uOttawa

L'Université canadienne
Canada's university

FACULTÉ DES ÉTUDES SUPÉRIEURES ET POSTOCTORALES

uOttawa

L'Université canadienne
Canada's university

FACULTY OF GRADUATE AND POSDOCTORAL STUDIES

Frédéric Caron
AUTEUR DE LA THÈSE / AUTHOR OF THESIS

M.A.Sc. (Civil Engineering)
GRADE / DEGREE

Department of Civil Engineering
FACULTÉ, ÉCOLE, DÉPARTEMENT / FACULTY, SCHOOL, DEPARTMENT

Repair and Retrofit of Non-Ductile Reinforced Concrete Frames with Diagonal Steel Compression Struts

TITRE DE LA THÈSE / TITLE OF THESIS

Dan Palermo
DIRECTEUR (DIRECTRICE) DE LA THÈSE / THESIS SUPERVISOR

CO-DIRECTEUR (CO-DIRECTRICE) DE LA THÈSE / THESIS CO-SUPERVISOR

Hassan Aoude

David Lau

Gary W. Slater
Le Doyen de la Faculté des études supérieures et postdoctorales / Dean of the Faculty of Graduate and Postdoctoral Studies

Repair and Retrofit of Non-Ductile Reinforced Concrete Frames with Diagonal Steel Compression Struts

By

Frédéric Caron

Thesis submitted to the

Faculty of Graduate and Postdoctoral Studies

in partial fulfillment of the requirements

for the degree Master of Applied Science in

Civil Engineering

Department of Civil Engineering

Faculty of Engineering

The University of Ottawa

Your file Votre référence
ISBN: 978-0-494-74140-5
Our file Notre référence
ISBN: 978-0-494-74140-5

Acknowledgements

As the author of this research dissertation, I would like to express sincere appreciation to my supervisor Dr. Dan Palermo for all his help and guidance. Special thanks to all of the students and the laboratory technician Mr. Muslim Majeed from the University of Ottawa Structural Laboratory that provided help and guidance with the experimental and analytical research.

I would like to acknowledge the financial support provided by the Natural Sciences and Engineering Research Council of Canada (NSERC) for the Canadian Seismic Research Network (CSRN).

I would also like to thank my family and friends who have helped, encouraged and supported me during my study.

Finally, I would like to acknowledge the University of Ottawa for providing me with the opportunity to pursue this study.

Abstract

Reinforced concrete frames built before the 1970s were designed prior to the enactment of seismic codes. These frames were designed with strong beams and weak columns, which is contradictory to the capacity design philosophy currently employed. These frames lack sufficient shear and confinement reinforcement. The joints, columns, and beams are susceptible to shear failures, thus preventing these frames from reaching their full flexural capacity. Such premature failures have no warning and are characterised by inadequate ductility, which is one of the key performance indicators in seismic design. There are two general methods to rehabilitate a concrete frame. The first would be to add new structural elements such as infill walls or steel bracing, and the second would be to strengthen the structural elements: the joints, beams, and columns. The latter has been studied using fibre reinforced polymers (FRP) and steel jackets.

The main objective for this research is to evaluate the response of repaired and retrofitted non-ductile reinforced concrete frames which are vulnerable to earthquake loading. The main focus is to investigate a quick, easy and inexpensive retrofit method that could be used before or after a structure is damaged. The retrofit method utilizes diagonal X-bracing fabricated from square steel hollow sections, which are designed as compression struts to retrofit non-ductile reinforced concrete frames in an attempt to increase stiffness and lateral load capacity.

The advantage is the elimination of costly and detailed connections necessary to exploit the tension capacity of the brace. Two, single-storey, one-bay, non-ductile reinforced concrete frames were first repaired. One frame was tested to assess the seismic performance of the repair strategy and the second frame was retrofitted with steel X-bracing.

Experimental and analytical results for both the retrofitted and repaired frames are presented. Code prescribed calculations and finite element analyses were performed to evaluate the frames and to provide comparisons between code-expected performance and advanced modelling predictions.

Table of Contents

List of Figures

Chapter 2

Chapter 3

Chapter 4

Chapter 5

Chapter 6

Appendix A

Appendix B

List of Tables

Chapter 3

Chapter 4

Chapter 5

Chapter 6

Notations

$A_{i \to i+50}$ -Area of steel between distance i and i + 50 mm

A_s -Area of steel (mm^2)

A_{si} -Area of steel at the distance d_i (mm^2)

α_1 - Ratio of average stress in rectangular compression block to the specified concrete strength

b -Width (mm)

b_i -Width of member i (mm)

β_1 -Ratio of depth of rectangular compression block to depth of the neutral axis

c -Distance from extreme compressive fibre to the neutral axis (mm)

C_c -Force due to concrete in compression (kN)

C_r -Compressive resistance of a member (kN)

d_b -Diameter of rebar (mm)

d_i -Distance from the compression face to the reinforcement (mm)

d_v -Effective shear depth, taken as the greater of *0.9d* or *0.72h* (mm)

E_s -Steel modulus of elasticity (MPa)

E_{sh} -Steel strain hardening modulus (MPa)

ε_c -Strain in the concrete (mm/mm)

ε_x -Strain in the concrete at a certain point (mm/mm)

ε_{cc} -Crushing strain of concrete (mm/mm)

ε_{rup} -Buckling strain of the square hollow section (mm/mm)

ε_{si} -Strain in the steel at the distance d_i (mm/mm)

ε_{sh} -Strain hardening strain (mm/mm)

ε_u	-Ultimate strain (mm/mm)
ε_y	-Yielding strain (mm/mm)
f'_c	-Concrete compressive strength (MPa)
F_i	-Force due to the steel at the distance d_i (kN)
F_k	-Web buckling stress (MPa)
f_{si}	-Stress in the steel at the distance d_i (MPa)
f_y	-Steel yield strength (MPa)
f_u	-Steel ultimate strength (MPa)
h	-Height of beam or column (mm)
h_i	-Height of member i (mm)
I	-Moment of inertia (mm^4)
I_e	-Effective moment of inertia (mm^4)
I_g	-Gross moment of inertia (mm^4)
k_i	-Development length modification factor
L	-Length of a member (mm)
l_d	-Development length (mm)
λ	-Factor to account for low density concrete
M_n	-Nominal moment capacity (kNm)
$M_{n\ bot}$	-Nominal moment at the bottom of a column (kNm)
$M_{n\ top}$	-Nominal moment at the top of a column (kNm)
N	-Axial load (kN)
N_i*	-Connection resistance, as an axial force in member i (kN)
θ	-Angle of inclination of diagonal compressive stresses to the longitudinal axis (°)
P_n	-Nominal axial force (kN)
P_{no}	-Maximum nominal axial force (kN)

r -Radius of gyration (mm)

t -Thickness (mm)

t_b -Width of a steel plate (mm)

t_i -Thickness of member i (mm)

T_n -Nominal tension force (kN)

t_p -Thickness of steel plate (mm)

V -Lateral force acting on the concrete frame (kN)

V_c -Shear resistance of the concrete (kN)

V_n -Nominal shear force (kN)

V_s -Shear resistance of steel stirrups (kN)

$\bar{x}$ -Centre of eccentricity (mm)

Chapter 1

1 Introduction

1.1 General

Earthquake design has significantly evolved during the past 40 years. However, reinforced concrete frames built before the 1970s were designed before seismic requirements were introduced. These frames were designed primarily for wind and gravity loading, resulting in strong beams and weak columns, which is contradictory to the capacity design philosophy currently employed. These frames have a number of structural deficiencies; they lack sufficient shear, buckling and confinement reinforcement, the lap splice lengths and locations are also inappropriate. Therefore, the joints, columns, and beams of these concrete frames are susceptible to non-ductile modes of failure and, therefore, prevent the frame from developing the required displacement capacity to resist the seismic demands. These premature failures have no warning and are characterized by inadequate ductility, which is one of the key performance indicators in seismic design.

Completely replacing a building that does not conform to current earthquake design methods is not economically feasible or viable. Therefore, retrofit methods have been developed and are still being developed to enhance, in most cases, the lateral load carrying resistance and stiffness of non-ductile frames in an attempt to prevent excessive damage that could be caused by future earthquakes. This has been achieved by adding reinforced concrete shear walls, diagonal tension cables, diagonal FRP sheets, or steel X-bracing. By increasing the stiffness of the structure, the lateral load carrying capacity of the frames is increased, while reducing the inelastic ductility demands. These retrofit techniques are invasive and require significant detailing. This is particularly true when the tension capacity of the retrofitting material is the main contribution to the lateral resistance.

A challenging task is to convince building owners to seismically retrofit their structures, particularly when earthquakes may not have occurred in the past. Therefore, the scope of this study is to investigate repairing post-earthquake damaged reinforced concrete frames and to develop quick and simple retrofitting strategies to strength deficient non-ductile reinforced concrete frames.

1.2 Objective

The main objective for this research is to evaluate the response of repaired and retrofitted non-ductile reinforced concrete frames which are vulnerable to earthquake loading. The main focus is on developing a quick, easy and inexpensive retrofit method that could be used before or after a structure is damaged. The retrofit method utilizes diagonal X-bracing fabricated from square steel hollow sections, which are designed as compression struts to retrofit non-ductile reinforced concrete frames in an attempt to increase stiffness and lateral load capacity. The advantage is the elimination of costly and detailed connections necessary to exploit the tension capacity of the brace. Two, single-storey, one-bay, non-ductile reinforced concrete frames, previously damaged, were first repaired in this study. One frame was tested to assess the seismic performance of the repair strategy and the second frame was retrofitted with steel X-bracing. The frames were evaluated experimentally and analytically.

1.3 Scope

The scope of this research consists of:

- *Review previous research on repaired and/or retrofitted reinforced concrete frames*
- *Calculate the expected capacities according to the design standards of Canada for reinforced concrete and structural steel for the repaired and retrofitted frames*
- *Repair two reinforced concrete frames that were previously tested*
- *Design and retrofit one of the repaired frames by adding structural steel compressive braces*
- *Prepare and test both specimens*
- *Analyze the test frames using the nonlinear finite element program VecTor2*
- *Evaluate and compare the code predictions, analytical analysis and experimental test data*

1.4 Thesis Outline

The thesis is divided into seven chapters. Chapter 1 is an introduction that presents the outline, the objectives, and the scope of this thesis. Chapter 2 provides a literature review of previous repair and retrofit methods utilizing fibre reinforced polymers and steel bracing. Chapter 3 includes a description of the test specimens and the material properties. Furthermore, the capacities of the repaired and retrofitted frames, the design of the steel bracing for the retrofit, the repairs performed to both frames, and the experimental setup and loading program are included. Chapter 4 lists the experimental results of the repaired and retrofitted frames. Chapter 5 explains the models developed for the analysis of the frames, along with the results. Chapter 6 presents a comparison of the experimental and analytical results. Finally, Chapter 7 provides a summary and conclusions for this research project.

Chapter 2

2 Literature Review

2.1 Introduction

There are two general methods to retrofit reinforced concrete frame structures. The first includes the addition of new structural elements such as infill walls or structural steel bracing, while the second is intended to strengthen the individual structural elements of the frame: the joints, beams, and columns. Strengthening of structural elements has been investigated through the use of fibre reinforced polymers (FRP) and steel jackets. This chapter provides a review of research performed using FRPs, joint retrofit methods, beam retrofit methods, column retrofit methods, frame retrofit methods, and retrofit methods of existing buildings.

2.2 Research on Fibre Reinforced Polymers as a Retrofit Material

Toutanji and Balaguru (1998) researched the durability of concrete cylinders wrapped with FRP tow sheets and tested under axial loading. They subjected their test specimens to two different cycles: wetting and drying, and freezing and thawing. Their tests had two sets of elements retrofitted with two different types of FRPs. The first set of columns was wrapped with carbon fibre reinforced polymers (CFRP) and the second with glass fibre reinforced polymers (GFRP). Degradation of bond due to the exposure conditions was observed, therefore, the columns experienced a reduction in flexural strength. The strength of CFRP wrapped specimens were not greatly affected when exposed to the wet-dry cycle and an improvement in the stiffness was observed. On the other hand, the GFRP wrapped specimens did not exhibit any stiffness change when exposed to the wet-dry cycle, while they exhibited a 10% reduction in the compression strength. The freeze-thaw cycle significantly affected the strengths of both CFRP and GFRP specimens. A reduction of over 25% was observed. It was found that the specimens wrapped with CFRP were superior to those wrapped with GFRP when exposed to harsh environments.

Karbhari (2001) researched FRP in the rehabilitation of concrete structures. The advantages of FRP are that they do not take up much space, they can be applied quickly, they have higher strength than steel, and the fabrication process produces consistent materials. FRPs, however, have limitations such as: strain capacity, they do not yield or experience plastic deformations, they behave linear elastically, and they are anisotropic which means that they have different properties in the longitudinal and transverse direction. FRP sheets can be prefabricated with an adhesive or some sort of glue that can be applied as a wet layup. The wet layup process is associated with manual application and use of ambient curing conditions. The concerns for this process include quality control, resin mix, wet-out of fibres, uniform resin impregnation, voids, compaction, wrinkles and control of curing. Polyurethane and epoxies are the two main structural adhesives used for the wet layup application. Polyurethane generally contains moisture sensitive components and may undergo reversion in presence of heat and/or moisture and significant reduction in performance at elevated temperatures. Epoxies have a higher range compared to polyurethane and show less creep and shrinkage, but their overall peel strength is lower. Prefabricated shells have a pre-applied adhesive bond. They have better quality control, and are efficient and durable, but it is dependent on the integrity of the bond. Due to the ease of application, there is a lack of detailing provided for the application of FRPs. For example, corners of square/rectangular concrete columns must be rounded to increase the effectiveness of the confinement and decrease the chance of fibre fracture.

2.3 Reinforced Concrete Joint Retrofit Methods

Ghobarah and Biddah (1999) performed dynamic analyses on reinforced concrete frames which included joint shear deformations. The objective of the study was to develop simple and accurate macro-models. The models were intended to be representative of joints whose shear-distortion properties and bar bond-slip relationships are specified explicitly under reverse cycle loading. When inadequate joint reinforcement and detailing is present, local shear failure initiates before other flexural elements reach their capacities. There are two different mechanisms that cause joint deformations: shear stress transfer and slippage of the reinforcing bars due to bond failure. Crack openings are the reason for the rebar pulling out. These cracks cause fixed-end rotations. Joints were rehabilitated using steel jackets to develop a ductile system that would allow energy dissipation. The joints were represented by two rotational springs in series. One of the springs represented the joint shear deformation and the other represented the rebar bond-slip. The authors recommended rehabilitation of the top and intermediate floors of a frame by increasing the confinement of the columns, which would reduce the critical regions; and rehabilitate the joints with steel jackets to improve the shear strength of the joints. In the lower floors, it was recommended to connect the bottom reinforcing bars to the beams and check the columns for shear capacity.

Said and Nehdi (2004) researched the use of FRP for reinforced concrete frames in seismic zones. Two studies were conducted, but only the first part will be discussed here. Part 1 of their study was on the evaluation of FRP beam-column joint rehabilitation techniques. They first established that FRPs can be used for different structural shapes, but that it has a brittle failure and strength is lost when wrapped around corners. Furthermore, the FRP is susceptible to damage in fires.

Five different specimens were tested. Specimen T1 was the control specimen and designed with older codes. After T1 was tested, it was repaired using method A-1 and renamed T1R. An additional T1 specimen was tested and later repaired using method A-2 with cover plates and renamed T2R. Another specimen, T9, which was similar to T1, was retrofitted prior to testing using method A-3 with steel angles. A companion specimen, J1, was designed to current codes and tested as part of this program. The three different rehabilitation methods are shown in Figure 2.1.

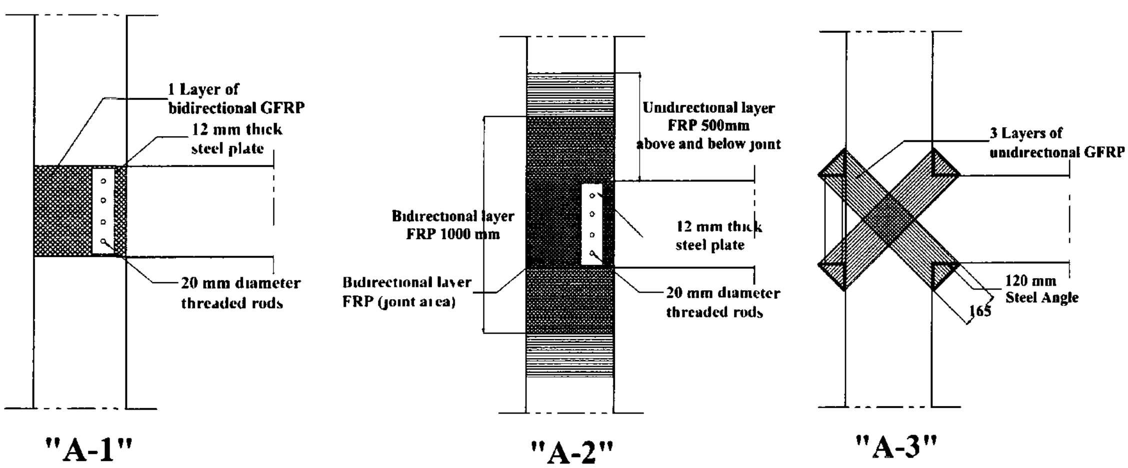

Figure 2.1: Different rehabilitation methods (Said and Nehdi, 2004)

Retrofit method A-1 consisted of one layer of a bidirectional GFRP jacket added at the joint and further confined with a 12 mm thick steel plate. Retrofit method A-2 included a uni-directional layer of FRP 500 mm above and below the joint, then a 1000 mm bi-directional layer of FRP was centered at the joint and, finally, an FRP bi-directional jacket was applied to the joint and confined by a 12 mm thick steel plate. Retrofit method A-3 involved adding two-three layered uni-directional GFRP strips diagonally across the joint forming an X. To aid the GFRP achieve its strength, small steel angles were added to the joints. It was found that the retrofitted specimens performed better than the control substandard specimen T1, but not as well as the standard specimen J1. The jacket of T1R was under-designed and the joint failed before a full flexural hinge could develop in the beams. A flexural hinge was observed when T2R failed. Confinement from the jacket delayed the deterioration of the joint but it did not prevent joint failure in specimen T9. The energy dissipation and maximum load capacity were increased for all three retrofitted specimens relative to T1, which can be observed in Figure 2.2.

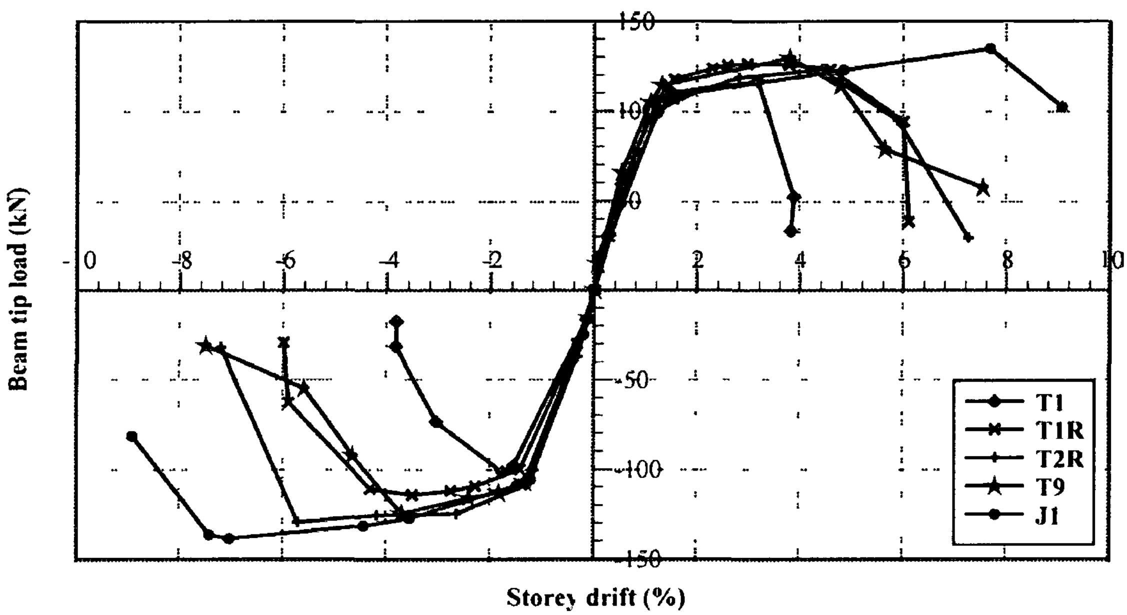

Figure 2.2: Load-storey drift envelopes (Said and Nehdi, 2004)

Said (2008) experimentally studied steel bracing to strengthen the joints of deficient reinforced concrete frames. The brace consisted of three pieces: two anchoring members which are bolted into the beam and column, and one I-shaped bracing member that is welded onto the anchoring members. Figure 2.3 demonstrates one joint retrofitted with four braces and another joint retrofitted with one steel bracing.

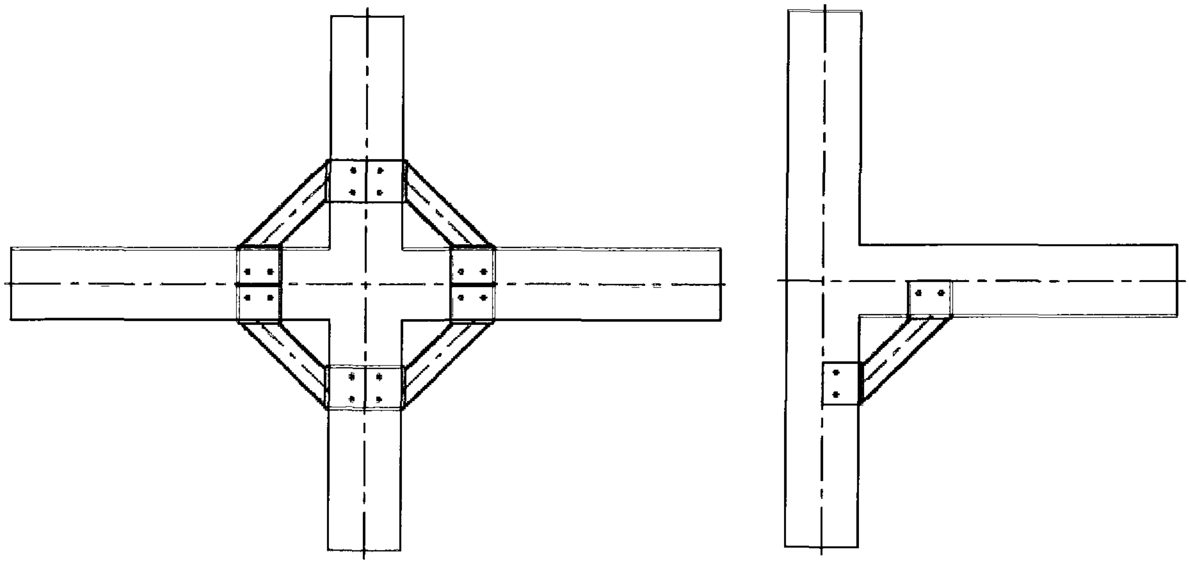

Figure 2.3: Example of configuration for local steel bracing system (Said, 2008)

Testing was performed on three specimens: one standard specimen designed to current codes, one substandard specimen, and one substandard retrofitted specimen. The specimens were constructed as a column with a cantilever beam which was pushed up and down during loading. The substandard specimen was retrofitted with two steel bracing units, one on top side of the beam and the other on the bottom side. The standard specimen reached a load of 107 kN corresponding to a tip displacement of 28 mm. The substandard specimen had a maximum tip displacement of 20 mm and a maximum load of 60.0 kN in the upward loading direction and 86.0 kN in the downward loading direction. The load for the retrofitted specimen was 150 kN upward and 142 kN downward. The corresponding tip displacements were 55 mm and 59 mm, respectively. The maximum loads in the top steel bracing were 239 kN in tension and 314 kN in compression. The maximum loads observed in the bottom steel bracing were 174 kN in tension and 225 kN in compression. The estimated forces experienced by the steel bracing system indicated that the steel bracing was within the elastic range. The steel bracing was able to delay joint shear failure and slippage of the beam's bottom reinforcement.

2.4 Reinforced Concrete Beam Retrofit Methods

Wand et al. (2004) conducted research on rehabilitation of cracked and corroded reinforced concrete beams retrofitted with fibre reinforced plastic patch strips. Different reinforced concrete beam rehabilitation options were evaluated as shown in Figure 2.4.

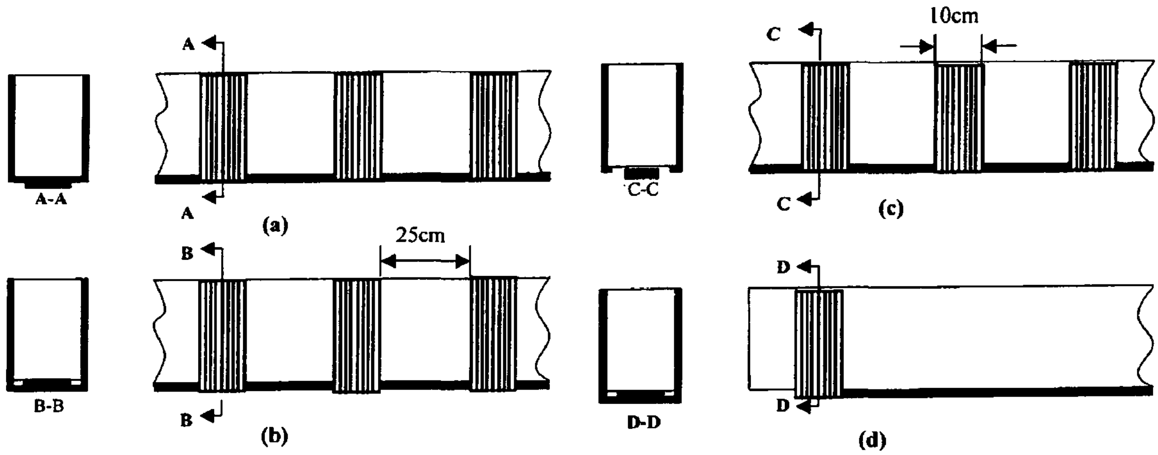

Figure 2.4: a) equally spaced U-shaped strips with longitudinal strips placed under; b) longitudinal strips with equally spaced U-shaped strips placed over; c) longitudinal strips with discontinuous equally spaced U-shaped strip; d) U-shaped strips placed at each end of the longitudinal strips (Wang et al., 2004)

The methods all included longitudinal strips of FRP placed under the beam to increase the flexural capacity of the beam and U-shaped FRP strips to increase the shear resistance of the beam. There were four different methods. The first was to apply equally spaced U-shaped strips and then apply the longitudinal strips under the beam. The second method was the opposite of the first; longitudinal FRP strips were applied and then the equally spaced U strips were bonded to the beam. The third method was to use discontinuous equally spaced U-shaped strips. The last method was to apply the longitudinal FRP strips and then hold them with only two U-shaped strips placed at each end of the longitudinal strips. When using longitudinal strips, the concerns are that either the longitudinal strips fail if the local strains are high or the anchoring system fails. It was determined that the application of FRP U-shaped strips could improve the loading capacity of a corroded concrete beam. When using equally spaced U-shaped strips to hold the longitudinal strips, the strain values were higher but the full usage of the FRP was not realized. It was found that the load carrying capacity of the beam can be attained with any design that can reduce stress concentrations at the intersection of the U-shaped anchor strips.

2.5 Reinforced Concrete Column Retrofit Methods

Li and Sung (2003) conducted a study on seismic repair and rehabilitation of shear-damaged circular bridge columns using carbon fibre reinforced plastic jacketing. In this research, a large circular bridge column was tested to induce shear failure due to seismic loading. First, the column was tested without any retrofitting. The cyclic loading test was terminated when one of the following occurred: spalling of concrete, rupturing of the vertical reinforcement bars, loosening of the horizontal reinforcement, or a 60% reduction in the maximum lateral force. After the first test was performed, the column was repaired by removing the spalled concrete and cleaning the surface with a high pressure air gun. Then, non-shrink mortar was used to repair the concrete, epoxy was injected using a high-pressure air pump to seal cracks, and, finally, CFRP jacketing was placed on the column. It was clear that the strength of the column was significantly improved. The energy dissipation capacity increased compared to a repaired companion column. The column failure mode changed from shear failure to flexural failure.

2.6 Reinforced Concrete Frame Retrofit Methods

Maheri and Sahebi (1997) performed an experimental study using steel bracing to reinforce concrete frames. Four different specimens were investigated: a control specimen without any bracing, a specimen with diagonal tension bracing, a specimen with diagonal compression bracing, and a specimen with a combination of compression and tension X-bracing. The braces were welded to plates situated at each inner corner of the concrete frame. The analytical strength was estimated as 3.9 tons for the repaired frame, 14.1 tons for the frame reinforced with the tension-only brace, 14.8 tons for the frame reinforced with the compression-only brace, and 27.2 tons for the frame reinforced with the compression and tension X-bracing. The frames were subjected to horizontal cyclic loading. The control specimen was able to support an ultimate load of 4.0 tons as expected. The concrete frame reinforced with the compression and tension X-bracing reached a maximum load of 12.5 tons. This was lower than expected, and failure was observed in the brace under tension. The concrete frame reinforced with the compressive-only brace buckled when the load reached 10.0 tons. The concrete frame reinforced with the tension brace failed when the load reached 9.0 tons. It was also concluded that the connections were weak and did not allow the full capacity of the braces to be developed.

Ghobarah and Abou Elfath (2001) studied the rehabilitation of reinforced concrete frames using eccentric steel bracing. The advantages of steel bracing are the ability to accommodate openings, the minimal added weight to the structure, and minimum disruption to the occupants when building an external system. The researchers noted that combined concrete and steel systems were not used as a retrofit method due to the lack of sufficient research and design information. A three-storey office building rehabilitated with eccentric steel bracing placed in the interior bays of the frames was investigated in this study as shown in Figure 2.5.

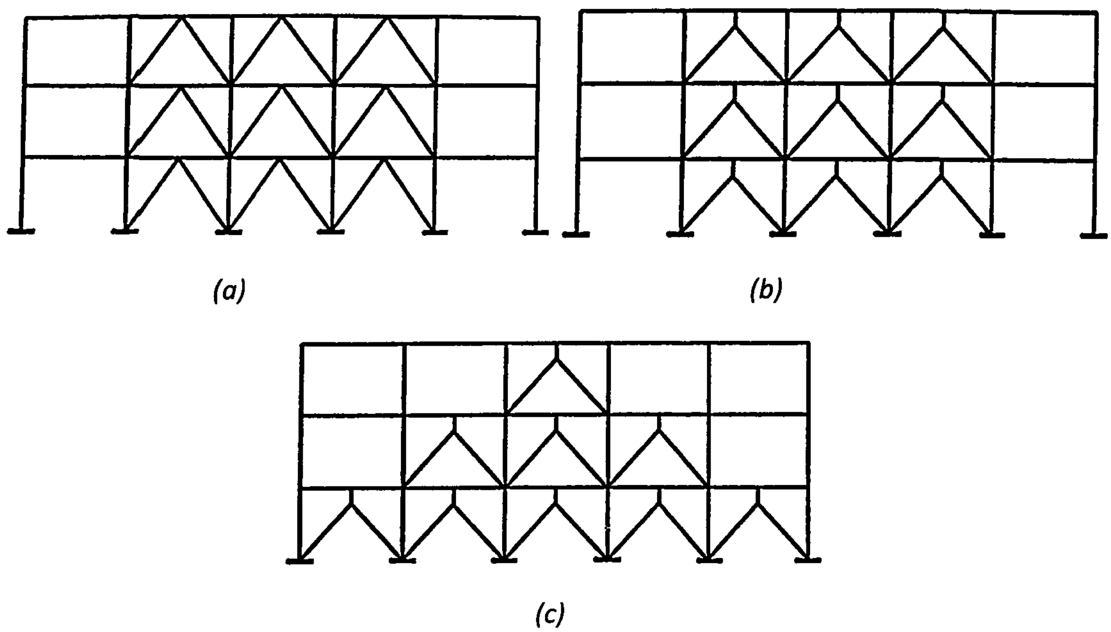

Figure 2.5: a) Inverted V-bracing placed in the interior frames; b) Inverted V-bracing with a vertical steel link placed in the interior frames; c) Inverted V-bracing with a vertical steel link placed in the interior frames as a pyramid (Ghobarah and Abou Elfath, 2001)

The three different bracing strategies investigated were: inverted-V-bracing placed in the interior frames; inverted-V-bracing with a vertical steel link placed in the interior frames; and inverted-V-bracing with a vertical steel link placed in the interior frames as a pyramid. For the inverted V-bracing, hinging started in the beams of the first and second floors due to pullout of the bottom reinforcement and yielding of the top reinforcement. The damage then spread to the columns of the first and second floors. After the loading was complete, splice failures at the bottom of the columns and yielding of the reinforcement of the first storey columns were noted. Even with an increase in earthquake intensity, the columns and beams of the third storey remained undamaged. At the first and second storeys, some of the steel bracing members buckled, as well as three of the steel members of the third storey. For the inverted V-bracing with a vertical steel link, hinging started in the beams of the first and second floors. The damage then spread to the columns of the first and second floors. After an increase in earthquake intensity, the columns and beams of the third storey still remained undamaged. For the inverted V-bracing with a vertical steel link placed as a pyramid, hinging started in the beams of the second floor and columns of the third floor. The damage then spread to the beams of the first floor and to the second-storey columns. Finally, the damage spread to the columns of the first storey. For both the inverted V-bracing with a vertical steel link and inverted V-bracing with a vertical steel link placed as a pyramid, it was observed that the shear steel links experienced shear yielding and that the bracing members behaved elastically.

The number of plastic hinges found in the inverted V-bracing with a vertical steel link placed as a pyramid system was greater than in the inverted V-bracing with a vertical steel link. This was due to the fact that the improved plastic mechanism led to the participation of more reinforced concrete elements in the building's inelastic response. In the case of the inverted V-bracing with a vertical steel link placed as a pyramid, significantly lower deformations in damage areas were noted than in the case of the inverted V-bracing with a vertical steel link. This was due to the uniformity of the storeys' displacement which, in turn, produced small variations in the maximum shear force. It was determined that the inverted V-bracing with a vertical steel link placed as a pyramid was the best system which demonstrated less damage. Another advantage of inverted V-bracing with a vertical steel link compared to a simple inverted V-bracing is that in the first case only three connections with the concrete were needed, while four were needed in the second case. As observed, it was suggested that the distribution of the brace strengths be distributed to obtain a uniform distribution with the storey drift.

Shalouf (2005) studied seismic retrofit of reinforced concrete frames with diagonal prestressing or FRP strips. Four frames were considered in the program. The first frame was BR-1, a concrete frame with a brick infill wall. The second frame, BR-2, was a reinforced concrete frame with a brick infill wall that was retrofitted with diagonal prestressing cables. The third frame, BR-3, was also filled with a brick wall; the columns were wrapped with CFRP, and diagonal prestressing cables were also included as part of the retrofit as shown in Figure 2.6. The fourth frame, BL-3, had an infill concrete block wall and was retrofitted with diagonal CFRP strips as illustrated in Figure 2.7.

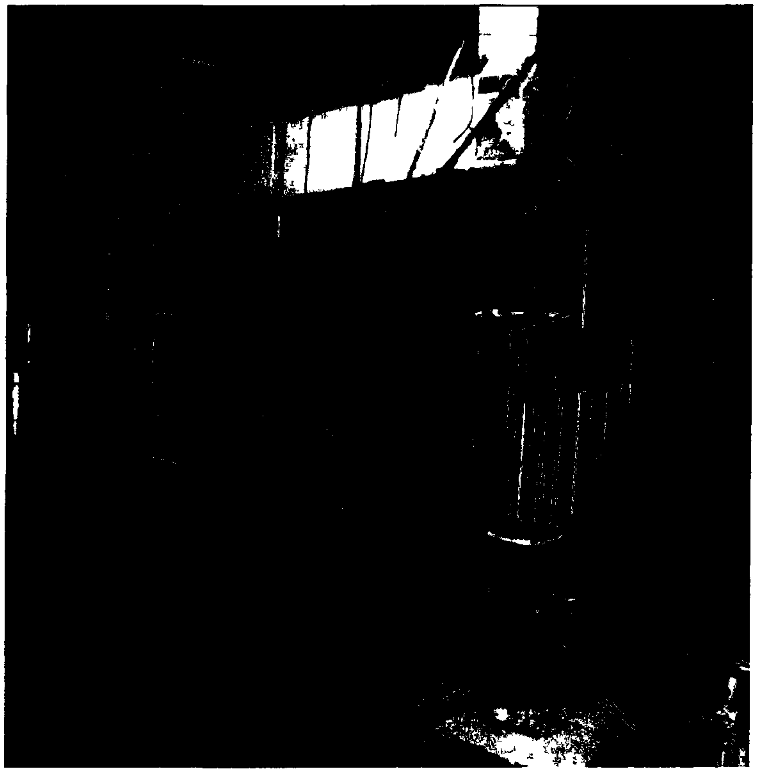

Figure 2.6: Retrofitted reinforced concrete frame BR-3

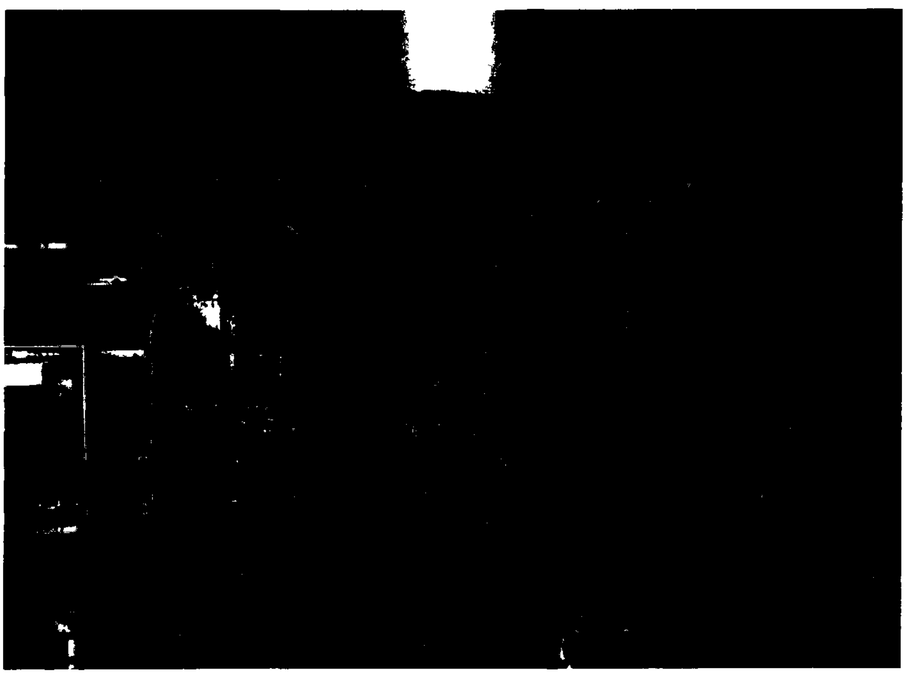

Figure 2.7: Retrofitted reinforced concrete frame BL-3

The four frames were tested under the same loading protocol. The gravity load was applied through prestressing cables. The horizontal load was imposed along the top beam with a 1000 kN hydraulic actuator. Measurements were recorded in relation to the foundation of the frame. A linear variable displacement transducer (LVDT) was used to measure the lateral displacement at the location of the applied load, while a backup LVDT was mounted at the other end of the top beam with a light metal frame. Strain gauges were also placed on the reinforcement. The test setup is illustrated in Figure 2.8 and the layout of the reinforcement and location of the strain gauges on the reinforcement is provided in Figure 2.9.

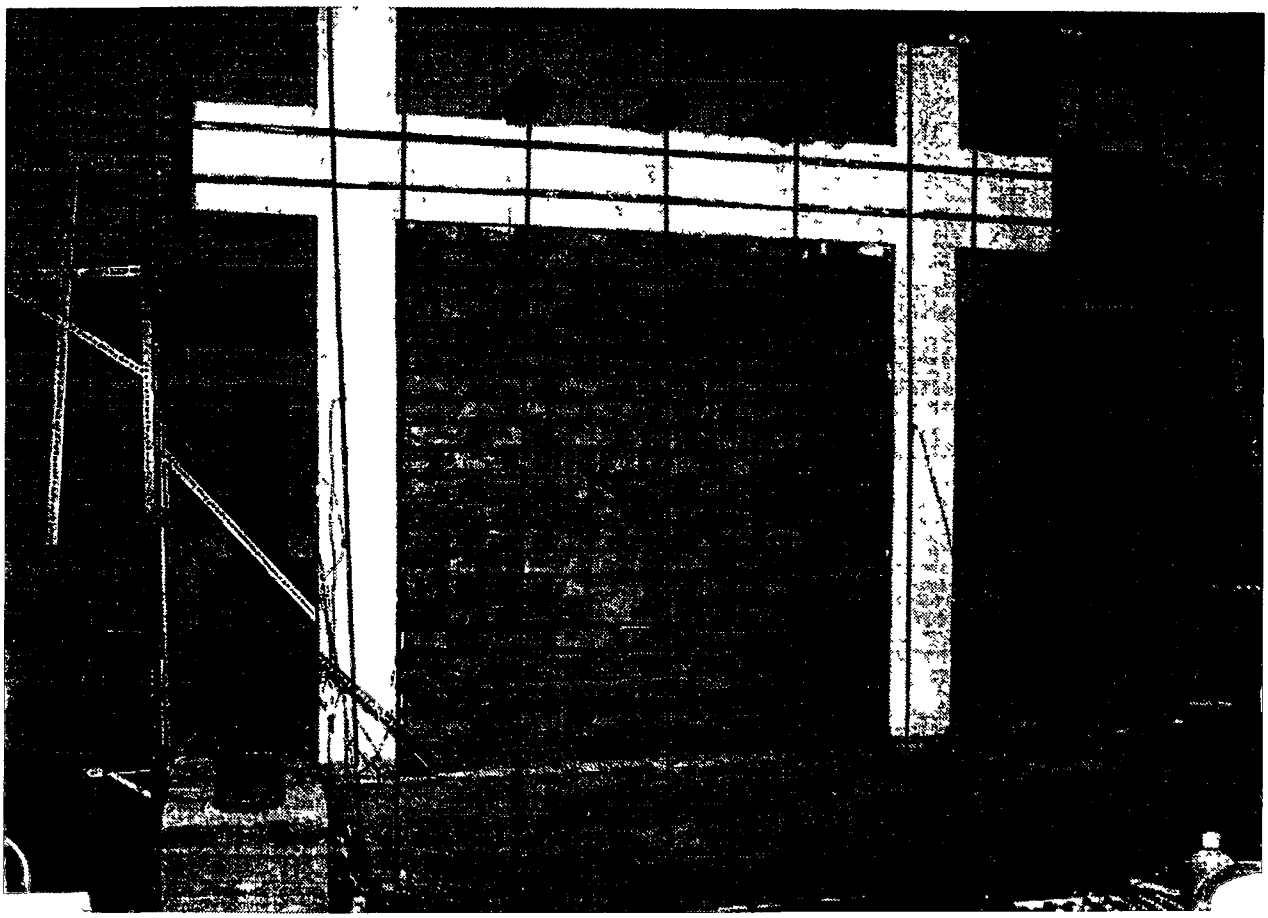

Figure 2.8. Typical test setup (Shalouf, 2005)

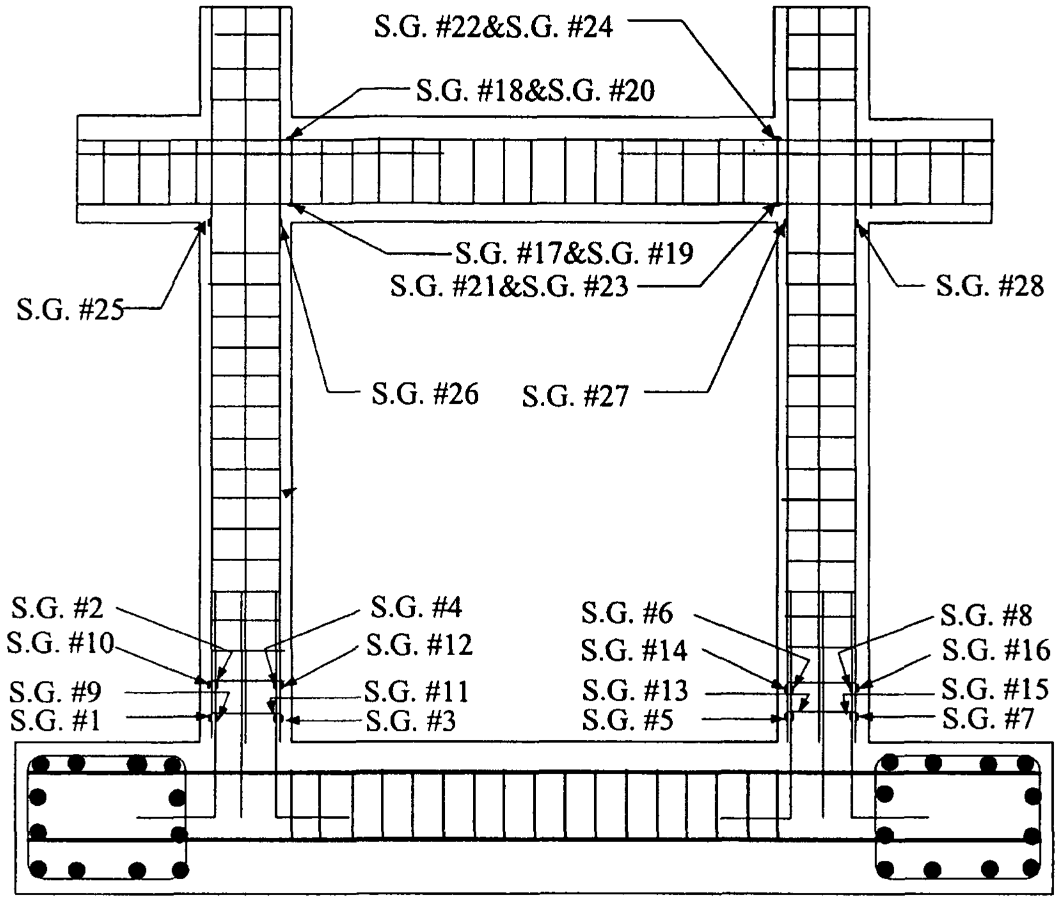

Figure 2.9: Typical reinforcement layout and strain gauge placement (Shalouf, 2005)

The strength of an identical repaired frame was estimated in a previous study by Serrato (2002). Frame BR-1 was tested as the reference specimen for Frames BR-2 and BR-3. It reached a peak horizontal load of 400 kN after displacing 35 mm. The diagonal prestressing cables for BR-2 were prestressed to 75 kN and for BR-3 to 125 kN. Frame BR-2 reached a peak horizontal load of 746 kN at a corresponding displacement of 25 mm, while Frame BR-3 reached a peak load of 715 kN at 20 mm of displacement. Failure in BR-2 was gradual, where an abrupt shear failure was experienced in one column of BR-3. Frame BL-3 reached a peak lateral load of 659 kN at a displacement of 15 mm. A significant portion of the strength gain due to the FRP diagonal strips was lost at 2% drift ratio. The research program demonstrated that the retrofitting methods investigated only increased the strength and stiffness but not the ductility of the frames. The lateral load versus the lateral displacement responses for the four tests is displayed in Figures 2.10 to 2.13.

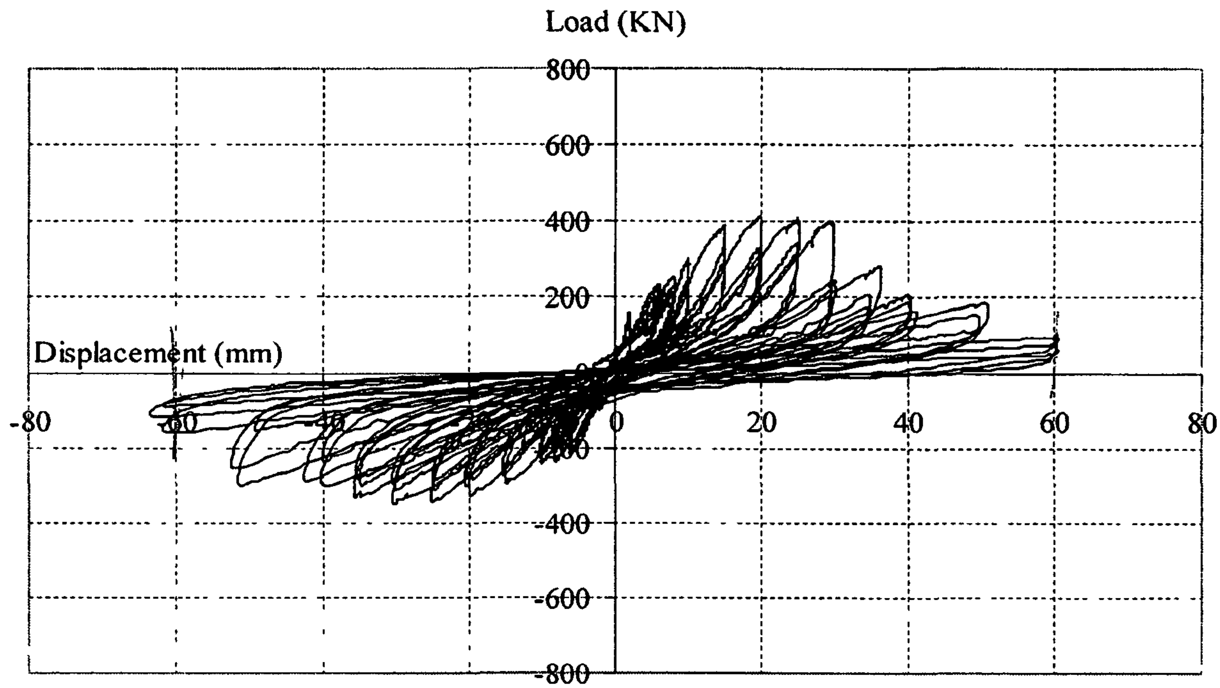

Figure 2.10: Lateral load versus lateral displacement relationship for BR-1 (Shalouf, 2005)

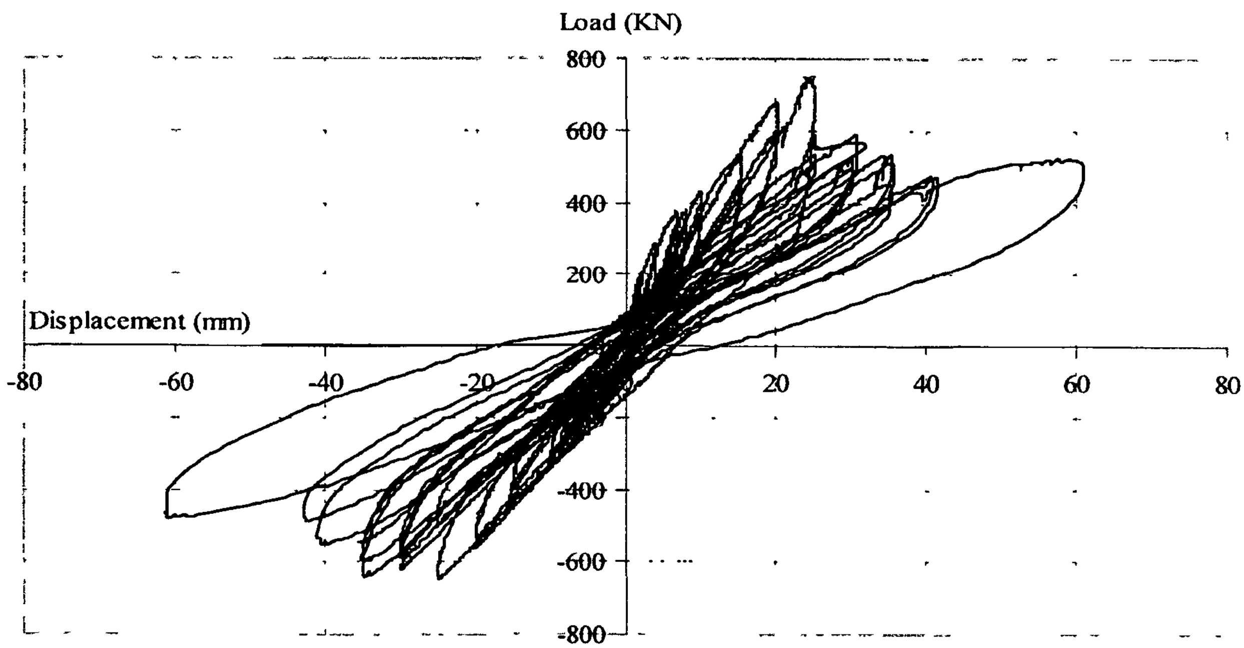

Figure 2.11: Lateral load versus lateral displacement relationship for BR-2 (Shalouf, 2005)

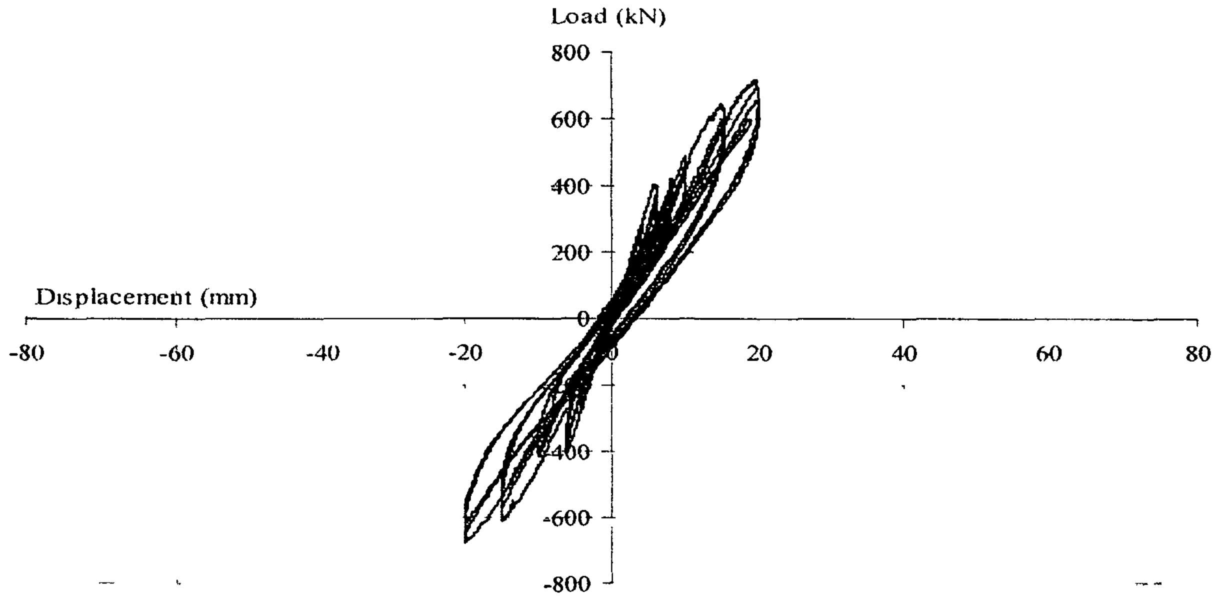

Figure 2.12: Lateral load versus lateral displacement relationship for BR-3 (Shalouf, 2005)

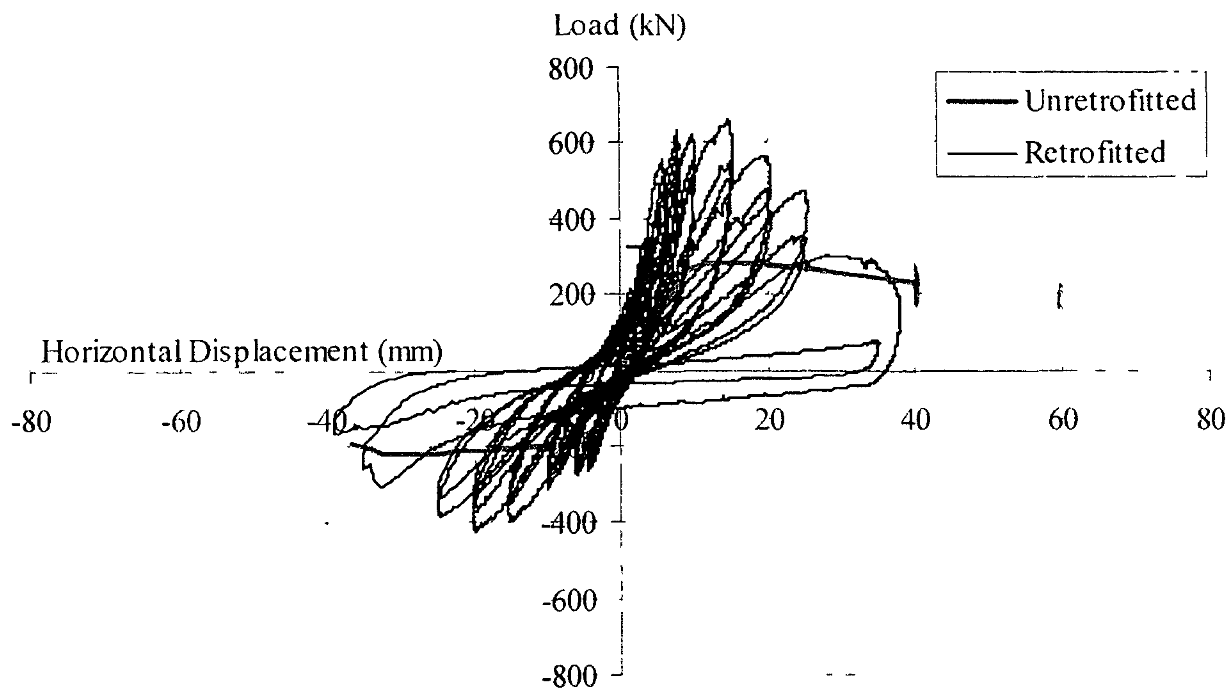

Figure 2.13: Lateral load versus lateral displacement relationship for BL-3 (Shalouf, 2005)

Duong et al. (2007) conducted an experimental investigation on the seismic behaviour of a shear-critical reinforced concrete frame. The focus of the research was to provide knowledge on the behaviour of shear-critical reinforced concrete structures and to provide experimental data that could be used in future projects. A single-span, two-storey reinforced concrete frame with shear-critical beams was constructed and tested. After testing the frame under reverse cycling loading, the severely shear damaged beam was repaired with CFRP and then retested. The failure mode of the frame was altered from brittle flexural-shear in the original test to ductile failure after repair. The displacement ductility was improved by a factor of more than 1.7, the maximum displacement was increased by a factor of more than 3.7, and the energy dissipation was increased by a factor of more than 5.7. An increase in the shear capacity of more than 30% was noted for the repaired frame. The test was terminated due to the actuators exhausting their stroke capacity; therefore, complete failure was not experienced, indicating that the repaired frame would have demonstrated additional enhancement in behaviour. It was recommended that the flexural capacity of the beams be increased such that the CFRP wrap would rupture.

Li et al. (2007) performed theoretical and experimental studies on repaired and rehabilitated reinforced concrete frames. In the study, it was determined that it was more economical to rehabilitate the columns that had sustained shear failure to satisfy requirements of current seismic codes than to demolish and reconstruct the entire building.

The proposed rehabilitation method is to be implemented in two stages. First, immediately following a major earthquake, non-shrink mortar is used to repair the columns and steel cables are used to prevent the building from failing during aftershocks. This was considered a good first step since the required materials are readily available and less experienced workers could perform the work without significant problems. The second stage takes place after the aftershocks. It involves the use of CFRPs to enhance the strength and ductility of the columns. The second step was found to be advantageous because no heavy equipment is required and it is implemented quickly. The CFRPs were preferred given its resistance to corrosion, light weight, workability and constructability, high strength-to-weight ratio, high elastic modulus, and high resistance to environmental degradation.

Three different frames were tested as shown in Figure 2.14: the first, BMNF – benchmark non-ductile frame; the second, BMNFH10B – benchmark non-ductile frame with half height brick wall; and the third, BMNF10B – benchmark non-ductile frame with full height brick wall. After retrofitting, the frames were renamed: BMNF-FC – benchmark non-ductile frame repaired with steel wire cable, non-shrink mortar and CFRPs; BMNFH10B-FC – benchmark non-ductile frame with half height brick wall repaired with steel wire cable, non-shrink mortar and CFRPs; and BMNF10B-FC – benchmark non-ductile frame with full height brick wall repaired with steel wire cable, non-shrink mortar and CFRPs.

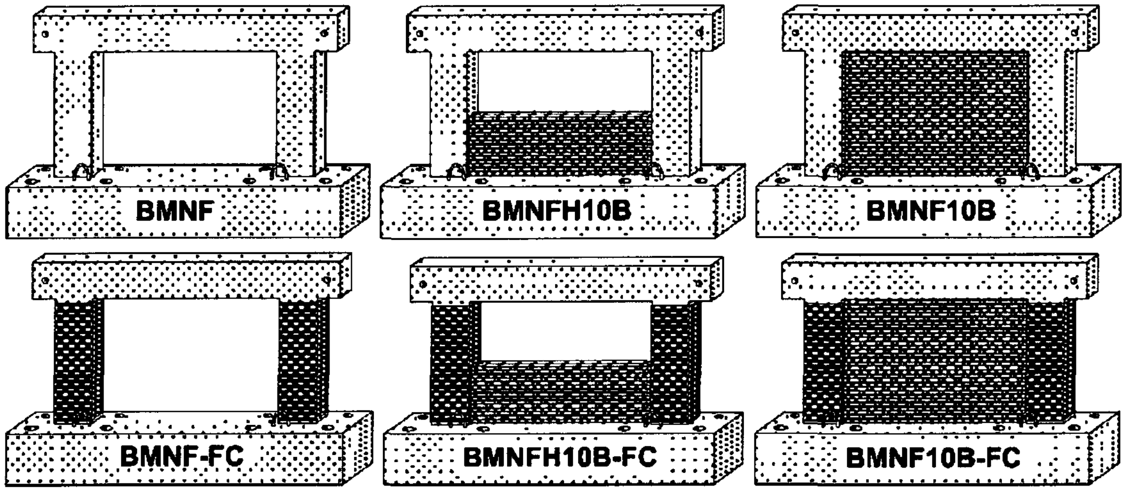

Figure 2.14: Tested frames (Li et al., 2007)

The repair procedure, which is illustrated in Figure 2.15, includes removal of spalled concrete, wrapping of the column with a 16 mm steel wire cable and then application of non-shrink mortar to replace the concrete that was removed from the column. Next, epoxy is applied to the surface of the concrete, followed by a primer, and then the carbon fibre sheet is applied. Removal of the bricks adjacent to the columns, followed by repair of the columns and then replacement of the bricks was required in the repair of the frames that contained infill brick walls. It was found that the load carrying capacity was increased up to 20%. Also, the energy dissipation and the drift ratio of the rehabilitated reinforced concrete frames were more than twice that of the as-built frames. Finally, the frames with the brick infill walls had a higher increase in energy dissipation and load carrying capacity.

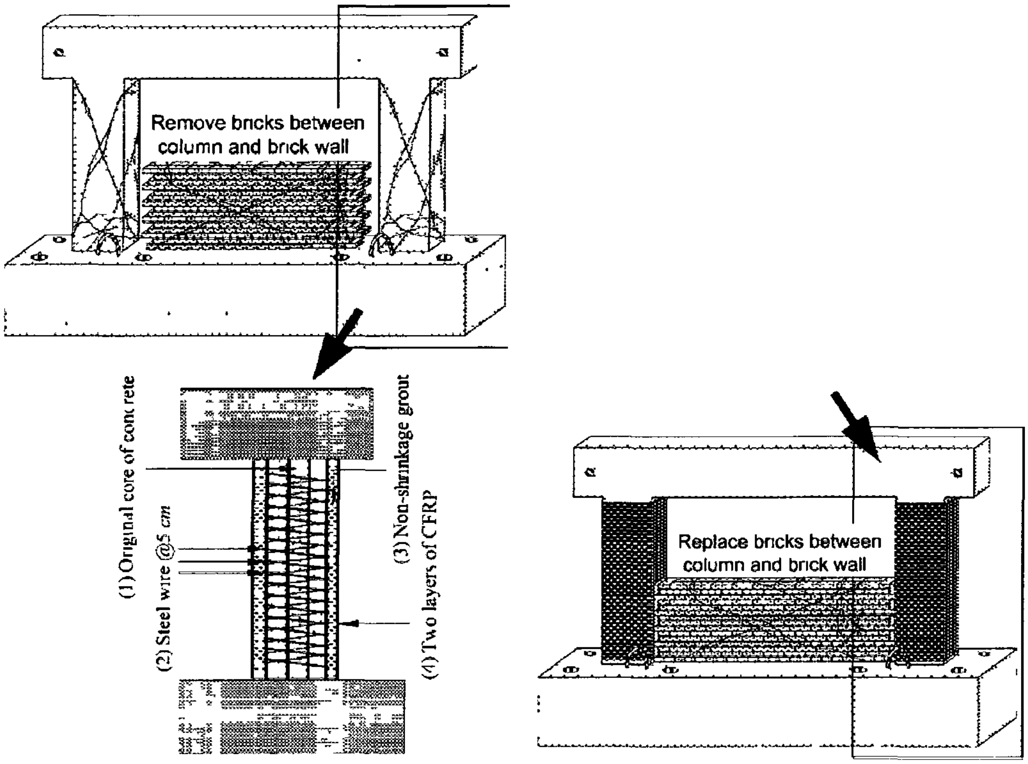

Figure 2.15: Repair and rehabilitation procedures (Li et al., 2007)

Ozcelik and Binici (2010) conducted research on the performance of post-installed internal steel frames (ISFs). They tested three retrofitted frames and one reference frame. The frames were subjected to constant gravity load and cyclic lateral displacements. Deficiencies in the frames were poor detailing of the transverse steel in the beams, joints and columns, and the bond of the longitudinal reinforcement. Low strength concrete was another deficiency.

The four specimens were one-bay, single-storey portal frames scaled by a factor of 1/3. They were built with 8 MPa concrete. Two different methods were used to install the ISFs. The first method did not implement anchors. To start, a thin layer of repair putty was used to create a smooth bonding surface with the reinforced concrete frame. Then, epoxy was used to bond the steel columns of the ISF to the concrete frame, and three days later the steel beams of the ISF were welded to the steel columns. This retrofit method is illustrated in Figure 2.16 a). The second method followed the same installation procedures implemented for the first method but, in addition, included the use of anchors. The steel beams and columns were anchored into the existing concrete frame as demonstrated in Figure 2.16 b).

Specimen SP1 was the reference specimen, while SP2 and SP3 were retrofitted using the first method and SP4 was retrofitted using the second method. The structural steel used for SP2 was an HSS section

(HSS 80 x 80 x 4 mm) and the structural steel used for SP3 and SP4 was an I-beam (I-140). A general schematic of the retrofitted frames is depicted in Figure 2.17.

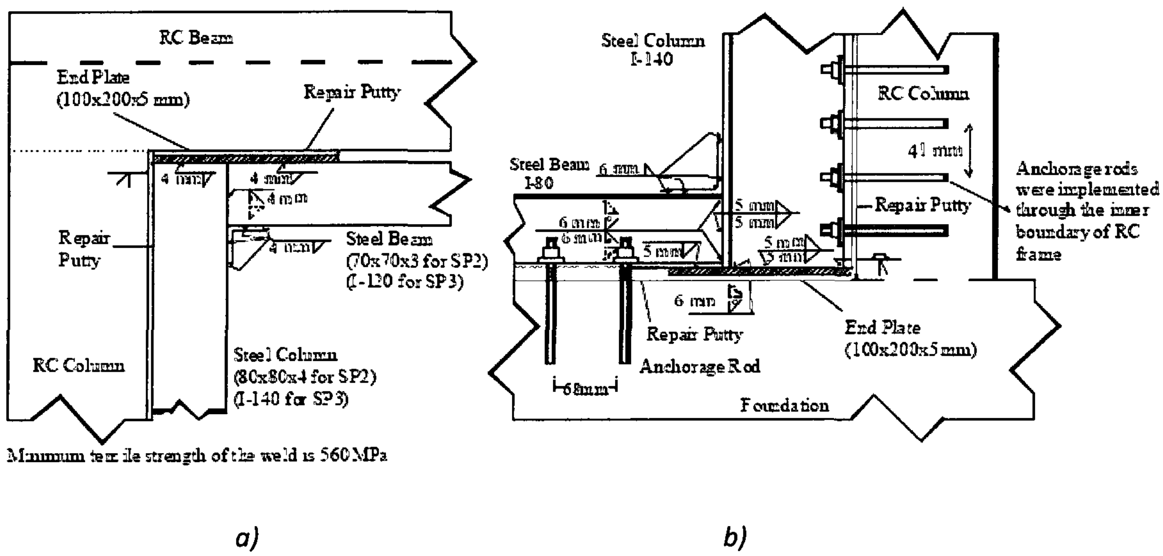

Figure 2.16: Retrofit methods; a) Method I; b) Method II (Ozcelik and Binici, 2010)

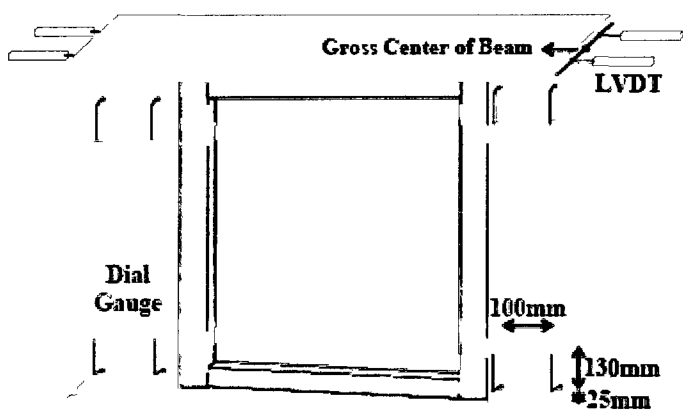

Figure 2.17: Retrofitted specimen (Ozcelik and Binici, 2010)

The reference frame, SP1, formed plastic hinges in the column, but with an increase in the lateral load the frame suffered pinching and severe stiffness degradation. SP2 exhibited a strength increase factor of 4.0 relative to the reference frame and a stiffness increase factor of 2.5. Failure was due to fracture of the steel beams. SP3 had a lateral strength increase factor of approximately 6.7 compared to the reference specimen. The stiffness was also increased by a factor of 4.8. The anchorless connection of the ISF with the concrete frame resulted in excessive damage at the beam-column joint. For Frame SP4 the stiffness was increased by a factor of 5 and the lateral strength increased by a factor of 8.6 in relation to the reference specimen. There was no failure observed in the anchors and joints. The failure mode was initiated by fracture of the steel beam. The superior performance in Frame SP4 was attributed to the anchor connection.

The study indicated that ISFs can increase the stiffness, strength, and energy dissipation capacity. The increase in lateral strength and energy dissipation capacity was due to a reduction in pinching in the hysteretic response, and a reduction of stiffness and strength degradation. This retrofit method is limited by the horizontal shear strength of the beam-column joints of the original concrete frame.

Sahoo and Rai (2010) investigated a seismic strengthening technique using aluminum shear links as energy-dissipating devices. The lateral strength and stiffness, and the energy-dissipation potential were the primary deficiencies for the buildings considered. The advantages of this retrofit method are that the shear links have low yield strength with high ductility and are resistant to fatigue. In addition, it is insensitive to load amplitude, frequency, and number of load cycles. Stable and symmetric hysteretic loops due to shear yielding can also be observed when shear links are used under cyclic loading.

The main objectives of this study were to study the behaviour of a strengthened reinforced concrete frame specimen with an aluminum shear link under lateral load, and to compare the results of the bare and retrofitted frames in terms of lateral strength, lateral stiffness, energy dissipation, and damage level.

Figure 2.18 shows the retrofitted specimen; a reduced-scale, (1:2.5) single-storey, one-bay reinforced concrete frame retrofitted with an aluminum shear link, a collector beam, a T-hangar, two-bracings, four steel collars, and four stiffeners. The collector beam was designed to sustain the maximum axial force equal to one-half of the storey shear and it reduces the need for drilling into the concrete to connect the shear link. The steel collars were formed by welding batten plates to four steel angle sections at the corners. The intent was to simplify the connections with the braces and collector beam to the reinforced concrete frame. The steel collars also confine the reinforced concrete columns and, to some extent, enhance the lateral strength and plastic rotational capacities of the columns.

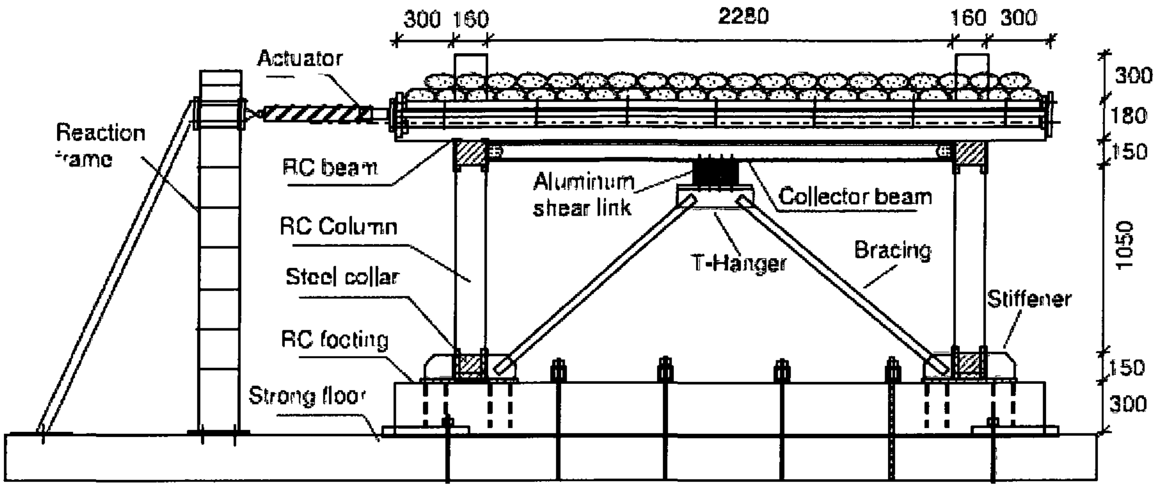

Figure 2.18: Strengthened specimen (Sahoo and Rai, 2010)

The bare reinforced concrete frame resisted a lateral load of 71.8 kN and experienced a maximum drift of 4.5%. Failure was due to inadequate shear strength of the columns which caused severe crushing of the concrete at both extremities.

The strengthened specimen sustained a maximum lateral load of 141.8 kN; 64.2 kN was carried by the reinforced concrete frame, and 77.6 kN was carried by the shear link. Apart from minor flexural and shear cracks, the concrete members of the strengthened specimen did not experience significant damage. The collector beam did not cause shear failure in the columns, and the shear link was able to yield without any connection failure. The shear link exhibited a stable and symmetric hysteretic loop with significant post-yield strain-hardening. Both of the bracing members behaved elastically with no sign of yielding or welding failures. The collector beam did not show any sign of buckling or yielding.

To summarize, the strengthened specimen provided an increase in lateral strength of 2.1, increase in lateral stiffness of 3.5, and increase in energy dissipation of 4.0 relative to the companion bare frame.

2.7 Retrofit Methods Implemented in Existing Reinforced Concrete Structures

Islam et al. (2010) presented a retrofit technique that was implemented on a 14-storey concrete residential tower located in California as shown in Figure 2.19. The building was constructed in the 1960's and posed a significant collapse hazard.

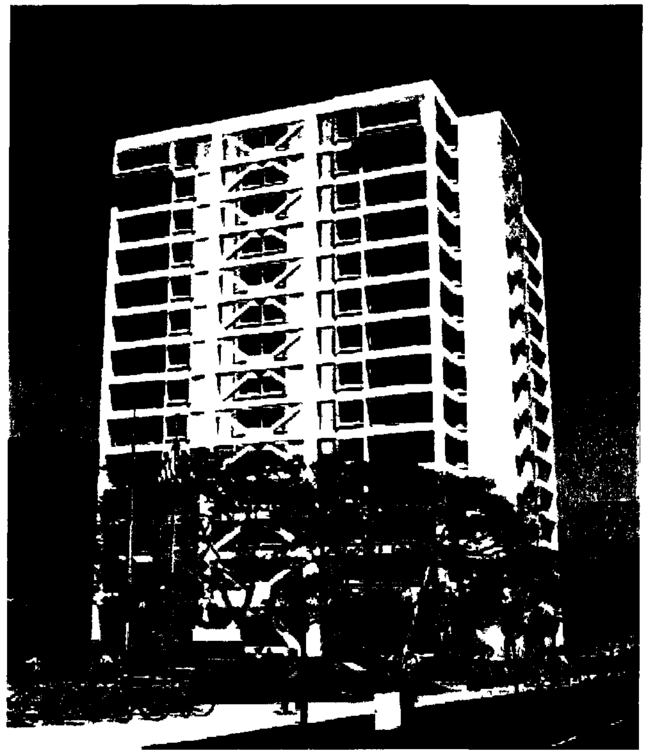

Figure 2.19: Residential tower after retrofit (Islam et al., 2010)

The residential tower consists of post-tensioned concrete flat slabs and post-tensioned perimeter concrete moment frames where the beam and columns contain non-ductile detailing. The primary concerns were: inadequate detailing for post-yield deformation capacity; reduction of ductility due to the post-tensioning of the beams; and the potential for brittle crushing of the concrete in the joints due to diagonal compression.

The objectives of the seismic upgrade were to mitigate the major seismic deficiencies and to meet the life safety (475-yr) and collapse (2475-yr) criteria of the current building code. The owner had the following requirements: a retrofit method that was aesthetically acceptable and non-intrusive, minimal interior construction, and open views for the occupants.

The addition of new Buckling Restrained Braced Frames (BRBF's) was proposed. These were added on all four faces of the building. New exterior beams and columns were added over the existing moment frames to mitigate the joint shear. This retrofit method was analyzed using a three-dimensional nonlinear model with Program RAM Perform-3D. The results demonstrated a reduction of approximately 50% in the seismic drift, and it was determined that the BRBF's would resist 70% of the total storey shear.

Skokan et al. (2010) described the seismic retrofit of the Huntington Beach City Hall Administration Building. This 6-storey building was constructed in 1971. The reinforced concrete beam-column moment frame systems are non-ductile. The deficiencies for this building include: non-ductile detailing, strong beam – weak column, excessive building deflections, inadequate shear capacity of the beam-column joints, and inadequate strength in the walls and foundations.

The seismic retrofit solution involved the addition of exterior braced frames. A performance-based approach was used to meet the "Life Safety" performance of the 500-year earthquake. The behaviour of the buckling restrained braces and the existing concrete beam-column frame systems were evaluated with a three-dimensional non-linear computer model.

The buckling of the braces was prevented by encasing the core steel plates within a mortar-filled hollow steel tube. This permits the braces to yield in tension and compression. Therefore, the energy dissipation of the upgraded structure will be based on a non-degrading hysteretic behaviour. The new buckling restrained braces, as shown in Figure 2.20, were connected to new concrete frames that, in turn, were connected to the exterior of the existing building. The braces were added to three sides of the building, while the remaining side was upgraded with a new concrete frame.

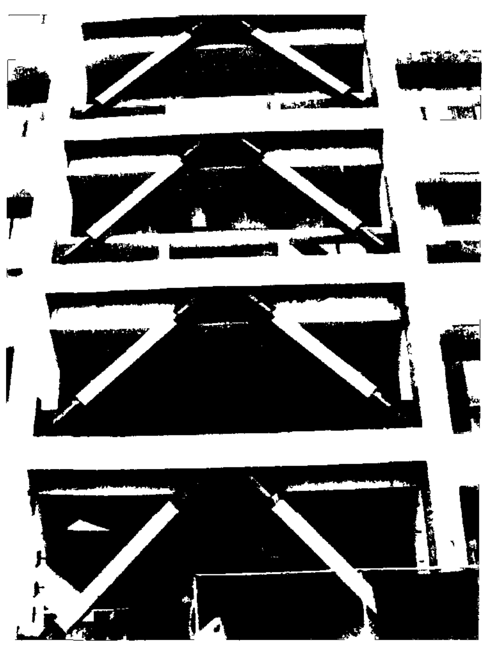

Figure 2.20: Retrofit scheme during construction, BRBF (Skokan et al. 2010)

The retrofit method was evaluated with Program SAP-2000. The retrofit was designed to limit the inter-storey drift to 1%; the analysis indicated a 0.8% drift. The analysis also demonstrated that the storey shear on the existing non-ductile concrete frames was reduced, and approximately 70% of the total storey shear was resisted by the new frames.

This retrofit system was able to do the following: provide partial views from the existing windows, provide less demolition than an interior retrofit scheme, be a cost-effective solution compared to an interior method, reduce the building drift, and reduce issues related to excessive stresses in the existing structural elements. Furthermore, the buckling restrained braces do not exhibit any strength degradation.

2.8 Summary

Various repair and retrofitting methods were reviewed in this chapter. The methods included FRPs and steel braces. The literature demonstrates that, in the past, steel braces were used predominantly as tension-resisting members. The repair and retrofit methods provided techniques for joints, beams, columns, and frames to prevent local shear failure and to promote flexural capacity or to stiffen the frame to respond in the elastic range. It was also noted that non-retrofitted elements should not fail in shear after a certain element of the frame has been retrofitted. A system should have a ductile failure or remain elastic. Many of the presented retrofit methods are complex, expensive, and invasive.

Retrofit methods utilizing FRPs tend to be expensive due to the cost of the material. They require preparation of the concrete surface for installation and may not be easy to install. FRPs are only as good as its bond and connection with the concrete. Steel bracing retrofitting methods that have been studied in the past have mostly been used as tension members (cables or members). These methods tend to have very complicated connections. Drilling into concrete to make these connections is not an easy or quick task, nor will it always be possible.

The research presented herein is focused to introduce a quick, economical, and non-invasive retrofit strategy. Steel (HSS sections) compression-only braces are being proposed. The installation of this system is quick and simple. The connections to the existing concrete frame are easy, there is minimal welding, and the HSS section can be cut to exact size with ease. All the components of the bracing system are situated within the frame's opening. Therefore, the procedure to install the proposed retrofit is less intrusive, and other structural elements, such as the slabs, beams, and column are not in the way of the installation. This research will also demonstrate that non-ductile reinforced concrete frames can be repaired and then retrofitted to satisfy requirements of currents codes.

Chapter 3

3 Experimental Program

3.1 Introduction

This chapter includes a description of the test specimens and the material properties. The capacity of the repaired frame and the failure mode will be discussed. The design of the steel bracing for the retrofitted frame is explained, as well as the repairing procedures for both frames. The chapter will end with a description of the experimental setup and loading protocol.

Both of the frames tested in this research program were originally designed and built by Shalouf (2005). Specimen BR-3 contained an infill brick wall and was retrofitted by wrapping the ends of the columns with FRP sheets, in addition to prestressing cables placed diagonally across the frame. This frame was repaired without the infill brick wall and was tested as the repaired frame for this research study. Frame BR-3 was renamed BR-3R. Specimen BL-3 contained an infill block wall and was retrofitted with diagonal FRP strips. This frame was first repaired and then retrofitted with diagonal steel X-bracing in this experimental program. Frame BL-3 was renamed BL-3R. Both frames were identically designed and built in the original study. The retrofit strategies in the original work resulted in higher lateral loads and increased stiffness, but damage was more extensive relative to the companion frames with infill walls. Frame BR-3 reached a maximum lateral load of 715 kN at a displacement of 20 mm, whereas Frame BL-3 reached a maximum lateral load of 659 kN at a displacement of 15 mm.

3.2 Specimen Description

The frames were designed according to ACI 318-63, which is the benchmark design standard used to build concrete test elements to represent structural concrete design practice prior to the enactment of seismic design provisions. These frames, therefore, possess a number of deficiencies. The frames have strong beams and weak columns, resulting in failure in the columns. The frames have deficient lap splice lengths, preventing the longitudinal reinforcing bars from attaining their full yield strength. The lap splices are often located at the base of the columns in potential plastic hinge regions, which is normally not permitted. This may result in the formation of a premature plastic hinge in this region, prior to the beams forming plastic hinges. There is also a lack of transverse reinforcement in the beam-column joints; this may result in joint shear failures. The columns and beams contain inadequate transverse reinforcement leading to problems with confinement and shear. Without proper shear reinforcement, the frames will not create the necessary plastic hinges to dissipate energy.

The single-storey, single-bay, half-scale frames in this study are built on I-shape foundations. The foundation is 500 mm deep, the width at each end is 1320 mm, the width between the columns is 480 mm, the entire length is 3270 mm, and the length of the wider sections is 480 mm. The columns are square with dimensions of 250 mm by 250 mm. The beams are 250 mm wide and 350 mm deep. The clear length of the columns and beams are 1825 mm. The ends of the beams and columns are extended by 400 mm beyond the frame to provide development length for the longitudinal reinforcement beyond the joints and to distribute the lateral loading to the frame. The details of the frames are shown in Figure 3.1, and the detailing of the beams and columns is shown in Figure 3.2.

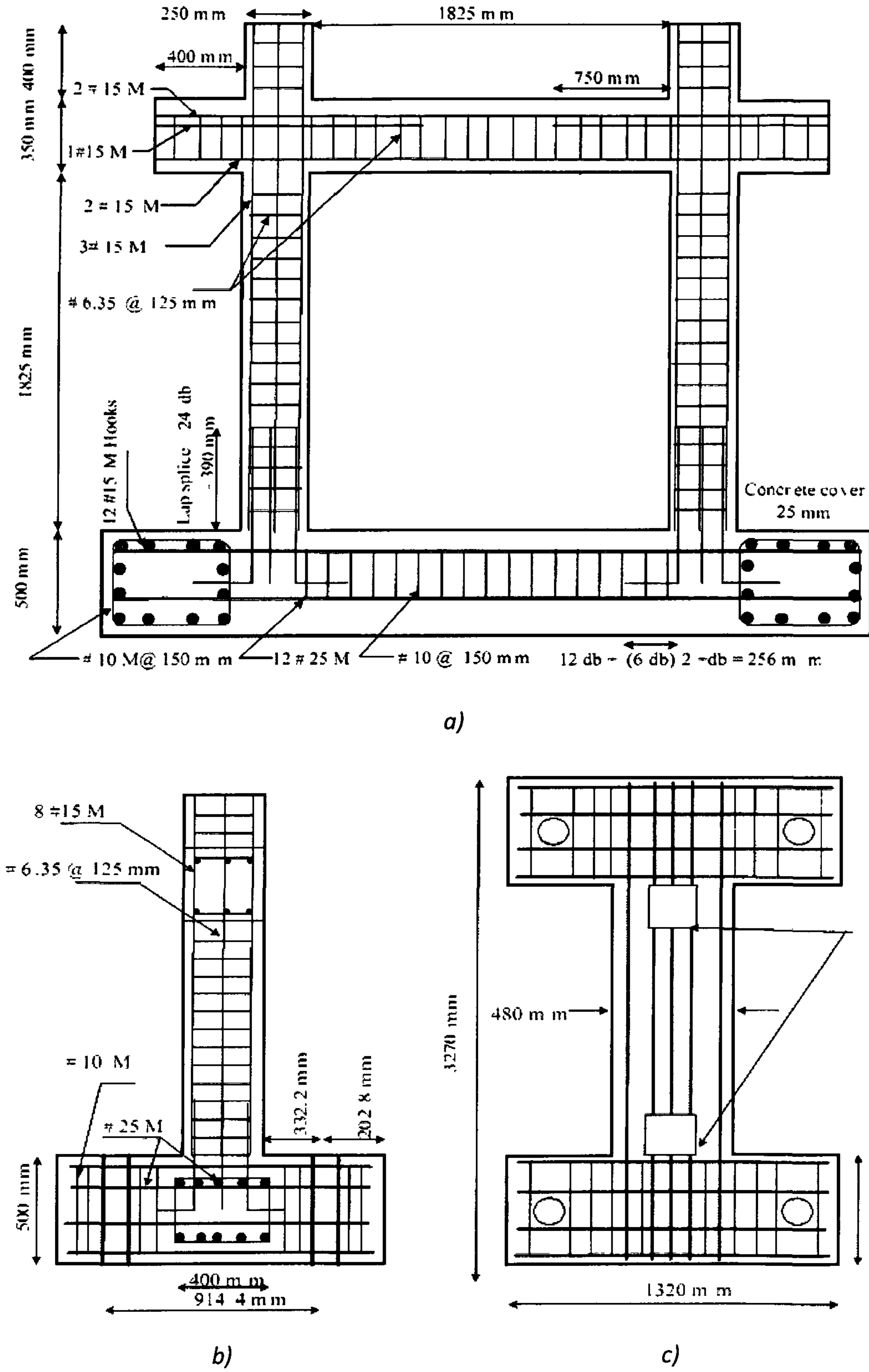

Figure 3.1: Detailing of the reinforced concrete frames: a) Front view; b) Side view; c) Top view (Shalouf, 2005)

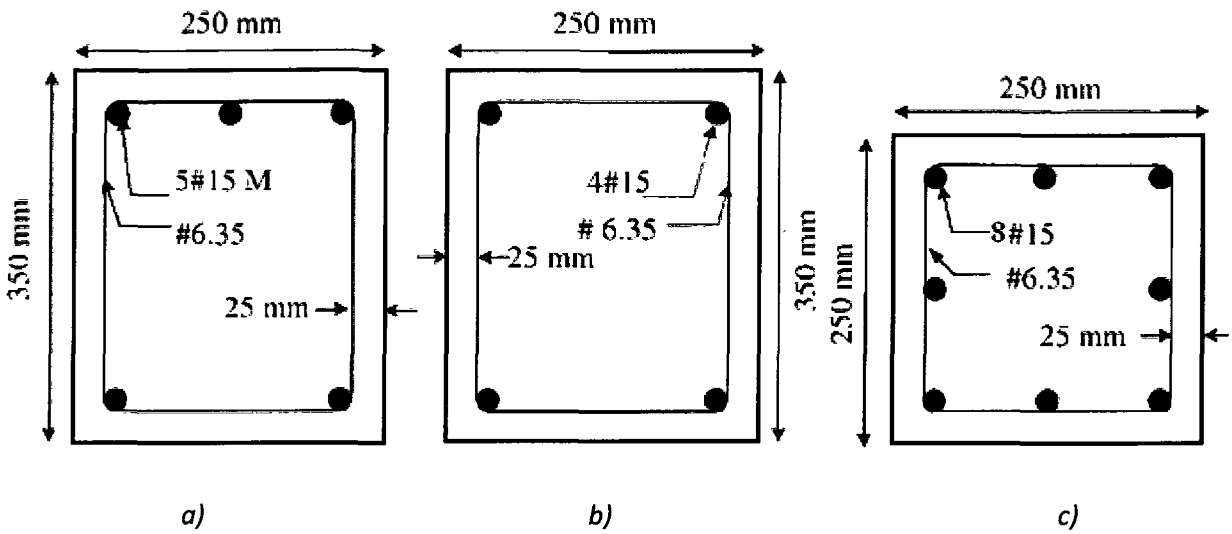

Figure 3.2: Cross sections: a) Beam at supports; b) Mid-span of beam; c) Column (Shalouf, 2005)

The concrete cover of the beams and columns is 25 mm. The transverse reinforcement for both the beams and columns consists of 6.35 mm diameter closed stirrups spaced at 125 mm. There are no stirrups in the joints. At the interior face of the columns, the longitudinal reinforcement in the beams consists of three No. 15 M bars at the top and two No. 15 M bars at the bottom. All four corner bars in the beams are continuous. The middle No. 15 M bar at the top of the beam extends 750 mm from the face of the columns. The columns contain eight No. 15 M bars. The lap splice length at the base of the columns for the longitudinal reinforcement is 390 mm.

3.3 Material Properties

The original frames were built using ready mix concrete with 10 mm maximum aggregate size. The mix design for the concrete used to repair the frames was different since the concrete was batched and mixed in-house; however, it was designed to match the strength of the concrete originally used in the frames. High early strength cement was used in the mix to repair the frames to reduce the curing time prior to testing. Three concrete mix designs are listed in Table 3.1. The mix designs for BR-3 and BL-3 correspond to the original concrete used to construct the frames, while the other mix design was prepared for this experimental program. Table 3.2 lists the average compressive strengths of the repair concrete at 7 and 28 days, and at the time of testing. Typical concrete stress-strain curves used in the three repairs made to the frames are illustrated in Figures 3.3 to 3.5.

Table 3.1:Concrete mix design

	BR-3	BL-3	Repair Concrete
Water-cement ratio	0.47	0.49	0.707
Water (kg)	129	130.9	239
Cement Type	Type 10	Type 10	Type HE
Cement (kg)	274.47	267.1	338
Slag (kg)	61.4	61.1	0
10 mm aggregate (kg)	1961.0	1960.4	1159
Sand (kg)	866	867	793

Table 3.2: Concrete compressive strengths (MPa)

Strength for the:	7 days	28 days	Day of test
Original frame, BR-3	27.9	31.7	33.2
Original frame, BL-3	27.3	31.1	32.1
Column repair, Frame BR-3R	26.5	30.3	34.1
Beam repair, Frame BR-3R	27.1	31.3	31.5
Column repairs, Frame BL-3R	25.8	33.4	42.0

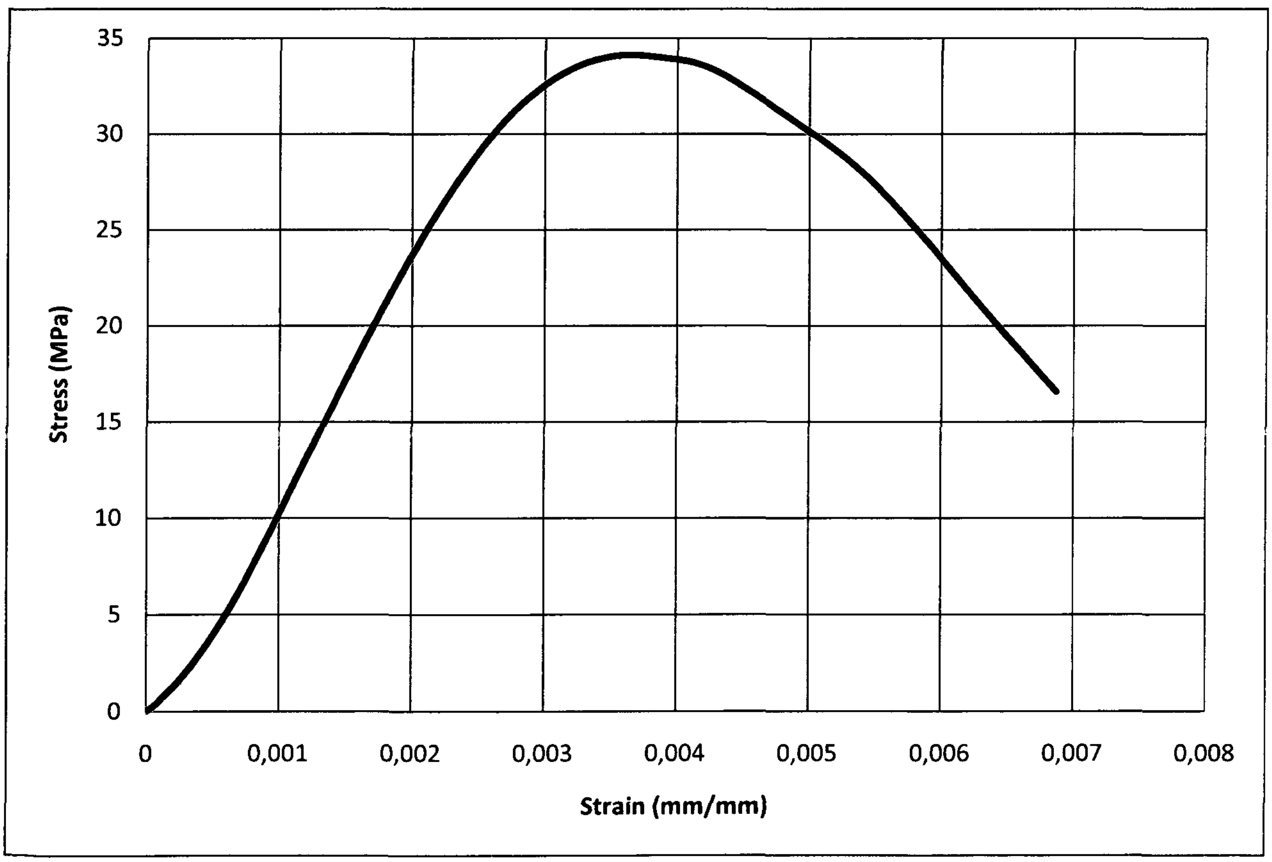

Figure 3.3: Stress-strain curve for concrete used to repair the beam of Frame BR-3R

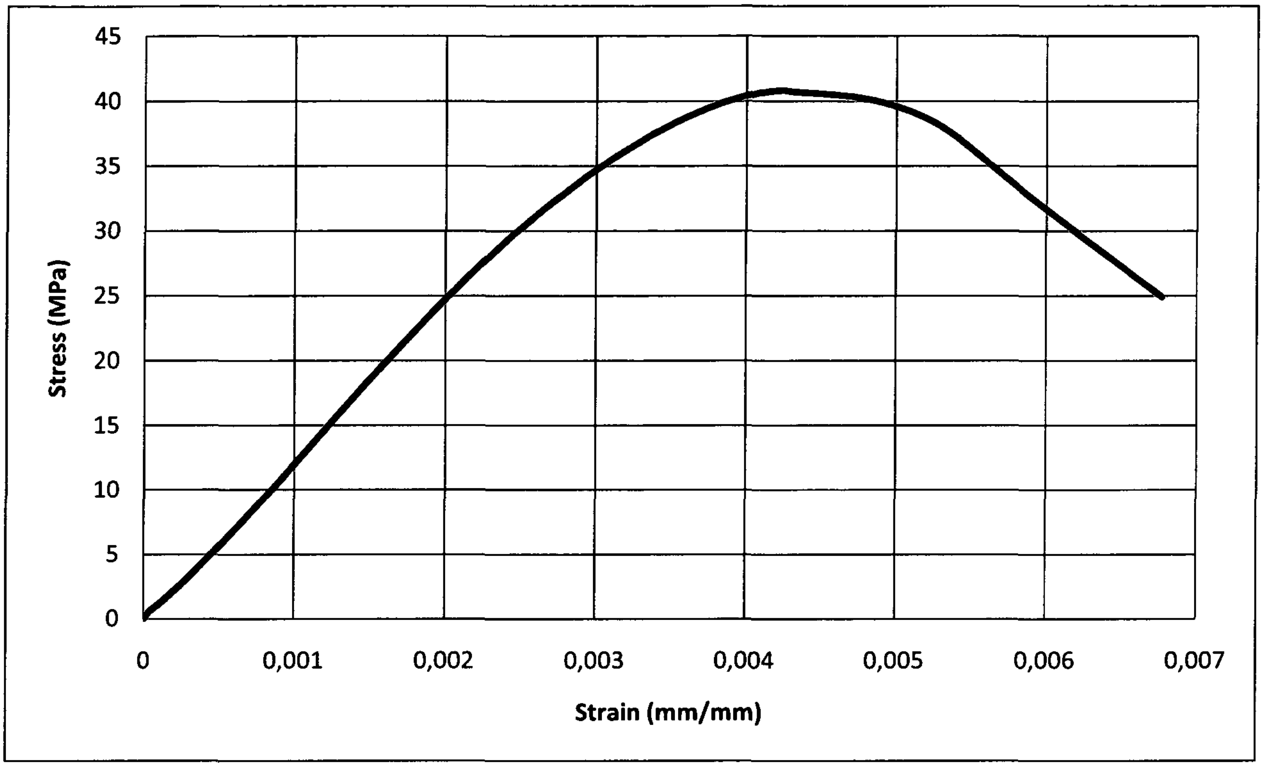

Figure 3.4: Stress-strain curve for concrete used to repair the column of Frame BR-3R

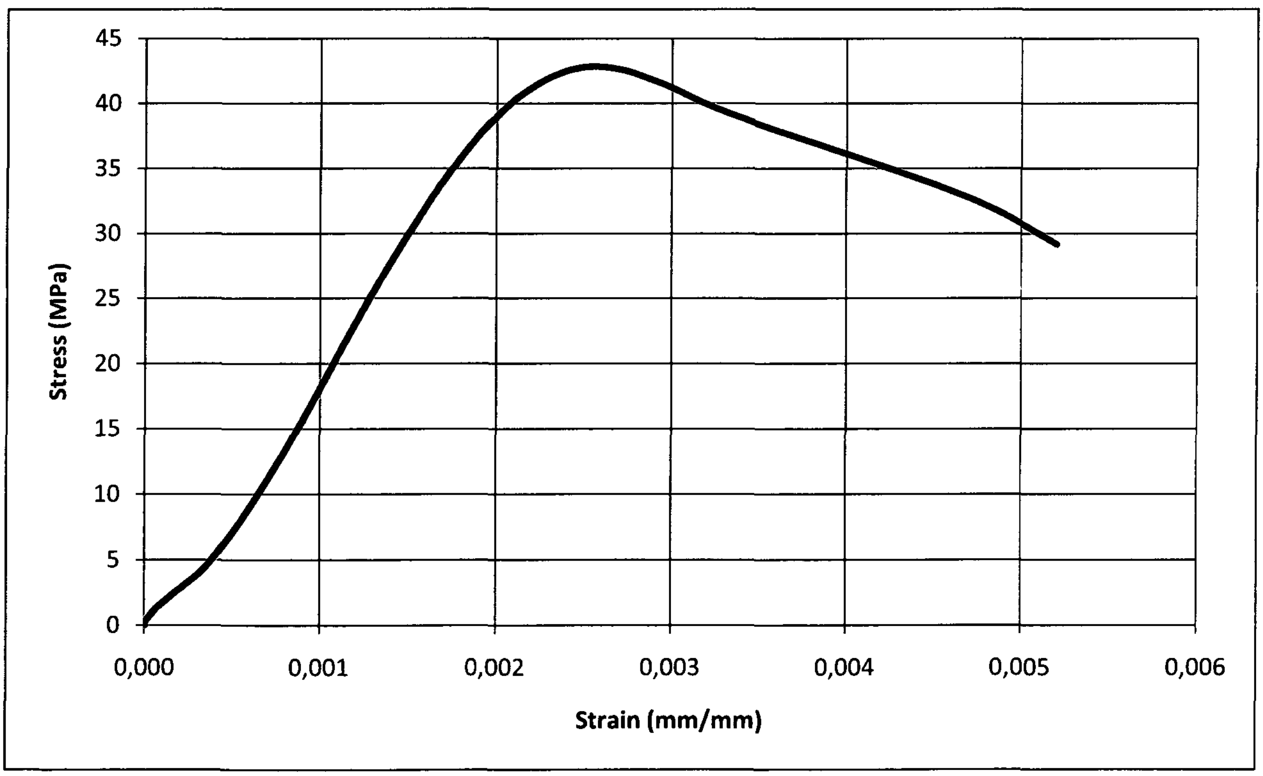

Figure 3.5: Stress-strain curve for concrete used to repair the columns of Frame BL-3R

The reinforcing steel used for the repair of the frames is similar to that reported for the original frames. The reinforcement properties reported by Shalouf (2005) are listed in Table 3.3. Samples of the reinforcement used to repair the frames in this study were tested. Table 3.4 and Figure 3.6 provide the measured steel properties

Table 3.3: Reinforcing steel properties, Shalouf (2005)

Reinforcement	Stirrup (6.35 mm smooth bar)	No. 15 M
Diameter, d_b (mm)	6.35	16
Area, A_s (mm^2)	31.7	200
Yield strength, f_y (MPa)	500	495
Ultimate strength, f_u (MPa)	525	525
Modulus of elasticity, E_s (MPa)	200 000	200 000

Table 3.4: Reinforcing steel properties

Reinforcement	Stirrup (6.35 mm smooth bar)	No. 15 M
Diameter, d_b (mm)	6.35	16
Area, A_s (mm^2)	31.7	200
Yield strength, f_y (MPa)	600	495
Ultimate strength, f_u (MPa)	795	569
Modulus of elasticity, E_s (MPa)	200 000	200 000

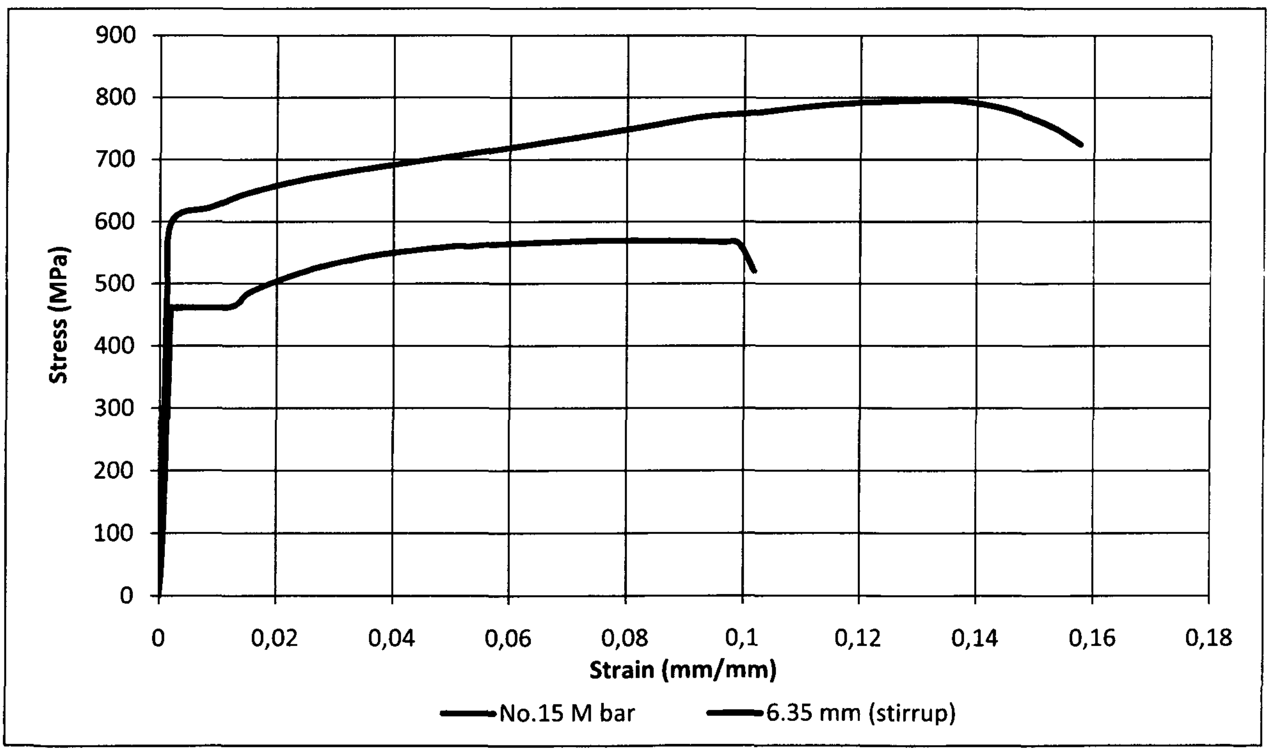

Figure 3.6: Typical steel stress-strain curves for the No. 15 M and 6.35 mm smooth bars

For the retrofitting of Frame BL-3R, hollow structural steel was used. A square section was selected (HSS 102 mm x 102 mm x 9.5 mm). The properties of the section are listed in Table 3.5, and a typical stress-strain curve obtained from a coupon sample is shown in Figure 3.7. The strength of the HSS section was based on an average strength of 445 MPa obtained from three coupon tensile tests. The response demonstrates a rounded response with a strength plateau at a corresponding strain of approximately 0.007(7000 $\mu\varepsilon$).

Table 3.5: Square steel hollow section properties

Properties	Value
Width, b (mm)	102
Thickness, t (mm)	9.5
Area, A_s (mm^2)	3280
Radius of gyration, r (mm)	36.9
Yield strength, f_y (MPa)	445
Ultimate strength, f_u (MPa)	468
Modulus of Elasticity, E_s (MPa)	200 000

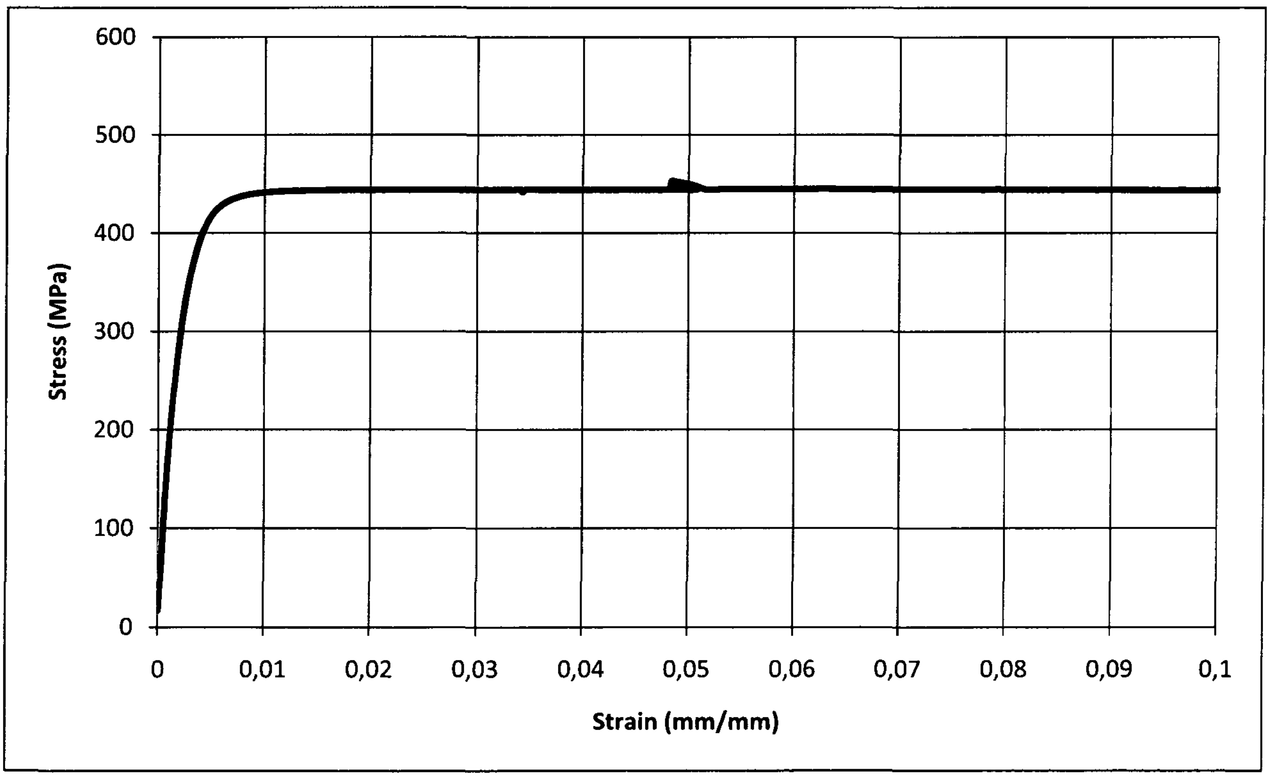

Figure 3.7: Typical steel stress-strain curve for hollow square section HSS 102 mm x 102 mm x 9.5 mm

3.4 Capacity of Repaired Frames

Canadian Standards Association (CSA) Standard A23.3-04 Design of Concrete Structures was used to determine the strength of the repaired frame. Since the frames were designed with the American Concrete Institute (ACI) Standard 318-63, certain prescriptions of A23.3-04 were not satisfied. The code requirements that were not satisfied included transverse reinforcement spacing, reinforcement splice lengths, and transverse reinforcement in the joints. The splices in the column are located at the base, adjacent the foundation, which is not permitted; and the splice lengths are not sufficient.

To determine the sectional strength of the columns and the beams, interaction diagrams were constructed using Program Response-2000 (Bentz, 2001) as shown in Figures 3.8 and 3.9. The shear strength of the columns for the repaired frame is 91 kN and was determined using the General Method of CSA A23.3-04. The shear strength capacity of the beams is 119 kN at the supports and 193 kN at mid-span. Since the frame was expected to remain within the elastic range or demonstrate limited inelasticity, the shear capacity included a concrete contribution. Detailed calculations are available in Appendix A.

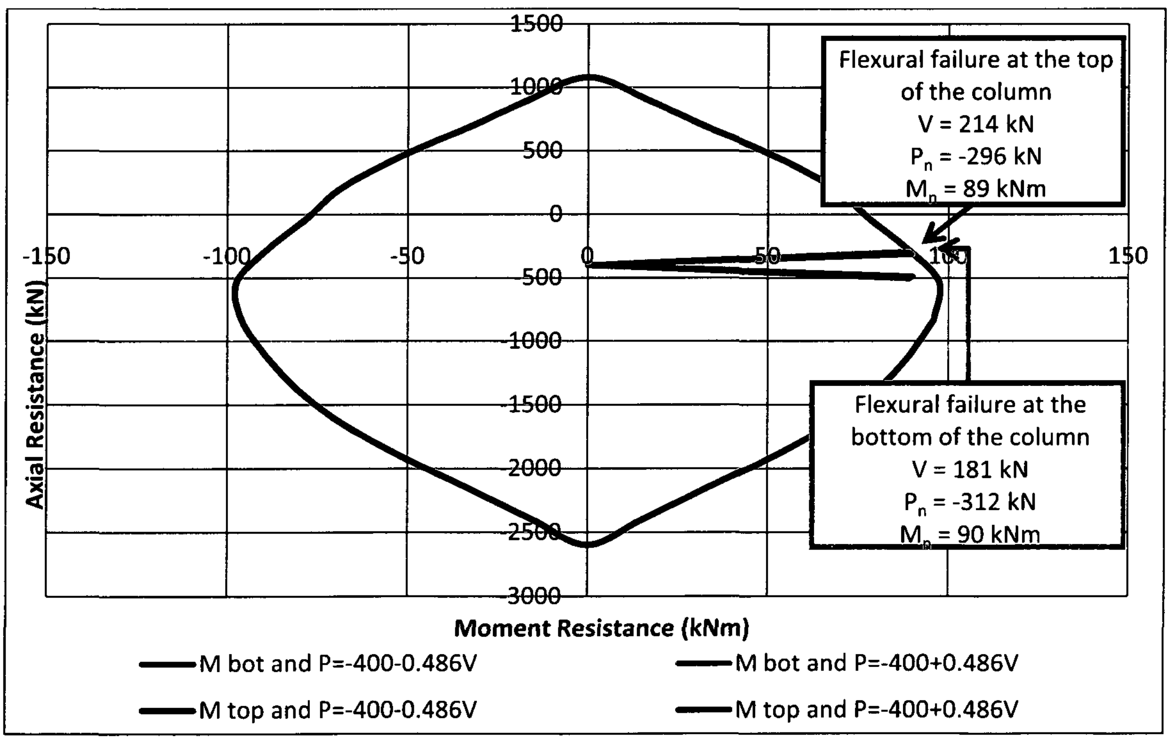

Figure 3.8: Column interaction diagram of the repaired frame

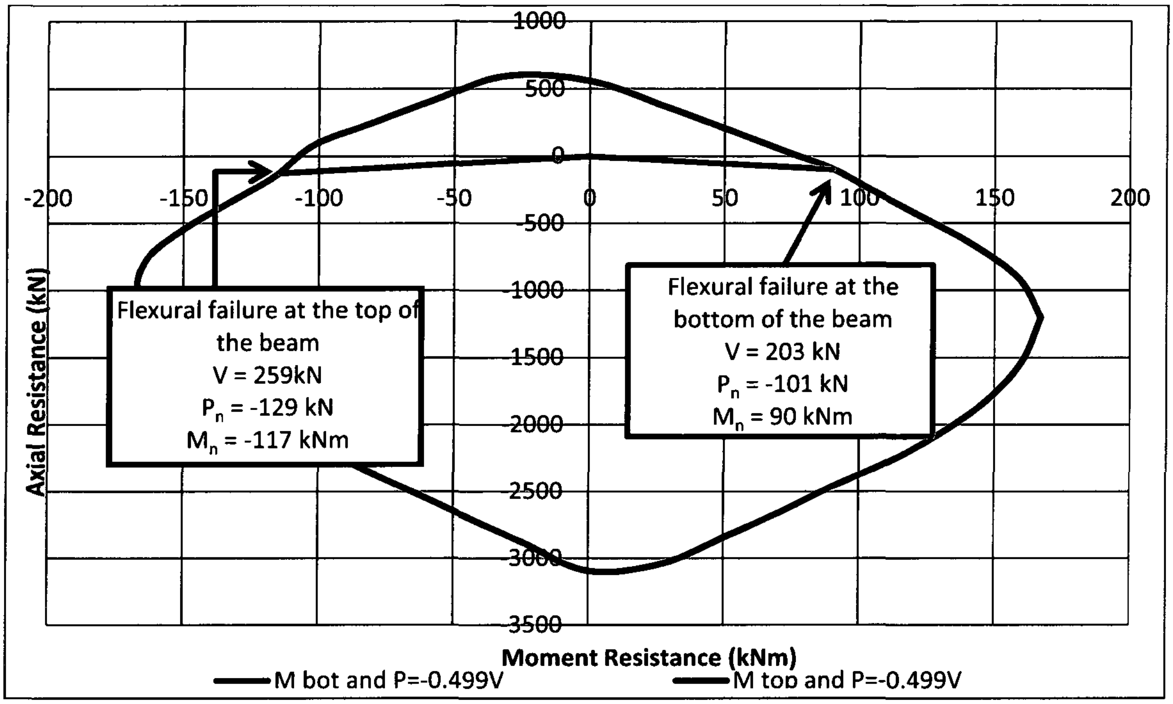

Figure 3.9: Beam interaction diagram of the repaired frame

3.5 Demands of Applied Loads

The elastic demands of the applied loading on the repaired and retrofitted frames were determined using Program SAP 2000, taking into account the cracked properties from Table 21.1 of CSA A23.3-04 Clause 21.2.5. The analysis was conducted in two steps. First, the member forces due to the gravity loads were determined followed by the member forces due to a unit lateral load. This resulted in relationships as functions of the applied lateral load for all members of the frame and was used to determine the mode of failure for the frames. The bracing system was not subjected to the gravity loads since it was installed in the frame after the gravity loads were applied; thus, simulating the installation of a bracing system in an existing building. Figures illustrating the applied loads acting on the frames, and the shear forces, axial forces, and bending moments on the members of the frames can be found in Figures A5, A6, and A7 in Appendix A. From these figures, the following relationships were determined:

Column: Repaired frame:

$$M_{bot} = 0.498V\ (kNm)$$

$$M_{top} = 0.417V\ (kNm)$$

$V = 0.501V\ (kN)$

$P = -400 - 0.486V\ (kN)$

$P = -400 + 0.486V\ (kN)$

Beam at support: Repaired frame:

$M = -0.442V\ (kNm)$

$M = 0.444V\ (kNm)$

$V = 0.486V\ (kN)$

$P = -0.499V\ (kN)$

Beam at mid-span: Repaired frame:

$M = 0\ (kNm)$

$V = 0.486V\ (kN)$

$P = -0.499V\ (kN)$

Column: Retrofitted frame:

$M_{bot} = 0.060V\ (kNm)$

$M_{top} = 0.048V\ (kNm)$

$V = 0.059V\ (kN)$

$P = -400 - 0.056V\ (kN)$

$P = -400 + 0.906V\ (kN)$

Beam at support: Retrofitted frame:

$M = 0.051V\ (kNm)$

$M = -0.051V\ (kNm)$

$V = 0.056V\ (kN)$

$$P = -0.059V\ (kN)$$

Beam at mid-span: Retrofitted frame:

$$M = 0\ (kNm)$$

$$V = 0.056V\ (kN)$$

$$P = -0.059V\ (kN)$$

HSS steel strut:

$$M = 0\ (kNm)$$

$$P = -1.224V\ (kN)$$

$$V = 0\ (kN)$$

From these equations and the capacities of each member, the expected lateral forces causing failure can be estimated. Note that the loading lines shown on the interaction diagrams of Figures 3.8 and 3.9 are based on the bending moments and the axial forces experienced by the member under the applied lateral and gravity loads. The failure load is based on the point where the loading line reaches the interaction diagram indicating the maximum capacity of the member.

The order of failure of each member for the repaired frame is listed in Table 3.6. Note that the calculated flexural capacities do not consider the lap splice or development lengths of the reinforcement. It was assumed that the reinforcement can sustain its full yield capacity, and that failure would occur in the members and not the joints.

Table 3.6: Order of failure in the repaired frame

Lateral force, V (kN)	Mode of failure
181	Flexural failure at the bottom of the column
182	Shear failure in the column
203	Flexural failure in beam at support – positive bending
214	Flexural failure at the top of the column
244	Shear failure in the beam at support
259	Flexural failure in the beam at support – negative bending
397	Shear failure in the beam at mid-span

From Table 3.6, failure should occur at the bottom of the column in flexure, provided deficiencies in requirements such as minimum shear reinforcement spacing, splice lengths, and joint reinforcement do control the failure mechanism in the frame.

3.6 Design of Steel Retrofitted Frame

Packer and Hendersen (1997) and the Handbook of Steel Construction (2004) were used to design the square steel hollow section used to brace the reinforced concrete frame. The steel brace was designed as a compression strut. Different sizes were considered. An HSS 102 mm x 102 mm x 9.5 mm was selected due to the actuator's loading capacity and to retrofit the frame to have a capacity of approximately 5 times the repaired frame, which would be in line with increases in seismic demands for this type of structure. The buckling capacity of the HSS section, assuming pinned-pinned end connections in the frame, was estimated at 827 kN. According to the elastic loading demands established in Section 3.5, a lateral load of 676 kN would be required to cause buckling of the brace and failure of the frame. Furthermore, according to Table 3.7, this would represent an increase in capacity of approximately 3.7.

The intersecting joint of the X-bracing system, as shown in Figure 3.10, required design considerations to ensure that the buckling capacity of the steel member would be utilized. It was determined that steel plates were necessary between the two intersection diagonal steel members to prevent local buckling of the walls of the HSS sections.

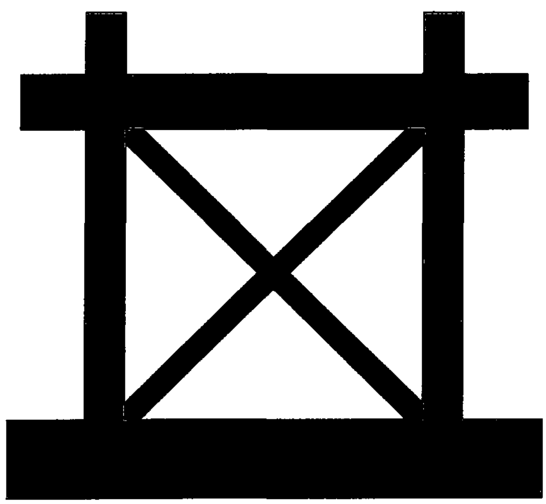

Figure 3.10: Steel bracing system

Figure 3.11 illustrates the intersecting joint of two rectangular steel hollow sections (Packer and Hendersen, 1997). The minimum thickness of the steel plate governed the design to prevent local buckling and, therefore, two-30 mm thick, 102 mm wide, and 204 mm long steel plates were used. Detailed calculations are provided in Appendix A.

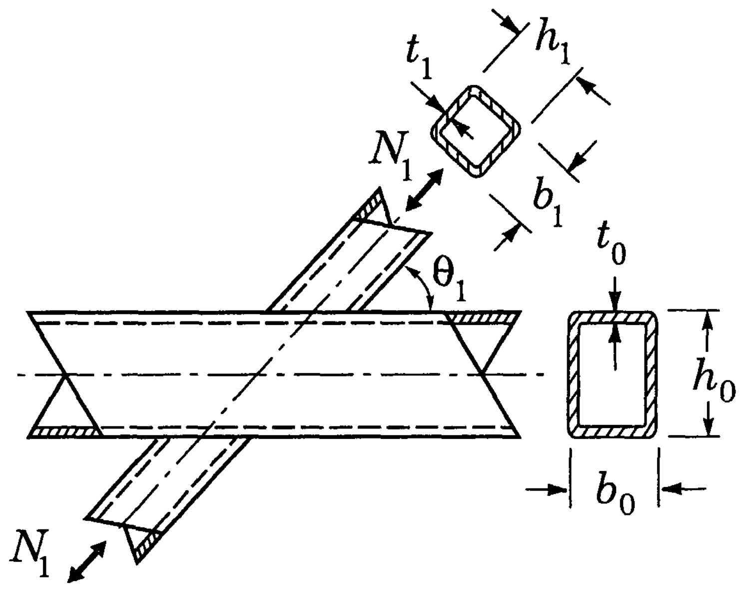

Figure 3.11: Description of the intersecting joint of rectangular steel hollow sections (Packer and Hendersen, 1997)

After the addition of the diagonal steel bracing retrofit, the order of failure was altered for the retrofitted frame as listed in Table 3.7. To determine the sectional strength of the columns and beams, the new loading lines were drawn on the interaction diagrams constructed with Program Response-2000 and are shown in Figures 3.12 and 3.13. The shear strength of the columns for the retrofitted frame was determined to be 66 kN using the General Method of A23.3-04. The bending moment capacity and shear strength of the beam did not change. The shear strength capacity of the beam is 116 kN at the support and 194 kN at mid-span. The frame was expected to remain within the elastic range or demonstrate limited inelasticity; therefore, the shear capacity included a concrete contribution. Detailed calculations are available in Appendix A.

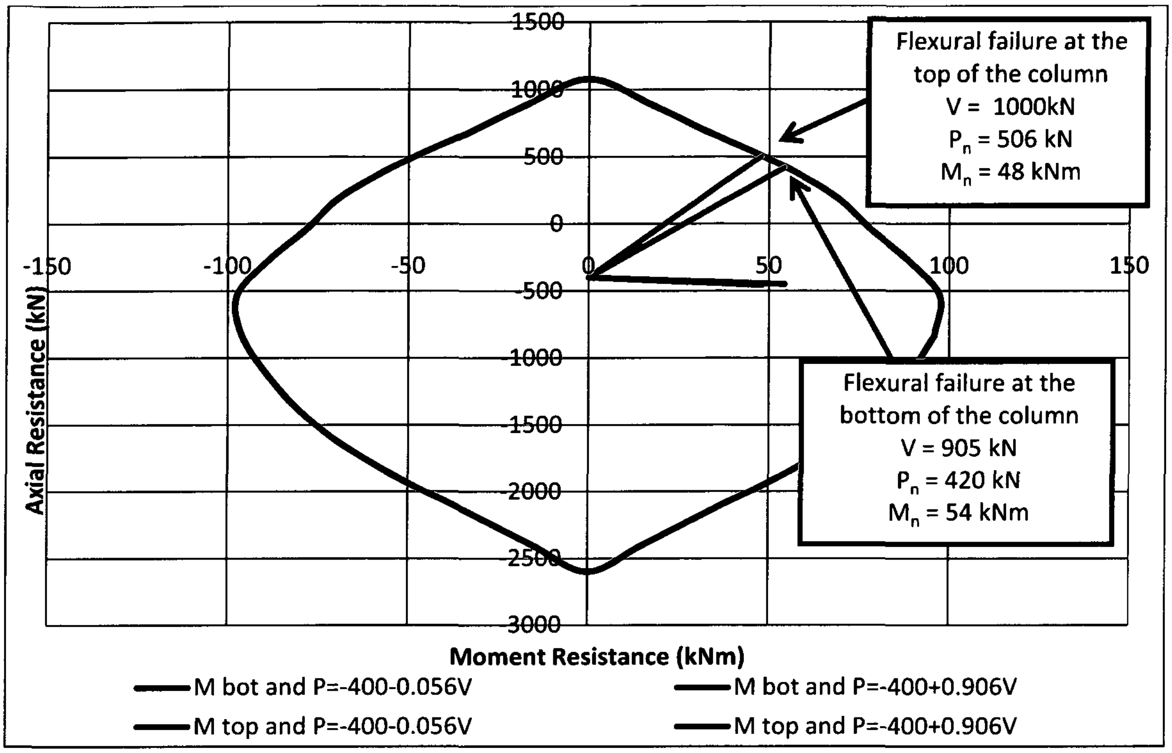

Figure 3.12: Column interaction diagram of the retrofitted frame

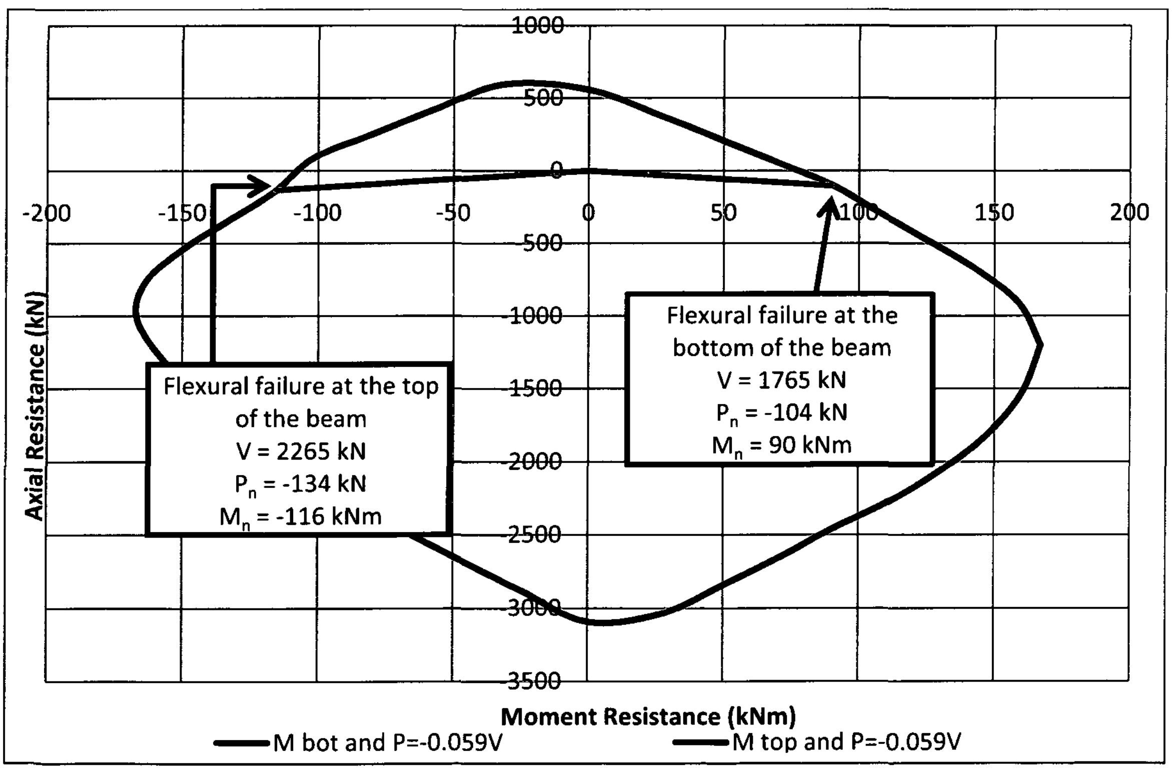

Figure 3.13: Beam interaction diagram of the retrofitted frame

Table 3.7: Order of failure in the retrofitted frame

Lateral force, V (kN)	Mode of failure
676	Buckling of the steel hollow section
905	Flexural failure at the bottom of the column
1000	Flexural failure at the top of the column
1119	Shear failure in the column
1765	Flexural failure in beam at support – positive bending
2071	Shear failure in the beam at support
2265	Flexural failure in beam at support – negative bending
3464	Shear failure in the beam at mid-span

3.7 Repair of Frame BR-3R

Frame BR-3 was received as illustrated in Figure 2.6. Damage was concentrated at mid-height in one of the columns. The longitudinal reinforcement at this section was buckled and the transverse ties had also been removed. In addition, the extension of beam beyond the frame on the same side as the damaged column did not have any concrete or stirrups. The longitudinal bars, however, were not damaged. Prior to repairing the frame, the prestressing cables used to apply the gravity loads and the diagonal tension forces were removed along with the infill brick wall. A vertical steel post was then added to support the beam, while the column was stabilized with four steel hollow sections. The four hollow sections could be tightened in both directions with threaded rods and nuts. After the buckled segments of the longitudinal reinforcement were cut and removed, the beam was aligned in the out-of-plane direction using a pulling system that was connected to another frame. The braces surrounding the column were also slowly tightened in many steps to align the column, while ensuring the beam did not displace out-of-plane. The vertical steel support was then adjusted to level the beam. Figure 3.14 displays the various bracing and support mechanisms.

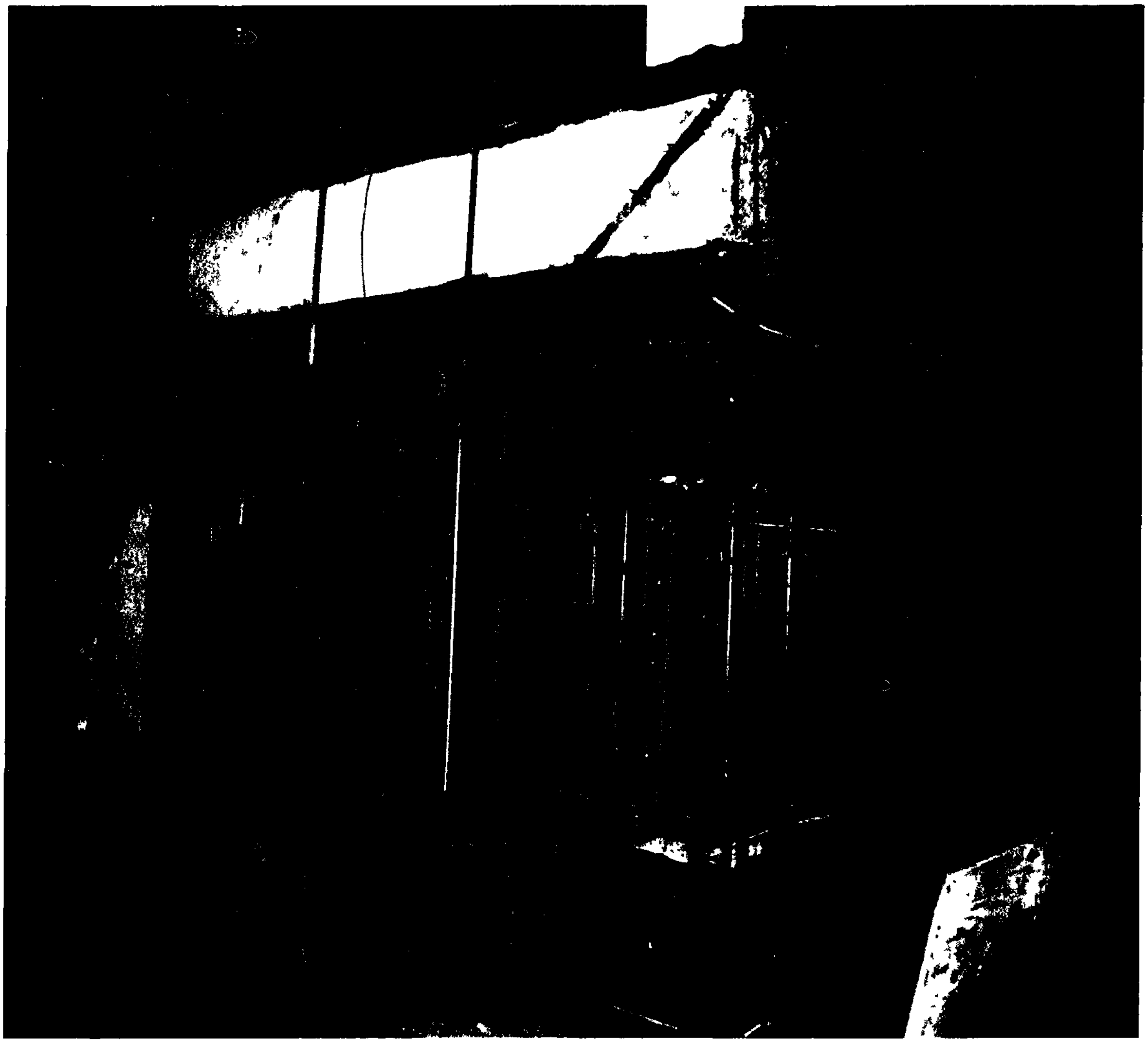

Figure 3.14: Frame BR-3R after being aligned

After aligning the frame, new transverse ties were added in the column. The ties, 6.35 mm in diameter, were inserted through the openings of the cut longitudinal reinforcement and placed at the bottom of the opening. New pieces of longitudinal bars, consisting of No. 15 M (similar to the existing reinforcement), were welded to the remaining reinforcement to replace the portions of the reinforcement that had buckled. The ties were then spaced at 125 mm and tied to the longitudinal reinforcement as shown in Figure 3.15.

Figure 3.15: Newly installed longitudinal reinforcement and transverse ties in Frame BR-3R

New stirrups were added to the extension of the beam that was not intact, along with new bolts to connect the actuator. Formwork was erected for the beam extension and around the bracing system of the column. The concrete was poured for both the beam extension and column at the same time and is illustrated in Figure 3.16.

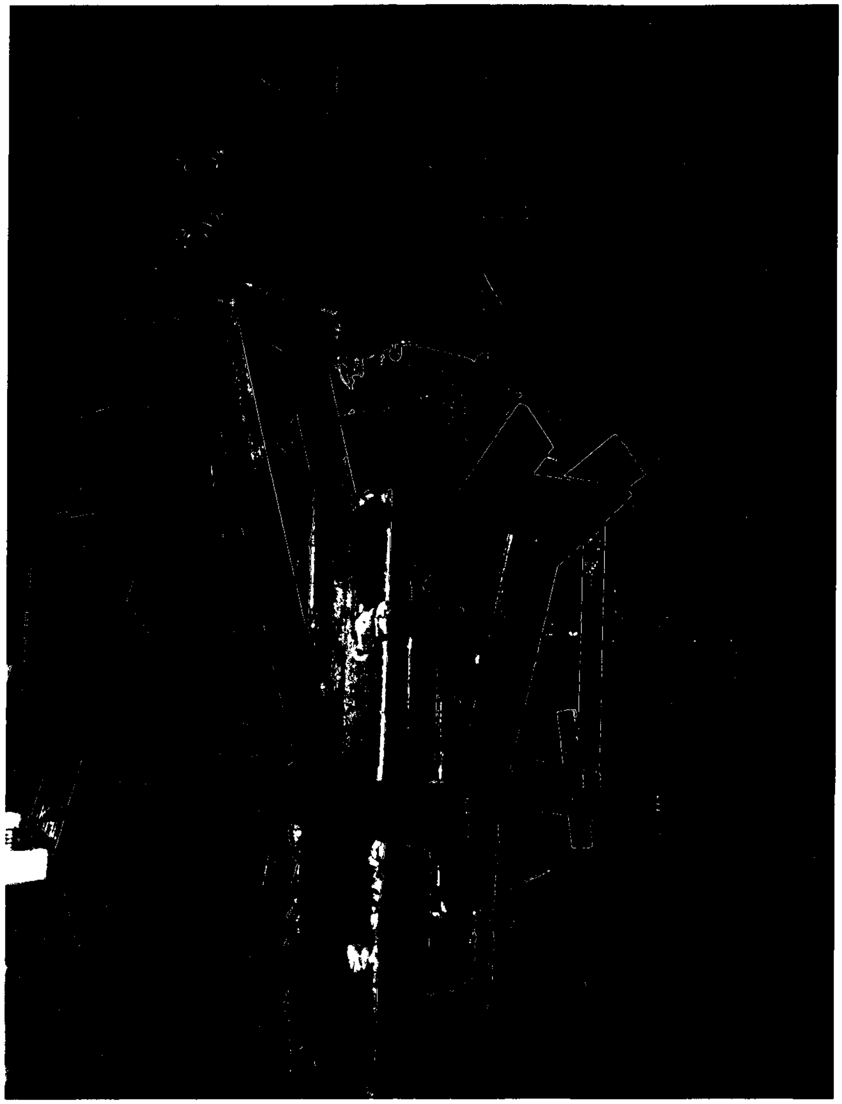

Figure 3.16: Formwork used to repair the column and the beam extension of Frame BR-3R

After the concrete was casted, the FRP situated at the top and bottom of the columns was removed. In addition, during the test setup while the gravity loads were being applied to the beam, significant shear cracking developed. This necessitated full replacement of the concrete and stirrups in the beam. The concrete in the beam was removed and the stirrups were replaced. It was determined that the longitudinal reinforcement was in good condition and did not require replacement. The damage and repair process of the beam is shown in Figures 3.17, 3.18 and 3.19. After the new beam was cast, Frame BR-3R was fully repaired (Figure 3.20).

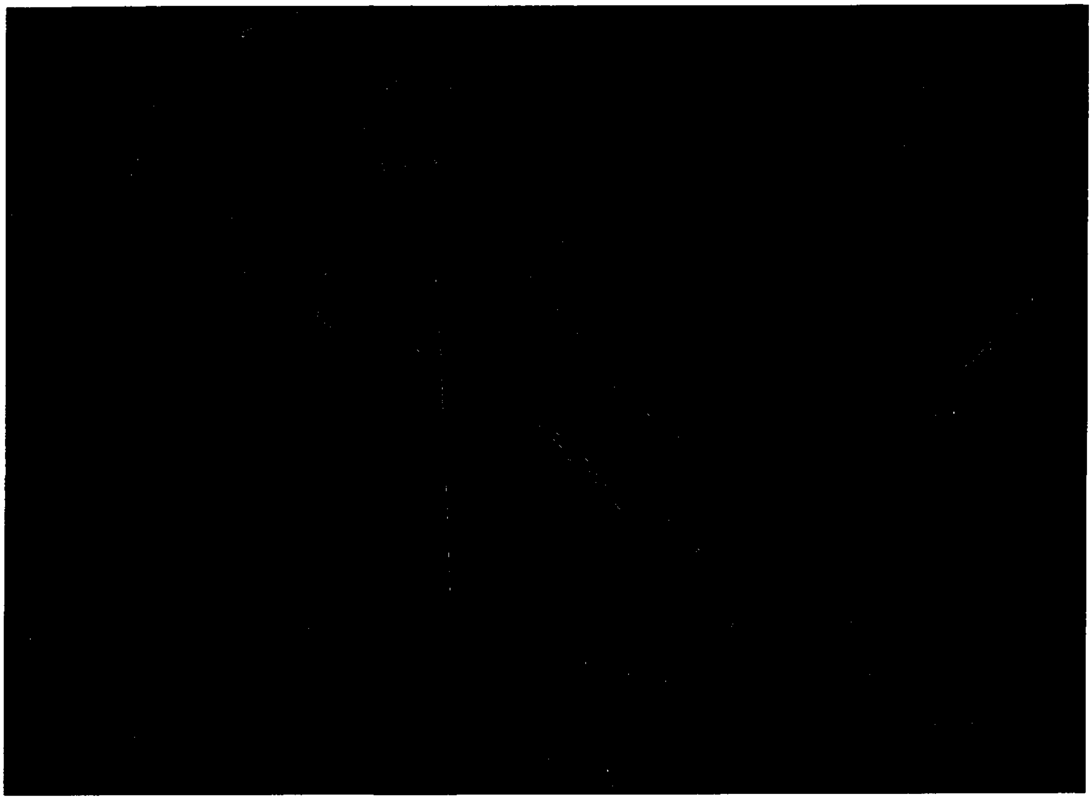

Figure 3.17: Shear cracks in the beam of Frame BR-3R

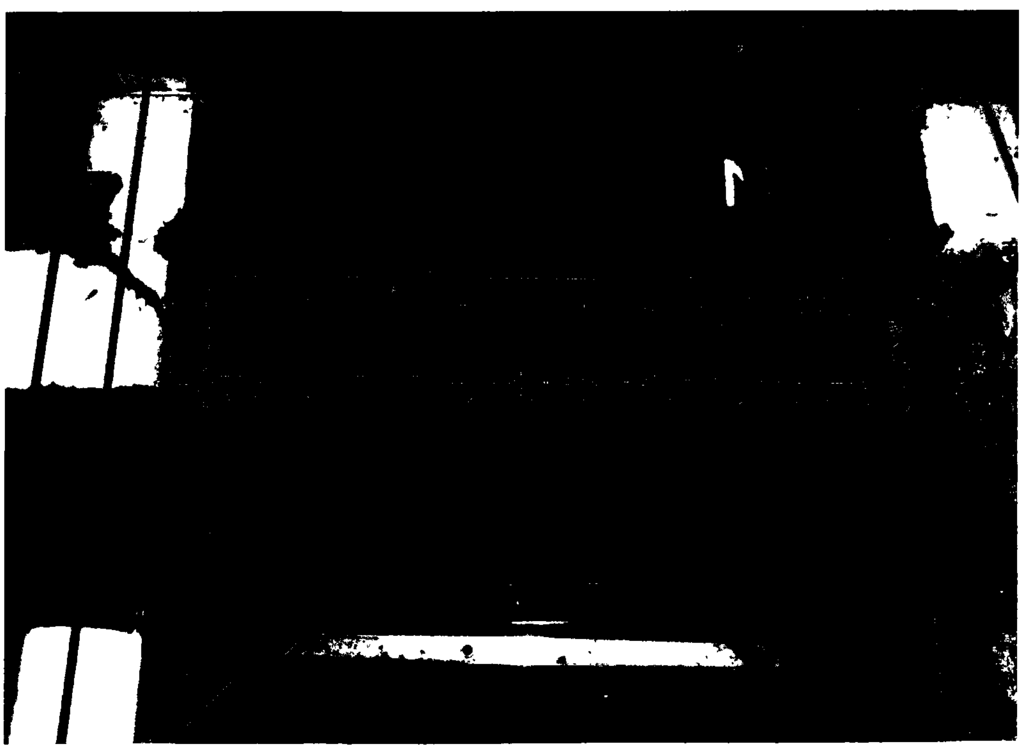

Figure 3.18: Frame BR-3R after the replacement of beam concrete and installation of new stirrups

Figure 3.19: Beam formwork for Frame BR-3R

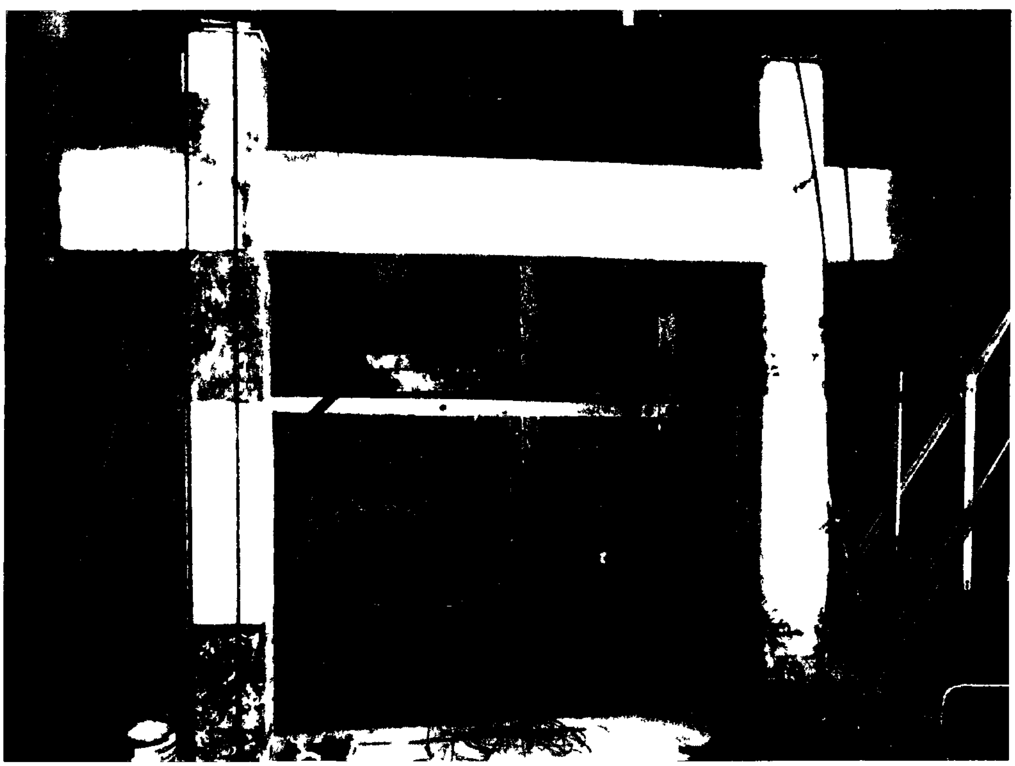

Figure 3.20: Fully repaired frame BR-3R

3.8 Repair and Retrofit of Steel Braced Retrofitted Frame, BL-3R

Frame BL-3 was received as shown in Figure 2.7. First, the FRP and infill concrete block wall were removed. This frame was damaged at the top of the columns. The concrete in those regions was removed. Then, two vertical steel posts to support the beam were added and the columns were stabilized with two sets of four steel hollow sections that could be tightened in both directions with threaded rods. The longitudinal reinforcement in the left column was significantly buckled and therefore removed. The longitudinal reinforcement in the right column was slightly buckled but not removed. The beam was then levelled in-plane using the vertical steel post supports, and out-of-plane in alignment with the columns by slowly tightening the steel braces surrounding the columns. Figure 3.21 illustrates the supports used to align the frame.

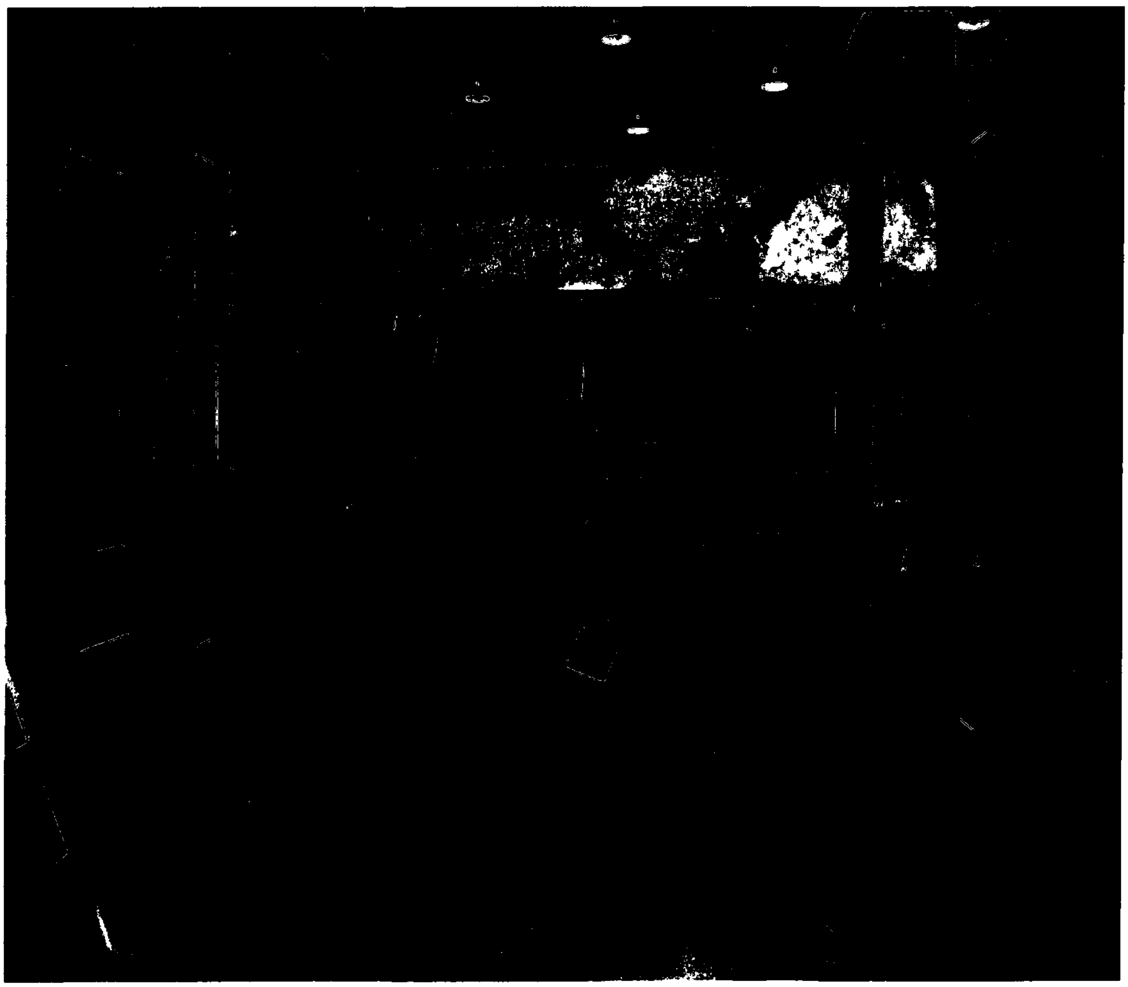

Figure 3.21: Frame BL-3R after being aligned

After aligning the frame, new transverse ties were added in the left column. The ties (6.35 mm diameter) were inserted through the openings of the cut reinforcement and placed at the bottom of the opening. New No. 15 M longitudinal reinforcement pieces were welded to the remaining reinforcement to replace the portions that had buckled in the left column. The ties were then spaced at 125 mm. For the right column, new No. 15 M longitudinal reinforcement pieces were welded directly to the existing reinforcement. The ties in the right column were then replaced and spaced at 125 mm. Given that the longitudinal reinforcement was not removed in this column, the ties could not be inserted in one piece. Therefore, two U-shaped stirrups were inserted around the longitudinal reinforcement and welded together to form closed ties in the right column. The replaced steel for Frame BL-3R can be observed in Figure 3.22. The formwork was then built around the bracing system. Small gaps were observed at the top of the left column after the formwork was removed as shown in Figure 3.23. The small gaps were filled with mortar. The repaired frame, BL-3R, is shown in Figure 3.24.

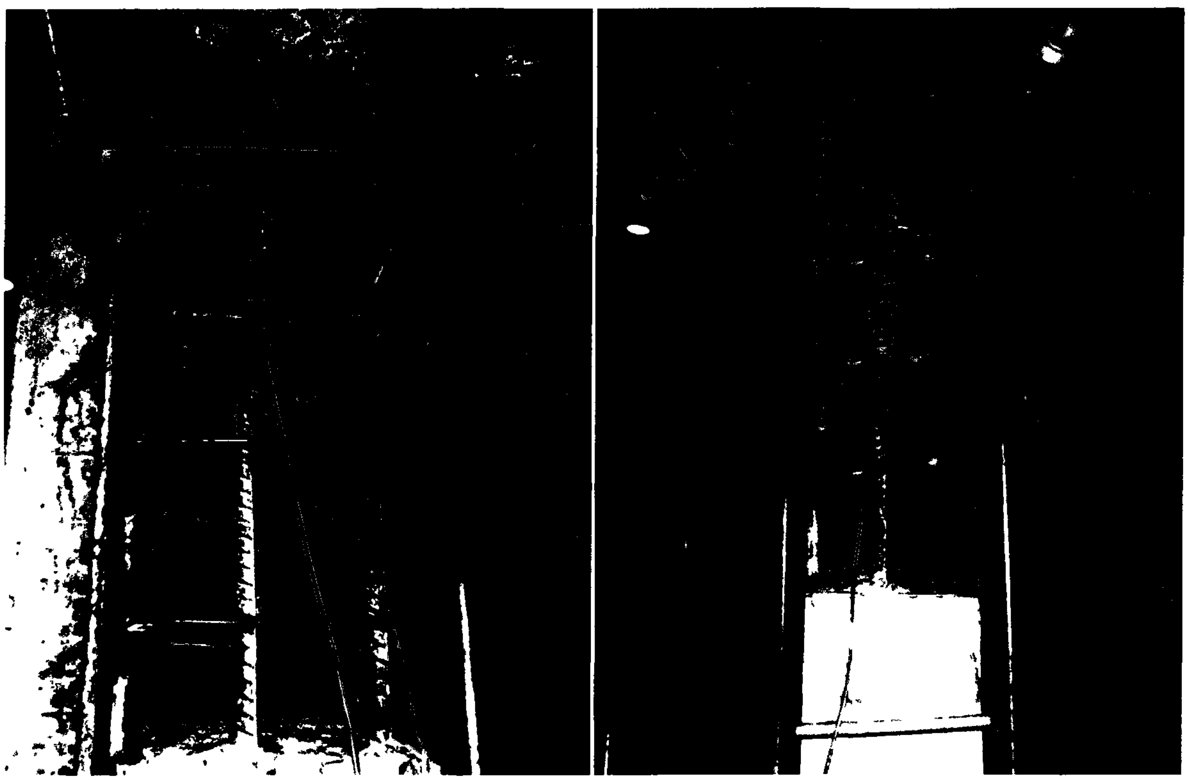

a) b)

Figure 3.22: Newly installed longitudinal reinforcement and ties in Frame BL-3R: a) Left column b) Right column

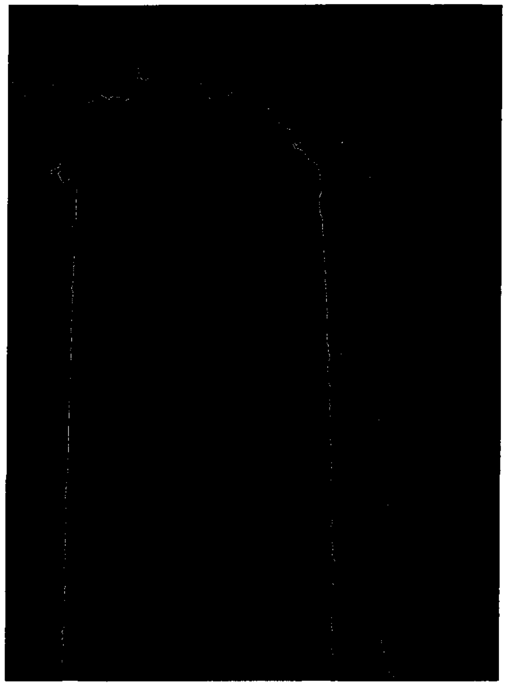

Figure 3.23: Small gaps at top of left column in Frame BL-3R

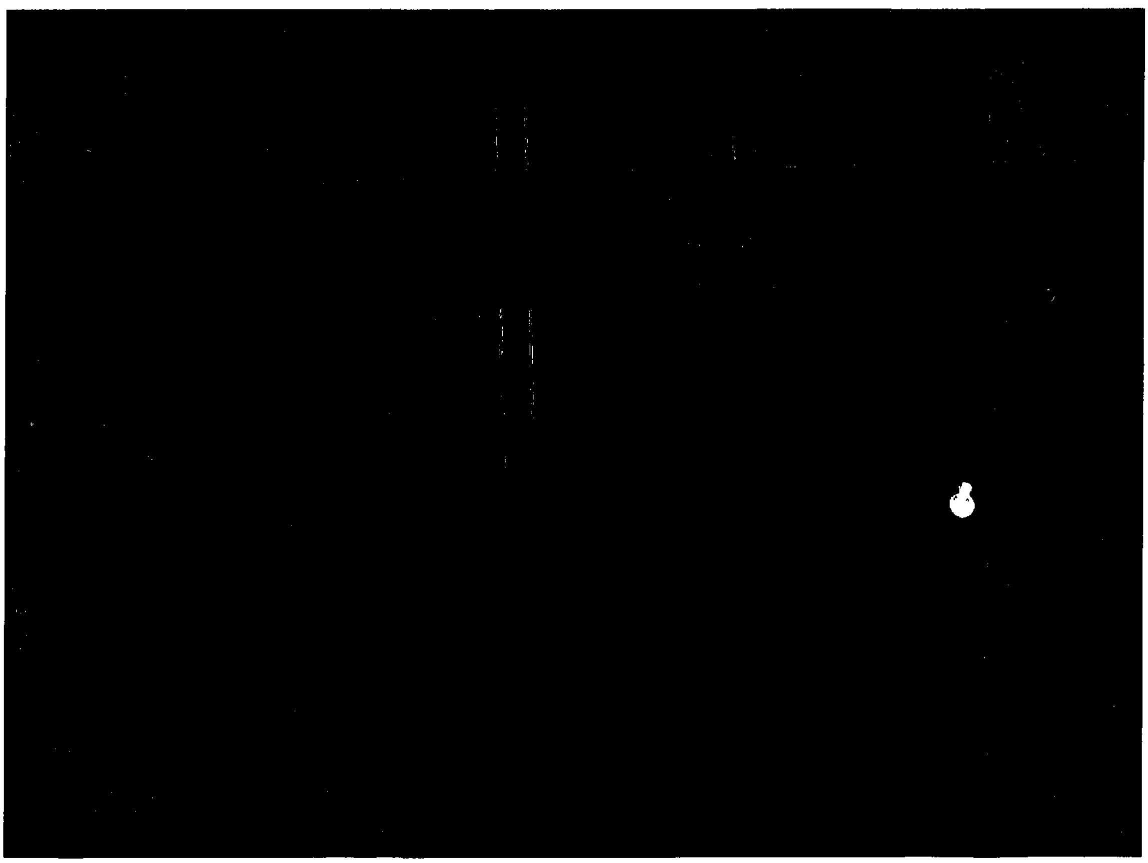

Figure 3.24: Fully repaired frame BL-3R

3.9 Construction of Steel X-Brace Retrofit in BL-3R

As described in the previous sections, the steel bracing system only acts in compression and was installed after the gravity loads were applied on the frame. Steel assemblies were built to ensure that the square hollow section (HSS 102x102x9.5) was aligned with the frame and did not move out-of-plane during the test. The assemblies also served to evenly distribute the compression stresses resisted by the HSS section to the concrete to avoid local crushing. The four assemblies were built (one for each corner) using four-250 mm long 152 mm x 152 mm x 9.5 mm steel angle pieces and eight square steel plates (152 mm x 152 mm x 9.5 mm). The angles were secured to the frame using a single bolt. This process is illustrated in Figure 3.25.

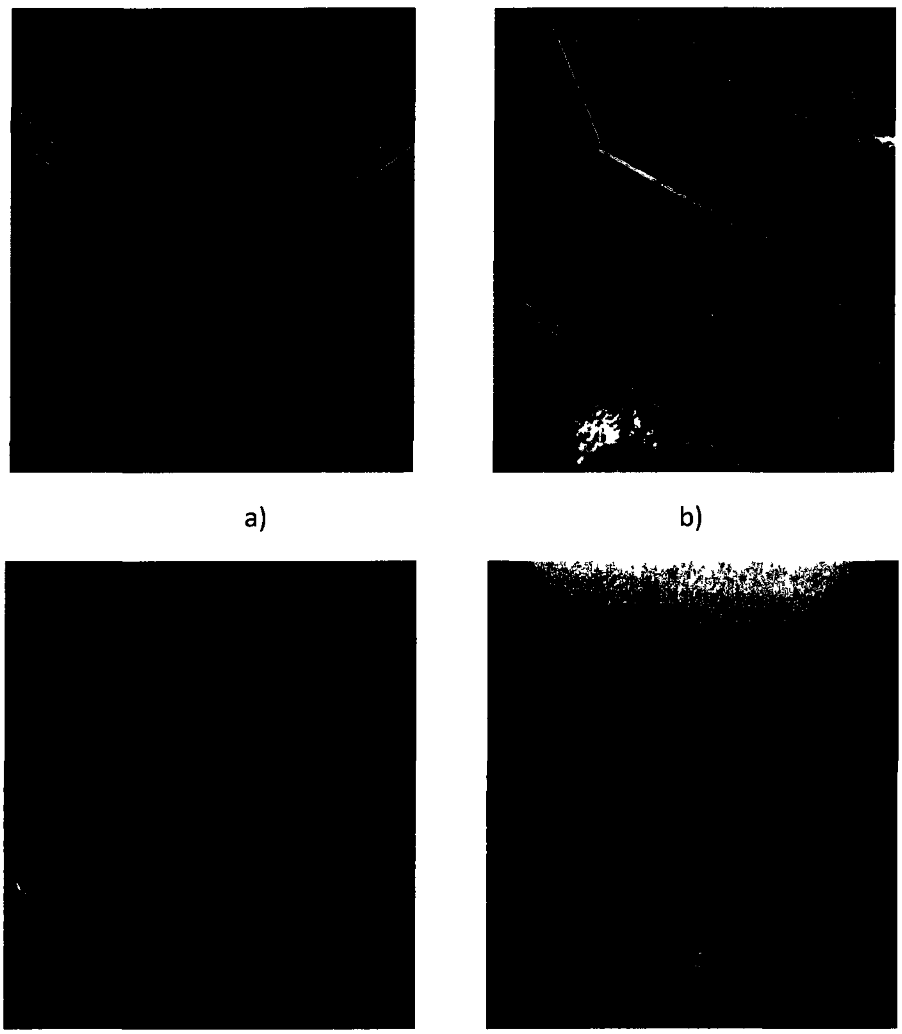

a) b)

c) d)

Figure 3.25: Bolting of angle support pieces for bracing system: a) Empty corner; b) Drilled angle; c) Drilled hole in corner; d) Bolted steel angle

The square hollow steel section was then cut into three pieces to fit snug tight with the frame. The first piece was cut to fit the full diagonal opening (2581 mm). Both ends of the first bracing member were cut into a V shape with 45° angles as shown in Figure 3.26 to bear properly onto the steel angles located at each corner of the frame. The first bracing member was placed in the frame and then four square steel plates were welded to the steel angles to keep the brace member in place. Two of the square steel plates were used at each end; one on each side of the square hollow section (Figure 3.27).

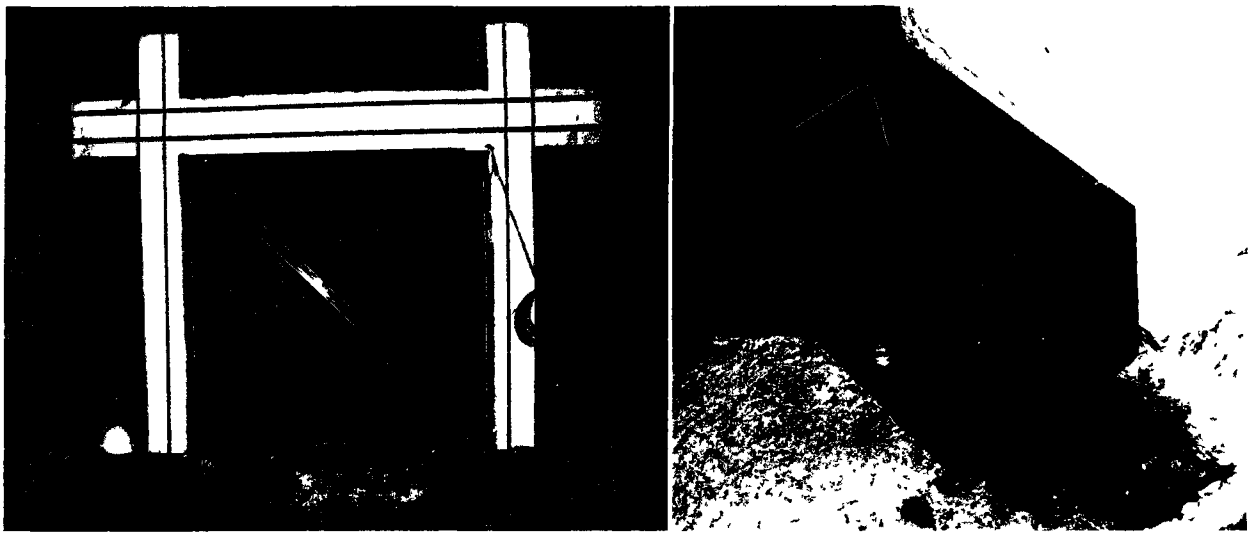

a) *b)*

Figure 3.26: First bracing member: a) First bracing member in place; b) View of 45° cut of the first bracing member

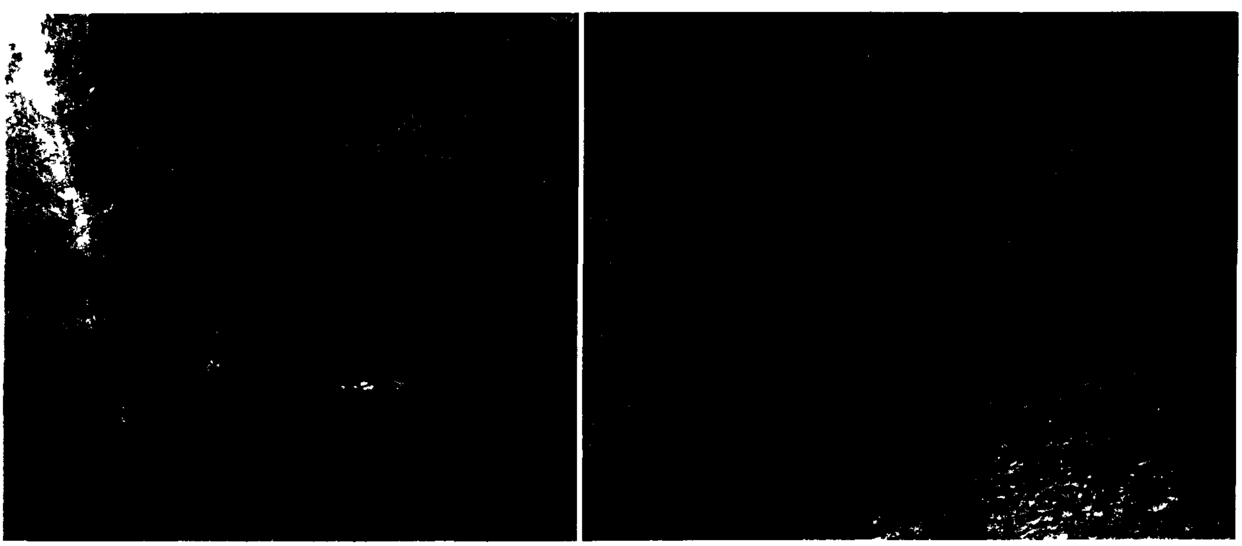

Figure 3.27: Welded square steel plates for the first steel member

The other two bracing members were cut to fit the opposite diagonal length, less the space occupied by the first bracing member (1125 mm). Both bracing members had one end cut flat to bear against the steel bearing plate placed between the intersecting brace members, while the other end was cut into a V shape similar to the first member to bear against the steel angles at the corner of the frame. First, the steel bearing plates were welded at the centre of the first bracing member. Next, the other two bracing members were welded to the steel bearing plates and then secured to the steel angles in the corners of the frame similar to the first bracing member. The complete steel bracing system is illustrated in Figures 3.28 and 3.29.

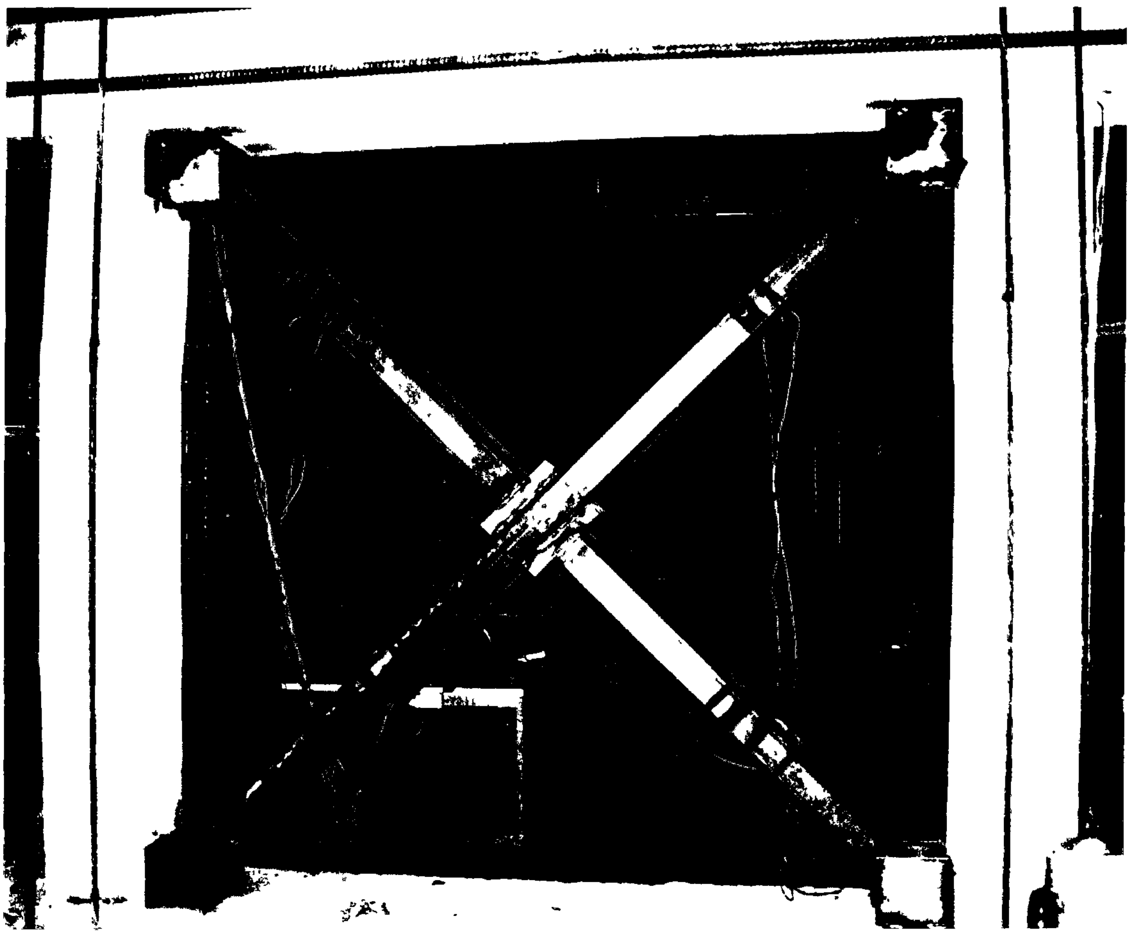

Figure 3.28: Fully installed steel bracing system

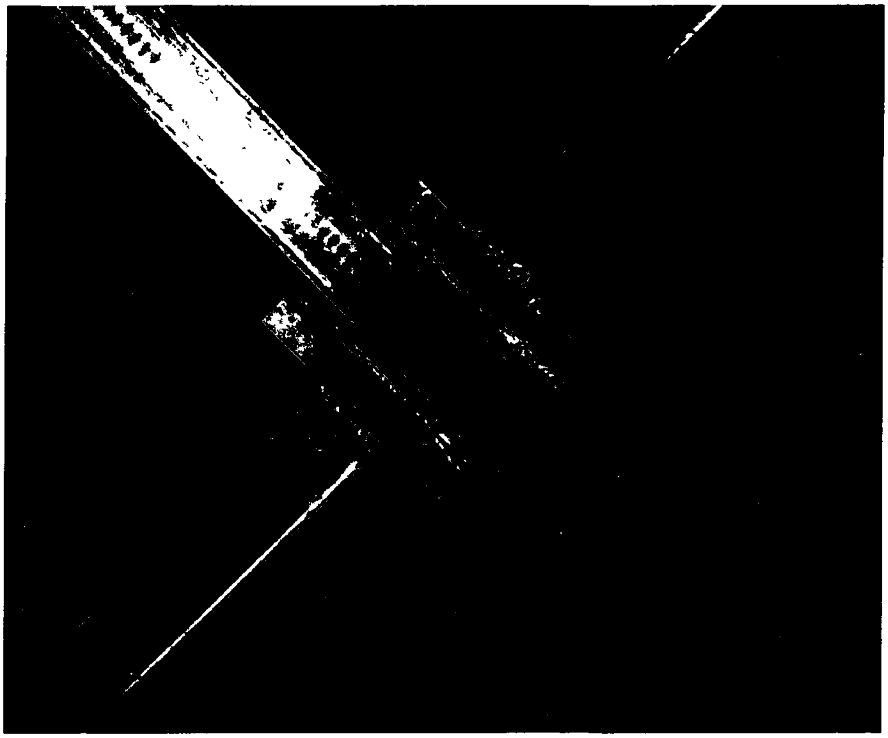

Figure 3.29: Detail of the steel bearing plates

3.10 Instrumentation and Test Setup

The test setup was identical for both tests and is shown in Figure 3.30. The specimens were subjected to reverse cyclic loading using an MTS hydraulic actuator. The capacity of actuator is 1000 kN, with a stroke limit of 500 mm; thus, for a reverse cyclic test, a specimen can pushed and pulled to a maximum of 250 mm in each direction. The actuator's load cell was used to monitor the lateral loading imposed during the tests. The actuator was mounted to a steel reaction frame at the same height of the beam (2375 mm) above the strong floor, and the other end was connected to a stiff loading steel plate attached to the frame as shown in Figure 3.31.

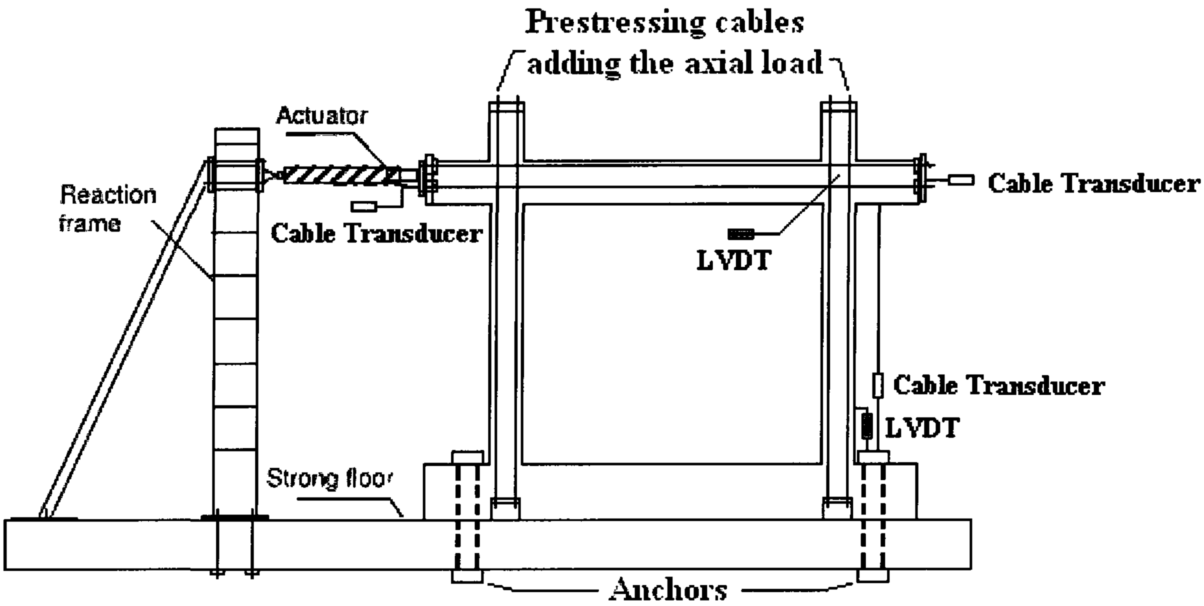

Figure 3.30: Test setup

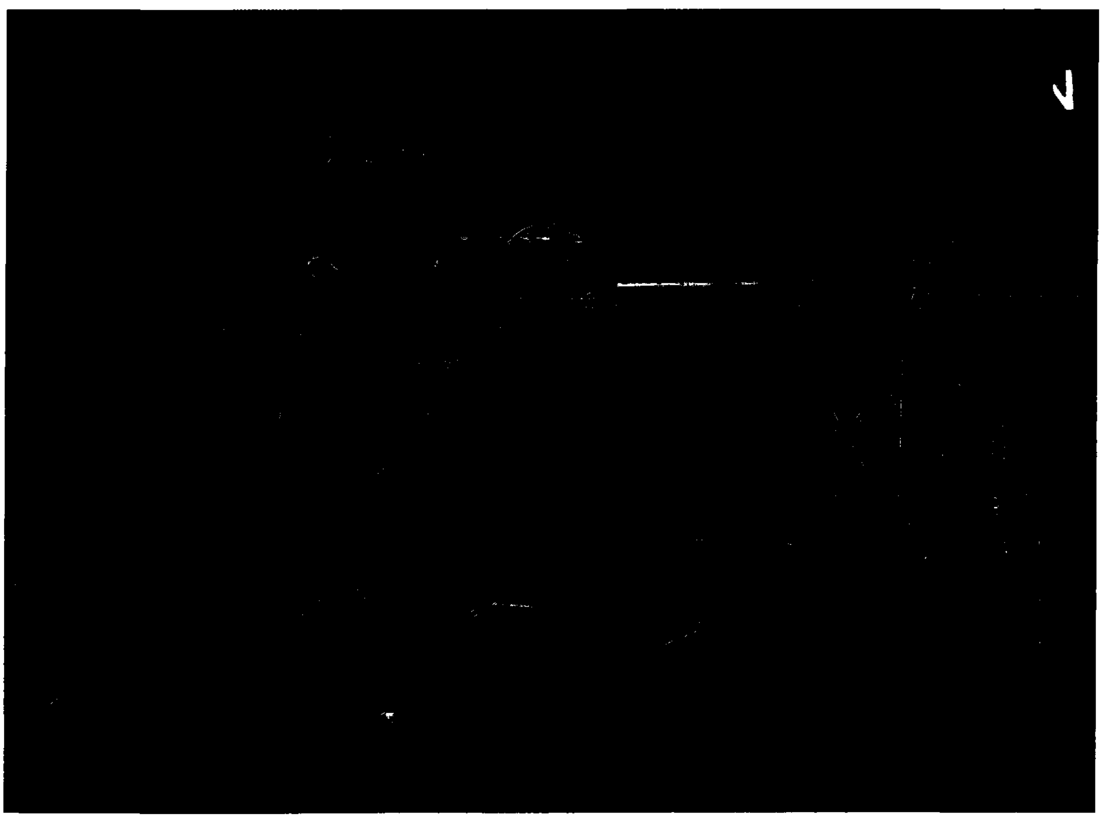

Figure 3.31: Mounted actuator

A stiff steel loading plate was placed at each end of the beam. The two plates were connected together with four-1000 MPa Dywidag prestressing bars; two bars on each side of the beam. The purpose of the prestressing bars was to permit loading in the pulling direction (towards the frame). When the actuator is pulling, the prestressing bars bear against the stiff loading plate at the other end of the frame, resulting in a pushing action on the opposite end of the specimen. Due to the lateral loads applied on the concrete frame and the reaction frame, both the foundation of the concrete frame and the footing of the reaction frame were secured to the strong floor of the laboratory with four high-strength bolts each. Gravity loads were applied to both columns of the concrete frame with four vertical prestressing cables per column to achieve a total load of 400 kN on each column. Two hydraulic jacks were used to post tension the cables to 100 kN each.

Two light steel frames were fixed to the foundation of the concrete frame, one at each end to mount the measuring instrumentation. All measurements recorded were relative to the motion of the foundation, thus eliminating the influence of any base slip or rocking of the foundation of the concrete frame during loading. For the tests, three displacement cable transducers (DCTs) and two linear variable displacement transducers (LVDTs) were used. One of the DCTs was used to measure the lateral displacements of the frame and was placed at the far end of the frame (opposite end to the actuator). It was connected at the mid-height of the beam as shown in Figure 3.32. A second DCT was used as a backup measurement device for the lateral displacements and was connected at the bottom of the beam on the actuator side to avoid any contact with the actuator. This setup is illustrated in Figure 3.33. The third DCT was used to measure the vertical displacement between the top of the base foundation and the bottom of the loading beam. It was connected on the outside of the column and on the opposite end to the actuator as shown in Figure 3.34. In addition, one of the LDVTs was used to measure the base anchorage slip of the column. This LDVT was connected on the outside of the column adjacent to the DCT measuring the vertical displacement (Figure 3.34). The second LVDT, as shown in Figure 3.35, was used to measure the out-of-plane displacements of the top loading beam. It was placed at the mid-height of the joint away from the actuator.

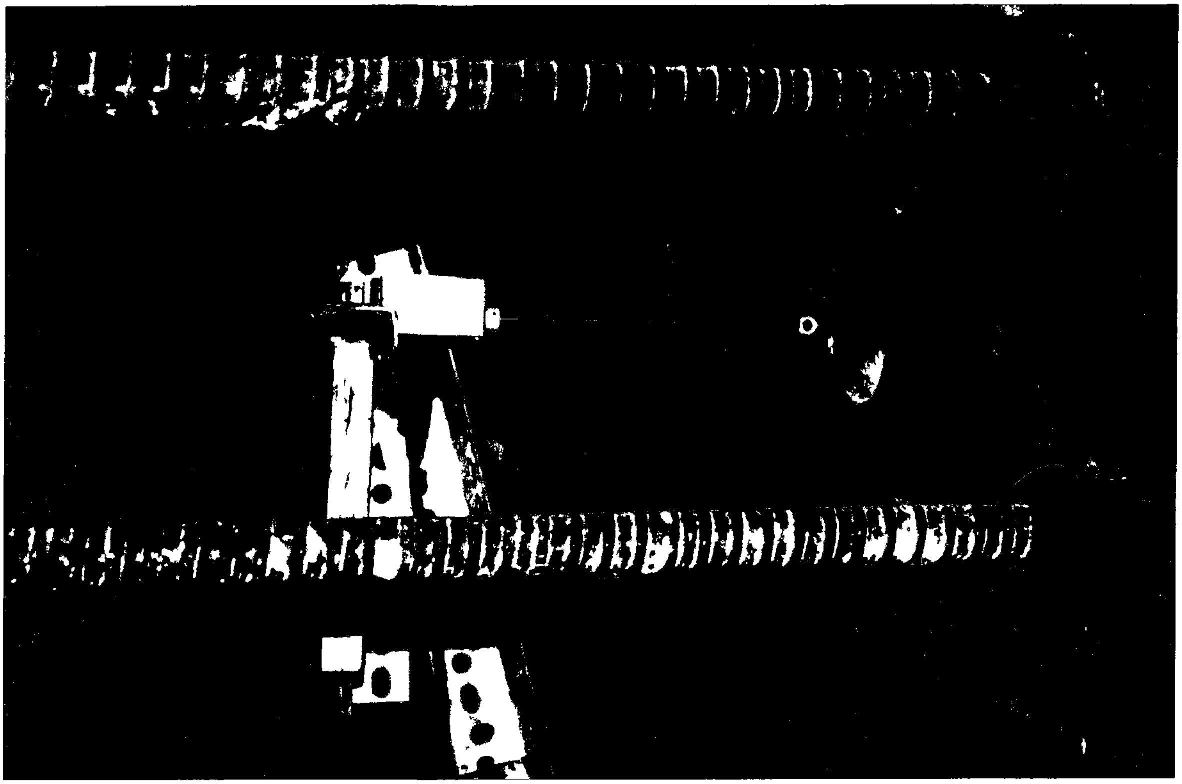

Figure 3.32: Lateral displacement measurements with displacement cable transducer

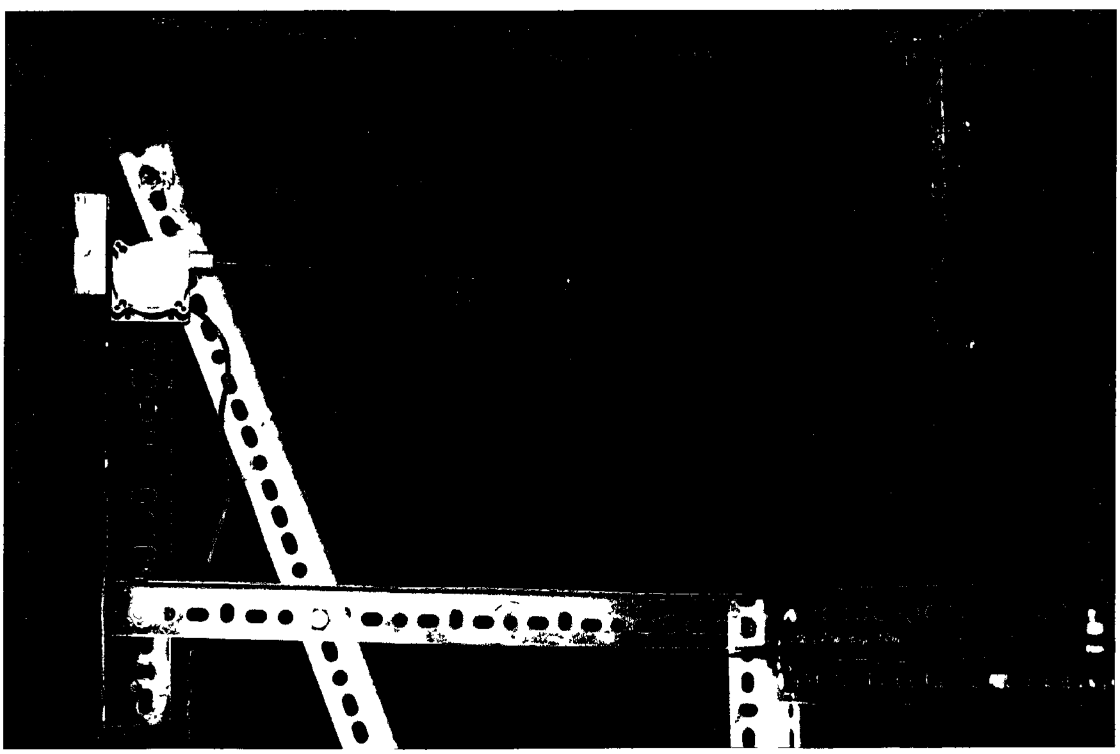

Figure 3.33: Backup lateral displacement measurements with displacement cable transducer

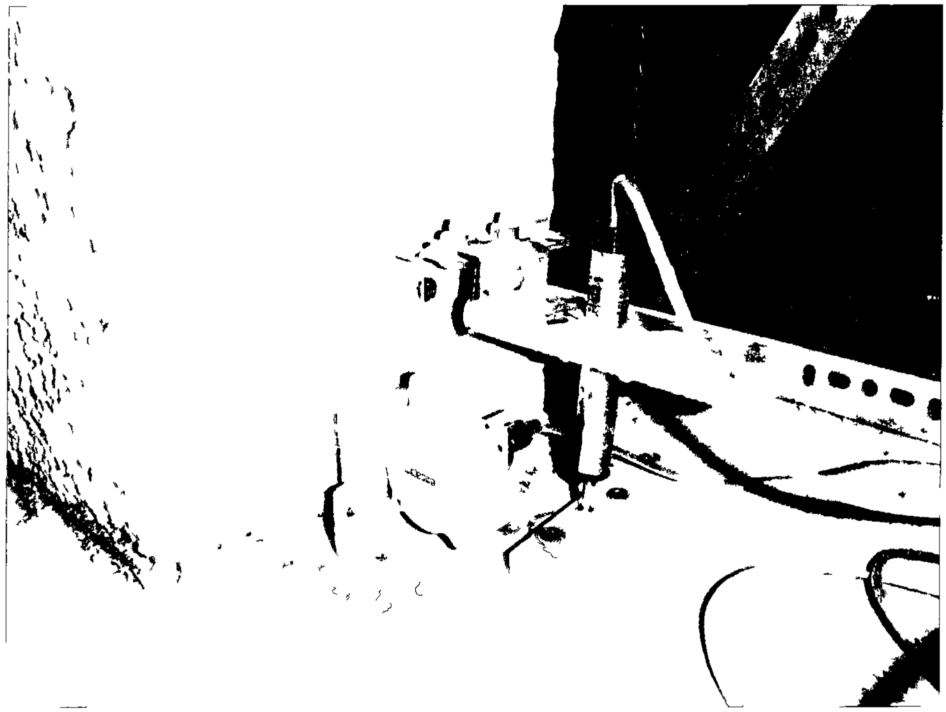

Figure 3.34: Displacement cable transducer and LVDT to measure vertical displacements

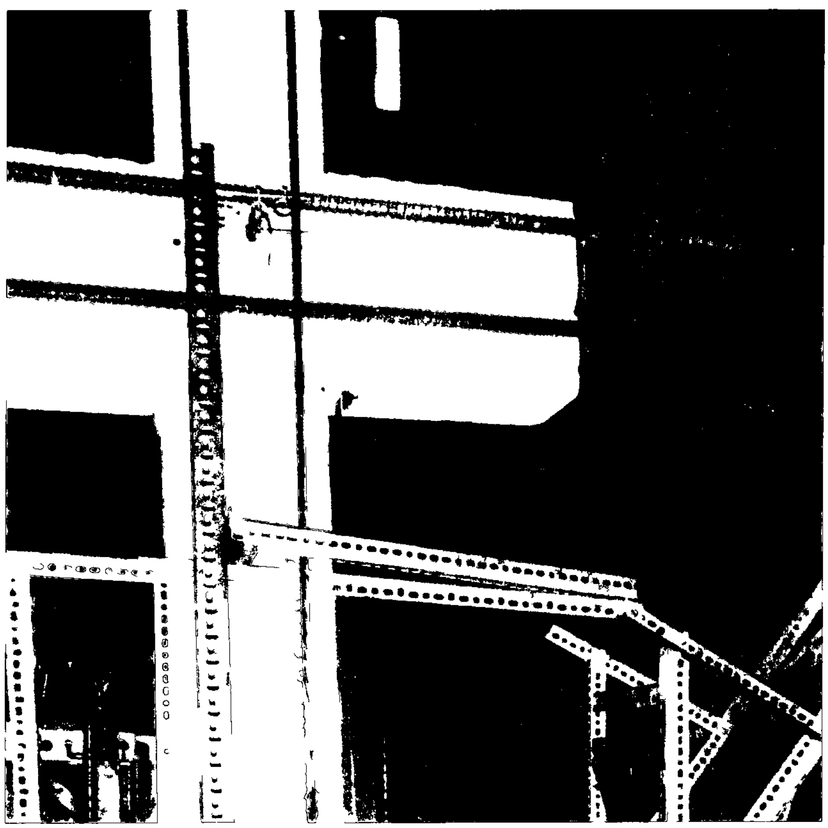

Figure 3.35: LVDT measuring the out-of-plane displacements

For the retrofitted frame, BL-3R, 16 strain gauges were used to record strains in the steel. Half of the strain gauges were used to monitor the strains in the new pieces of longitudinal reinforcement that were added to the columns, while the remaining eight were used to trace the strains experienced by the HSS X-bracing that was added to the frame. Figure 3.36 illustrates the location of each strain gauge along with the notation used to identify each measuring device. In the figure, S.G. refers to strain gauge, LC refers to left column, RC refers to right column, and X refers to HSS X-bracing.

The displacements devices, strain gauges, and load cells were connected to a data acquisition computer system which collected all the data.

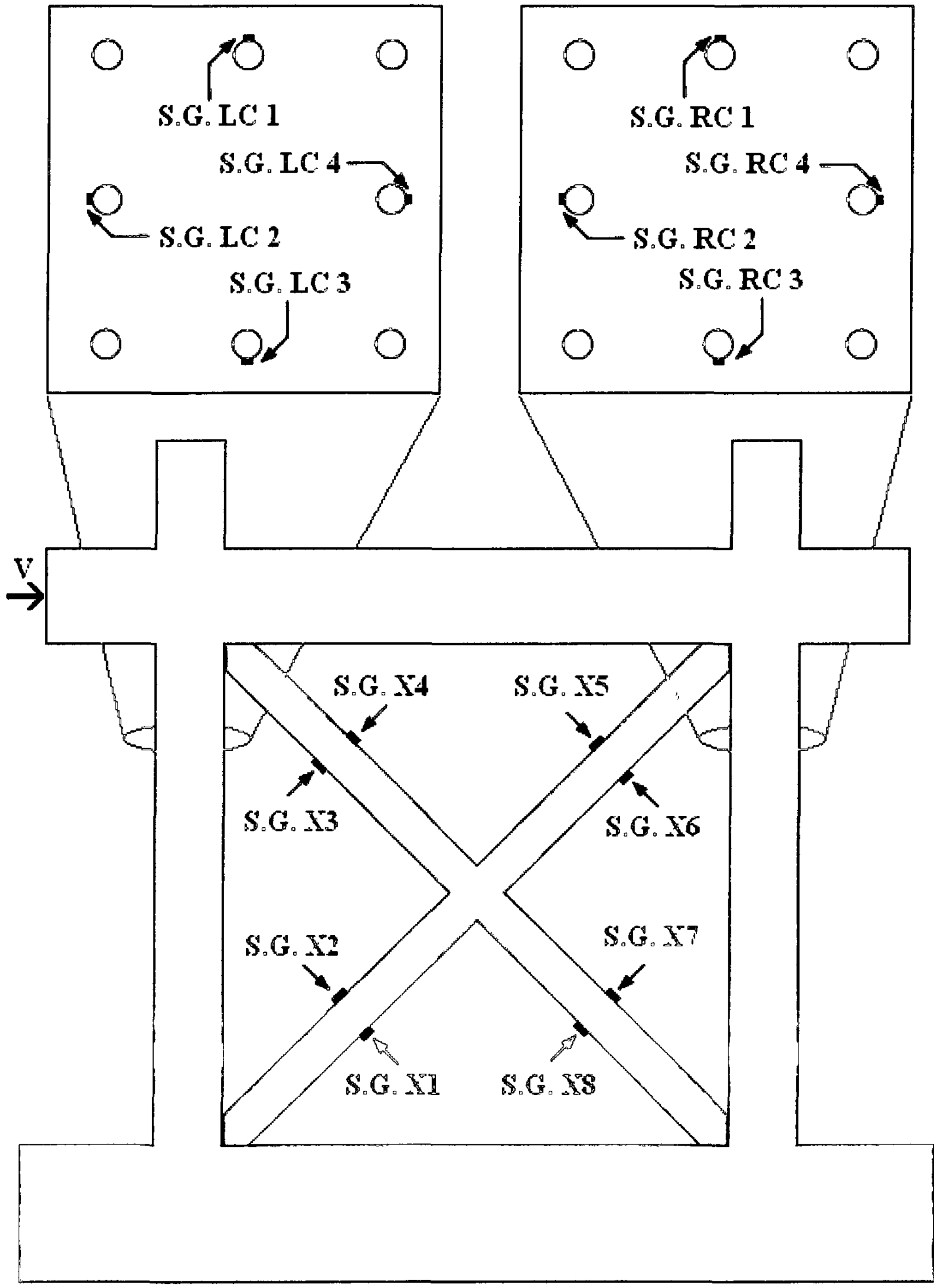

Figure 3.36: Locations of strain gauges on Frame BL-3R

3.11 Loading Program

A different loading program was used for each test. This was necessitated due to the significantly higher stiffness of the retrofitted frame. The repaired frame followed the same loading pattern as reported by Shalouf (2005) and is provided in Table 3.8. The loading program for the retrofitted frame was based on smaller amplitude increases in the lateral loading as listed in Table 3.9. Each loading cycle consisted of three repetitions, and the lateral displacements were based on the displacement recorded by the DCT located at mid-height of the loading beam. In addition to the lateral loading, each column was subjected to 400 kN of axial compression.

The test was terminated when there was a significant reduction in lateral load-carrying capacity or visible damage in the frame.

Table 3.8: Loading protocol for Frame BR-3R

Load cycle	Specimen lateral displacement (mm)	Lateral drift (%)
1	2	0.10
2	4	0.20
3	6	0.30
4	8	0.40
5	10	0.50
6	15	0.75
7	20	1.00
8	25	1.25
9	30	1.50
10	35	1.75
11	40	2.00
12	45	2.25
13	50	2.50
14	55	2.75
15	60	3.00

Table 3.9: Loading protocol for Frame BL-3R

Load cycle	Specimen lateral displacement (mm)	Lateral drift (%)
1	1	0.05
2	2	0.10
3	3	0.15
4	4	0.20
5	5	0.25
6	6	0.30
7	7	0.35
8	8	0.40
9	9	0.45
10	10	0.50
11	11	0.55
12	12	0.60
13	13	0.65
14	14	0.70
15	15	0.75

Chapter 4

4 Experimental Results

4.1 General

Two non-ductile reinforced concrete frames were tested in this research program to determine whether previously damaged frames could be repaired to their original capacity and retrofitted to sustain higher loads. As previously discussed, the frames were initially tested by Shalouf (2005) and were designed according to ACI 318-63, which did not contain specific seismic detailing prescriptions as is currently employed. This chapter includes the results and observations of two tests. A full description of the progression of damage, material failure, and crack patterns are described and accompanied with photos. Cracks existing from the initial tests in the repaired and retrofitted frame were marked in red before testing. This chapter provides plots of the applied lateral loads versus various measurements recorded during testing. The lateral load and lateral displacement along the top loading beam were assigned positive values to indicate pushing of the actuator. Conversely, the lateral load and lateral displacements are negative to indicate that the actuator was in a pulling motion. As a reference, the side connected to the actuator is denoted the left side of the frame.

4.2 Performance of Repaired Frame

Frame BR-3 from Shalouf (2005) was repaired and renamed BR-3R. This frame served as the companion repaired frame in this test program and was not retrofitted. As stated above, the lateral displacement, base anchorage slip of the column, vertical displacement of the column, and the out-of-plane displacement were measured and plotted against the applied lateral load in Figures 4.1 to 4.5. Throughout testing, the primary cable displacement transducer, situated at the end of the frame away from the actuator, was used as the reference lateral displacement reading. Specific readings for each phenomenon are discussed in the following paragraphs.

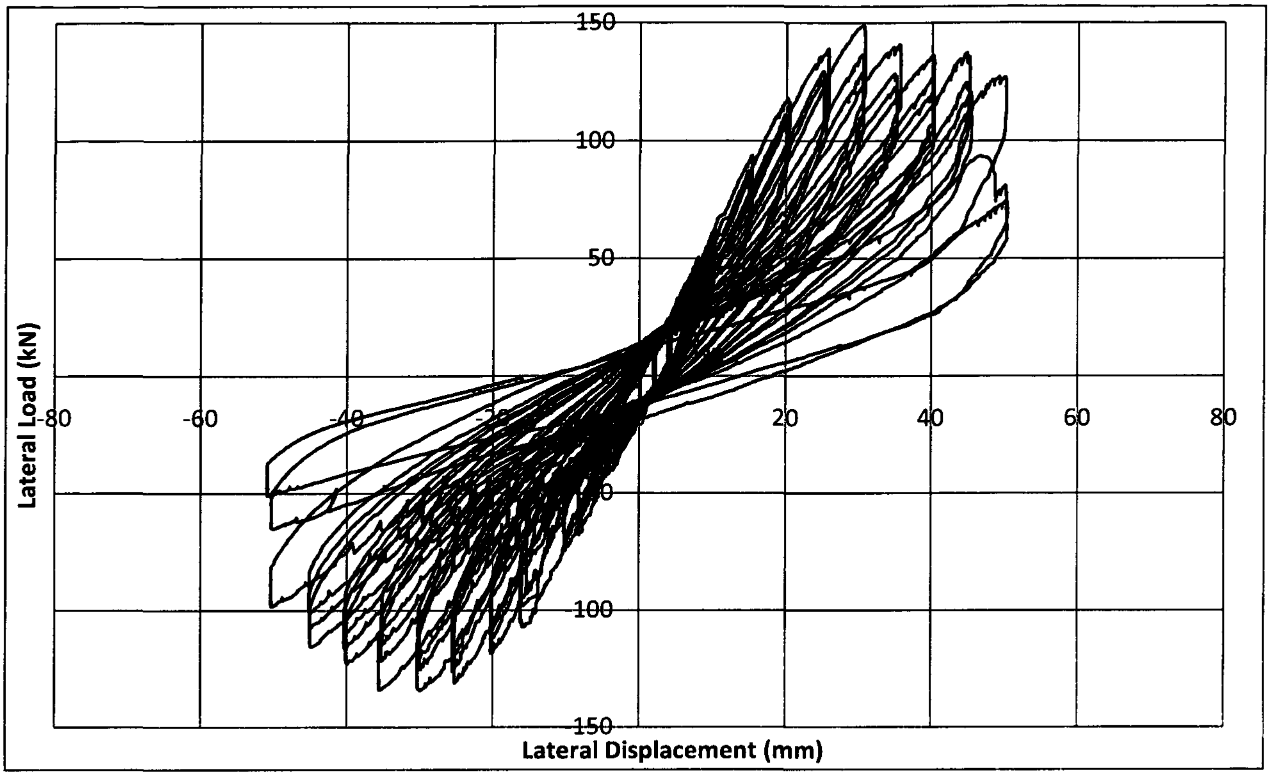

Figure 4.1: Lateral load versus lateral displacement response for BR-3R

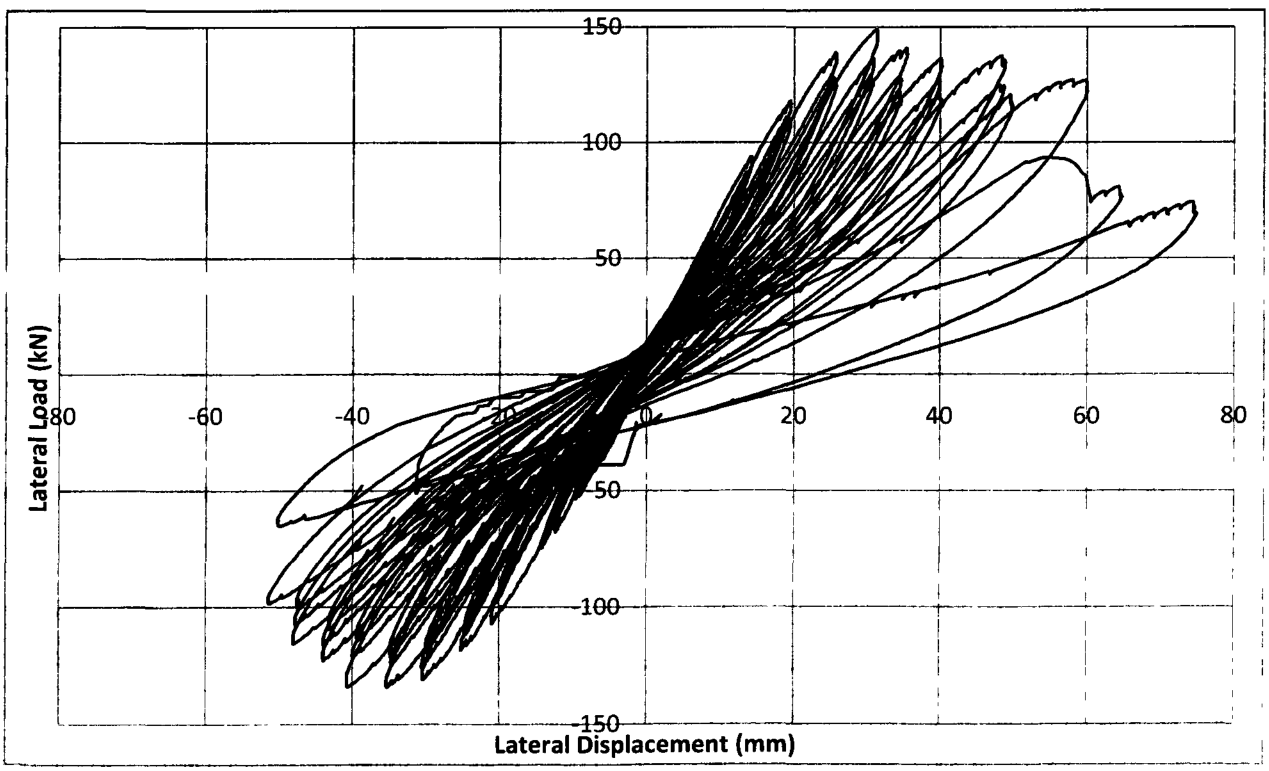

Figure 4.2: Lateral load versus lateral displacement response (backup) for BR-3R

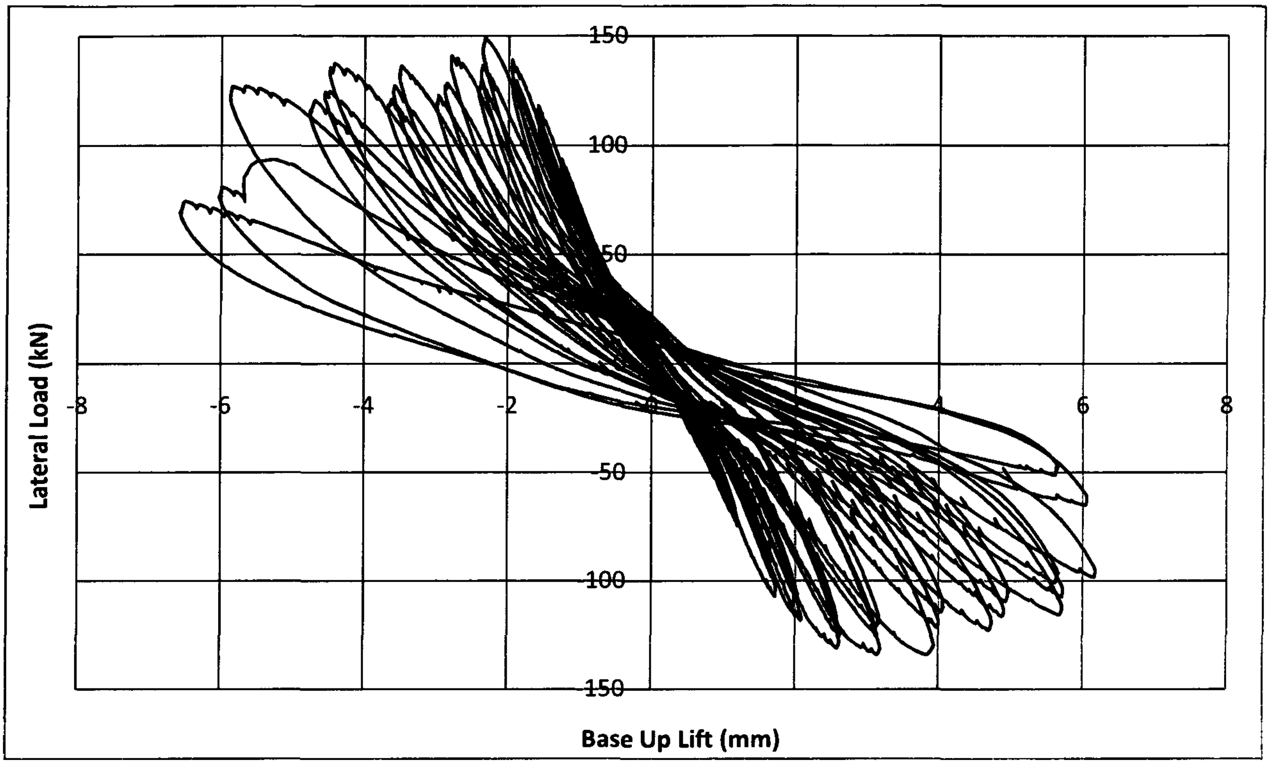

Figure 4.3: Lateral load versus base anchorage slip response for BR-3R

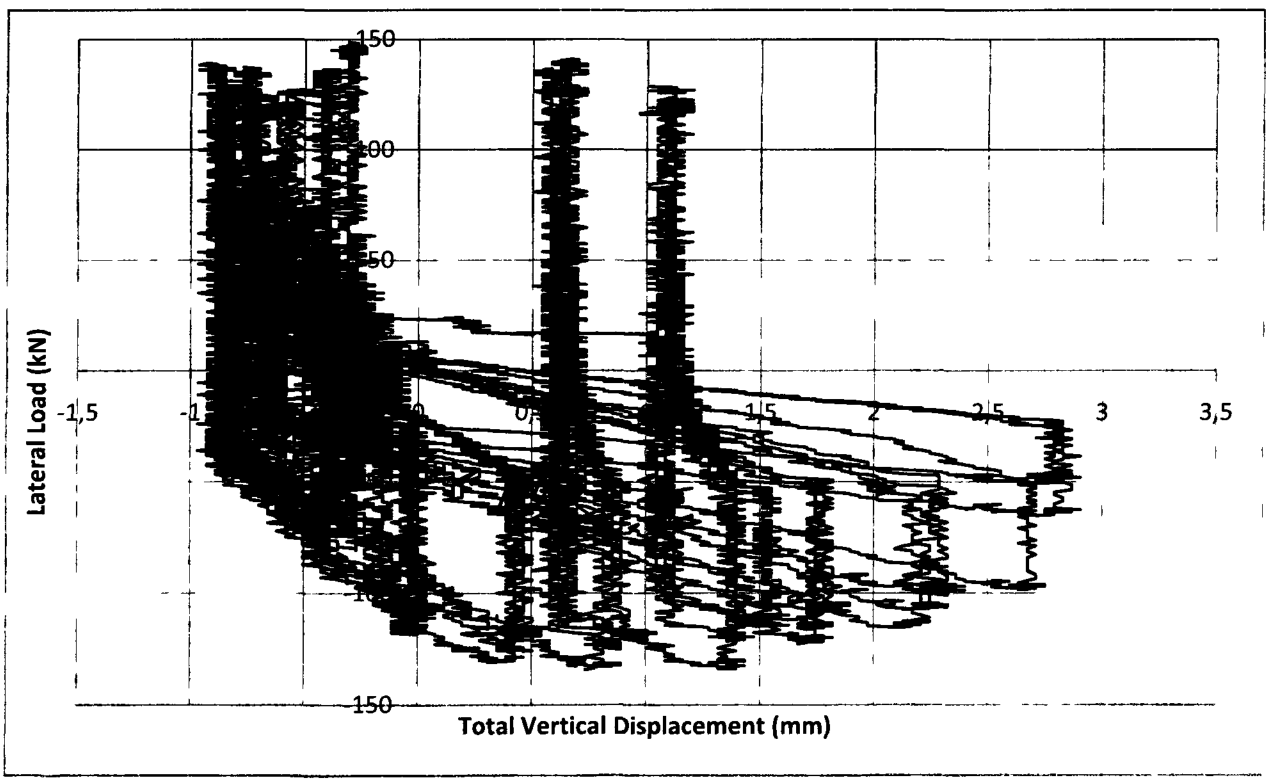

Figure 4.4: Lateral load versus vertical displacement response of column for BR-3R

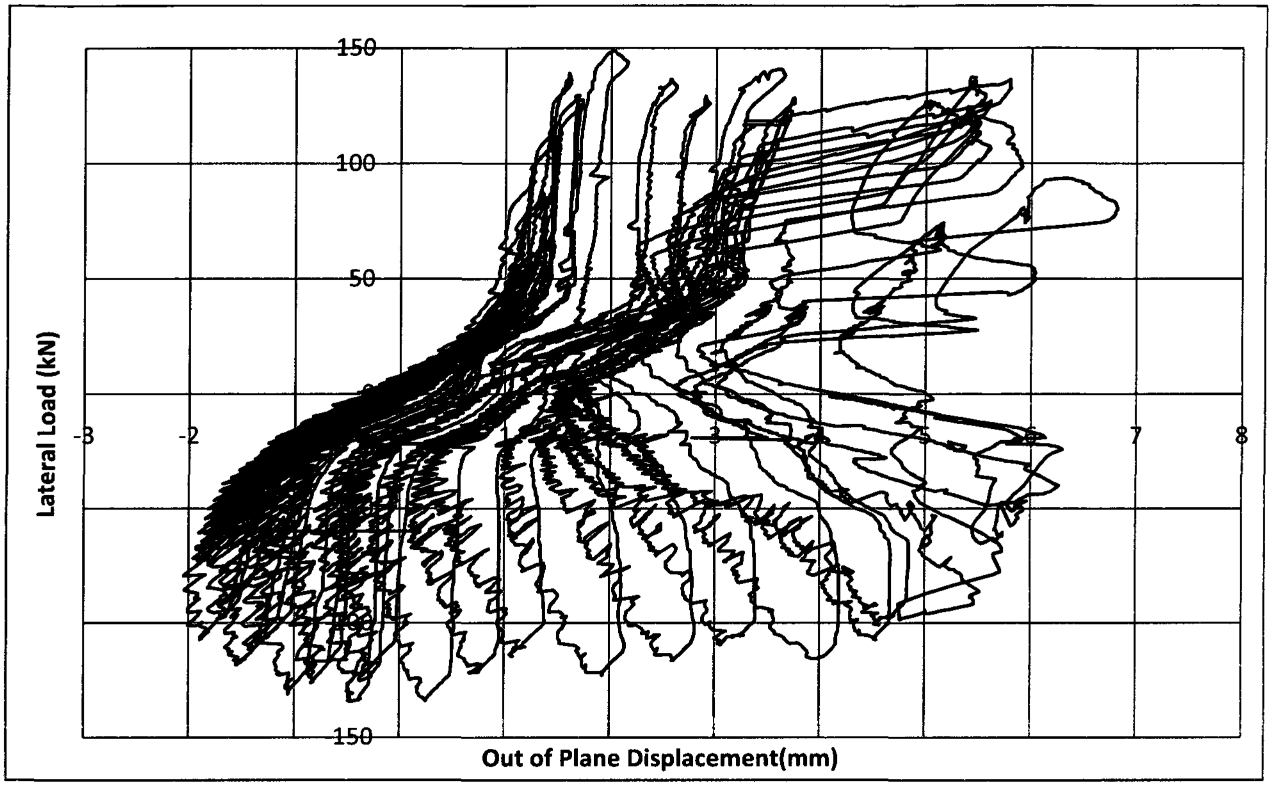

Figure 4.5: Lateral load versus out-of-plane displacement response for BR-3R

After the first load cycle to 0.1% lateral drift (2 mm), no new cracks were visible. For this drift level in the positive direction, the peak load was 13.1 kN, the out-of-plane displacement was 0.43 mm, the column base anchorage slip measured -0.18 mm, and the vertical displacement of the column was 0.00 mm. In the negative direction, the peak load was -31.5 kN, the out-of-plane displacement was -1.20 mm, the column base anchorage slip measured 0.55 mm, and the vertical displacement of the column was -0.16 mm.

The first shear cracks in the column surfaced during the second load cycle to 0.2% lateral drift (4 mm). Theses cracks were mostly extensions of previously existing cracks as indicated in Figure 4.6. For this drift level in the positive direction, the peak load was 25.6 kN, the out-of-plane displacement was 0.75 mm, the column base anchorage slip measured -0.35 mm, and the vertical displacement of the column was -0.16 mm. In the negative direction, the peak load was -41.7 kN, the out-of-plane displacement was -1.45 mm, the column base anchorage slip measured 0.72 mm, and the vertical displacement of the column was -0.27 mm.

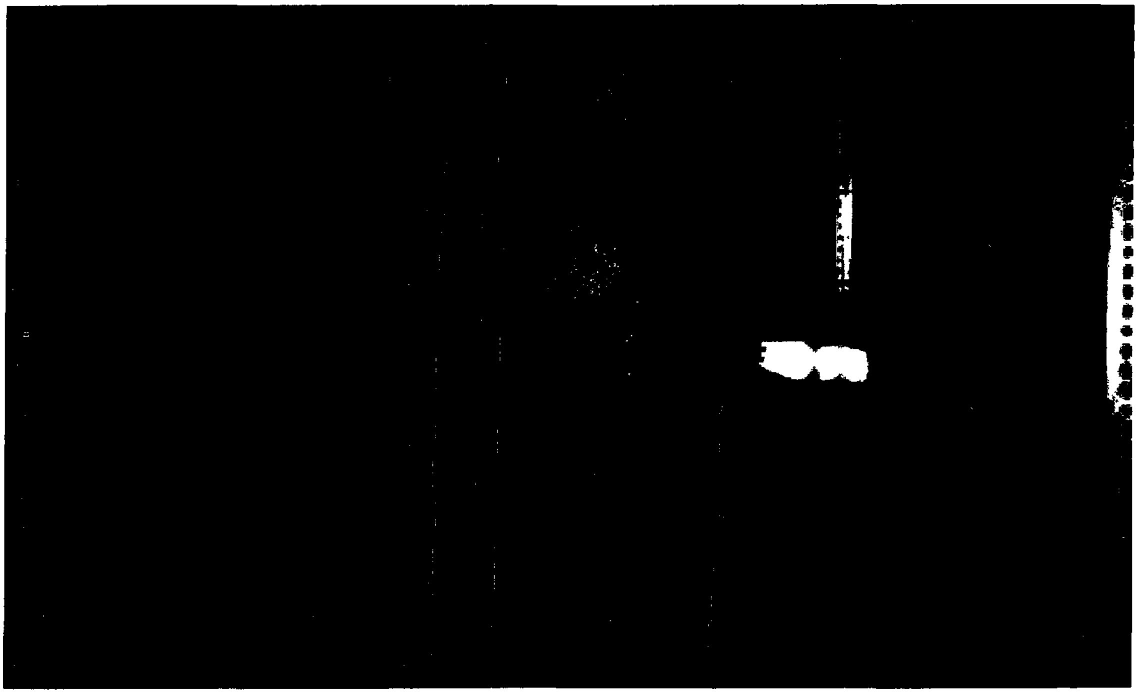

Figure 4.6: First shear cracks in column of Frame BR-3R (0.2% lateral drift)

No new cracks were noticeable after completing the third load cycle to 0.3% lateral drift (6 mm). In the positive direction, the frame reached a peak load of 39.2 kN, out-of-plane displacement of 1.07 mm, column base anchorage slip of -0.57 mm, and vertical displacement of column of -0.23 mm. In the negative direction, the peak load reached -53.6 kN, the out-of-plane displacement was -1.69 mm, the column base anchorage slip measured 0.91 mm, and the vertical displacement of the column was -0.27 mm.

At the fourth load cycle, 0.4% lateral drift (8 mm), small anchorage slip cracks at the base of the columns were visible as illustrated in Figure 4.7. Figure 4.8 shows the first flexural cracks in the beam and the first shear crack in the joints. In the positive direction, the peak load was 39.2 kN, the out-of-plane displacement was 1.07 mm, the column base anchorage slip measured -0.57 mm, and the vertical displacement of the column was -0.23 mm. In the negative direction, the peak load was -53.6 kN, the out-of-plane displacement was -1.69 mm, the column base anchorage slip measured 0.91 mm, and the vertical displacement of the column was -0.27 mm.

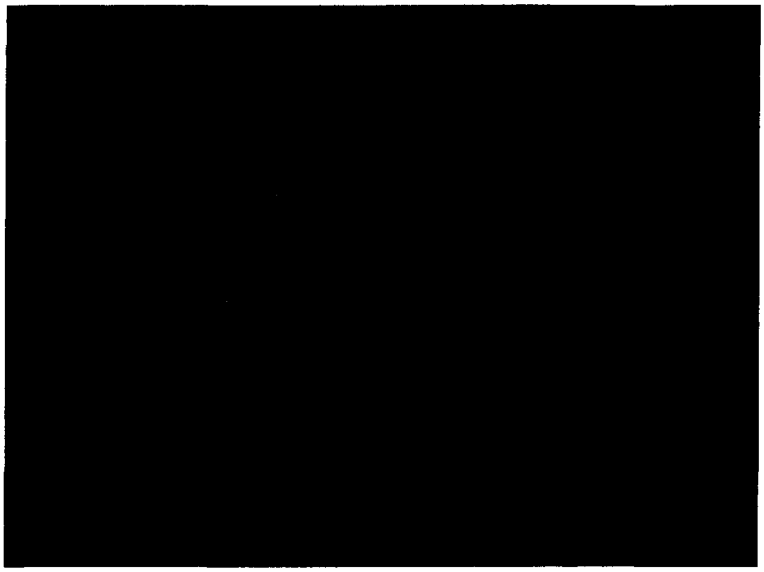

Figure 4.7: First visible up-lift crack in BR-3R (0.4% lateral drift)

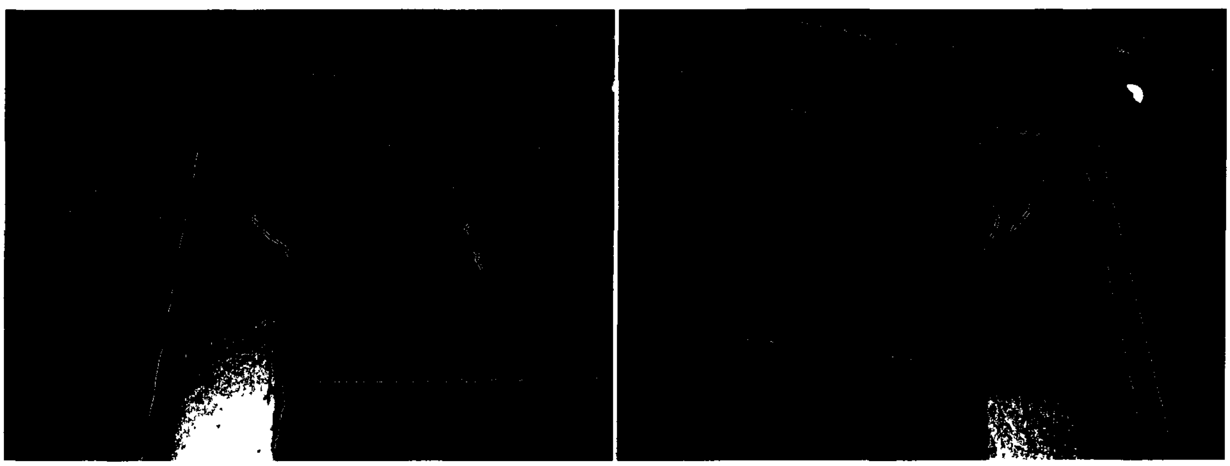

a) *b)*

Figure 4.8: First flexural cracks in the beam and first shear cracks in the joints of BR-3R (0.4% lateral drift): a) Left side joint; b) Right side joint

The shear cracks in the joints and the flexural cracks in the beam were more visible after the fifth load cycle to 0.5% lateral drift (10 mm) as displayed in Figure 4.9. In the positive direction, the peak load was 62.2 kN, the out-of-plane displacement was 1.22 mm, the column base anchorage slip measured -0.89 mm, and the vertical displacement of the column was -0.50 mm. In the negative direction, the peak load was -74.6 kN, the out-of-plane displacement was -1.81 mm, the column base anchorage slip measured 1.20 mm, and the vertical displacement of the column was -0.39 mm.

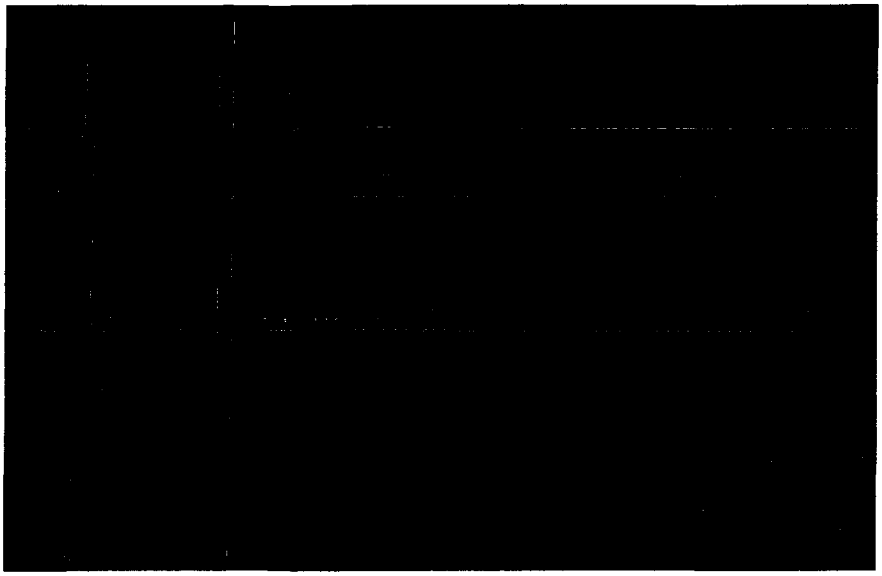

Figure 4.9: Flexural cracks in the beam and shear cracks in the joint of BR-3R (0.5% lateral drift)

At the sixth load cycle, the lateral drift was 0.75% (15 mm). The cracks in the joints did not change, but new flexural cracks in the beam were observed as shown in the photo of Figure 4.10. In the positive direction, the peak load was 93.9 kN, the out-of-plane displacement was 1.24 mm, the column base anchorage slip measured -1.27 mm, and the vertical displacement of the column was -0.62 mm. In the negative direction, the peak load was -107.3 kN, the out-of-plane displacement was -1.89 mm, the column base anchorage slip measured 1.72 mm, and the vertical displacement of the column was -0.08 mm.

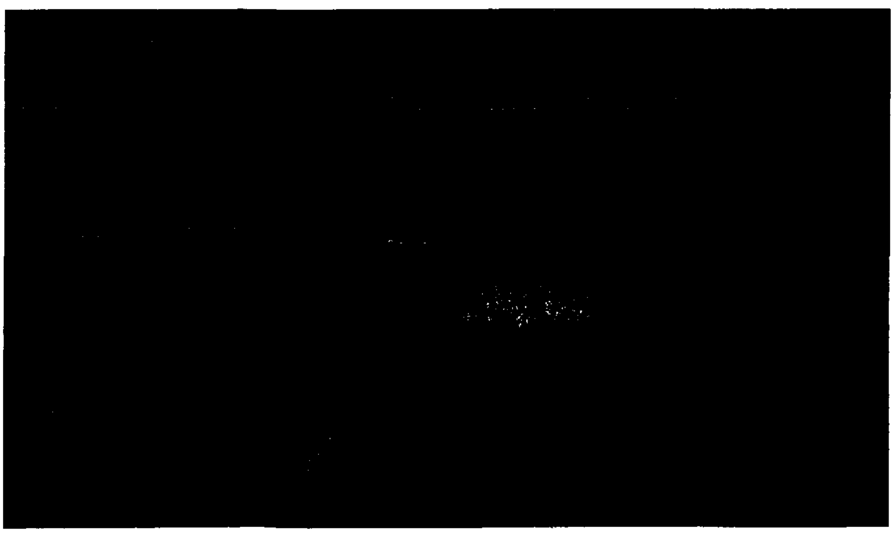

Figure 4.10: New flexural cracks in the beam of Frame BR-3R (0.75% lateral drift)

During the seventh load cycle to 1% lateral drift (20 mm), the first visual sign of rebar de-bonding and slipping was observed in the splice area of the left column. Figure 4.11 shows the vertical cracks indicating de-bonding of the longitudinal steel reinforcement. There was also an increase in number of shear cracks in the beam, columns and joints, and an increase in flexural cracking in the beam as depicted in Figure 4.12. In the positive direction, the peak load was 118.2 kN, the out-of-plane displacement was 1.47 mm, the column base anchorage slip measured -1.60 mm, and the vertical displacement of the column was -0.89 mm. In the negative direction, the peak load was -118.3 kN, the out-of-plane displacement was -1.54 mm, the column base anchorage slip measured 2.08 mm, and the vertical displacement of the column was 0.00 mm.

Figure 4.11: Vertical cracks at the splice location of BR-3R (1% lateral drift)

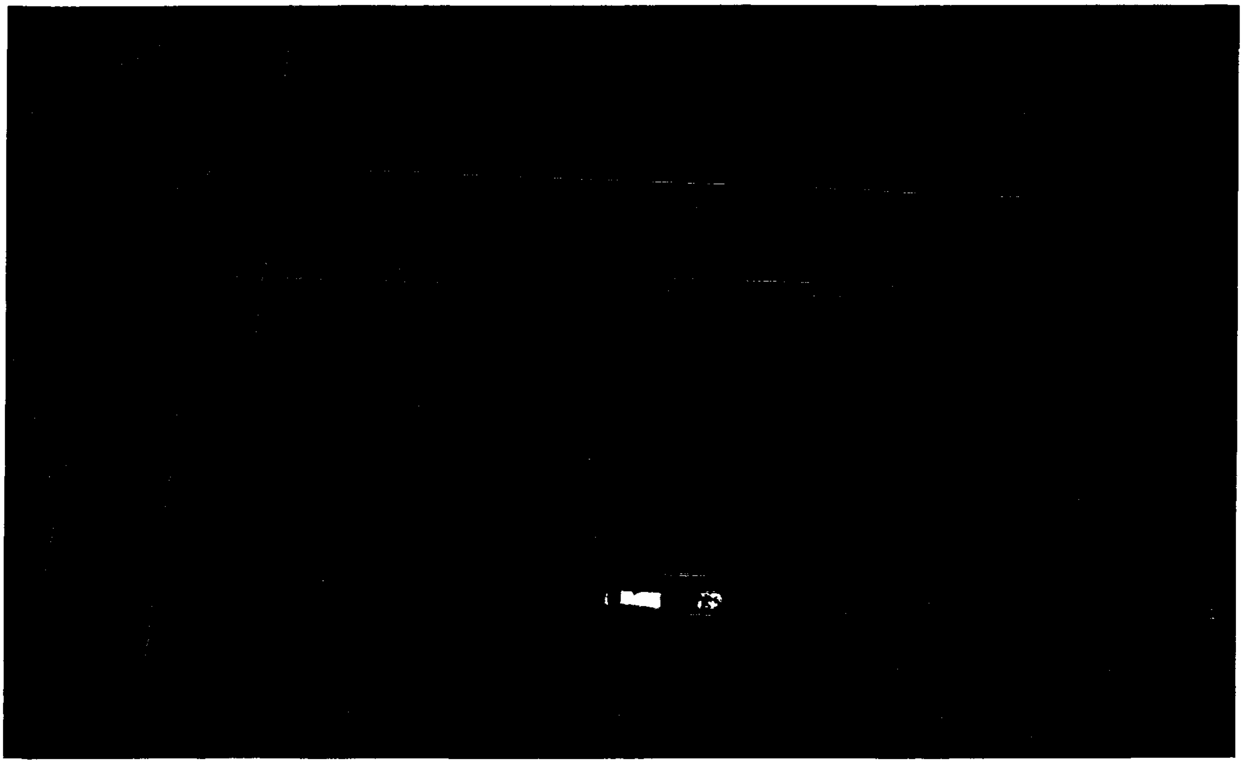

Figure 4.12: Shear cracking in the joints, beam and columns, and flexural cracks in the beam of BR-3R (1% lateral drift)

As illustrated in Figure 4.13, the vertical cracks at the base of the columns became more visible after the eighth load cycle to 1.25% lateral drift (25mm). This indicates that more bars were de-bonding at the splice location. There was an increase in shear cracks in the columns, and a small increase in the flexural and shear cracks in the beam as shown in the photo of Figure 4.14. In the positive direction, the peak load was 139.1 kN, the out-of-plane displacement was 1.60 mm, the column base anchorage slip measured -1.96 mm, and the vertical displacement of the column was -0.93 mm. In the negative direction, the peak load was -131.1 kN, the out-of-plane displacement was -1.05 mm, the column base anchorage slip measured 2.60 mm, and the vertical displacement of the column was 0.31 mm.

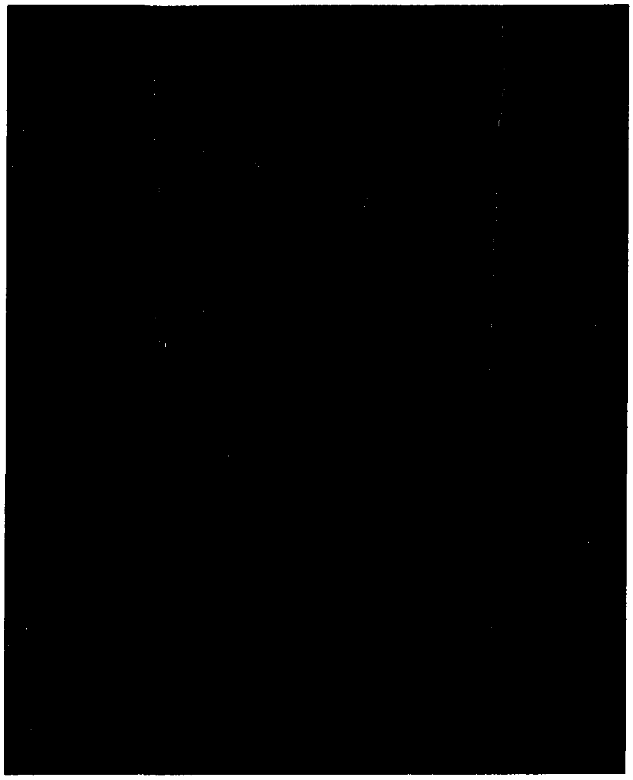

Figure 4.13: Vertical cracks in the column of BR-3R (1.25% lateral drift)

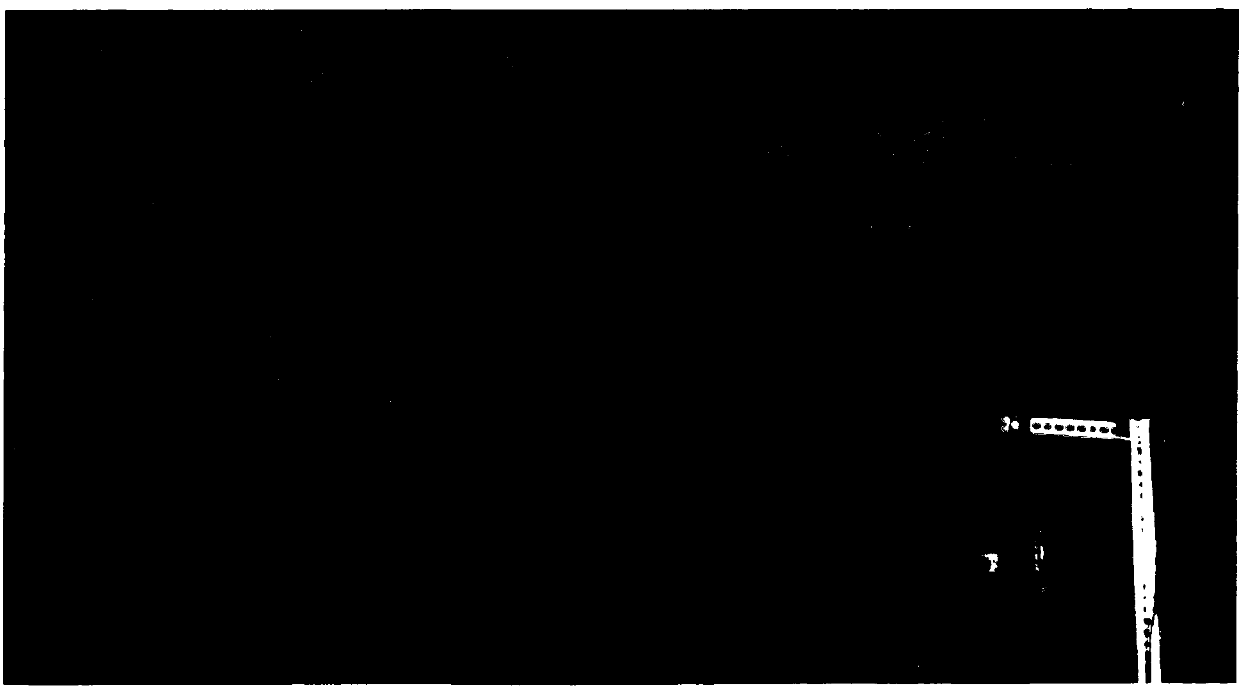

Figure 4.14: Shear cracks in the columns, and flexural and shear cracks in the beam of BR-3R (1.25% lateral drift)

During the ninth load cycle, 1.5% lateral drift (30 mm), there was a further propagation of vertical cracks at the splice location at the base of both columns. Flexural cracking also continued to surface near the base of the columns. Figure 4.15 provides photos of the cracking in the columns. There was a marginal increase in the flexural and shear cracks in the beam; the upper portion of the columns and the joints remained unchanged as shown in Figure 4.16. In the positive direction, the peak load was 149.1 kN, the out-of-plane displacement was 2.02 mm, the column base anchorage slip measured -2.33 mm, and the vertical displacement of the column was -0.31 mm. In the negative direction, the peak load was -134.4 kN, the out-of-plane displacement was -0.46 mm, the column base anchorage slip measured 3.16 mm, and the vertical displacement of the column was 0.74 mm.

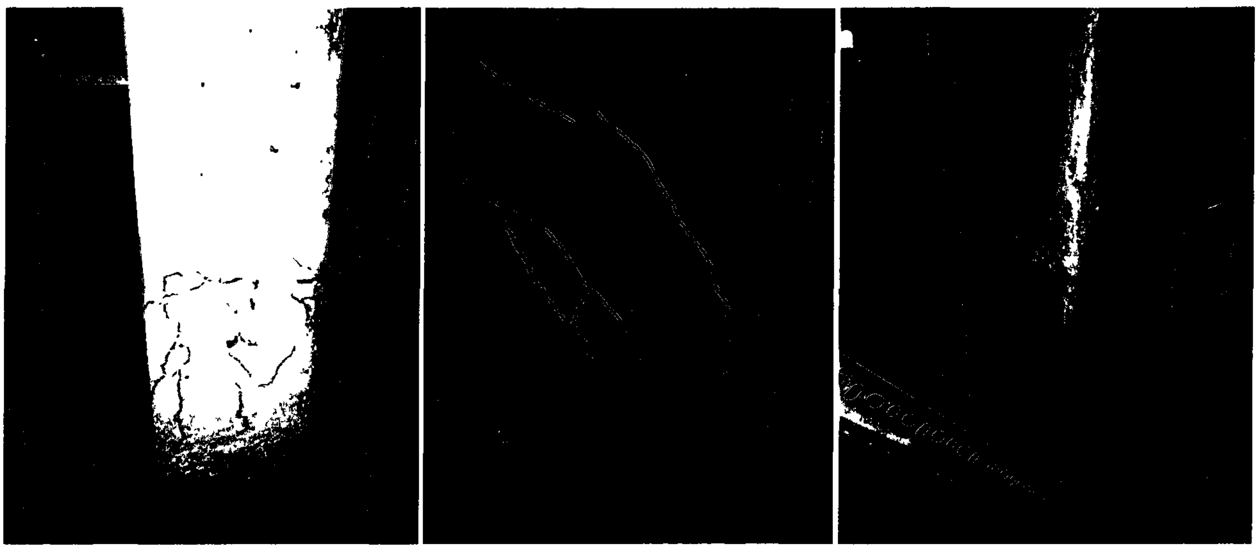

a) *b)* *c)*

Figure 4.15: Vertical and flexural cracks in columns of BR-3R (1.5% lateral drift): a) Left column; b) Right column; c) Right column

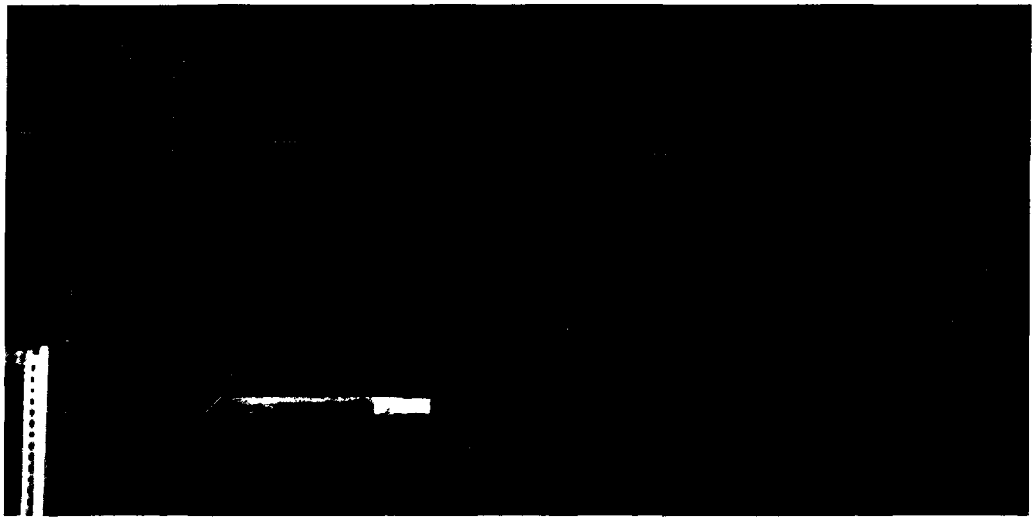

Figure 4.16: Flexural and shear cracks in the beam of BR-3R (1.5% lateral drift)

There was a significant increase in the vertical cracks at the splice location in the columns after the tenth load cycle to 1.75% lateral drift (35 mm). There was also spalling of the concrete cover in the left column in the vicinity of the splices as illustrated in Figure 4.17. Figures 4.18 and 4.19 demonstrate an increase in shear cracks in the joints. In Figure 4.19, a small increase in flexural and shear cracks in the beam and columns can also be observed. In the positive direction, the peak load was 140.9 kN, the out-of-plane displacement was 3.59 mm, the column base anchorage slip measured -2.79 mm, and the vertical displacement of the column was 0.66 mm. In the negative direction, the peak load was -134.1 kN, the out-of-plane displacement was 0.26 mm, the column base anchorage slip measured 3.84 mm, and the vertical displacement of the column was 1.40 mm.

a) *b)* *c)*

Figure 4.17: Vertical and flexural cracks and spalling in the columns of BR-3R (1.75% lateral drift): a) Left column; b) Right column; c) Right column

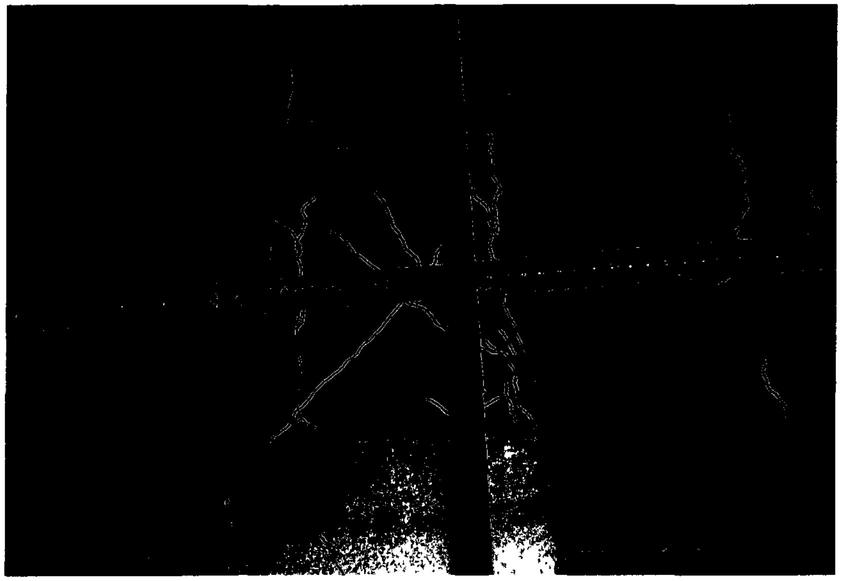

Figure 4.18: Shear cracks in the right joint of BR-3R (1.75% lateral drift)

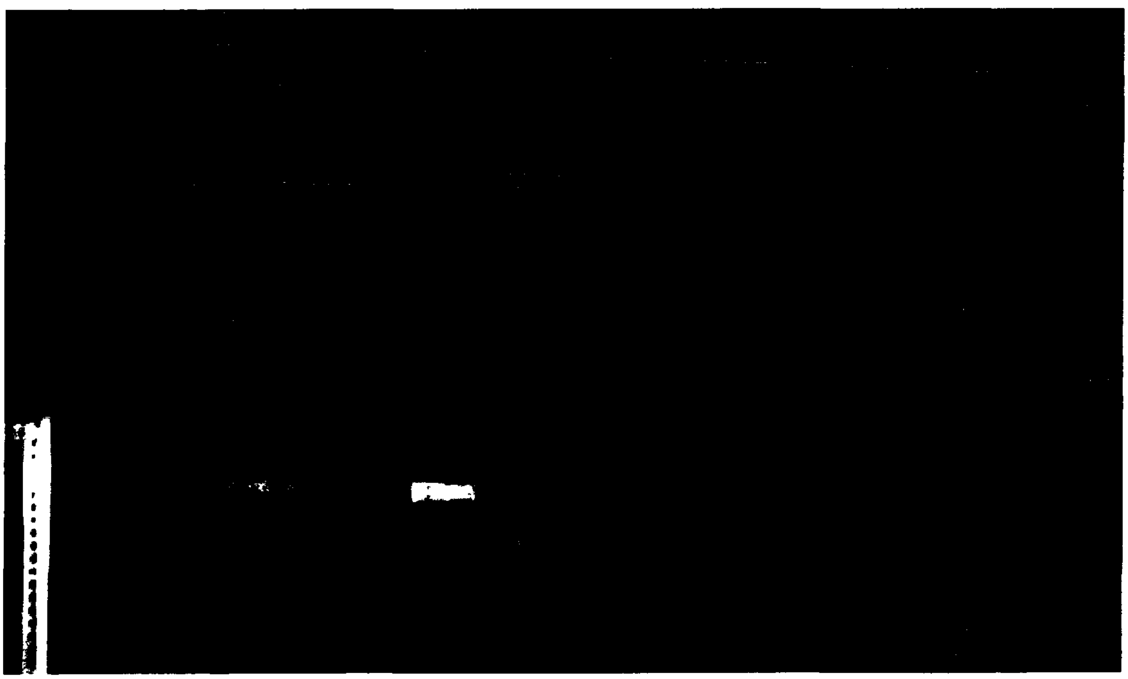

Figure 4.19: Flexural and shear cracks in the beam and columns of BR-3R (1.75% lateral drift)

Following the eleventh load cycle to 2% lateral drift (40 mm), there was no visible increase in shear and flexure cracks in the beam. There were numerous new small flexural and shear cracks in the columns as illustrated in Figure 4.20. There was a further increase in the vertical cracks and additional spalling of the concrete in the columns near the splice location as shown in Figure 4.21. In the positive direction, the peak load was 136.3 kN, the out-of-plane displacement was 5.80 mm, the column base anchorage slip measured -3.50 mm, and the vertical displacement of the column was -0.35 mm. In the negative direction, the peak load was -122.9 kN, the out-of-plane displacement was 1.94 mm, the column base anchorage slip measured 4.69 mm, and the vertical displacement of the column was 1.67 mm.

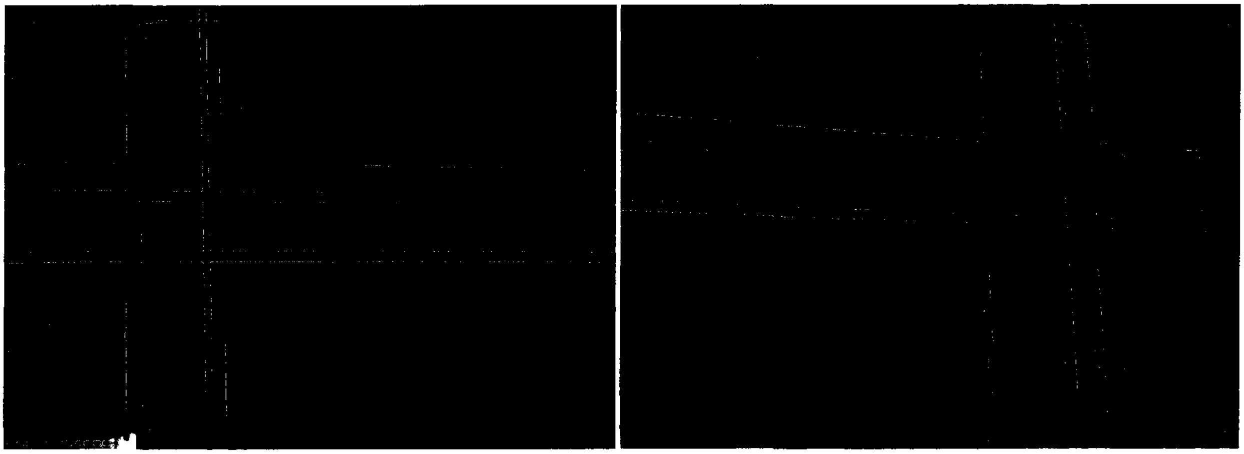

a) *b)*

Figure 4.20: Flexural and shear cracks in the columns of BR-3R (2% lateral drift): a) Left side; b) Right side

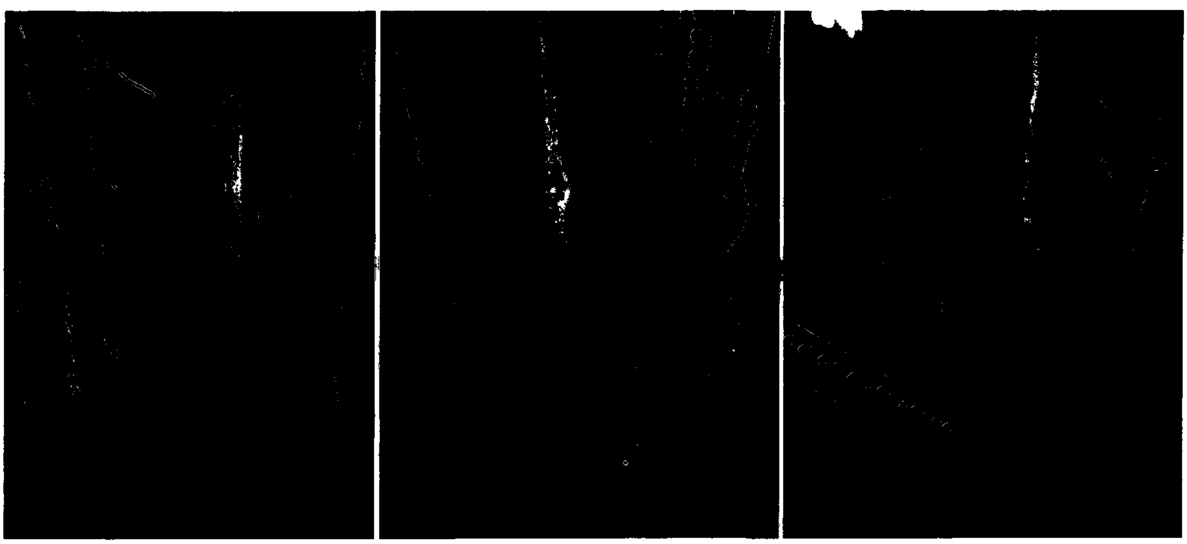

a) *b)* *c)*

Figure 4.21: Vertical and flexural cracks and spalling in the columns of BR-3R (2% lateral drift): a) Left column; b) Right column; c) Right column

As provided in Figure 4.22, after the twelfth load cycle to 2.35% lateral drift (45 mm), severe spalling of the concrete occurred at the splice location in the left column. Furthermore, vertical cracking increased in both columns. There was marginal increase in the flexural and shear cracks in the beam and columns (Figure 4.23). Some signs of de-bonding at the left end of the beam was observed as a longitudinal crack appeared near the bar cutoff location as shown in Figure 4.24. In the positive direction, the peak load was 137.4 kN, the out-of-plane displacement was 5.43 mm, the column base anchorage slip measured -4.42 mm, and the vertical displacement of the column was -0.78 mm. In the negative direction, the peak load was -115.6 kN, the out-of-plane displacement was 3.93 mm, the column base anchorage slip measured 5.65 mm, and the vertical displacement of the column was 2.09 mm.

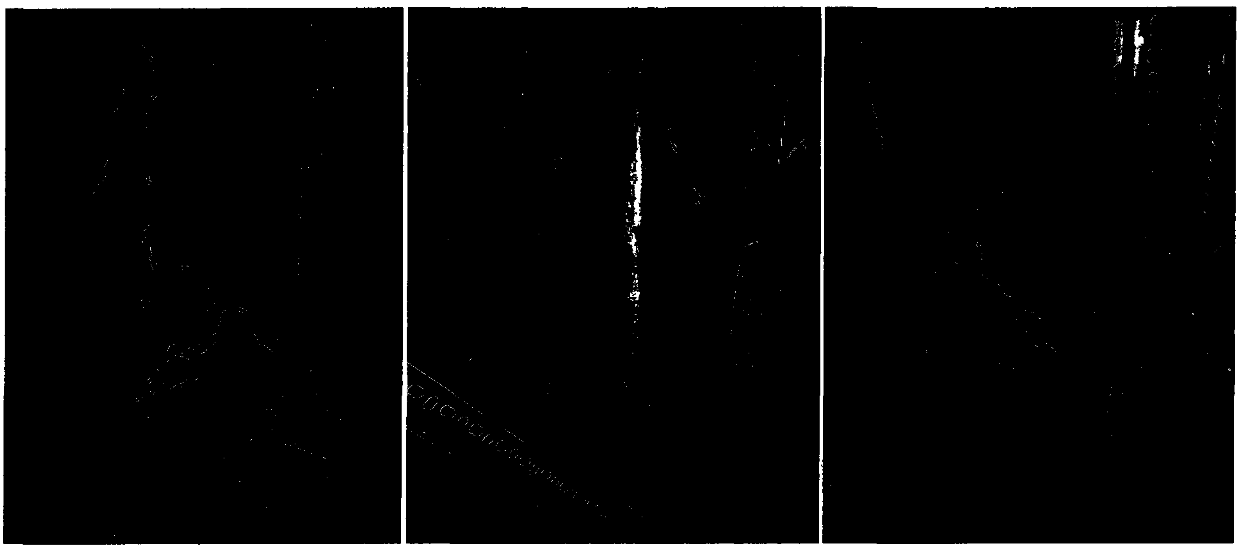

a) *b)* *c)*

Figure 4.22: Vertical and flexural cracks and spalling in the columns of BR-3R (2.25% lateral drift): a) Left column; b) Right column; c) Right column

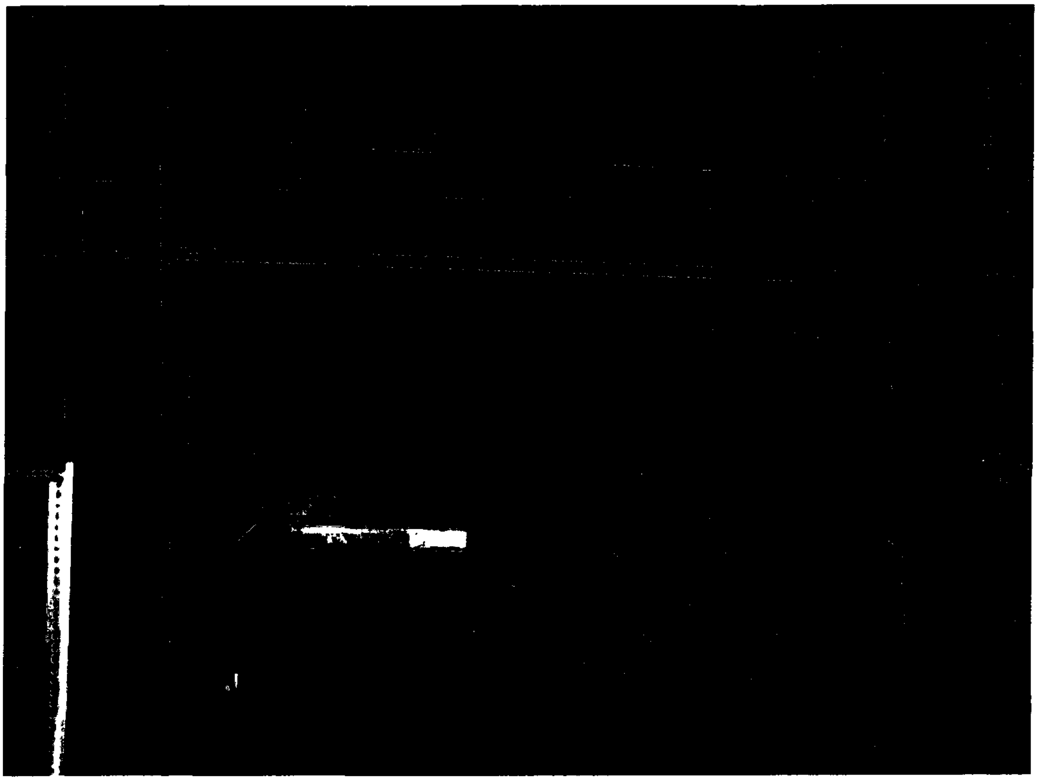

Figure 4.23 : Flexural and shear cracks in the columns and beam of BR-3R (2.25% lateral drift)

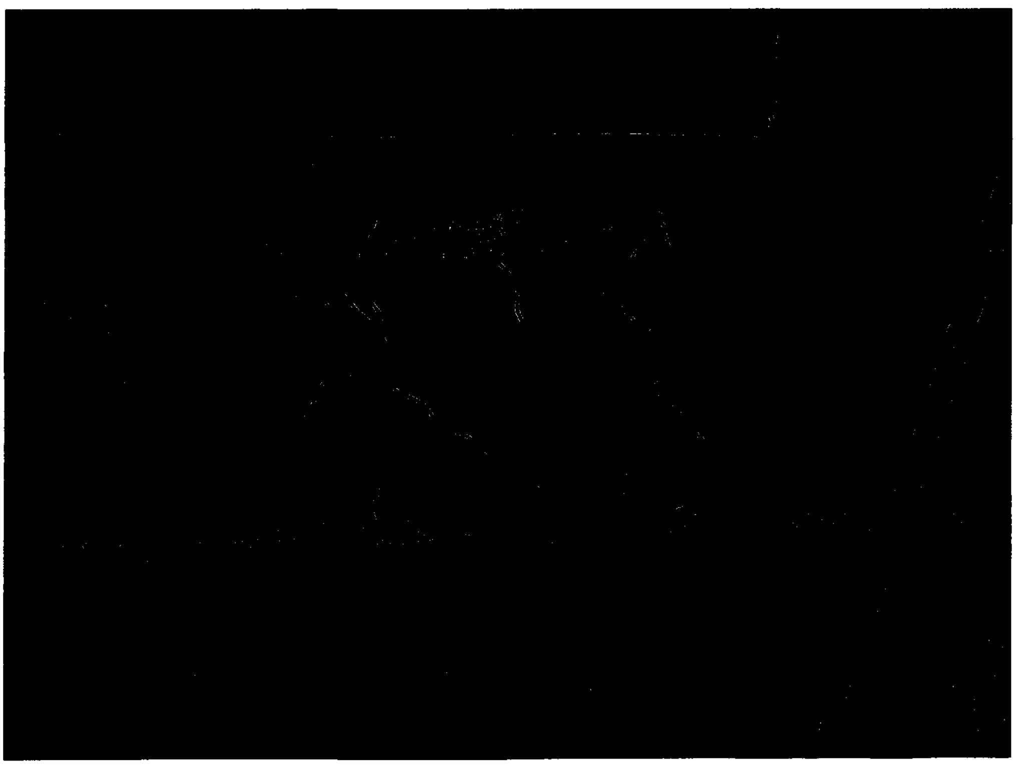

Figure 4.24: Longitudinal crack on the top of the beam of BR-3R (2.25% lateral drift)

Experimental Results

The final load cycle was the thirteenth after displacing to 2.5% lateral drift (50 mm). There were significant differences within the three repetitions in this final load cycle. When the frame was in the positive direction for the first cycle of 2.5% lateral drift, the peak load was 127.1 kN, the out-of-plane displacement was 5.04 mm, the column base anchorage slip measured -5.67 mm, and the vertical displacement of the column was -0.70 mm. In the negative direction, the peak load was -98.5 kN, the out-of-plane displacement was 4.78 mm, the column base anchorage slip measured 6.15 mm, and the vertical displacement of the column was 2.64 mm. When the frame was in the positive direction for the second cycle of 2.5% lateral drift, the peak load was 93.5 kN, the out-of-plane displacement was 6.32 mm, the column base anchorage slip measured -5.26 mm, and the vertical displacement of the column was -0.70 mm. In the negative direction, the peak load was -65.3 kN, the out-of-plane displacement was 5.54 mm, the column base anchorage slip measured 6.03 mm, and the vertical displacement of the column was 2.71 mm. When the frame was in the positive direction for the third and final cycle of 2.5% lateral drift, the peak load was 74.4 kN, the out-of-plane displacement was 5.17 mm, the column base anchorage slip measured -6.51 mm, and the vertical displacement of the column was -0.47 mm. In the negative direction, the peak load was -51.1 kN, the out-of-plane displacement was 5.83 mm, the column base anchorage slip measured 5.62 mm, and the vertical displacement of the column was 2.71 mm. Figure 4.25 displays the frame after the testing was completed. Figure 4.26 shows that there was no increase in the flexural and shear cracks in the columns or beam. As shown in Figures 4.27 and 4.28, failure in Frame BR-3R was controlled by the performance of the columns at the base including deficient reinforcement splice lengths. Furthermore, after the concrete had spalled at the splice locations, the longitudinal reinforcement was significantly bent under the lateral loading. Table 4.1 summarizes the experimental results of the repaired frame, BR-3R.

Figure 4.25: Frame BR-3R at the end of testing (2.5% lateral drift)

Figure 4.26: Flexural and shear cracks in the columns and beam of BR-3R (2.5% lateral drift)

Figure 4.27: Splice location of the right column of BR-3R (2.5% lateral drift)

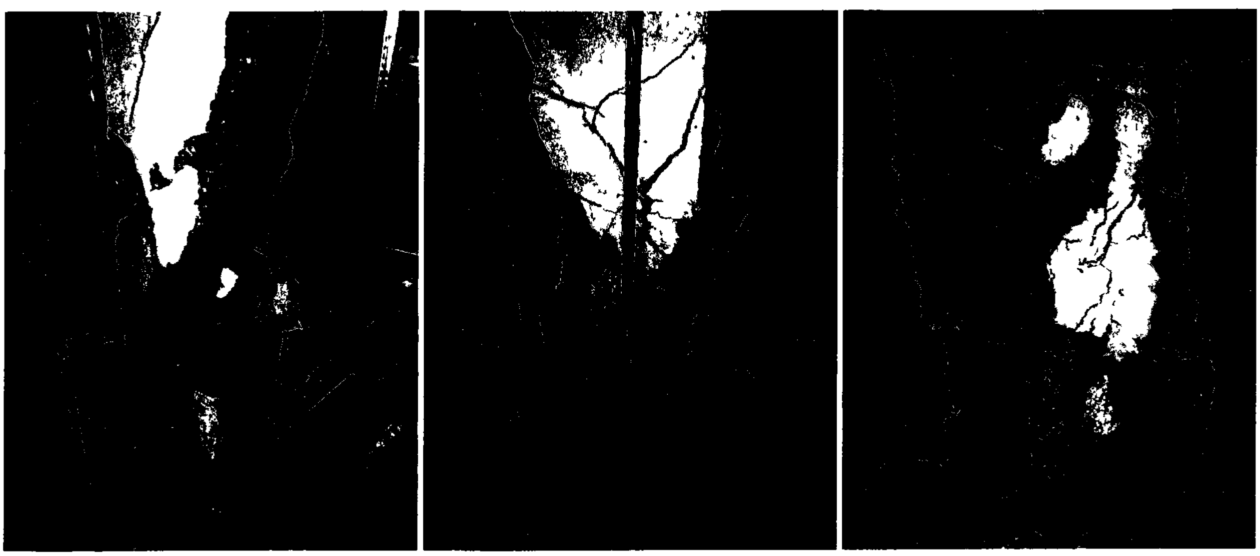

Figure 4.28: Splice location of the left column of BR-3R (2.5% lateral drift)

Table 4.1: Summary of Experimental Results for BR-3R

Positive Direction					Negative Direction				
Lateral Load (kN)	Lateral Disp. (mm)	Base Slip (mm)	Vertical Disp. (mm)	Out-of-Plane Disp. (mm)	Lateral Load (kN)	Lateral Disp. (mm)	Base Slip (mm)	Vertical Disp. (mm)	Out-of-Plane Disp. (mm)
13.1	2	-0.18	0.00	0.43	-31.5	-2	0.55	-0.16	-1.20
24.2	4	-0.33	-0.16	0.72	-40.1	-4	0.70	-0.27	-1.36
39.2	6	-0.57	-0.23	1.07	-52.3	-6	0.88	-0.27	-1.67
49.6	8	-0.72	-0.39	1.23	-67.8	-8	1.10	-0.39	-1.80
57.0	10	-0.83	-0.39	1.28	-74.6	-10	1.20	-0.39	-1.81
93.9	15	-1.27	-0.62	1.24	-107.3	-16	1.72	-0.08	-1.89
118.2	20	-1.60	-0.89	1.47	-118.3	-20	2.08	0.00	-1.54
139.1	26	-1.96	-0.93	1.60	-131.1	-25	2.60	0.31	-1.05
149.1	31	-2.33	-0.31	2.02	-134.3	-30	3.16	0.74	-0.46
140.9	36	-2.79	0.66	3.59	-134.1	-35	3.84	1.40	0.26
136.3	40	-3.50	-0.35	5.80	-122.9	-40	4.69	1.67	1.94
124.8	45	-4.49	-0.70	5.40	-107.4	-45	5.71	2.13	4.55
127.1	49	-5.67	-0.70	5.04	-98.5	-50	6.15	2.64	4.78
93.5	47	-5.26	-0.70	6.32	-65.3	-50	6.03	2.71	5.54
74.4	50	-6.51	-0.47	5.17	-51.1	-51	5.62	2.71	5.83

4.3 Performance of Retrofitted Frame

Frame BL-3 from Shalouf (2005) was repaired and retrofitted, then renamed BL-3R for this research program. The lateral displacement, base anchorage slip of the column, vertical displacement of the column, and the out-of-plane displacement were measured and plotted against the applied lateral load in Figures 4.29 to 4.31. There were also 16 strain gauges. Strain gauges RC1 and LC4 were defective and the data recorded from strain gauge X5 could not be used. Figures 4.32 and 4.33 display the strains measured from strain Gauges X3 and X6. These two strain gauges will be used throughout the damage and measurement explanations that were observed during testing. The gauges were situated at the same level and location on the steel bracing. Gauge X3 was situated on the long brace member, while Gauge X6 was situated on the member that was cut and placed as the upper portion of the second steel brace. The data from the other strain gauges can be found in Appendix B. Due to problems encountered during testing, the primary cable displacement transducer did not provide accurate results, and thus the backup lateral displacement cable transducer situated on the same side as the actuator was used as the reference for the lateral displacement of the frame.

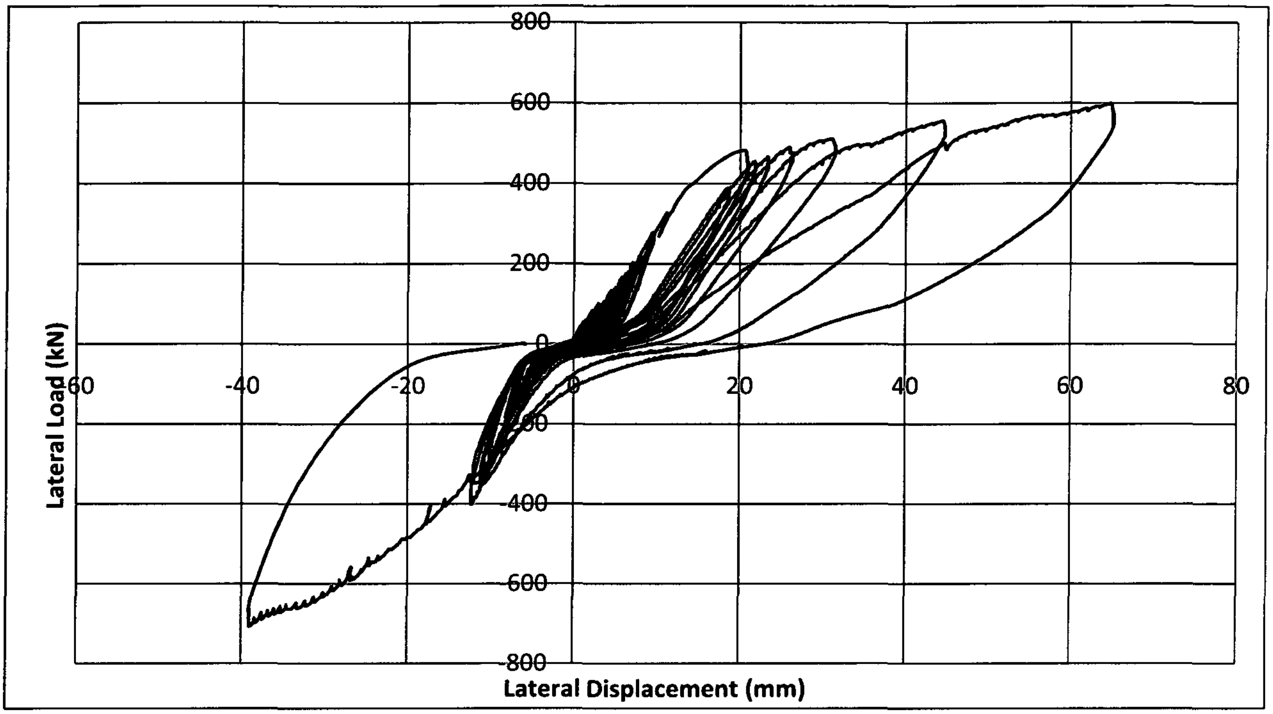

Figure 4.29: Lateral load versus lateral displacement response for BL-3R

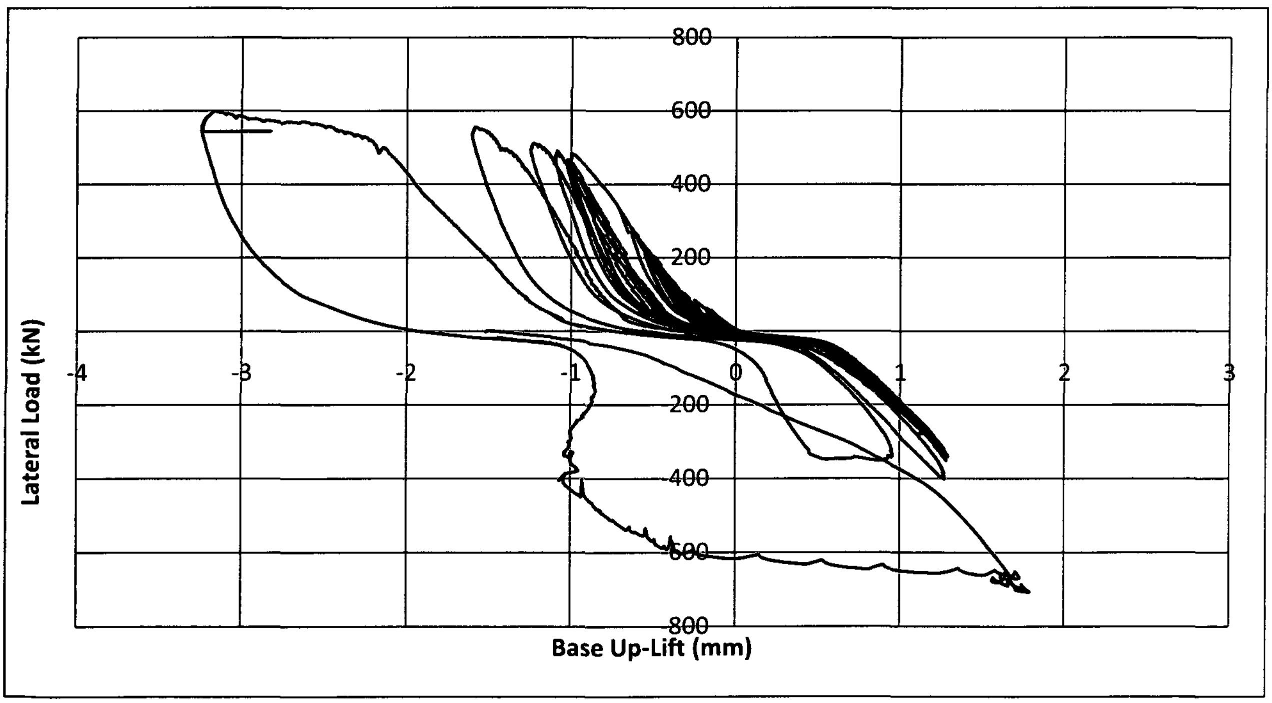

Figure 4.30: Lateral load versus base anchorage slip response for BL-3R

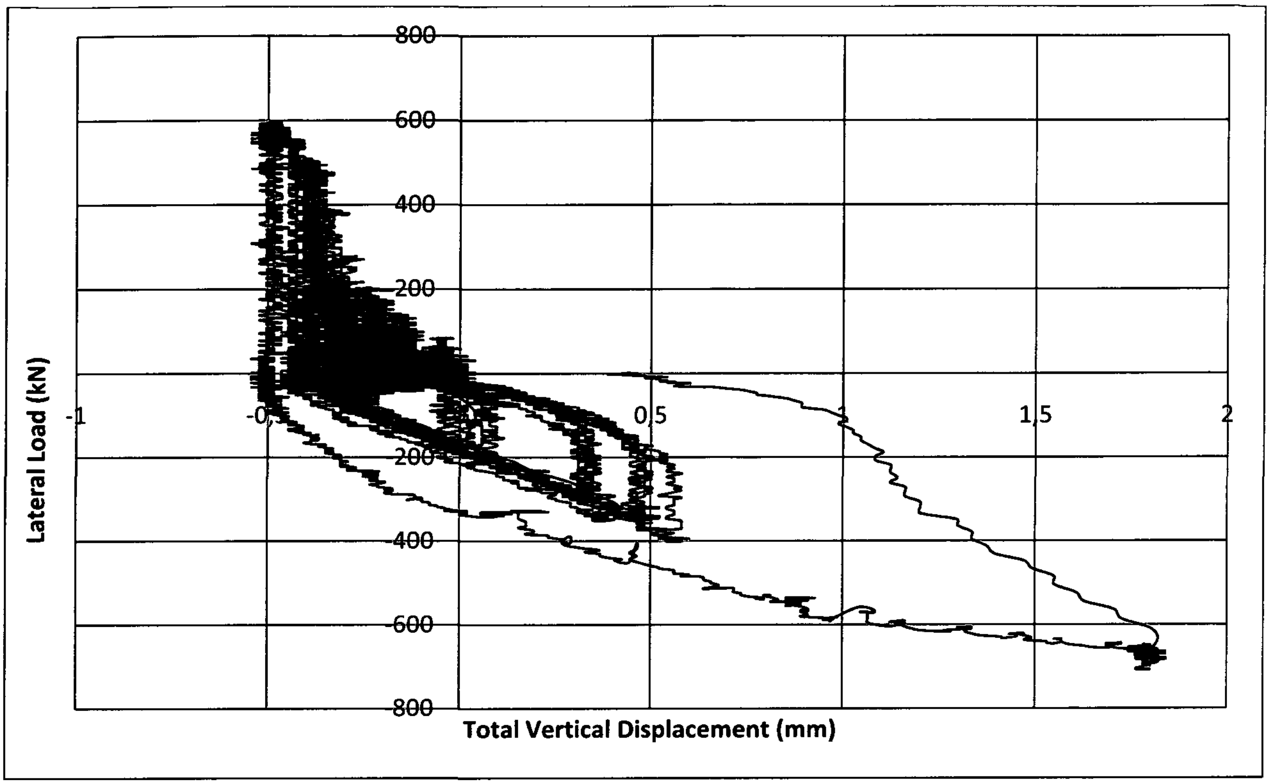

Figure 4.31: Lateral load versus vertical displacement response of column for BL-3R

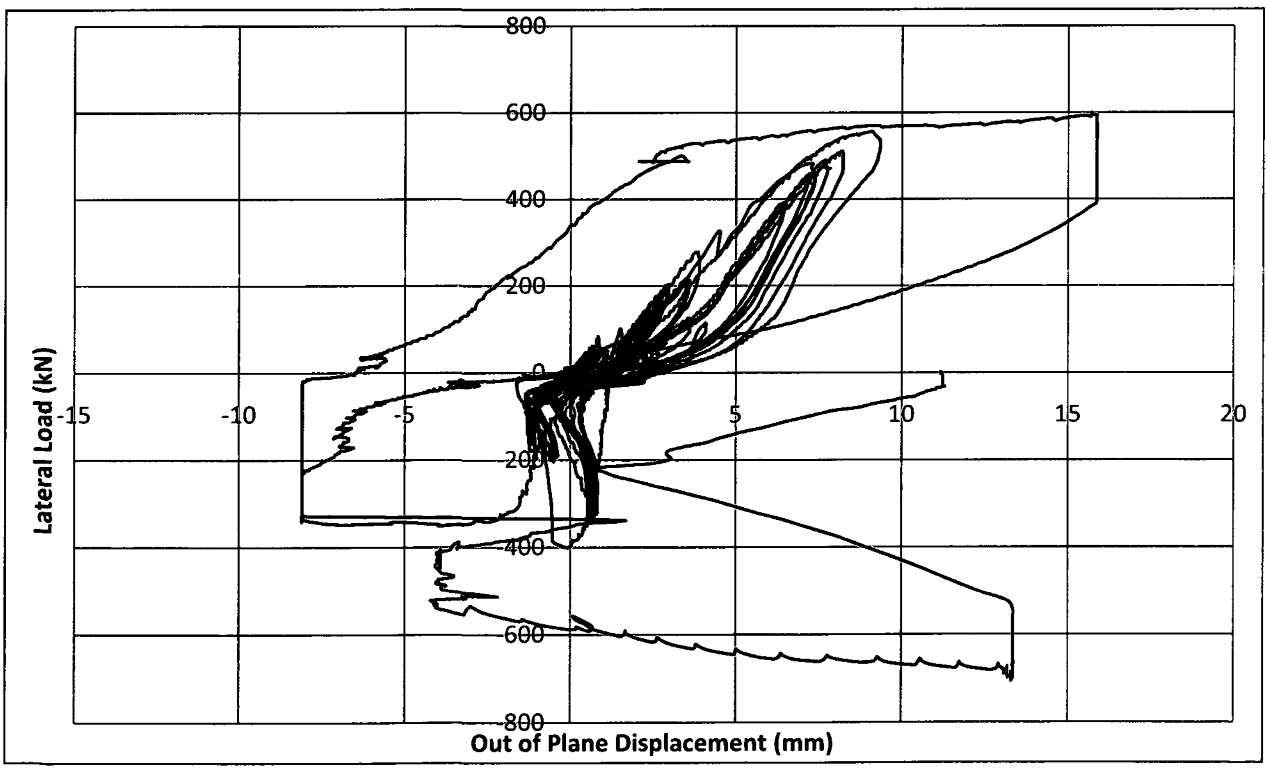

Figure 4.32: Lateral load versus out-of-plane displacement response for BL-3R

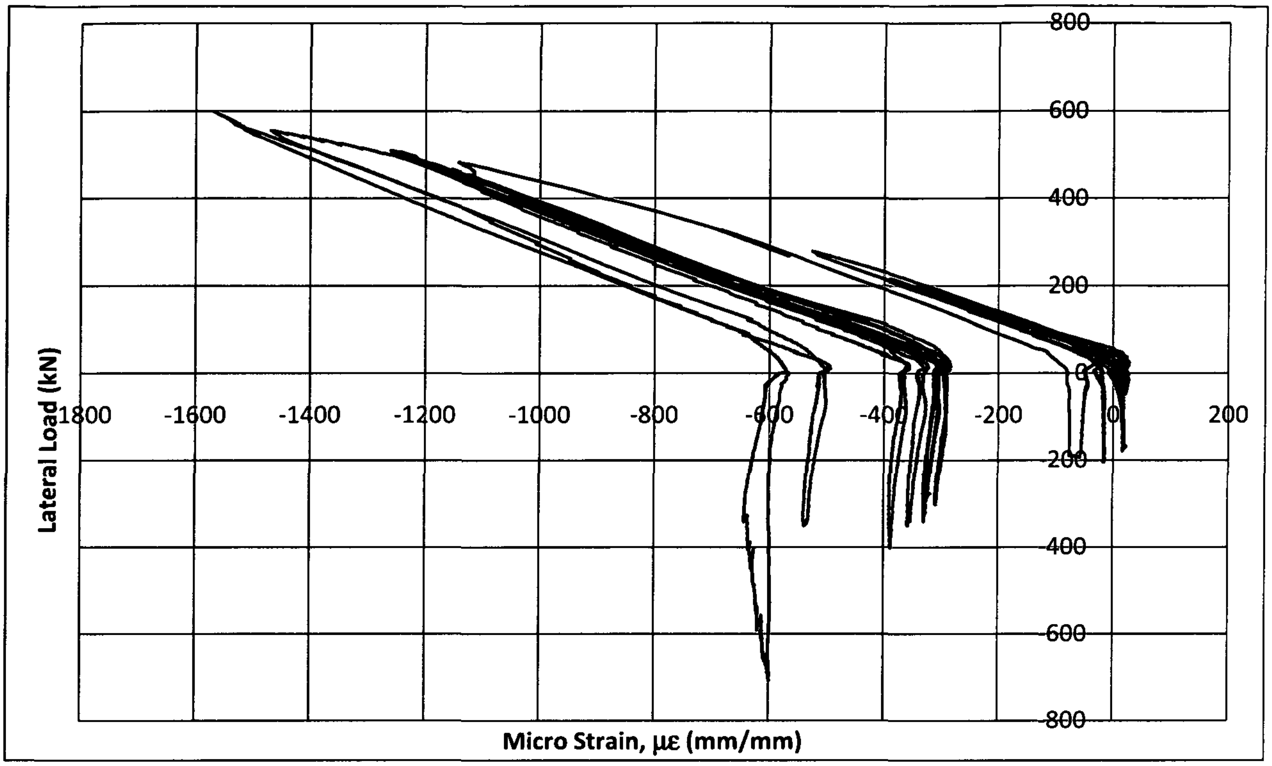

Figure 4.33: Lateral load versus strain response for Gauge X3 in BL-3R

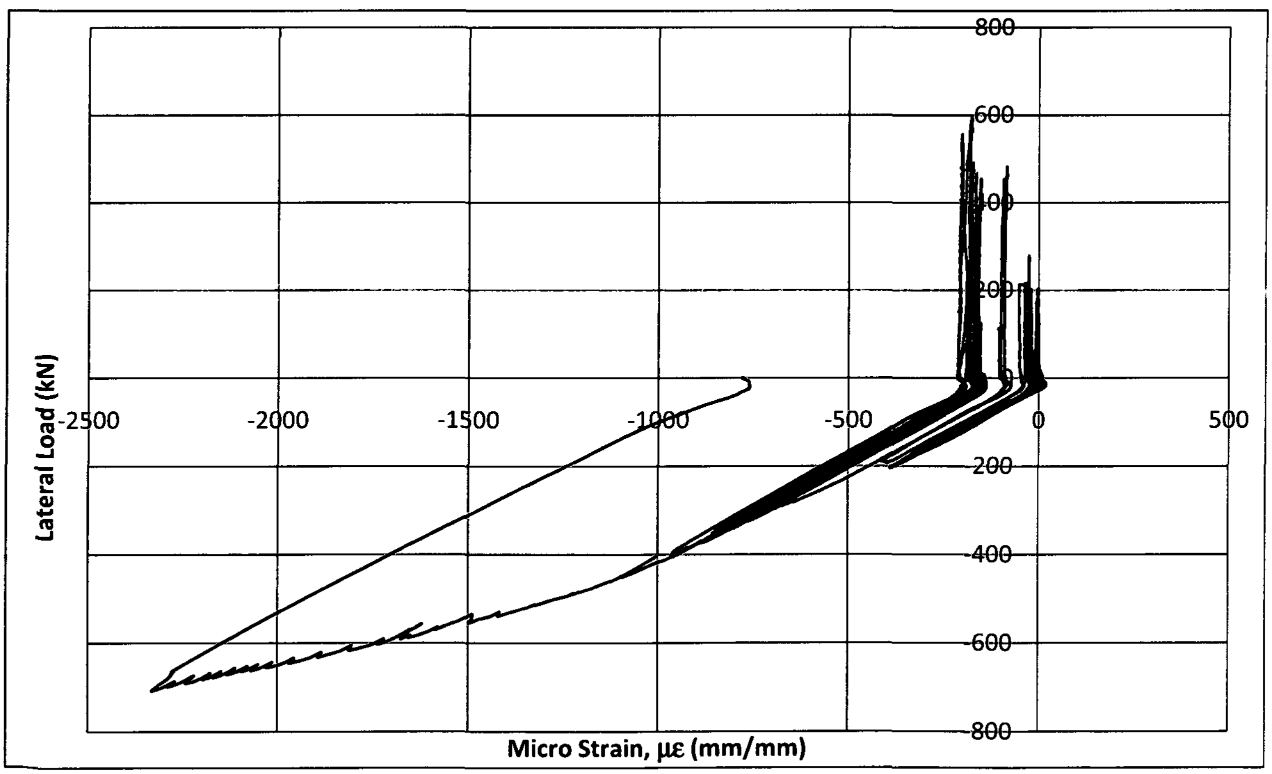

Figure 4.34: Lateral load versus strain response for Gauge X6 in BL-3R

Experimental Results

After the first load cycle to 0.05% lateral drift (1 mm), no new cracks were visible. Figure 4.35 shows BL-3R after the first load cycle. All the cracks marked on the frame at this point were pre-existing. In the positive direction, the peak load was 46.9 kN, the out-of-plane displacement was 0.52 mm, the column base anchorage slip measured -0.13 mm, the vertical displacement of the column was -0.04 mm, the strain in Gauge X3 measured -40 $\mu\varepsilon$, and the strain in Gauge X6 measured -4 $\mu\varepsilon$. In the negative direction, the peak load was -13.9 kN, the out-of-plane displacement was -0.17 mm, the column base anchorage slip measured 0.12 mm, the vertical displacement of the column was -0.06 mm, the strain in Gauge X3 measured 12 $\mu\varepsilon$, and the strain in Gauge X6 measured -2 $\mu\varepsilon$.

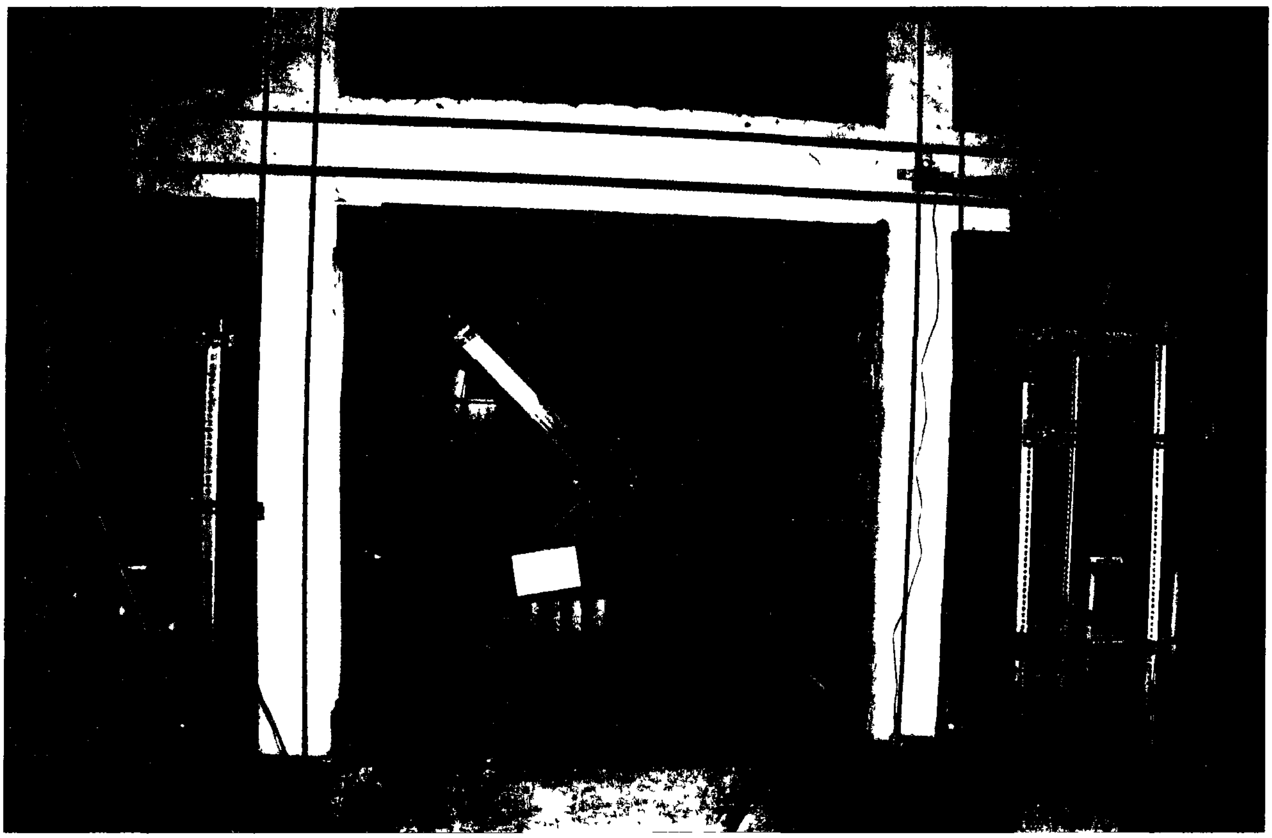

Figure 4.35: Frame BL-3R after the first load cycle to 0.05% lateral drift

There were no new cracks after the second load cycle to 0.10% lateral drift (2 mm). In the positive direction, the peak load was 78.4 kN, the out-of-plane displacement was 0.81 mm, the column base anchorage slip measured -0.24 mm, the vertical displacement of the column was -0.04 mm, the strain in Gauge X3 measured -92 $\mu\varepsilon$, and the strain in Gauge X6 measured -6 $\mu\varepsilon$. In the negative direction, the peak load was -25.4 kN, the out-of-plane displacement was -0.42 mm, the column base anchorage slip measured 0.23 mm, the vertical displacement of the column was -0.06 mm, the strain in Gauge X3 measured 15 με, and the strain in Gauge X6 measured -18 με.

Small cracks surfaced in the corners of the frame after the third load cycle (0.15% drift) as indicated in Figure 4.36. In the positive direction, the peak load was 99.0 kN, the out-of-plane displacement was 1.54 mm, the column base anchorage slip measured -0.32 mm, the vertical displacement of the column was -0.14 mm, the strain in Gauge X3 measured -120 με, and the strain in Gauge X6 measured -6 με. In the negative direction, the peak load was -39.8 kN, the out-of-plane displacement was -0.35 mm, the column base anchorage slip measured 0.40 mm, the vertical displacement of the column was -0.21 mm, the strain in Gauge X3 measured 21 με, and the strain in Gauge X6 measured -32 με.

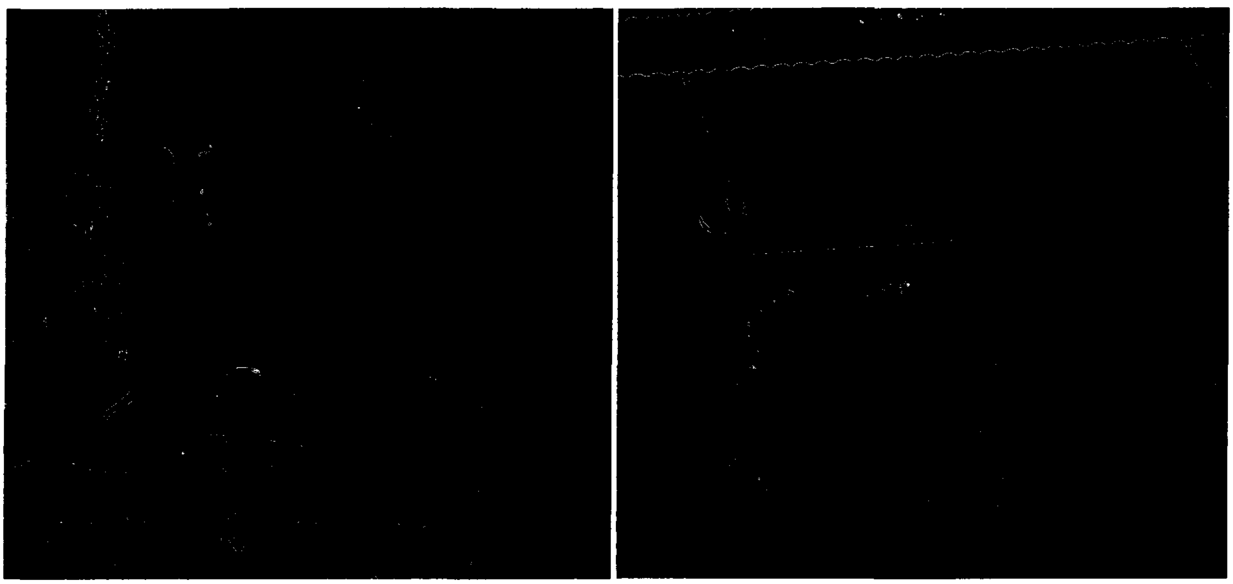

a) *b)*

Figure 4.36: Cracking in the corners of Frame BL-3R (0.15% lateral drift): a) Bottom left corner; b) Top left corner

The fourth load cycle to 0.20% lateral drift (4 mm) produced an additional crack in the corner, while existing cracks propagated (Figure 4.37). In the positive direction, the peak load was 118.1 kN, the out-of-plane displacement was 2.18 mm, the column base anchorage slip measured -0.35 mm, the vertical displacement of the column was -0.16 mm, the strain in Gauge X3 measured -158 με, and the strain in Gauge X6 measured -5 με. In the negative direction, the peak load was -67.2 kN, the out-of-plane displacement was -1.00 mm, the column base anchorage slip measured 0.55 mm, the vertical displacement of the column was -0.23 mm, the strain in Gauge X3 measured 16 με, and the strain in Gauge X6 measured -90 με.

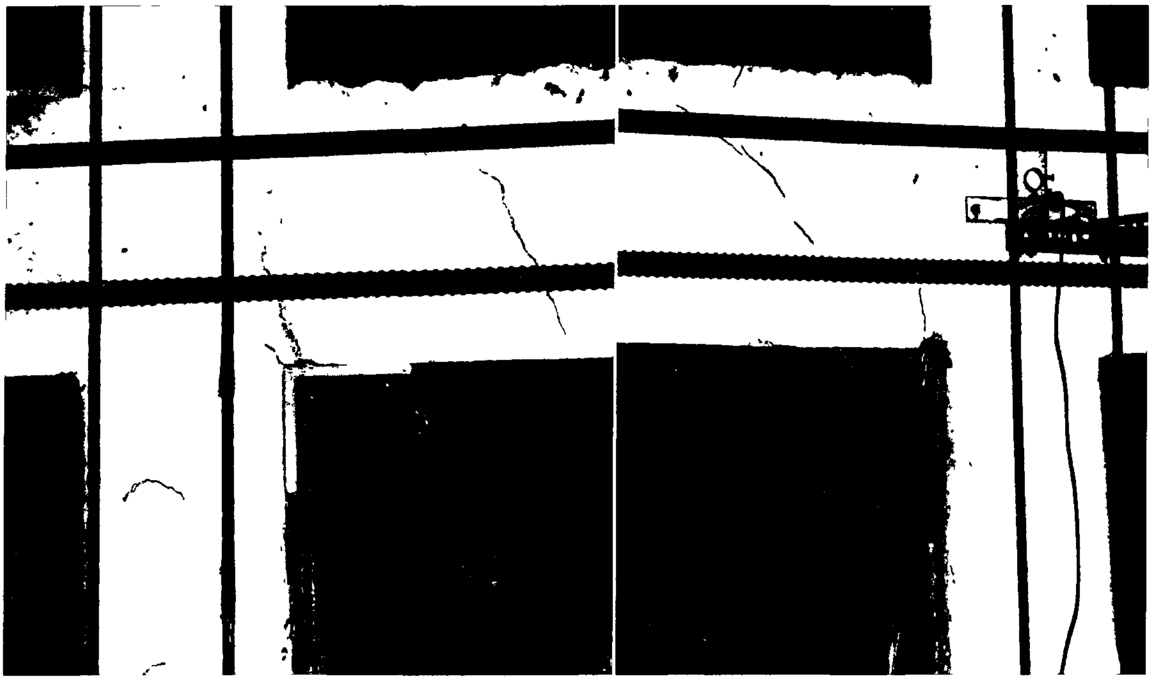

a) b)

Figure 4.37: Small cracks in the corners of BL-3R (0.20% lateral drift): a) Top left corner; b) Top right corner

No new cracks appeared during the fifth load cycle to 0.25% lateral drift. In the positive direction, the peak load was 142.3 kN, the out-of-plane displacement was 2.46 mm, the column base anchorage slip measured -0.41 mm, the vertical displacement of the column was -0.19 mm, the strain in Gauge X3 measured -201 με, and the strain in Gauge X6 measured -1 με. In the negative direction, the peak load was -101.6 kN, the out-of-plane displacement was -1.13 mm, the column base anchorage slip measured 0.66 mm, the vertical displacement of the column was -0.21 mm, the strain in Gauge X3 measured 16 με, and the strain in Gauge X6 measured -156 με.

At the sixth load cycle, the lateral drift was 0.30% (6 mm). Some concrete spalling was evident in the top left corner of the frame and extensions of existing cracks were also visible in the same corner as shown in the photos of Figure 4.38. In the positive direction, the peak load was 168.2 kN, the out-of-plane displacement was 2.65 mm, the column base anchorage slip measured -0.45 mm, the vertical displacement of the column was -0.23 mm, the strain in Gauge X3 measured -258 με, and the strain in Gauge X6 measured -3 με. In the negative direction, the peak load was -132.4 kN, the out-of-plane displacement was -1.25 mm, the column base anchorage slip measured 0.76 mm, the vertical displacement of the column was -0.16 mm, the strain in Gauge X3 measured 18 με, and the strain in Gauge X6 measured -219 με.

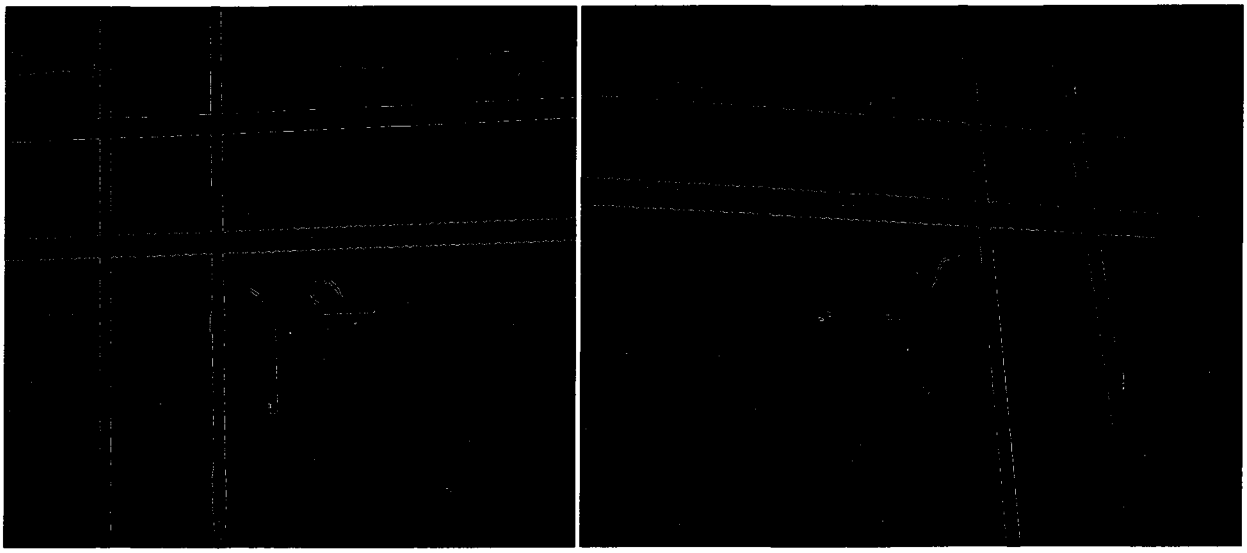

a) *b)*

Figure 4.38: Cracking and spalling in top left corner of BL-3R (0.30% lateral drift): a) Front top left corner; b) Back top left corner

After the seventh load cycle to 0.35% lateral drift (7 mm), more cracking and spalling in the top right corner was visible. The propagation of cracking and concrete spalling is shown in Figure 4.39. The cracking to this point was small in size. In the positive direction, the peak load was 198.9 kN, the out-of-plane displacement was 2.94 mm, the column base anchorage slip measured -0.49 mm, the vertical displacement of the column was -0.23 mm, the strain in Gauge X3 measured -330 με, and the strain in Gauge X6 measured -3 με. In the negative direction, the peak load was -161.3 kN, the out-of-plane displacement was -1.20 mm, the column base anchorage slip measured 0.84 mm, the vertical displacement of the column was -0.08 mm, the strain in Gauge X3 measured -19 με, and the strain in Gauge X6 measured -286 με.

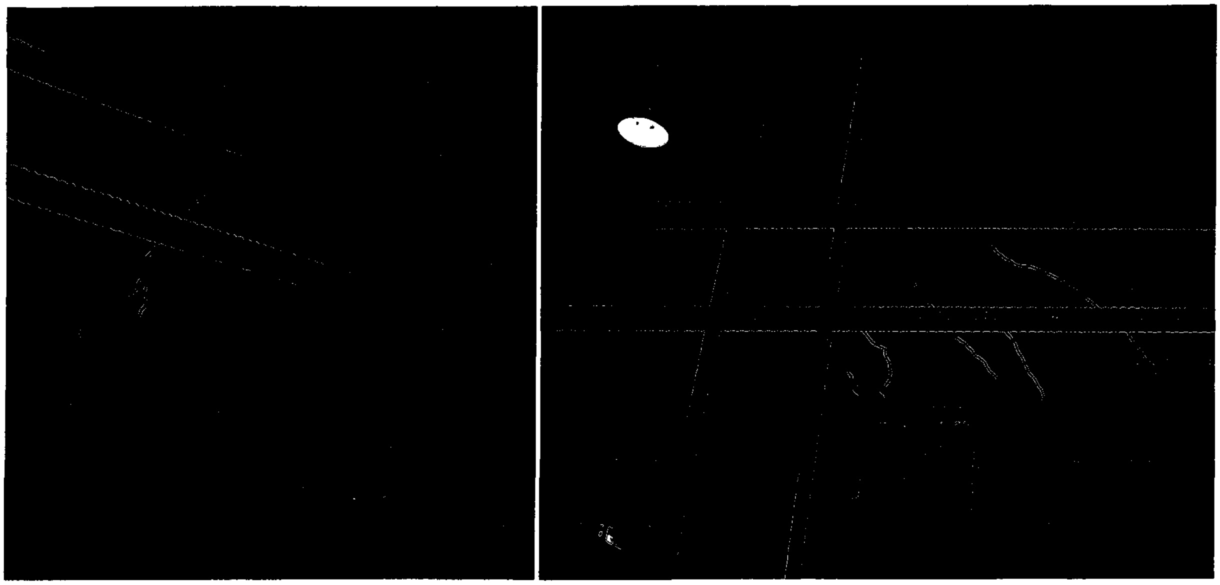

a) b)

Figure 4.39: Cracking and spalling in top right corner of BL-3R (0.30% lateral drift): a) Front top right corner; b) Back top right corner

Figures 4.40 and 4.41 show the re-opening of pre-existing flexural and shear cracks after the eighth load cycle to 0.40% lateral drift (8 mm) was completed. These figures also demonstrate the elongation of the cracks located in the corners of the frame. In the positive direction, the peak load was 228.5 kN, the out-of-plane displacement was 3.29 mm, the column base anchorage slip measured -0.55 mm, the vertical displacement of the column was -0.29 mm, the strain in Gauge X3 measured -391 με, and the strain in Gauge X6 measured -26 με. In the negative direction, the peak load was -198.8 kN, the out-of-plane displacement was -0.52 mm, the column base anchorage slip measured 0.95 mm, the vertical displacement of the column was 0.08 mm, the strain in Gauge X3 measured 18 με, and the strain in Gauge X6 measured -377 με.

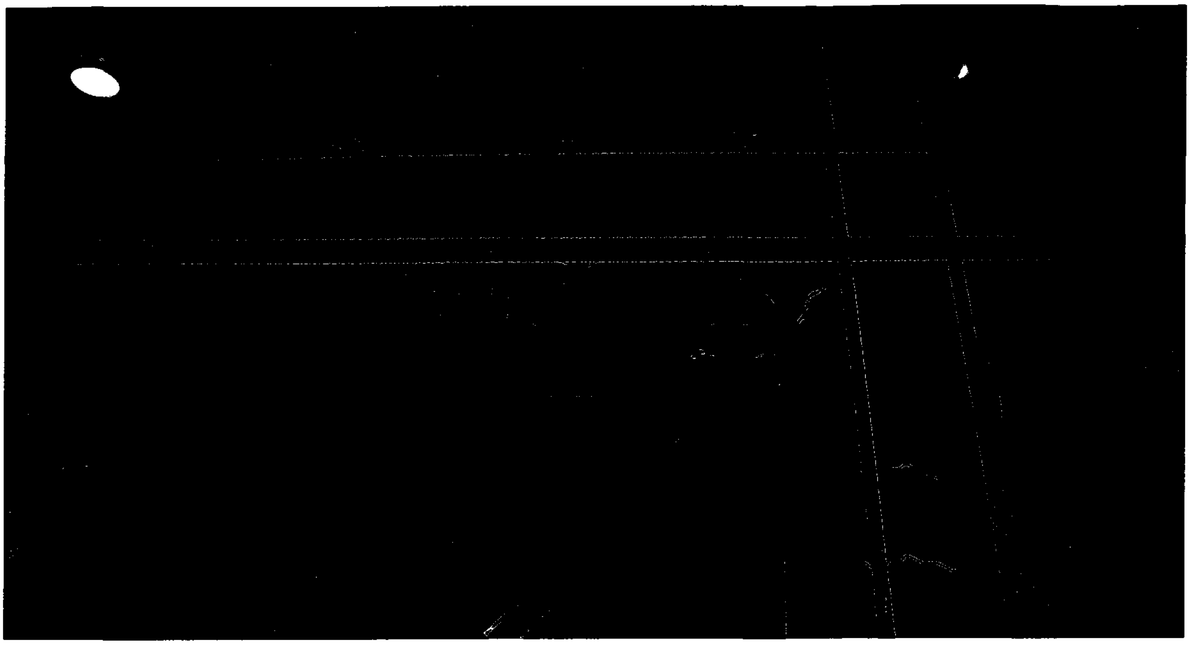

Figure 4.40: Flexural and shear cracks at the back left corner of BL-3R (0.40% lateral drift)

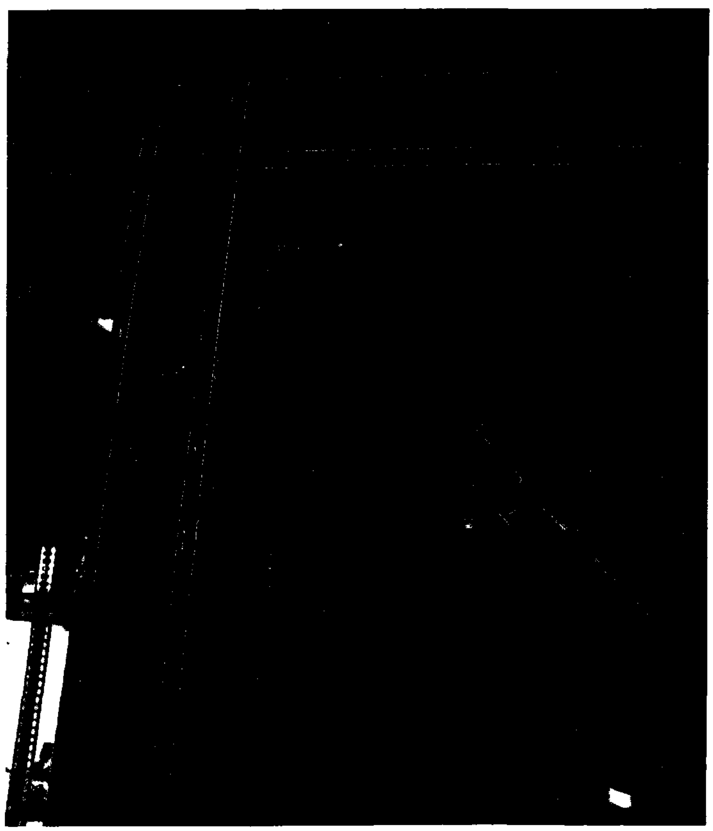

Figure 4.41: Flexural and shear cracks at the back right corner of BL-3R (0.40% lateral drift)

During the ninth load cycle, the imposed drift was 0.5% (10 mm) rather than 0.45% (9 mm) in the negative direction. This was the result of a problem encountered during the first repetition of loading at this drift level in the positive direction. The frame was accidentally pushed to 1.00% lateral drift (20 mm). Due to this jump in load, the foundation cracked in several places. Figure 4.42 provides a schematic of the cracks in the foundation, while Figure 4.43 provides photos of the cracking. The cracking in the foundation is denoted by the red lines. Beyond this load stage, the imposed drift in the negative direction continued to follow the initial loading protocol. In the positive direction, the frame was subjected to drifts exceeding 1.00% as given in the load-displacement response in Figure 4.29. The intent was to determine the maximum load and displacement capacity in the positive direction. The data collected beyond this point in the pushing (positive) direction was erratic due to the damage sustained in the foundation.

Most of the cracks on the frame after this load cycle were small and less than 1 mm in width. New shear cracks were evident in the top corners of the frame as illustrated in Figures 4.44 to 4.46. Pre-existing shear cracks in the beam are also evident in Figure 4.44 and pre-existing flexural cracks in the columns as shown in Figure 4.47 reopened. When the frame was displaced 20 mm in the positive direction, the peak load was 482.8 kN, the out-of-plane displacement was 7.32 mm, the column base anchorage slip measured -1.00 mm, the vertical displacement of the column was -0.39 mm, the strain in Gauge X3 measured -1142 $\mu\varepsilon$, and the strain in Gauge X6 measured -84 $\mu\varepsilon$. When the frame displaced 10 mm in the negative direction, the peak load was -301.3 kN, the out-of-plane displacement was 0.63 mm, the column base anchorage slip measured 1.22 mm, the vertical displacement of the column was 0.29 mm, the strain in Gauge X3 measured -309 $\mu\varepsilon$, and the strain in Gauge X6 measured -706 $\mu\varepsilon$.

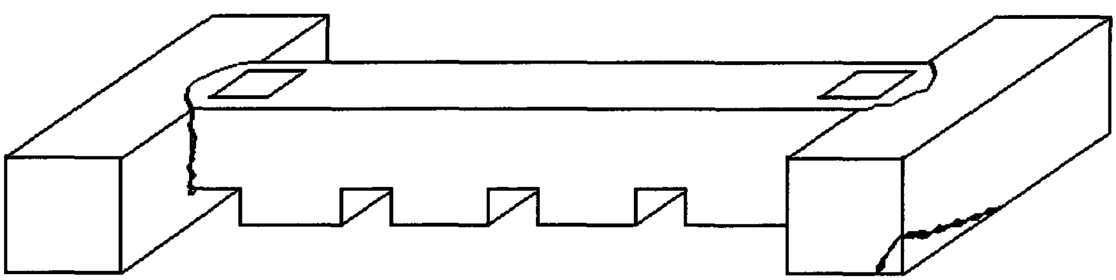

Figure 4.42: Schematic representation of the cracking in the foundation in BL-3R (0.50% lateral drift)

a) I-junction of the foundation away from the actuator

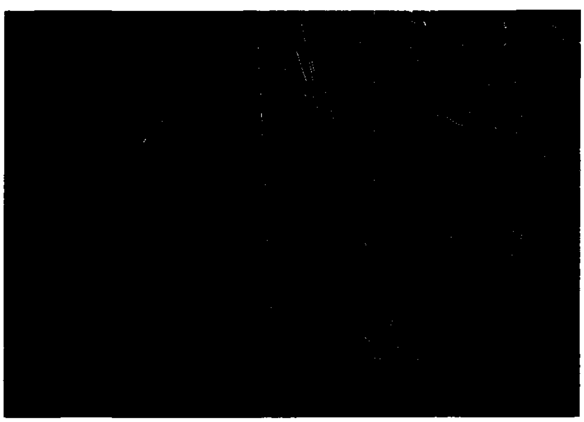

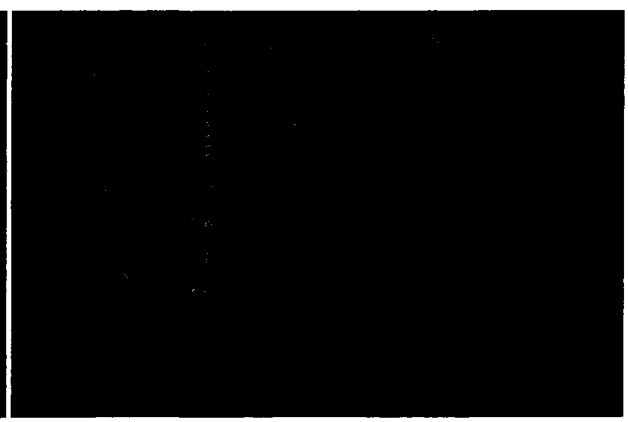

b) I-junction of the foundation at the actuator side   *c) Bottom of foundation away from the actuator*

Figure 4.43: Cracking in the foundation in BL-3R (0.50% lateral drift)

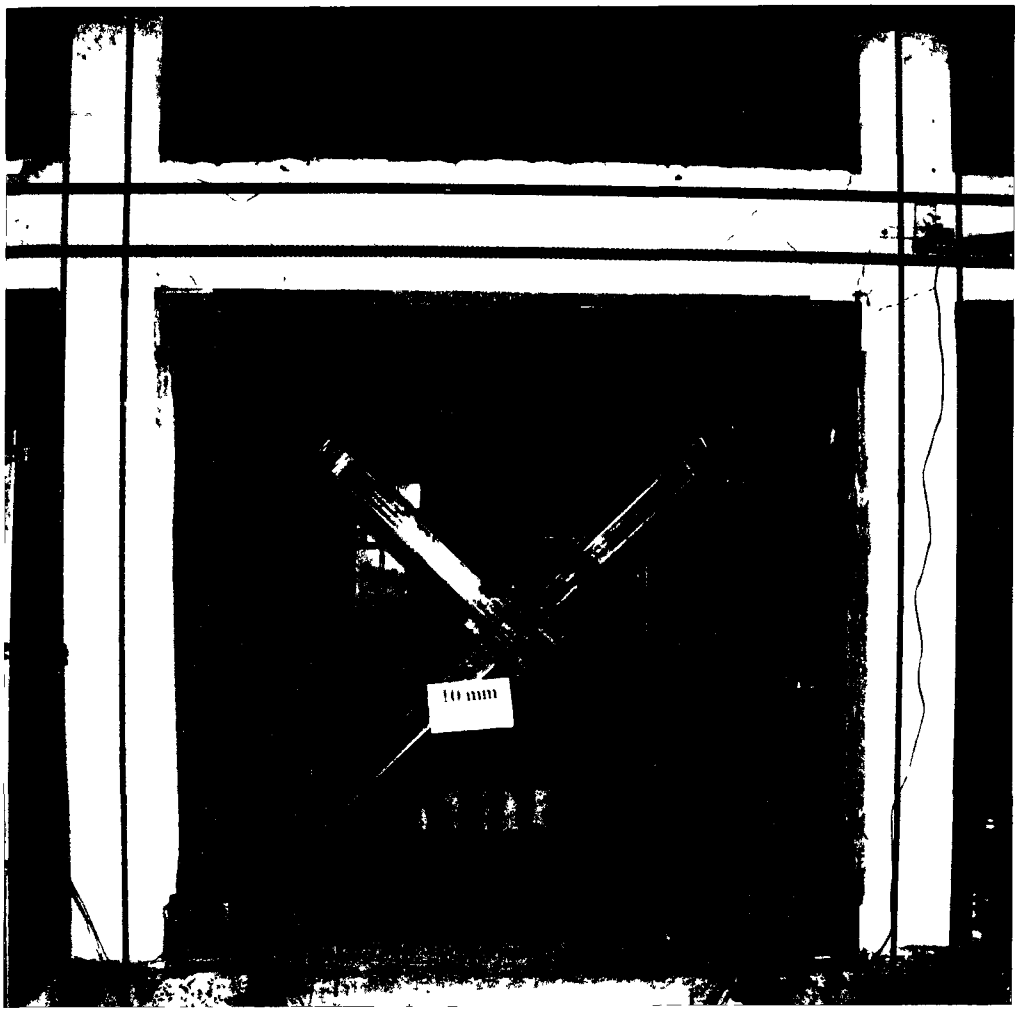

Figure 4.44: Cracking in Frame BL-3R (0.5% lateral drift)

Figure 4.45: Back of the top left corner in BL-3R (0.5% lateral drift)

Figure 4.46: Back top right corner in BL-3R (0.5% lateral drift)

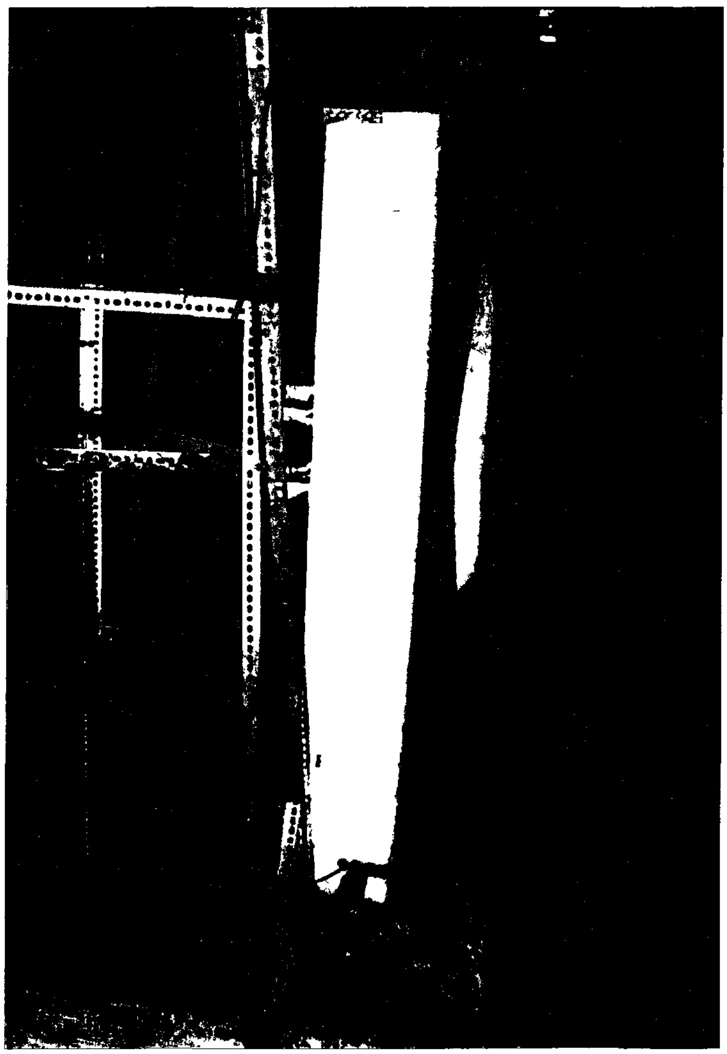

Figure 4.47: Re-opening of flexural cracks in column of BL-3R (0.5% lateral drift)

Following the tenth load cycle to 0.55% lateral drift (11 mm), the cracks were still slightly less than 1 mm wide and are shown in Figure 4.48. A small portion of concrete spalled off in one of the corners of the frames. Many of the pre-existing cracks reopened in the columns (Figure 4.49). In the negative direction, the peak load was -324.1 kN, the out-of-plane displacement was 0.76 mm, the column base anchorage slip measured 1.27 mm, the vertical displacement of the column was 0.48 mm, the strain in Gauge X3 measured -328 $\mu\varepsilon$, and the strain in Gauge X6 measured -765 $\mu\varepsilon$.

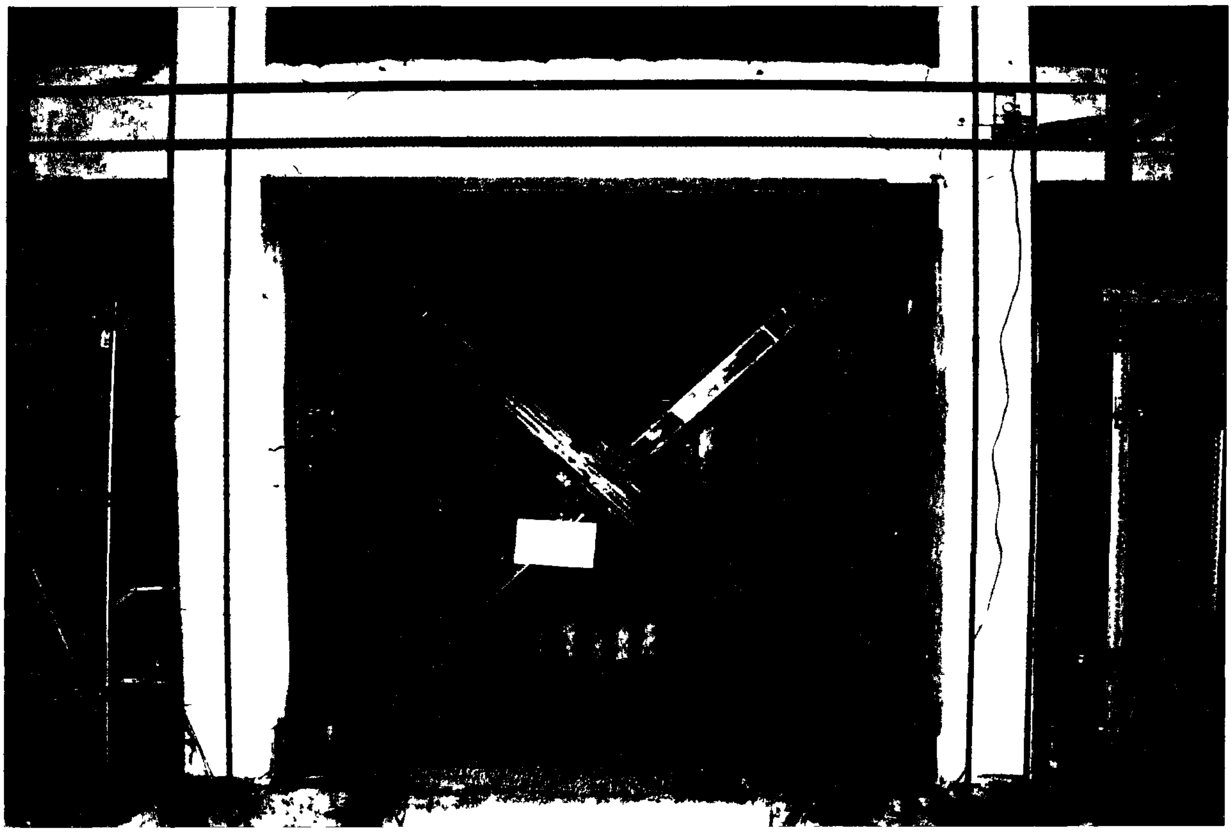

Figure 4.48: Cracking in Frame BL-3R (0.55% later drift)

a) *b)*

Figure 4.49: Re-opening of flexural cracks in the columns of BL-3R (0.55% lateral drift): a) Left column; b) Right column

The final load cycle was the eleventh after displacing to a drift of 0.60% (12 mm). The first displacement was in the negative direction. When the frame was displaced in the positive direction, the response indicated significant out-of-plane twisting. The frame behavior was controlled by the out-of-plane response. The out-of-plane displacements of the frame are evident in Figure 4.50. Figure 4.32 also demonstrates that the out-of-plane displacement was greater than the LVDT could measure. After having completed the three-12 mm cycles in the negative direction, the frame was then displaced in the negative direction to failure, which occurred in the foundation as depicted in Figures 4.54 and 4.55. The last loading was intended to determine the maximum capacity of the retrofitted frame and to determine the mode of failure. There were no visible signs that the steel frame reached its load carrying capacity (Figure 4.53). This was also evident in the recorded strains of the steel braces. The largest strain measured was less than -3300 $\mu\varepsilon$, which is significantly less than the strain (7000 $\mu\varepsilon$) corresponding to the yielding strength determined from coupon samples. Figure 4.51 shows vertical cracks formed at the base of the left column due to the out-of-plane displacements during the last loading in the positive direction. The top of the left column also cracked during the same displacement (Figure 4.51). Additional spalling occurred at the back top right corner as illustrated in Figure 4.52, which also shows an increase of shear cracks in the corners of the frame. Larger cracks were also observed and measured. The left column base anchorage slip crack was 6.4 mm, a crack on the left column at the base measured 3.4 mm, a 5.8 mm crack was noted on the beam, a 3.2 mm crack was measured at the top of the right column, and the right column base anchorage slip crack was 6.1 mm.

The last load cycle of 0.60% lateral drift in the negative direction generated a peak load of -401.1 kN, the out-of-plane displacement was -0.06 mm, the column base anchorage slip measured 1.27 mm, the vertical displacement of the column was 0.58 mm, the strain in Gauge X3 measured -388 $\mu\varepsilon$, and the strain in Gauge X6 measured -963 $\mu\varepsilon$.

In the positive direction, the last displacement measured 64 mm, the corresponding peak load was 598.9 kN, the out-of-plane displacement exceeded 15.71 mm, the column base anchorage slip measured -3.17 mm, the vertical displacement of the column was -0.48 mm, the strain in Gauge X3 measured -1569 $\mu\varepsilon$, and the strain in Gauge X6 measured -177 $\mu\varepsilon$.

When the frame was displaced (39 mm) in the negative direction to failure, the peak load was -707.1 kN, the out-of-plane displacement exceeded 13.3 mm, the column base anchorage slip measured 1.78 mm, the vertical displacement of the column was 1.76 mm, the strain in Gauge X3 measured -599 $\mu\varepsilon$, and the strain in Gauge X6 measured -2332 $\mu\varepsilon$. Table 4.2 summarizes the experimental results of the retrofitted frame, BL-3R.

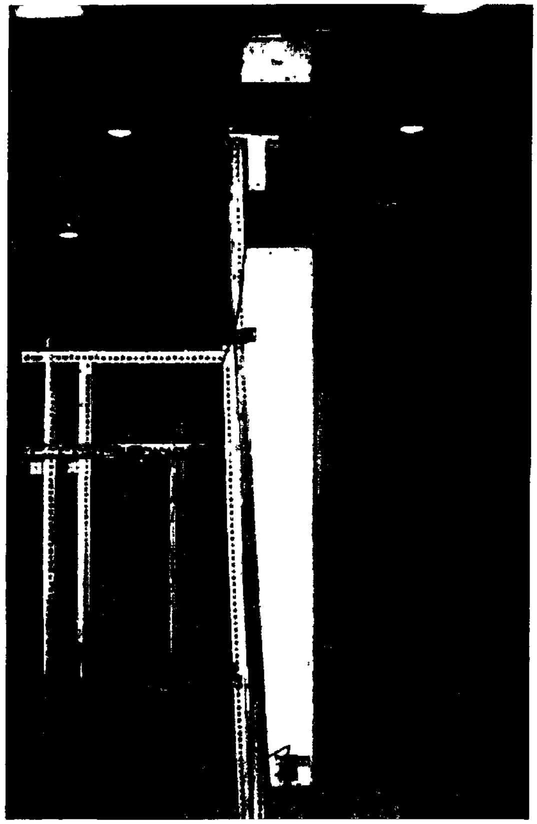

Figure 4.50: Out-of-plane twisting of BL-3R (0.60% lateral drift)

Figure 4.51: Cracking in BL-3R (0.60% lateral drift)

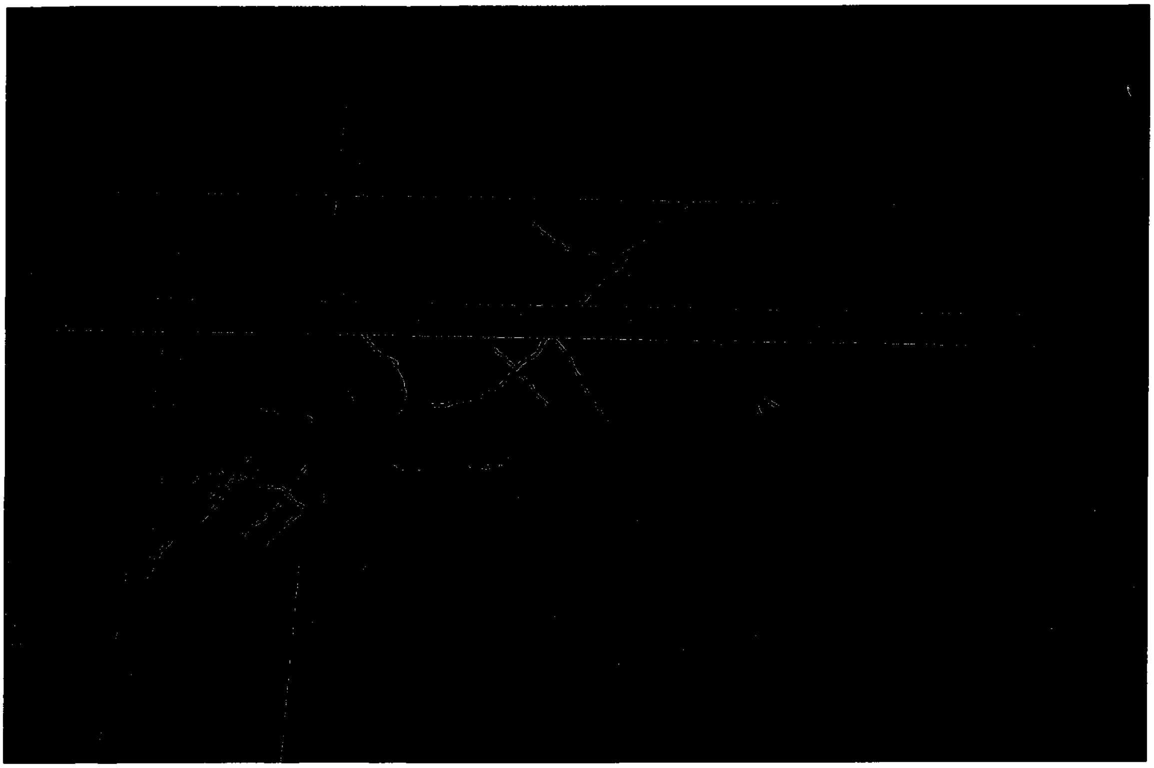

Figure 4.52: Cracking at the back top right corner of BL-3R (0.60% lateral drift)

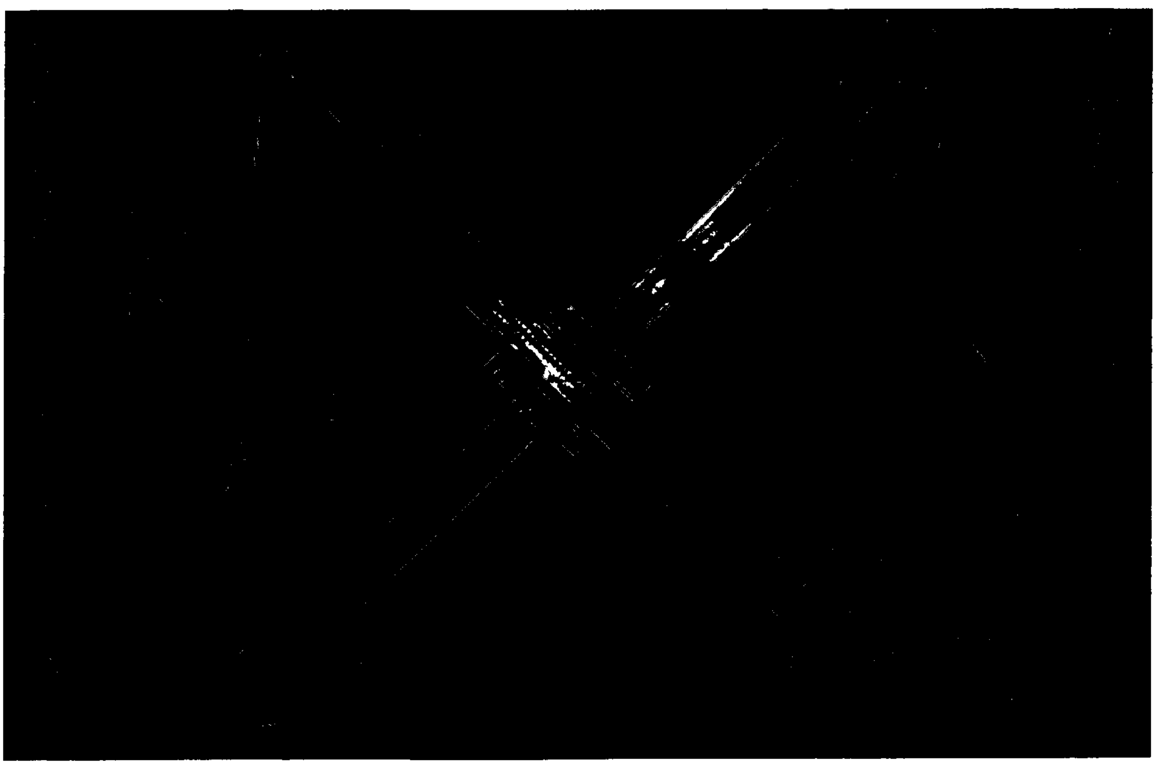

Figure 4.53: Steel bracing of BL-3R (0.60% lateral drift)

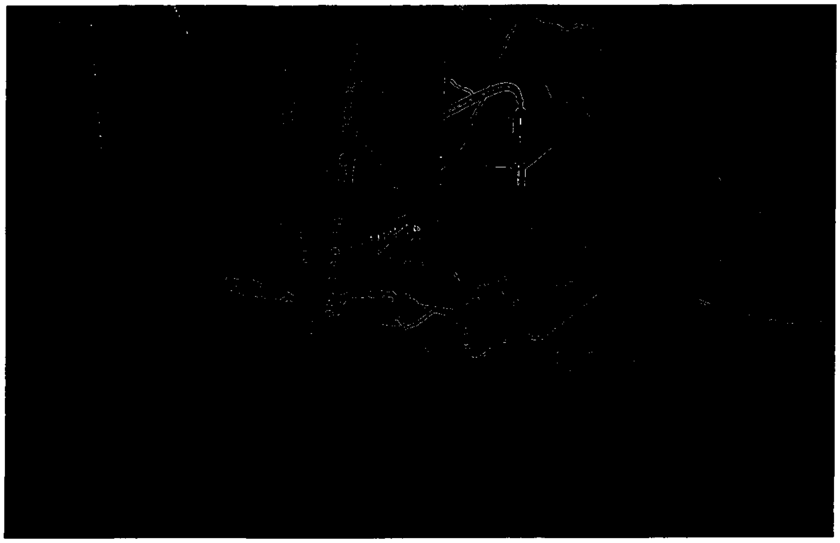

Figure 4.54: Foundation failure of BL-3R (0.60% lateral drift)

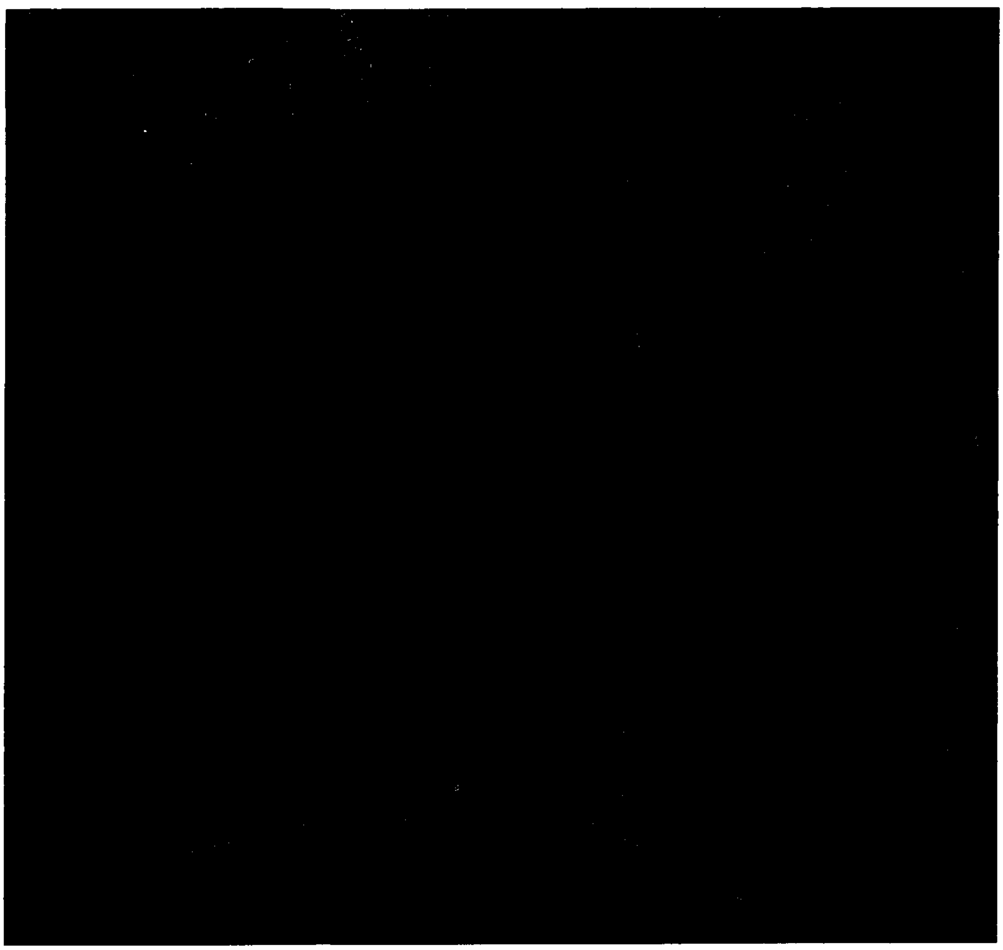

Figure 4.55: I-junction of the foundation, away from the actuator, of BL-3R (0.60% lateral drift)

Table 4.2: Summary of Experimental Results for BL-3R

Positive Direction					Negative Direction				
Lateral Load (kN)	Lateral Disp. (mm)	Base Slip (mm)	Vertical Disp. (mm)	Out-of-Plane Disp. (mm)	Lateral Load (kN)	Lateral Disp. (mm)	Base Slip (mm)	Vertical Disp. (mm)	Out-of-Plane Disp. (mm)
46.9	1	-0.13	-0.04	0.52	-13.9	-1	0.12	-0.06	-0.17
78.0	2	-0.24	-0.04	0.81	-25.4	-2	0.23	-0.06	-0.42
99.0	3	-0.32	-0.14	1.54	-39.8	-3	0.40	-0.21	-0.35
118.1	4	-0.35	-0.16	2.18	-67.2	-4	0.55	-0.23	-1.00
142.3	5	-0.41	-0.19	2.46	-101.6	-5	0.66	-0.21	-1.13
168.2	6	-0.45	-0.23	2.65	-132.4	-6	0.76	-0.16	-1.25
199.0	7	-0.49	-0.23	2.94	-161.3	-7	0.84	-0.08	-1.20
228.5	8	-0.55	-0.29	3.29	-198.8	-8	0.95	0.08	-0.52
262.6	9	-0.60	-0.29	3.65	-301.3	-10	1.22	0.29	0.63
482.8	21	-1.00	-0.39	7.32	-324.1	-11	1.27	0.49	0.76
					-401.1	-12	1.27	0.58	-0.06

Chapter 5

5 Analytical Program

5.1 General

Program VecTor2 (Wong and Vecchio, 2002) was utilized to perform the analytical component of this research. VecTor2 is a nonlinear finite element analysis (NLFEA) program for the analysis of two-dimensional reinforced concrete membrane structures subjected to quasi-static load conditions. VecTor2 uses a smeared, rotating-crack formulation for reinforced concrete based on the Modified Compression Field Theory and the Disturbed Stress Field Model. The program's solution algorithm is based on a secant stiffness formulation using a total-load iterative procedure.

Incorporated into the program's analysis algorithms are second-order effects such as compression softening due to transverse cracking, tension stiffening, shear slip along crack surfaces, and other mechanisms important in accurately representing the behaviour of cracked reinforced concrete structures. Recent enhancements include provisions for the consideration of: nonlinear expansion and confinement, cyclic loading, effects of slip distortion on element compatibility relations, bond slip of rebars, and application to the analysis of repaired or rehabilitated structures. A wide range of behaviour models are available for representing each of the various constitutive responses and mechanisms considered.

The analysis approach taken by VecTor2 is to use many low-powered elements in representing a structural element. Hence, the element library is limited to a 4-node rectangular or quadrilateral element (8 DOF), a 3-node triangular element (6 DOF), and a 2-node truss bar element (4 DOF). Reinforcement can be modeled either as smeared within the solid elements, or as discrete bars using the truss elements. For modeling mechanisms relating to bar slip and adhesion loss, a 2-node bond link element and a 4-node contact element are also available.

Analytical Program

The default constitutive models of Program VecTor2 were selected for the response of the concrete. The pre-peak compressive response of concrete in compression was modeled with Hognestad's Parabola, while the post-peak was based on the Modified Park-Kent Model. The hysteretic response of the concrete in compression and tension were based on the nonlinear model with plastic offsets. Compression softening, which accounts for the reduction in compressive strength and stiffness due to co-existing transverse tensile straining was modeled with Vecchio's 1992-A model (Vecchio and Collins 1993). This model considers both strength and strain softening. Tension stiffening was modeled by the modified Bentz model (Vecchio 2000b), which determines the tensile stresses that exist in concrete between cracks due to the bond action between the reinforcement and the concrete. This model accounts for the effect on surrounding elements not containing reinforcement. The post-cracking tensile stresses present in plain concrete, known as tension softening, was modeled with a linear descending response after cracking (Vecchio 2000b). This phenomenon plays an important role in situations where an element has little to no reinforcement, but still contributes to the strength and stiffness of the structure. The lateral expansion of concrete caused by internal micro cracking, which increases as the compressive stresses increase, was modeled with a variable Poisson's ratio based on the work of Kupfer (Kupfer *et al.* 1969). In addition, the Kupfer/Richart confined strength model (Vecchio 1992) accounted for the strength enhancement of concrete in compression due to tri-axial stress conditions. This model is an extension of the formulation presented by Kupfer *et al.* (1969), which accounts for strength enhancement in a bi-axial compression state, to include the tri-axial effect of reinforcement that confines the lateral expansion of concrete in the out-of-plane direction (Richart *et al.* 1928). The cracking strength of concrete which can differ from the concrete tensile strength due to co-existing transverse compressive stresses was considered with the Mohr-Coulomb stress criterion. Consideration was also given to the width of cracks, which can cause a reduction in the compressive stresses when crack widths exceed a specified limit (Vecchio 2000a); a limit of 20% of the aggregate size was used for the crack width check. The crack shear-slip deformations, which represent the main compatibility feature of the DSFM, were evaluated with the Vecchio-Lai model (Vecchio and Lai 2004).

For the reinforcement, the default constitutive models were also chosen. The Seckin Model (Seckin 1981) was selected to capture the hysteretic response of steel reinforcement. The model includes a linear elastic region followed by a yield plateau and strain hardening. The unloading and reloading response includes the Bauschinger effect (Vecchio 1999). Dowel action of the reinforcement, which arises from crack slip occurring transversely to the axes of the reinforcement, was considered using the

Tassios crack-slip model (Vintzeleou and Tassios 1987, He and Kwan 2001). Note that the steel braces were based on a bi-linear response. The intent was to capture the initial loading response followed by a reduced stiffness which was ultimately governed by the buckling capacity.

Both the repaired frame and the retrofitted frame were modeled using VecTor2 as fully repaired with no residual damage. A full description of the modeling procedure is provided in this section as well as the analytical results.

5.2 Modeling

5.2.1 Repaired Frame

The frame was modeled to the exact dimensions as the laboratory specimen including the base foundation as described in Chapter 3. Figure 5.1 shows the repaired frame finite element model that was created for analysis. This model contains a total of 2344 rectangular elements, 18 triangular elements, and 698 truss elements. The triangular elements were necessary due to geometric constraints between the concrete elements and the truss bar elements. The model was defined with 12 different zones for the concrete and 44 different truss bars for the reinforcement. The large number of concrete zones was used to describe differences in the smeared transverse reinforcement, concrete cover, and thickness of the elements. The different truss bars were employed to model the development length of the longitudinal reinforcing steel.

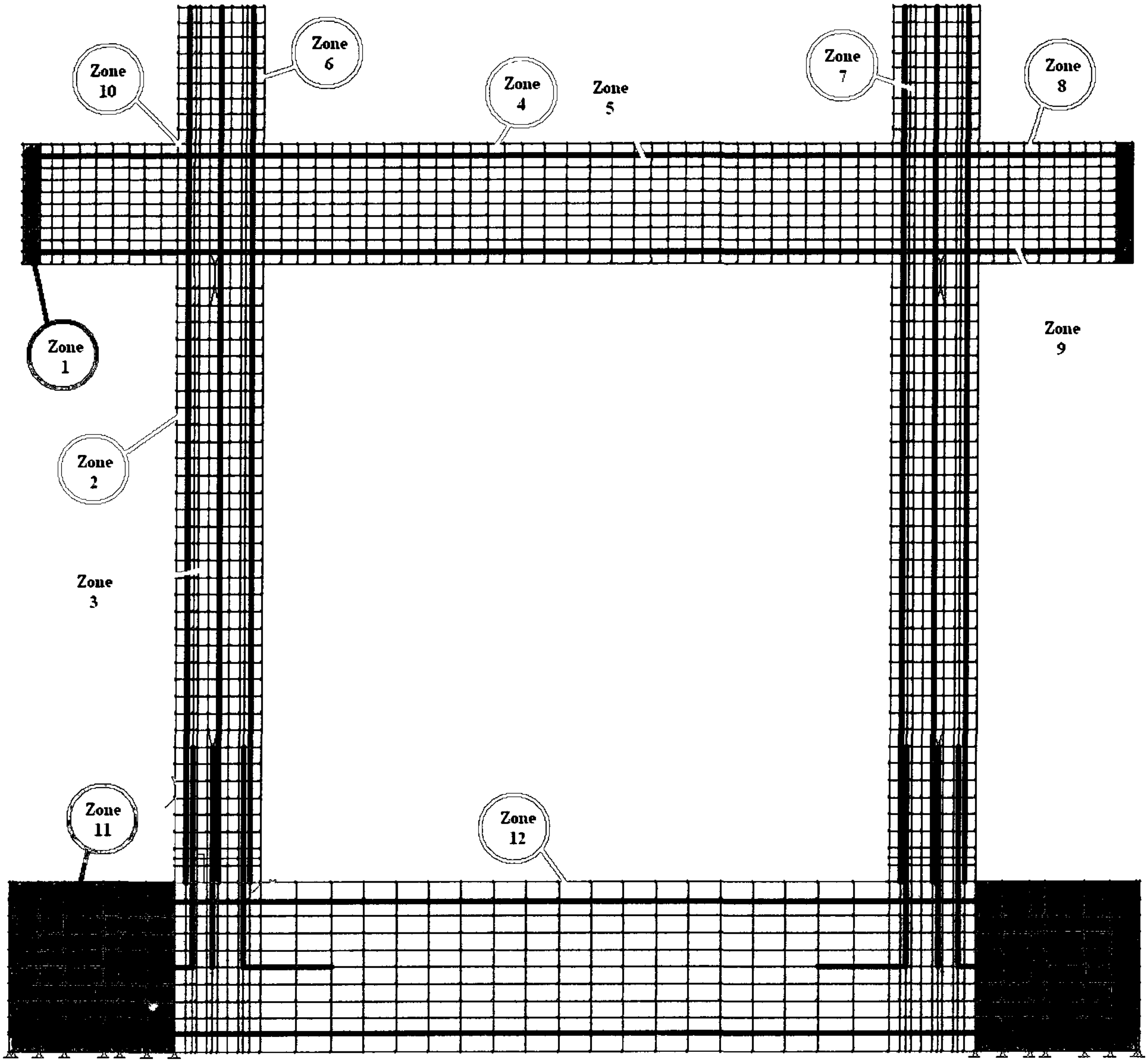

Figure 5.1: Finite element model of the repaired frame

One of the objectives was to develop a simple numerical model. The concrete strength was assumed the same throughout the entire frame; 32.1 MPa as provided by Shalouf (2005). An extra layer of 50 mm was added at each end of the loading beam, represented as zone 1 (brown ☐) in Figure 5.1, to simulate the large steel loading plates that were used during testing to transfer the lateral load from the actuator to the frame. This layer also prevented local crushing of the concrete in the middle of the beam where the lateral displacement was applied during the analysis. The properties of this concrete material were defined with compressive and tensile strengths of 1000 MPa. The tensile strength of the other layers of concrete was reduced to 0.1 MPa to account for cracking in the members that was present from the initial testing of the frames. Therefore, due to the cracking, it was assumed that the concrete in the frames was not capable of resisting tensile stresses. Note that a value of zero in the VecTor2 input files is reserved for the default tensile strength which the program calculates from the concrete compression strength that is provided. The transverse reinforcement was smeared in the concrete elements representing the core of the members, thus the concrete cover layers for the columns (zone 2 ■, zone 6 ■) and beam (zone 4 ■, zone 8 ■) contained no steel reinforcement. The joints, zone 10 (green ■), did not have any smeared tie or stirrup reinforcing steel. The percentage of smeared reinforcement in the out-of-plane direction was determined by the area of the transverse reinforcement legs extending out-of-plane divided by the width of the member (less the cover) and the spacing of the transverse reinforcement. The percentage of smeared transverse reinforcement in the in-plane direction was determined by the area of transverse reinforcement divided by the thickness of the member and the spacing of the transverse reinforcement. Due to the large amount of steel and the lack of information, the base foundation was assumed to contain smeared reinforcement throughout the foundation.

The longitudinal reinforcing steel was modeled with discrete truss bars and placed at the center line of the actual position in the test specimens. Therefore, the longitudinal bars were positioned at a distance equal to the concrete cover plus half the diameter of the bar (33 mm) from the concrete face for the longitudinal reinforcement at the edges of the beam and columns. Thus the concrete cover in the model was also 33 mm in width. At the splice location at the bottom of the column, the hooked bars extending from the foundation and the longitudinal reinforcement that terminated at the base of the column were separated by a 1 mm gap to differentiate between the two reinforcement components in the columns. Starting from the left side of the column, the three No. 15 bars (600 mm^2) were positioned 33 mm from the face of the column, the two No. 15 bars (400 mm^2) in the middle of the column were placed at 125 mm, and the other three No. 15 bars (600 mm^2) were placed at 217 mm from the left face. The first three No. 15 hooked bars (600 mm^2) were placed at 50 mm from the left face. The two middle No. 15 hooked bars (400 mm^2) were placed 108 mm from the left face. The last three No. 15 hooked bars (600 mm^2) were placed 200 mm from the left face. The No. 15 M bars in the beam were placed 33 mm away from the concrete face. The top truss bar in the beam represents three No. 15 bars (600 mm^2) to a distance of 750 mm from the face of the columns; thereafter, the truss bar represents two No. 15 bars (400 mm^2). The bottom truss bar represents two continuous No. 15 bars (400 mm^2). Two additional truss bars were used to model the reinforcement in the foundation, each representing five No. 25 bars (2500 mm^2). The truss bars in the repaired frame model had yield strength of 495 MPa, ultimate strength of 525 MPa, modulus of elastic of 200 000 MPa, strain hardening modulus of 10 000 MPa, and strain at the onset of strain hardening of 10 millistrain. The concrete zones with smeared reinforcement are described in Table 5.1. Note that the direction of 361° indicates out-of-plane reinforcement in the model.

Table 5.1: Description of the concrete zones in the finite element model

Member/ Zone	Thickness (mm)	Reinforcement					
		#	Direction (°)	Ratio (%)	d_b (mm)	f_y (MPa)	f_u (MPa)
Column Zone 3	250	1	0	0.2027	6.35	500	525
		2	361	0.2754	6.35	500	525
Beam Zone 5	250	1	90	0.2027	6.35	500	525
		2	361	0.1784	6.35	500	525
Beam Zone 9	250	1	90	0.2027	6.35	500	525
		2	361	0.1784	6.35	500	525
Column Zone 7 ■	250	1	0	0.2027	6.35	500	525
		2	361	0.2754	6.35	500	525
Foundation Zone 12 ■	480	1	90	0.2778	10	485	525
		2	361	0.2667	10	485	525
Foundation Zone 11 ■	1320	1	0	0.2667	10	485	525
		2	90	0.2778	10	485	525
		3	361	1.0000	25.2	485	525

The development lengths of the longitudinal reinforcement in the columns and beam were modeled by reducing the area of the reinforcement to correspond to the strength of bar over the development length. Figure 5.2 demonstrates that the effective area was based on a linear strength development. At the terminated end of the reinforcement, the effective area of the steel was zero. The effective area of the steel linearly increased, reaching the full area (full yield strength) at the development length of 654 mm for the 15 M reinforcing bar.

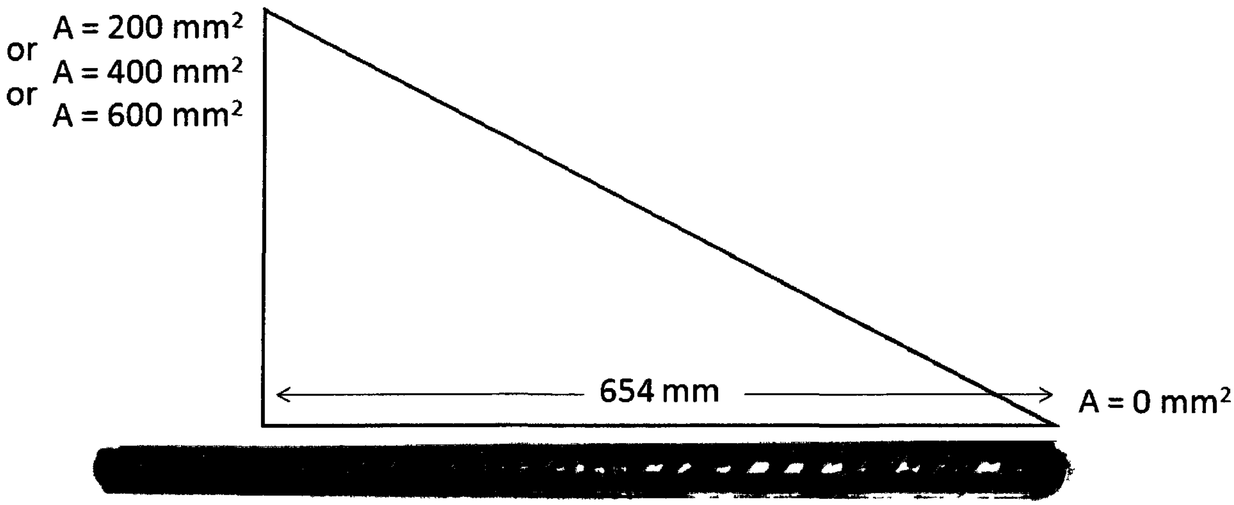

Figure 5.2: Effective area of the reinforcing steel over the development length

Appendix C provides details of the calculations for the effective area over the development length. The effective areas were divided in 50 mm sections. Each section was assigned its own averaged area. The reinforcement in the splice region of the column, including the hooked bars, and the terminated reinforcement at the top of the beam were subjected to the reduction of area over the development length. The reduction in area was not applied to the portion of the beam extending beyond the columns or the extension of the columns above the loading beam since these areas were not critical in the behaviour of the frame. Table 5.2 lists the effective area of reinforcement that was assigned to each section of the three locations containing different numbers of 15 M reinforcing bars. This included the single 15M bar that was terminated at the top of the beam, the three-15 M bars located at the edges of the columns, and the two-15 M bars located in the middle of the columns. Note that the top truss bar in the beam was modeled with the effective area in addition to the two continuous 15 M bars at the same level. Therefore, the area of steel assumed in the numerical model over the development length of this truss bar are the values listed in Table 5.2 for one-15 M bar plus the 400 mm^2 of the other two-15 M bars.

Table 5.2: Development length area distribution

Sections (mm)	Area of steel (mm^2)		
	Beam 1 No. 15 bar A = 200 mm^2	Column 2 No. 15 bars A = 400 mm^2	Column 3 No. 15 bars A ≈ 600 mm^2
0 – 50	7.7	15.4	23.1
50 – 100	23.0	46.2	69.2
100 – 150	38.5	76.9	115.4
150 – 200	53.8	107.7	161.5
200 – 250	62.3	138.5	207.7
250 – 300	84.6	169.2	253.8
300 – 350	100.0	200.0	300.0
350 – 400	115.4	230.8	346.2
400 – 450	130.8	261.5	392.3
450 – 500	146.2	292.3	438.5
500 – 550	161.5	323.1	484.6
550 – 600	176.9	353.8	530.8
600 – 650	192.3	384.6	576.9

The loading of the frame included nodal loads to impose the gravity load on the columns and support displacements to impose the lateral load on the top loading beam. The lateral load was applied as a support displacement at the middle of the beam and at the face of the extended portions beyond the columns. The lateral displacements were applied to simulate a pushing motion similar to the laboratory testing. To simulate the action of the actuator pulling the frame in the laboratory, the support displacements were applied on the right side of the beam; while the pushing motion of the actuator on the frame was replicated by applying support displacements to the left side of the beam. The 400 kN gravity loading of each column was spread evenly across the top of each column as nodal loads. The loading program was similar to that used in the testing. Three repetitions were applied at each displacement level. The displacement was increased by 2 mm until 10 mm of lateral displacement. Thereafter, the displacements were incremented by 5 mm until failure.

5.2.2 Steel Bracing Retrofitted Frame

The retrofitted frame was modeled similar to the repaired frame with the exception of the steel X-bracing. To define the X-bracing retrofit, an additional concrete zone and an additional truss bar were added. Figure 5.3 illustrates the finite element model that was created for the retrofitted frame. This model contains a total of 2382 rectangular elements, 56 triangular elements, and 710 truss elements. The model is defined by 13 different concrete zones and 45 different truss bars.

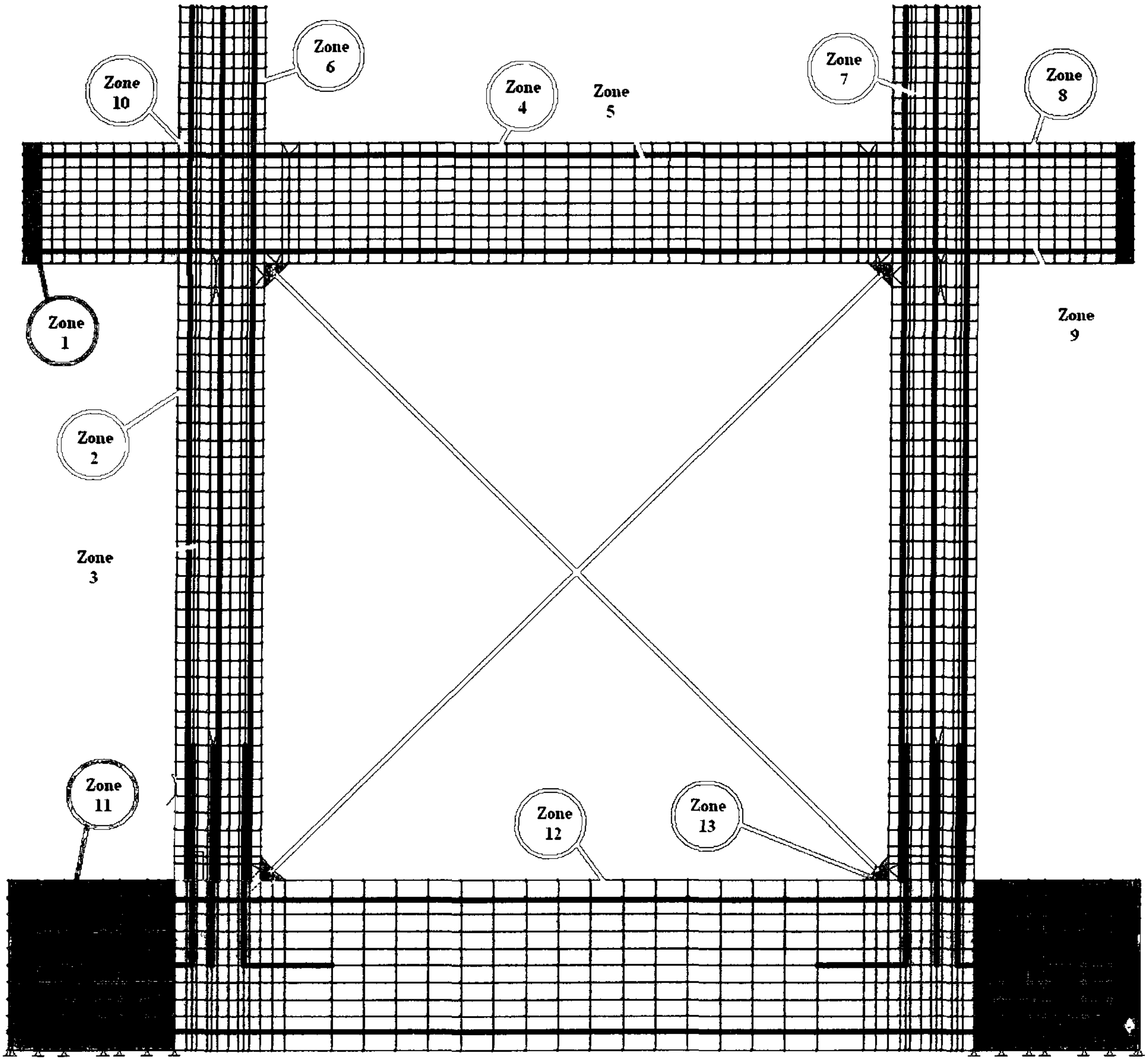

Figure 5.3: Finite element model of the retrofitted frame

Concrete zone 13 (bright green □) as shown in Figure 5.3 was added at the interior corners of the frame to represent the steel angle assembly that was used to ensure the steel bracing remained in place and to distribute the compressive stresses experienced by the HSS section to the concrete, thus eliminating local concrete crushing. These zones were modeled with the same width as the steel angle pieces (250 mm), and were assigned a concrete compressive strength of 1000 MPa and a minimal tensile strength of 0.1 MPa. Note, that this zone would only be subjected to compressive stresses imposed by the diagonal braces. Furthermore, the tensile strength was reduced to ensure the corners of the columns were not stiffened and strengthened by the assembly. The length and height were equal to the length and height of the 45° cut of the square hollow section (72 mm). The two new diagonal truss bars (■) were modeled as compression only and aligned with the interior corners of the beam-column joints. The properties assigned to the braces are listed in Table 5.3 and is represented in Figure 5.4. Detailed calculations for the stress-strain model are provided in Appendix C. The relationship was based on the theoretical buckling strength of the steel brace, equal to approximately 252 MPa. Thus, the stress-strain model in Figure 5.4 is terminated at this stress level to simulate buckling. Note that the response assumes a bi-linear model to best represent the stress-strain response of the steel coupon test. The first linear response is assumed to represent the elastic loading curve to approximately 150 MPa, while the subsequent linear response represents a post-elastic response leading to the buckling capacity. Figure 5.5 represents how VecTor2 interprets the steel properties provided by the user. The values given for the yield strength, ultimate strength, strain hardening modulus, and strain hardening strain were selected to represent the bi-linear response of Figure 5.4.

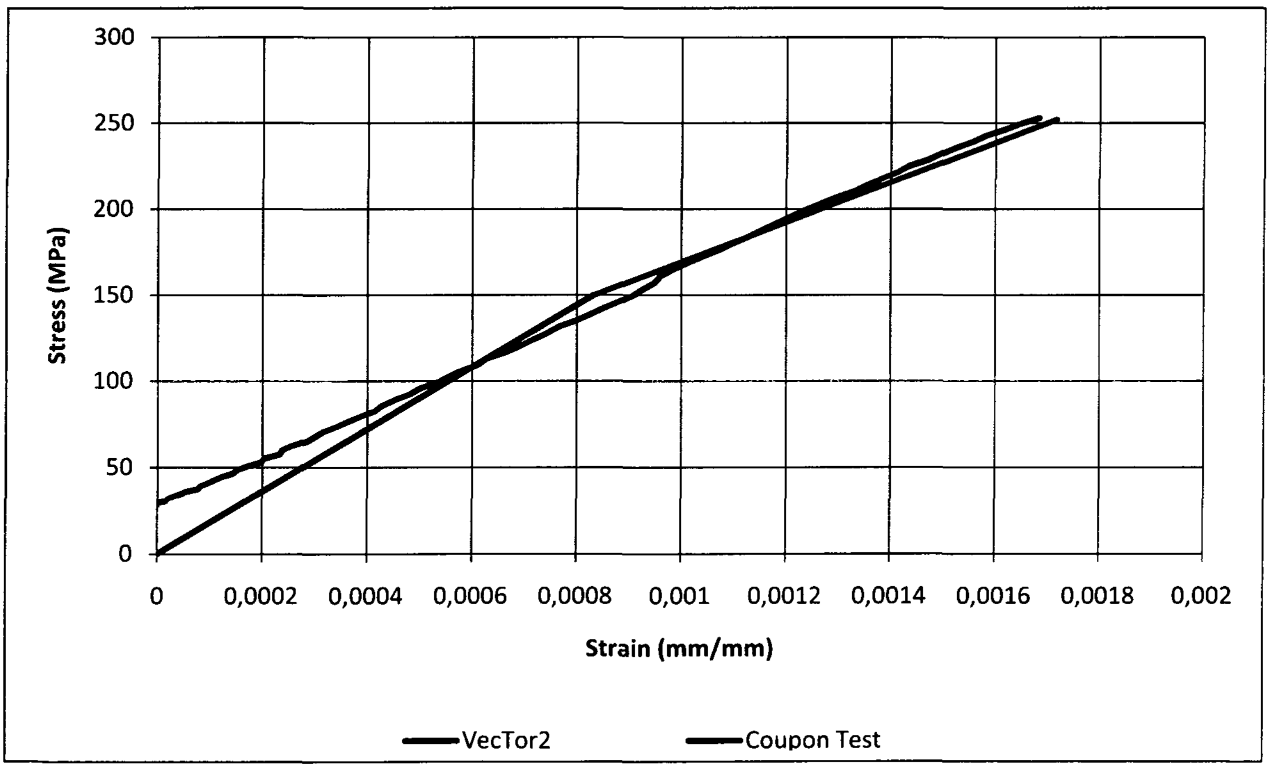

Figure 5.4: Representation of the properties provided in VecTor2 for the steel bracing truss bars

Table 5.3: Properties provided in VecTor2 for the steel bracing truss bars

Properties	Values
Cross-Sectional Area (mm^2)	3280
Reinforcement Diameter, d_b (mm)	102
Yield Strength, f_y (MPa)	150
Ultimate Strength, f_u (MPa)	252
Elastic Modules, E_s (MPa)	180 000
Strain Hardening Modulus, E_{sh} (MPa)	115 385
Strain Hardening Strain, ε_{sh} (mε)	0.834

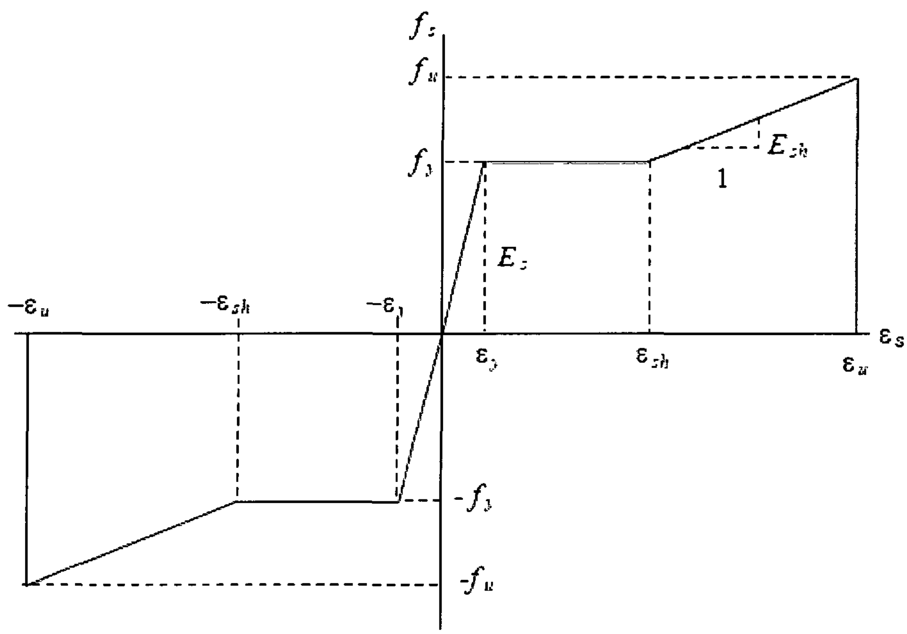

Figure 5.5: VecTor2 ductile steel stress-strain response (Wong and Vecchio, 2002)

Loading of the retrofitted frame was similar to the repaired frame. Nodal loads and support displacements were used. The lateral load was applied as a support displacement at the middle of the beam, while the 400 kN gravity loading was distributed across the top of each column as nodal loads. The loading program included three repetitions applied at each displacement level and the displacements were increased by 2 mm until failure.

5.3 Analytical Results

5.3.1 Repaired Frame

The analytical results for the repaired frame are presented in this section. The lateral load versus the lateral displacement response is shown in Figure 5.6. The predicting cracking and displacements at failure are shown in Figure 5.7.

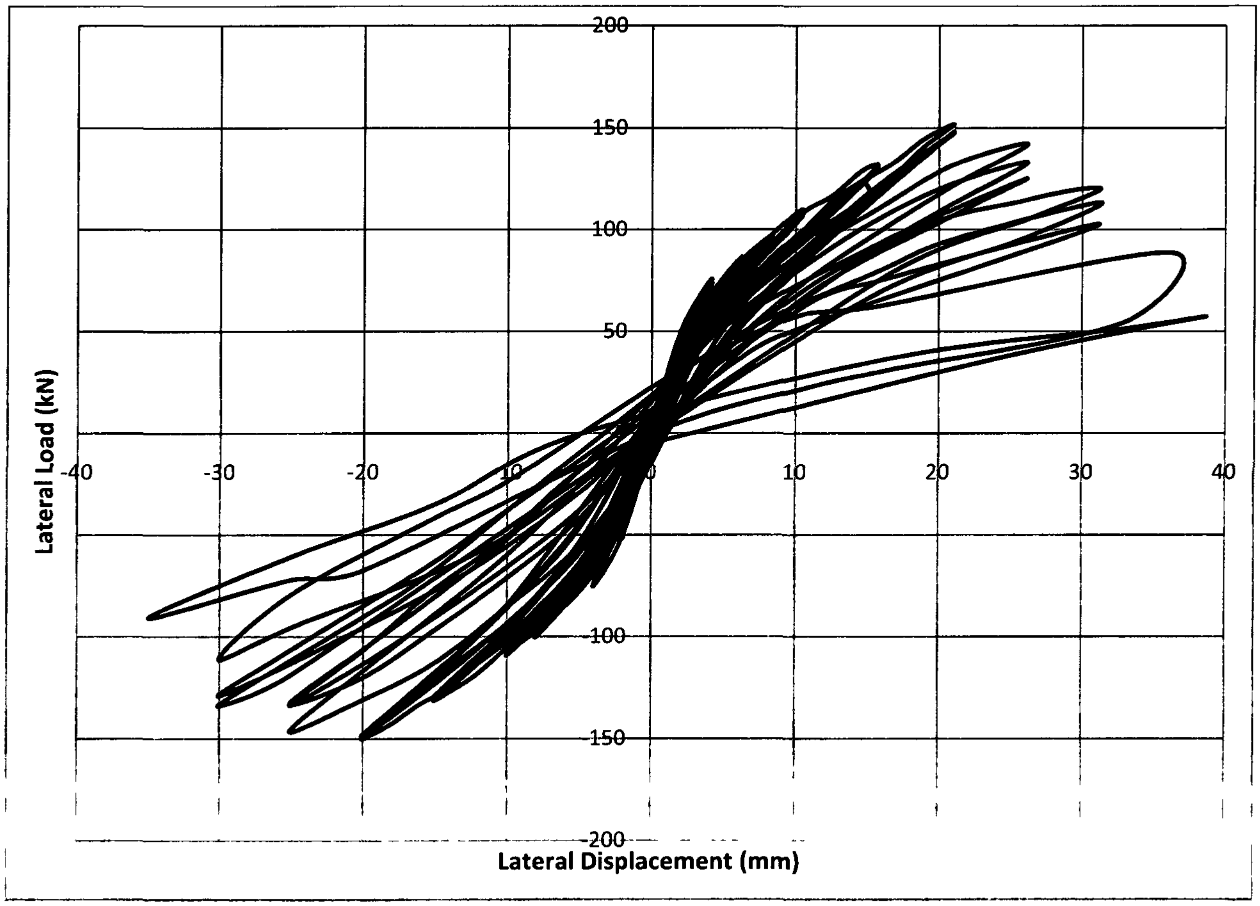

Figure 5.6: Predicted lateral load versus lateral displacement response for the repaired frame

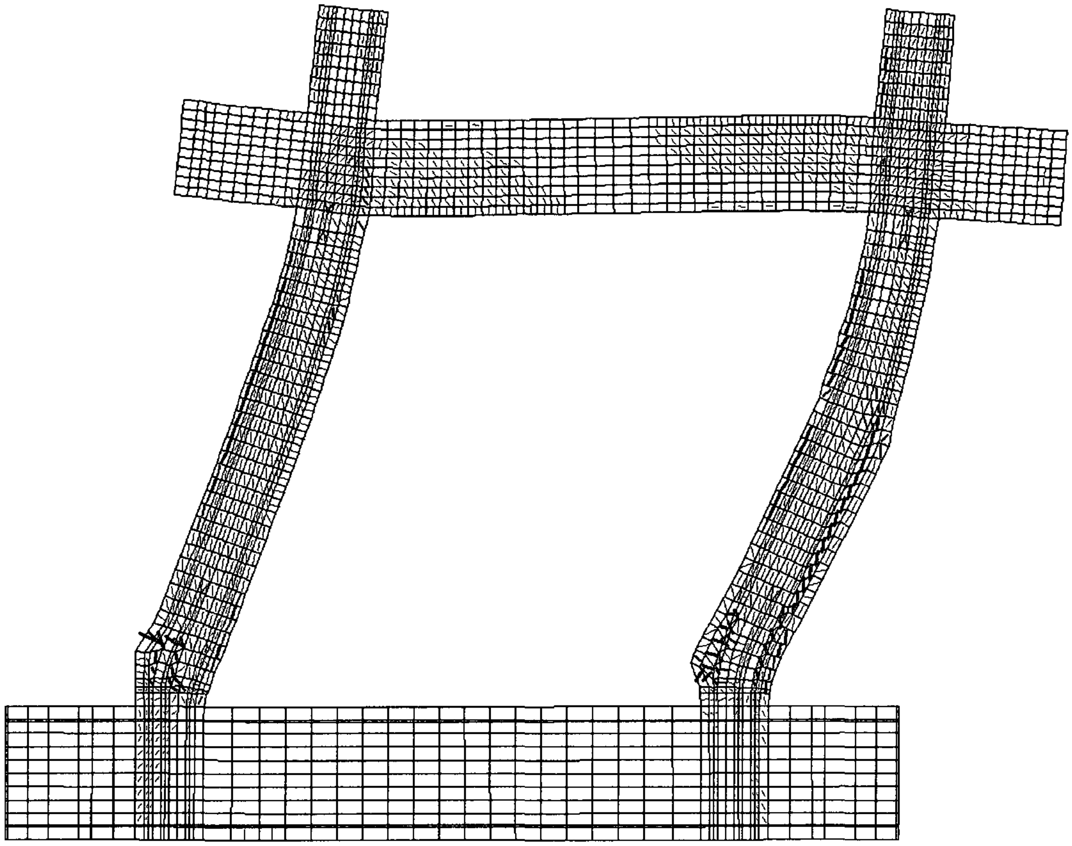

Figure 5.7: Predicted failure condition of the repaired frame

As observed in Figure 5.7, the predicted failure mode of the repaired frame was controlled by the columns at the base of the frame. Peak loads of -150.1 kN and 151.7 kN were sustained during loading to 1.00% lateral drift (20 mm). The up-lift of the column was approximately 1.80 mm at this drift level. The final load cycle was 1.75% lateral drift (35 mm). After having displaced to 38.7 mm, the lateral load dropped more than 50% of the peak load to 57.8 kN.

Throughout the entire simulation, only the truss bars at the base of the columns in the splice region indicated yielding. This was due to the reduction of the truss bar area simulating the development length effectiveness of the reinforcement in this area.

Large cracks of 2.00 mm or more in width were observed in the concrete cover at the onset of lateral loading. This was expected since there was no steel holding the concrete in this layer. Apart from the concrete cover, all the cracks in the beam were less than 1 mm.

The first sign of reinforcement de-bounding in the repaired frame model was observed at the base of the column in the splice region during loading to 0.75% lateral drift (15 mm). Vertical cracks of 1.69 mm width surfaced between the truss bars in the splice regions at the base of both columns. During the subsequent load stage to 1.00% lateral drift (20 mm), where the peak load was sustained, there was a small increase in width of the vertical cracks; approximately 2.20 mm in width. At 1.25% lateral drift (25 mm), large cracks (3.5 mm in width) along the entire reinforcement lap region at the base of the columns was predicted, separating the truss bars in the column closest to the inside of the frame and the hooked truss bars extending down into the foundation. At the next load cycle to 1.50% lateral drift (30 mm), the truss bars situated toward the outside edge of the column and the hooked truss bars extending into the foundation also experienced significant vertical cracking suggesting de-bonding of the reinforcement. The first large cracks to appear in the other portions of the columns were observed during the last load cycle to 1.75% lateral drift (35 mm). The middle top portion of the right column opened up due to a large vertical crack between the middle and outer truss bars.

5.3.2 Steel Bracing Retrofitted Frame

The analytical results for the retrofitted frame are described in this section. The lateral load versus the lateral displacement response is provided in Figure 5.8, while the cracking and displacements experienced by the frame during the last displacement are shown in Figure 5.9.

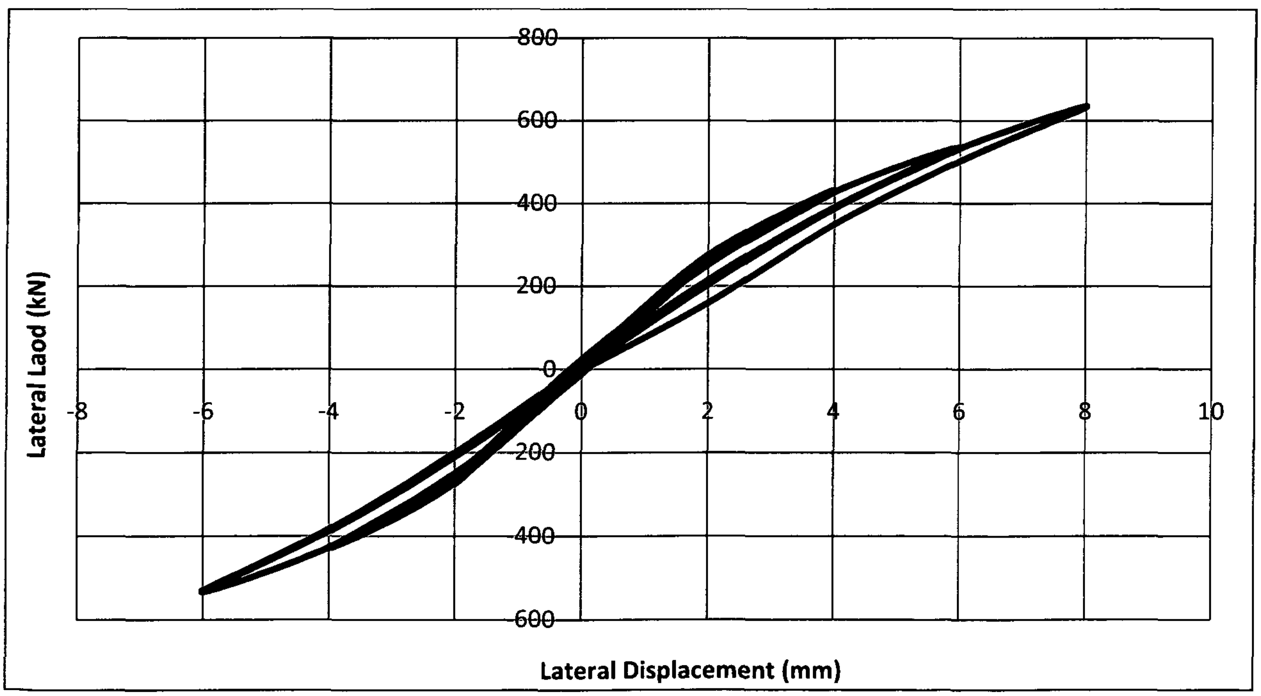

Figure 5.8: Predicted lateral load versus lateral displacement response for the retrofitted frame

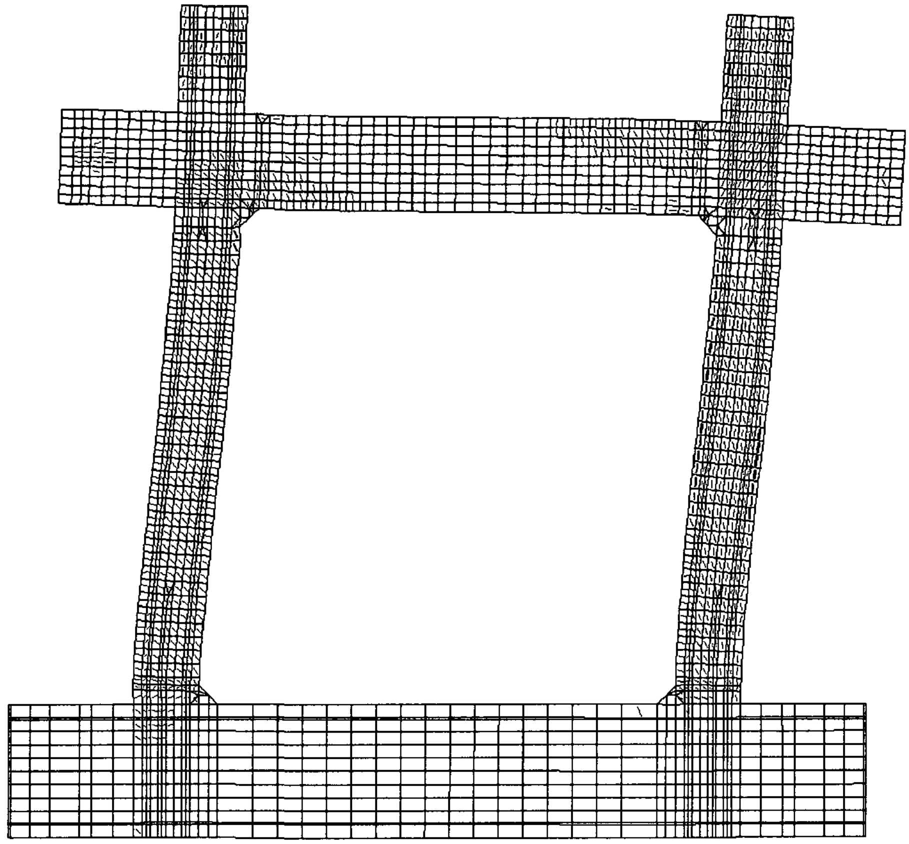

Figure 5.9: Predicted failure condition of the retrofitted frame

Failure of the retrofitted frame was predicted as buckling of the diagonal steel brace. The frame sustained a peak load of 634.5 kN in the positive direction during loading to 0.40% lateral drift (8 mm), which corresponded to the onset of buckling of the brace. The uplift of the column was approximately 0.72 mm.

Throughout the entire simulation, only the truss bars at the base of the columns in the splice region indicated yielding. This was due to the reduction of the truss bars area simulating the development length effectiveness of the reinforcement in this area.

There were no cracks that were larger than 0.72 mm in width except for the zones representing the concrete cover. This was due to the small displacements experienced by the frame. There were also no signs of de-bonding in the splice area.

Chapter 6

6 Discussion of Results

6.1 General

Chapters 4 and 5 presented the experimental and numerical results, respectively. This chapter provides a comparison of the results. First, the experimental results of the repaired and retrofitted frame are compared, including the lateral loads, the lateral displacements, the base anchorage slip, the vertical displacements, and the out-of-plane displacements. Thereafter, the numerical results for the repaired and retrofitted frame are compared. The second part of this chapter discusses the experimental and numerical results. To facilitate the comparisons, the envelope responses of the data are used. The envelopes are formed from the peak load for each load cycle. Table 6.1 provides a summary of the failure mode and ultimate loads according to A23.3-04, experimental testing, and Program VecTor2.

Table 6.1: Ultimate loads and failure modes

	Repaired Frame		Retrofitted Frame	
	Ultimate lateral load (kN)	Failure Mode	Ultimate lateral load (kN)	Failure Mode
A23.3-04	181	Flexural failure at the bottom of the column	676	Buckling of the HSS steel brace
Experimental testing	149	Flexural failure at the bottom of the column – deficient splice lengths	707	Foundation failure and out-of-plane twisting
VecTor2	151	Flexural failure at the bottom of the column – deficient splice lengths	635	Buckling of the HSS steel brace

The ultimate load and failure mode for the repaired frame are similar for the experimental testing and VecTor2. The differences with A23.3-04 are attributed to the deficiencies in the reinforcement splice length that was not taken into account. The retrofitted frame in the experimental program reached a higher load due to the twisting of the frame and end restraint of the brace, which increased the buckling capacity. The CSA standard A23.3-04 and VecTor2 predicted the same failure mode. Program VecTor2 predicted a smaller failure load due to the assumed bi-linear response of the HSS brace to simulate the buckling capacity.

6.2 Comparison of Repaired and Retrofitted Frames

6.2.1 Experimental Results

In this section, the envelope results of Frames BL-3R and BR-3R are compared, including the lateral displacement, the base anchorage slip of the column, the vertical displacement of the column and the out-of-plane displacement. These phenomena are plotted against the lateral load and are shown in Figures 6.1 to 6.4.

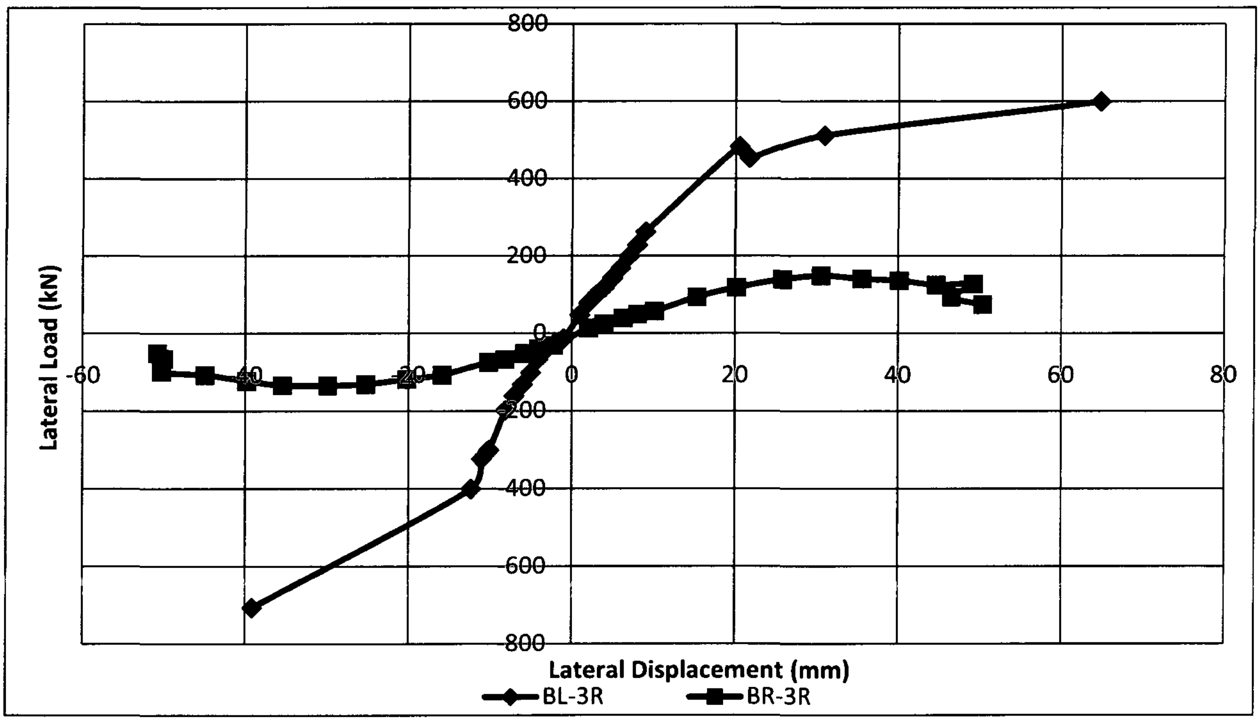

Figure 6.1: Lateral load versus lateral displacement envelope response

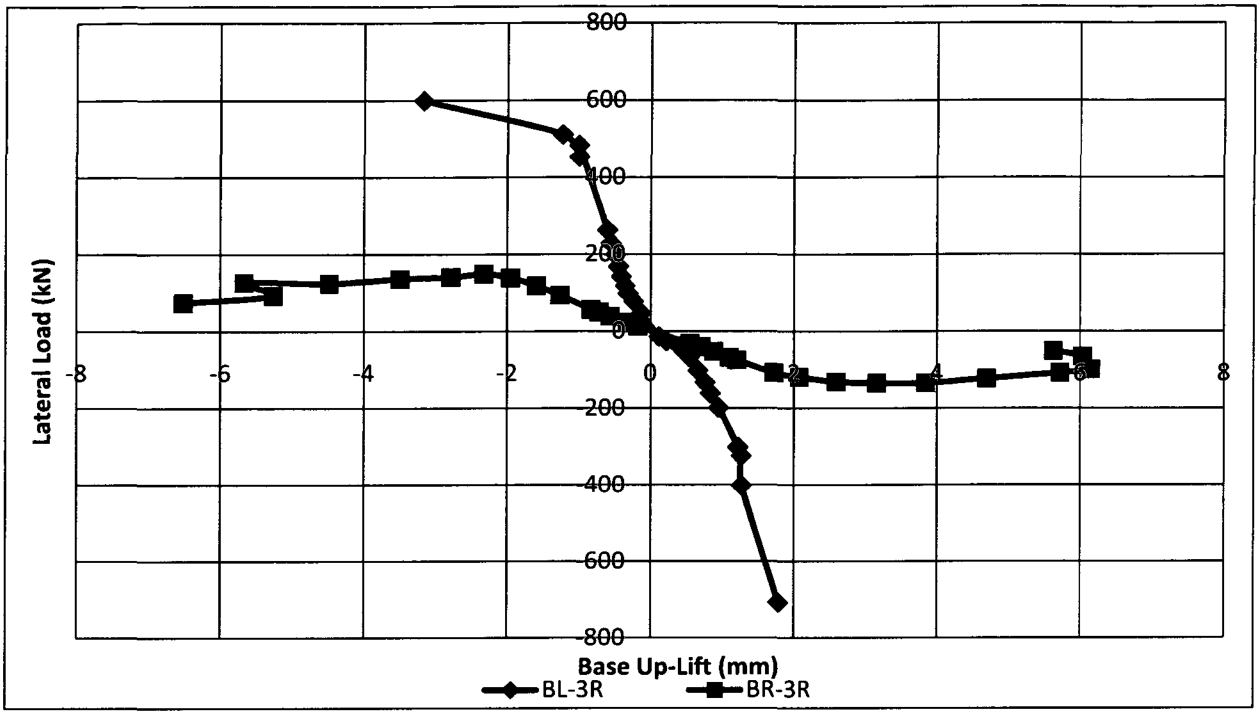

Figure 6.2: Lateral load versus base anchorage slip envelope response

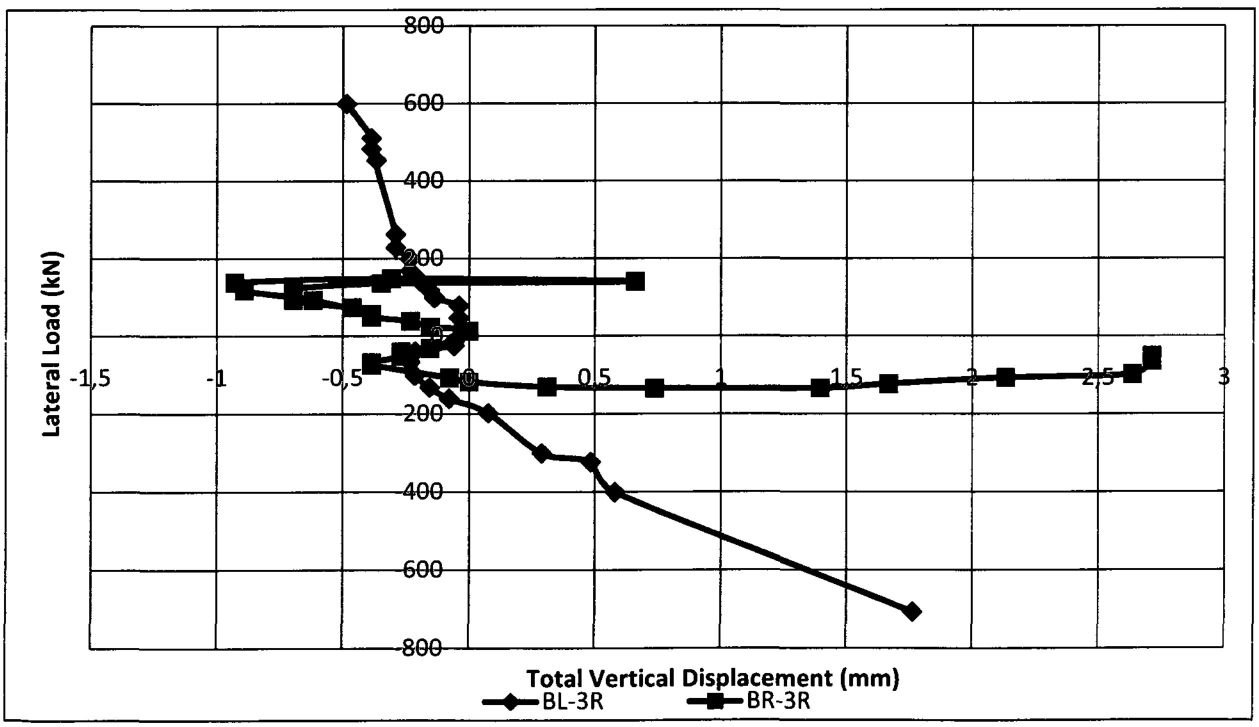

Figure 6.3: Lateral load versus vertical displacement envelope response of column

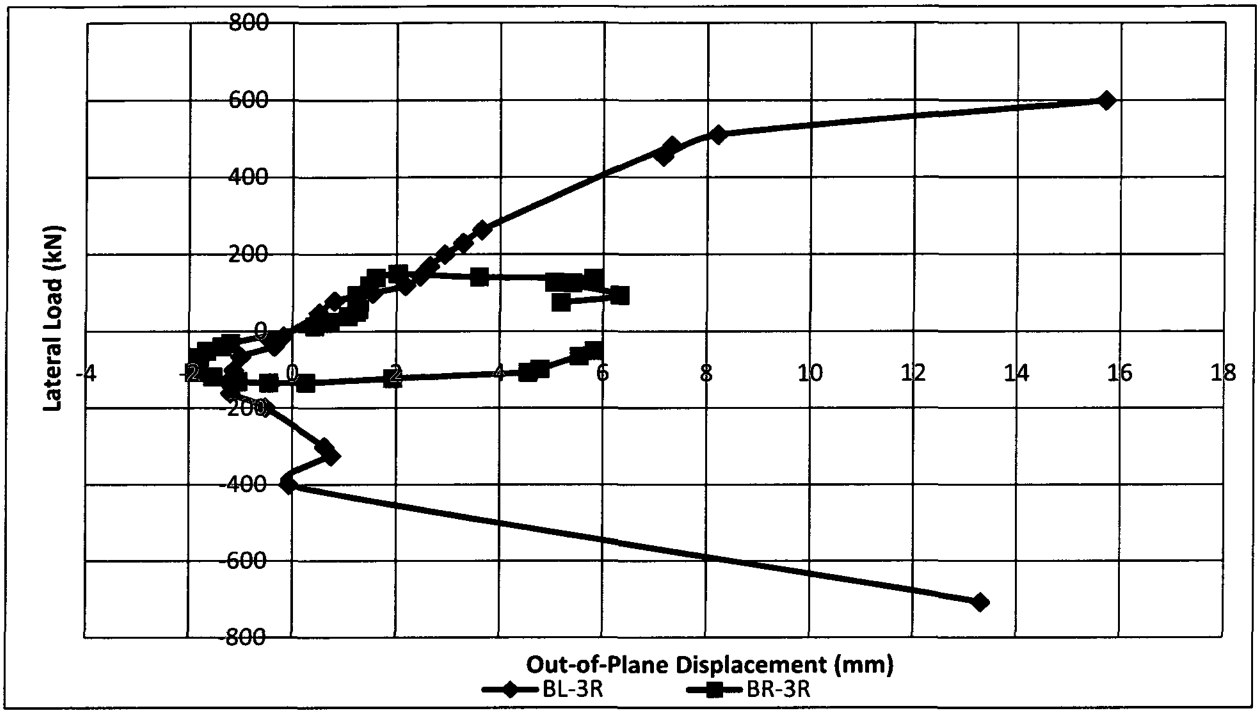

Figure 6.4: Lateral load versus out-of-plane displacement envelope response

The repaired frame, BR-3R, sustained a maximum lateral load of 149 kN at 30 mm of displacement in the positive direction and 134 kN at a corresponding displacement of 40 mm in the negative direction. The retrofitted frame, BL-3R, experienced a maximum lateral load of 599 kN corresponding to a displacement of 65 mm in the positive direction and 707 kN at a displacement of 40 mm in the negative direction. The response of Frame BR-3R demonstrates non-ductile behaviour since the load-displacement response is rounded, and beyond the peak lateral load capacity there is a gradual degradation in strength. Frame BL-3R demonstrated enhancement in strength and stiffness compared to Frame BR-3R. Note that beyond 20 mm of displacement, the frame's response was dominated by the out-of-plane behaviour. Due to the out-of-plane twisting, the retrofitted frame did not experience the actual in-plane lateral load capacity; however, an increase in lateral load capacity of approximately 5 times the strength of the repaired frame was realized. This enhancement is in line with increases in the elastic seismic forces prescribed by current design standards relative to those in practice and corresponding to the design standard used to design the original frames. This can be observed in Figure 6.1.

Even though Frame BR-3L sustained a significant increase in lateral loading, the base anchorage slip was less than Frame BR-3R as shown in Figure 6.2. Apart from the last displacement in the positive direction of Frame BL-3R, the base anchorage slip is contained between +/- 2 mm, while for Frame BR-3R, the base anchorage slip is contained between +/- 6 mm. Similar behaviour in response is observed in the vertical displacement of the columns. Apart from the last displacement in the negative direction, the vertical displacement of the column for BL-3R ranges between +/- 0.5 mm. The vertical displacement of the column for BR-3R is between -1 mm to 2.5 mm (Figure 6.3). Therefore, the retrofitted frame experienced a vertical displacement of the columns in the order of 1/3 that of the repaired frame, indicating an increase in stiffness. Figure 6.4 indicates that the out-of-plane displacements are consistent relative to the lateral load experienced by the frame whether retrofitted or not. It is apparent that as the lateral load exceeds 400 kN in both the positive or negative directions, the out-of-plane displacements increase substantially, and thus the response of the frame was dominated by the out-of-plane behaviour thereafter.

The envelope secant stiffness-displacement response is provided in Figure 6.5. Note that the response is shown for the positive direction of loading and for the first repetition of displacements for clarity. The secant stiffness was calculated by dividing the peak lateral load by the corresponding displacement at each displacement level. The largest stiffness was experienced in both frames during the first repetition of loading in the positive direction. Frame BL-3R experienced a secant stiffness of approximately 47 kN/mm at 1 mm of lateral displacement, while Frame BR-3R experienced a secant stiffness of approximately 7 kN/mm at 2 mm of lateral displacement. Thus, the retrofit strategy resulted in an approximate increase in initial stiffness of approximately 7.

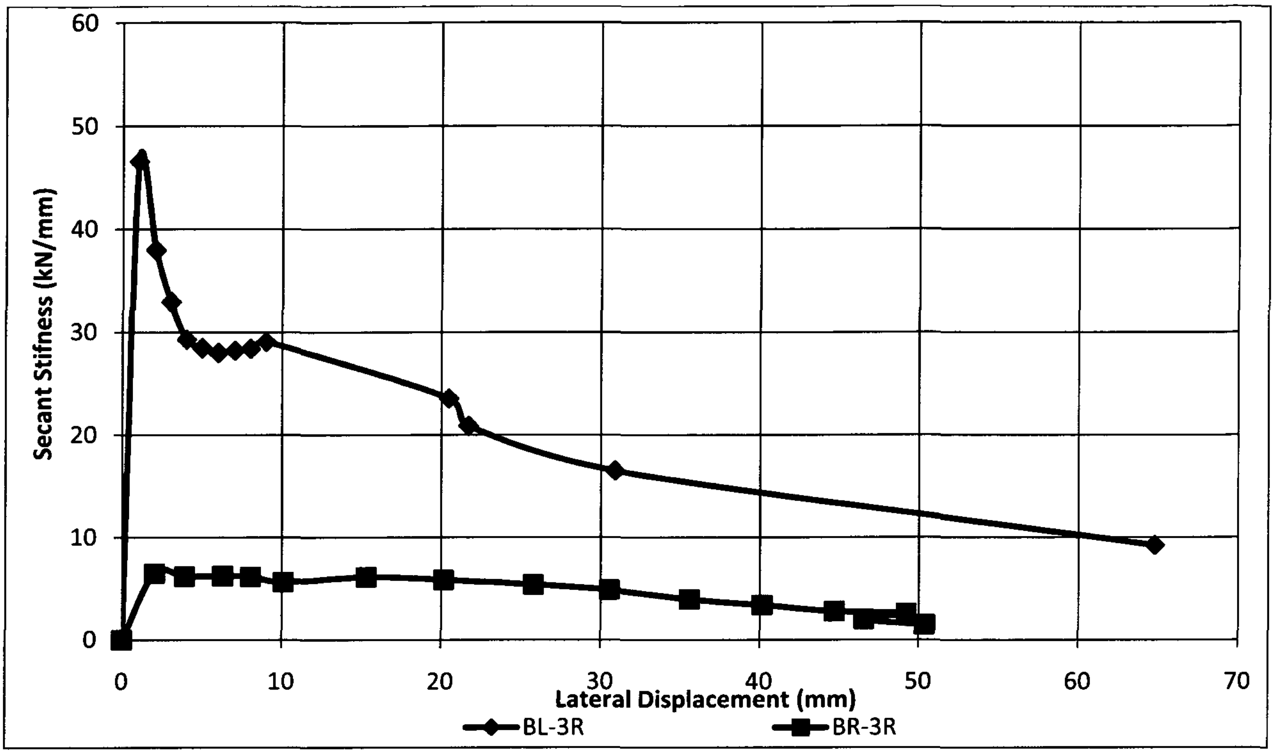

Figure 6.5: Secant stiffness-displacement responses of Frames BR-3R and BL-3R

6.2.2 Analytical Results

The finite element model of the repaired frame predicted a maximum lateral load of 152 kN at 20 mm of displacement in the positive direction and 150 kN at a corresponding displacement of 20 mm in the negative direction. The model of the retrofitted frame predicted a maximum lateral load of 635 kN corresponding to a displacement of 8 mm in the positive direction and 534 kN at a displacement of 6 mm in the negative direction. The response of the repaired frame demonstrates non-ductile behaviour since the load-displacement response is rounded, and beyond the peak lateral load capacity the strength gradually decreases. The retrofitted model illustrates enhancement in strength and stiffness compared to the repaired model; however, ductility was not improved. An increase in lateral load capacity of approximately 4 times the strength of the repaired frame was predicted as illustrated in Figure 6.6.

The increase in stiffness is represented by the secant stiffness-displacement response provided in Figure 6.7. The results are based on first repetition of loading in the positive direction, which provides the largest stiffness experienced by both frames. The retrofitted frame experienced a stiffness of approximately 137 kN/mm at 2 mm of lateral displacement and the repaired frame experienced a stiffness of approximately 24 kN/mm at 2 mm of lateral displacement. Thus, the retrofit strategy resulted in an approximate increase in initial stiffness of approximately 6. The increase in strength and stiffness obtained from the analytical results resemble the experimental results.

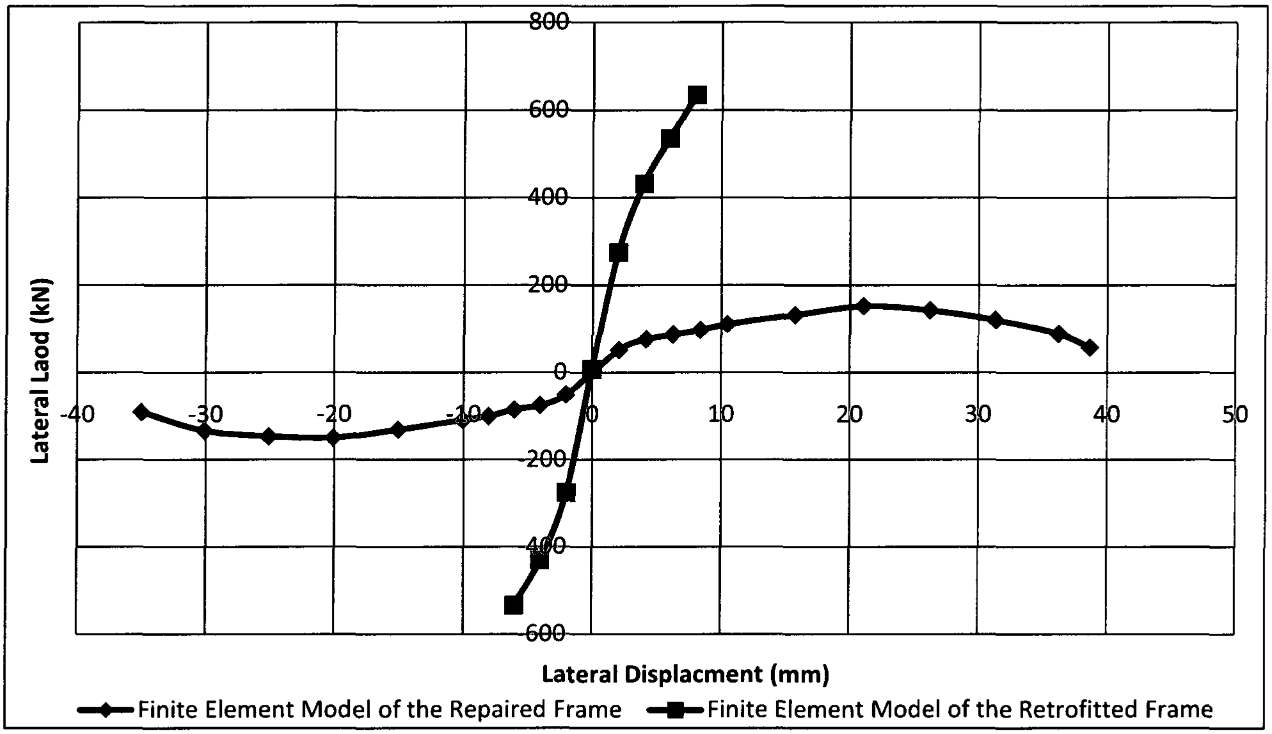

Figure 6.6: Lateral load versus lateral displacement envelope response of the finite element models

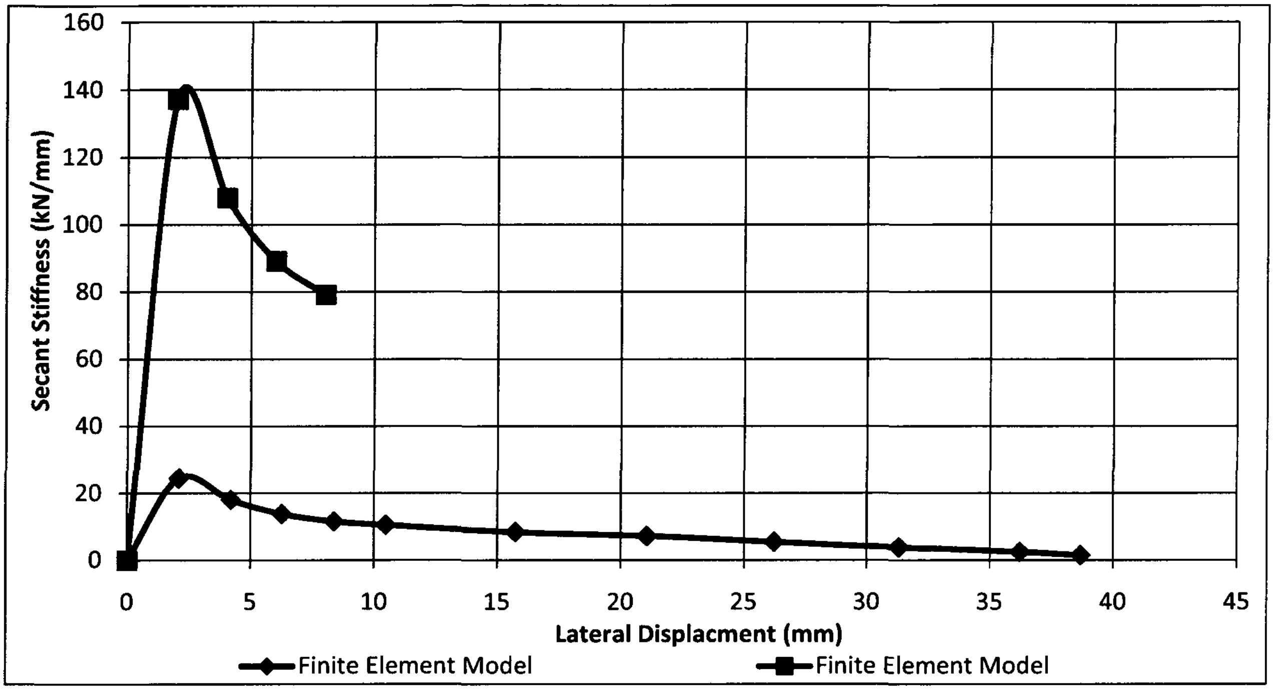

Figure 6.7: Secant stiffness-displacement responses of the finite element models

6.3 Comparison of Analytical and Experimental Results

6.3.1 Repaired Frame

The finite element model of the repaired frame sustained a maximum lateral load of 152 kN at 20 mm of displacement in the positive direction and 150 kN at a corresponding displacement of 20 mm in the negative direction. Experimentally, the repaired frame, BR-3R, sustained a maximum lateral load of 149 kN at 30 mm of displacement in the positive direction and 134 kN at a corresponding displacement of 40 mm in the negative direction. Both the predicted and observed behaviours are very similar and the peak lateral loads are approximately 150 kN. The peak loads did not occur at the same displacement. The finite element model predicted a stiffer response as shown in Figure 6.8. This is attributed to two causes: first, the analysis is based on a two-dimensional response and, thus, does not capture the out-of-plane displacements; and second, the model did not carry forward any residual damage in the frame from the original test. However, the general shape of the envelope responses is very similar. The failure mode was well predicted by the model in comparison to the observed failure. The finite element model and the observed response of Frame BR-3R indicated damage was concentrated near the base of the columns including deficiencies in the lap splice lengths. Slip of the reinforcement and concrete spalling were noticeable. This can be seen in Figure 6.9.

The difference in stiffness is evident in Figure 6.10. The finite element model predicted a secant stiffness of approximately 24 kN/mm at 2 mm of lateral displacement, while Frame BR-3R experienced a secant stiffness of approximately 7 kN/mm at 2 mm of lateral displacement during testing. Thus, the finite element model is approximately 3 times stiffer. However, beyond a lateral displacement of approximately 10 mm, the secant stiffness predicted by the finite element model and that observed during testing converge. This indicates that aside from the initial stiffness, the finite element model was in agreement with the observed behaviour.

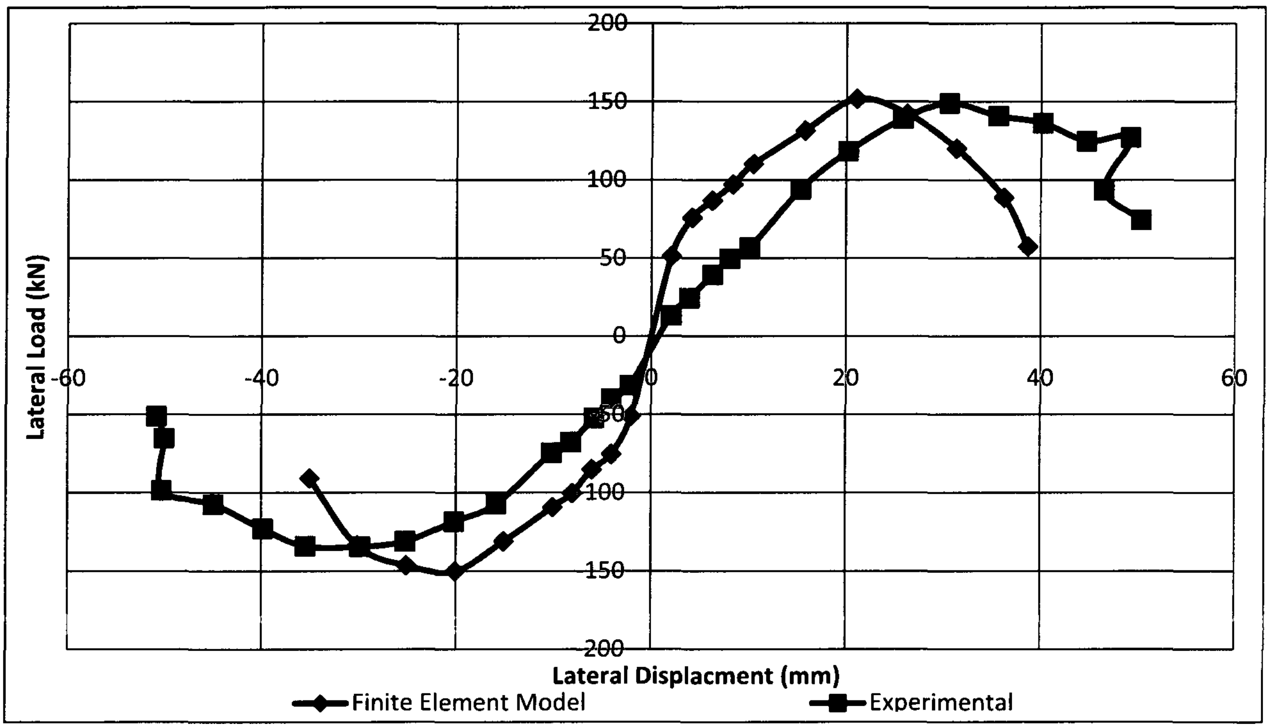

Figure 6.8: Lateral load versus lateral displacement envelope response of the repaired frame

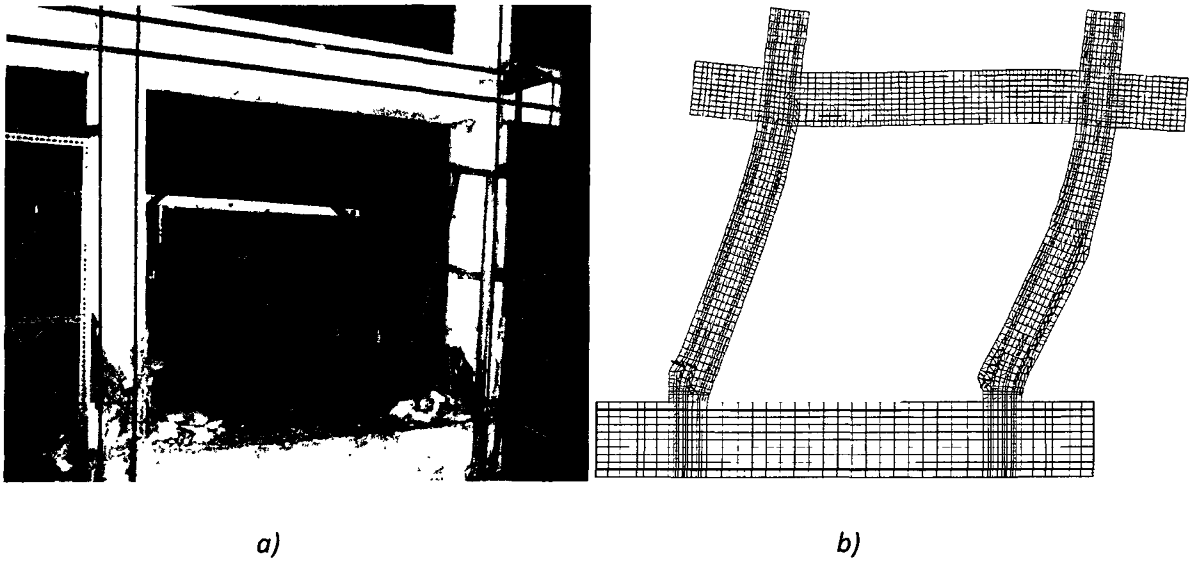

Figure 6.9: Failure Condition of Frame BR-3R: a) Experimental Observations; b) Finite Element Model

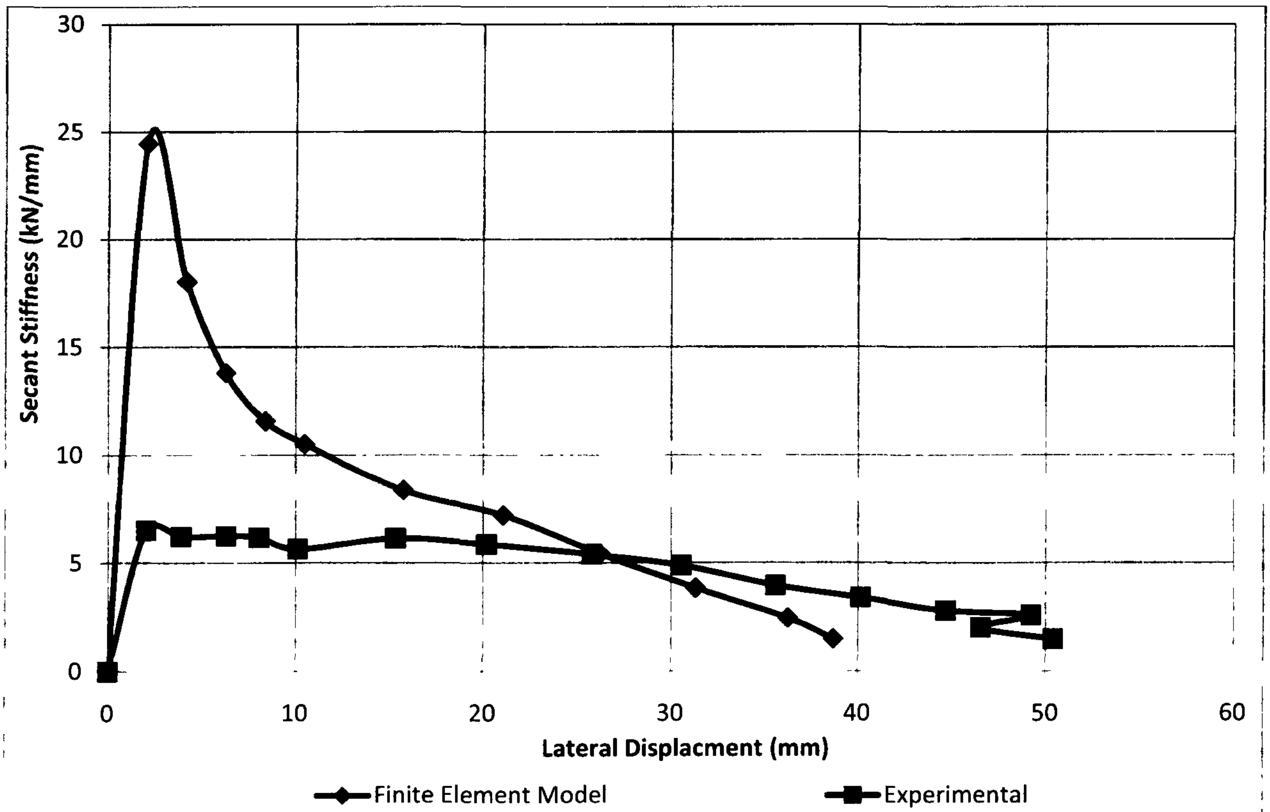

Figure 6.10: Secant stiffness-displacement response of the repaired frame

6.3.2 Steel Bracing Retrofitted Frame

The finite element model of the retrofitted frame predicted a maximum lateral load of 635 kN corresponding to a displacement of 8 mm in the positive direction and 534 kN at a displacement of 6 mm in the negative direction. Frame BL-3R experienced a maximum lateral load of 599 kN corresponding to a displacement of 65 mm in the positive direction and 707 kN at a displacement of 40 mm in the negative direction during testing. Both the peak lateral loads and corresponding lateral displacements demonstrate discrepancies between the model and observed behaviours as illustrated in Figure 6.11. There are many reasons for the differences in behaviour. The finite element model assumes a perfect alignment of the steel X-bracing with the frame. Furthermore, the model assumes no space between the X-bracing, the steel angle anchorage system that keeps the X-bracing in place, and the frame. In addition, the steel X-bracing could bend out-of-plane or rotate against the steel angle system that holds the X-bracing in place, which is not captured in the analysis. Recall, also, that the analysis is based on a two-dimensional in-plane response, and out-of-place displacements, which would reduce the stiffness of the frame, are not captured. All of these factors can, in turn, cause a reduction of stiffness in Frame BL-3R relative to the finite element model. Another contributing factor to the differences in behaviour is that the response of the steel X-bracing in the finite element model was assumed to be governed by the buckling strength, which results in a stiff and brittle response as shown in Figure 6.11. However, Frame BL-3R sustained significantly larger displacements prior to failure. The observed failure of Frame BL-3R was due to out-of-plane twisting of the frame and damage to the foundation. The predicted and observed failures are shown in Figure 6.12.

The difference in stiffness between the model and test specimen is provided in Figure 6.13. The finite element model predicted a secant stiffness of approximately 137 kN/mm at 2 mm of lateral displacement, while Frame BL-3R experienced a stiffness of approximately 47 kN/mm at 1 mm of lateral displacement during testing. Thus, the model is approximately 3 times stiffer than the observed response of Frame BL-3R. This is similar to the increase in stiffness predicted by the finite element model relative to the experimental response for the repaired frame BR-3R.

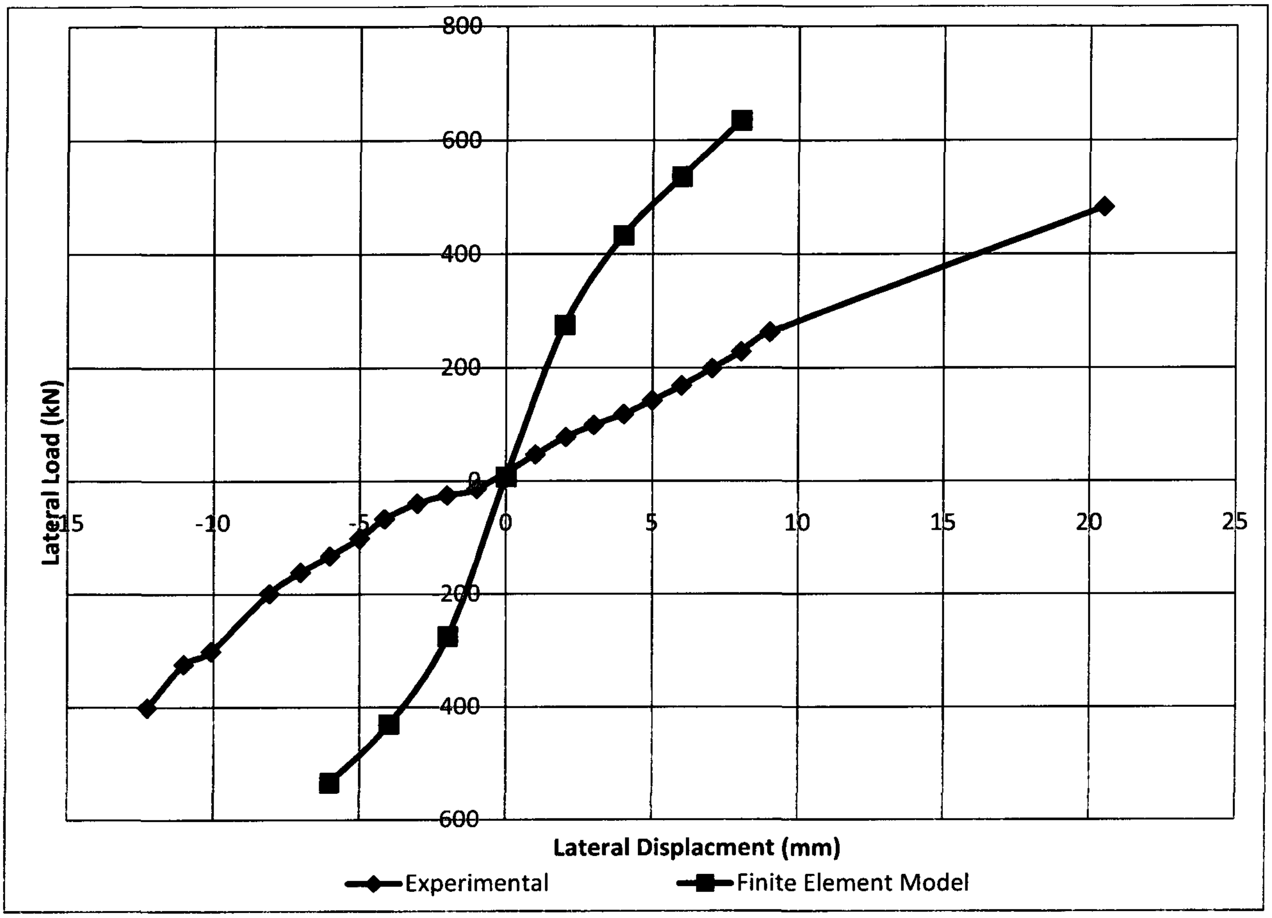

Figure 6.11: Lateral load versus lateral displacement envelope response of the retrofitted frame

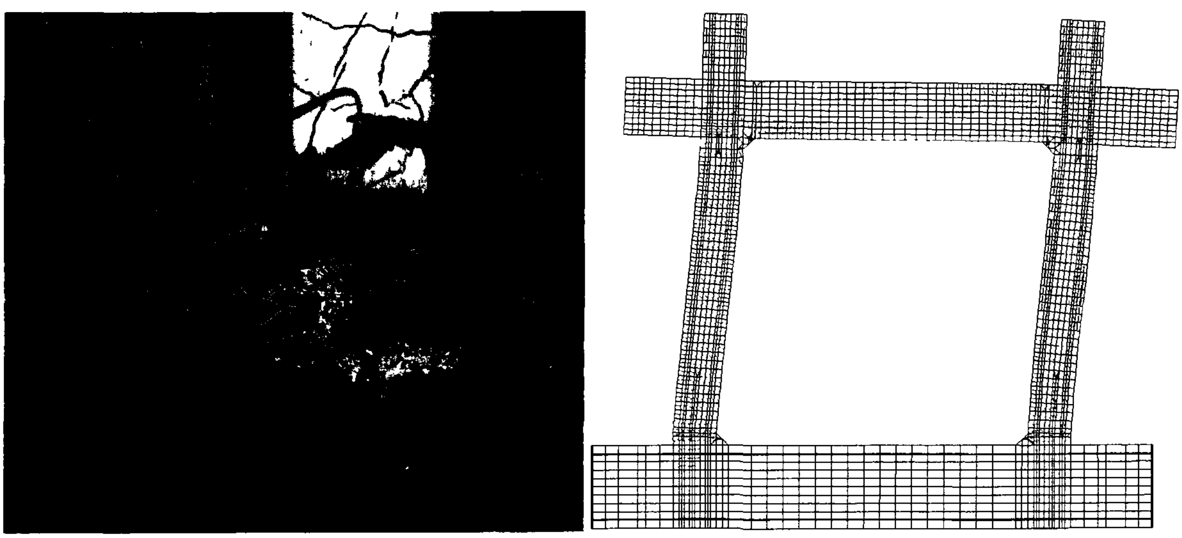

a) b)

Figure 6.12: Failure Condition of Frame BL-3R: a) Experimental Observations; b) Finite Element Model

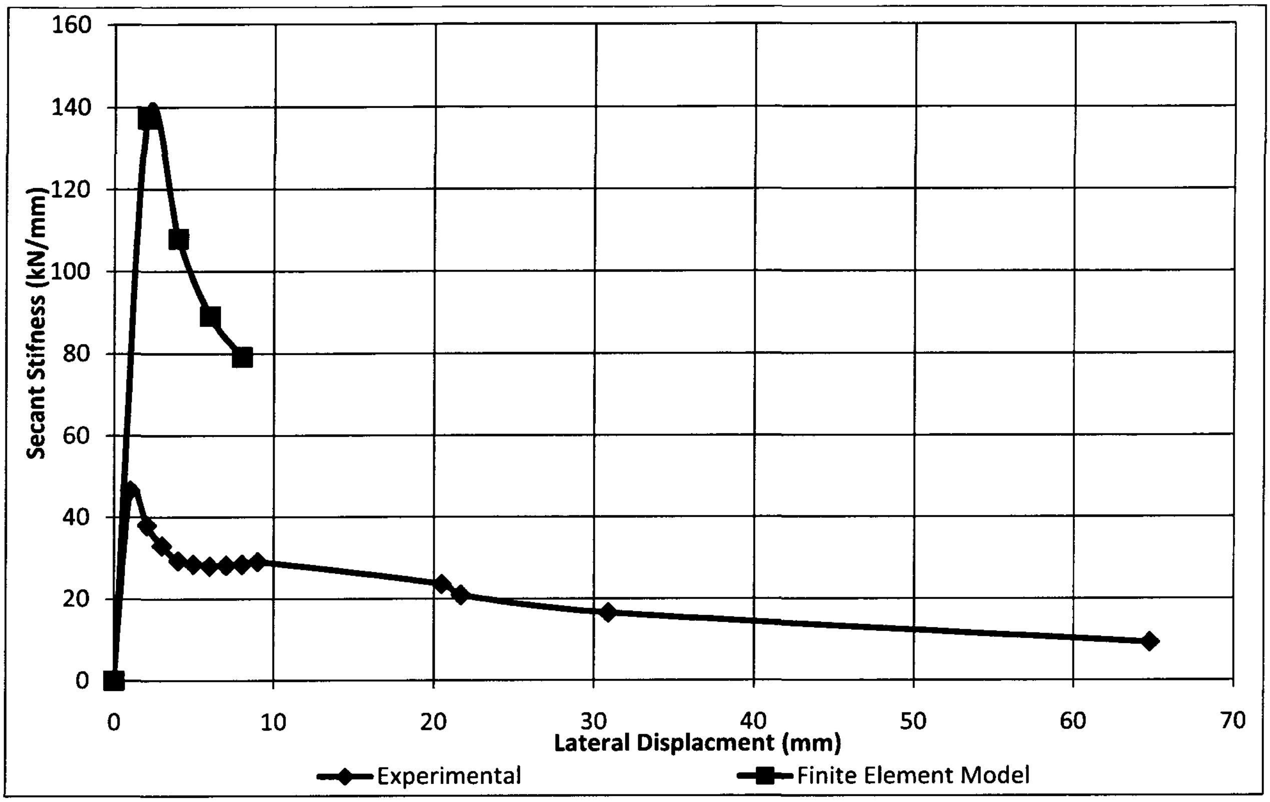

Figure 6.13: Secant stiffness-displacement response of the retrofitted frame

Chapter 7

7 Summary and Conclusions

7.1 Summary

Reinforced concrete frames built before the 1970s were designed according to provisions for wind and gravity loading. These frames were typically built with strong beams and weak columns, which represents a contradiction to the current seismic design philosophy. Completely replacing a building that does not conform to current earthquake design methods is not economically feasible or viable. Therefore, retrofit methods are used to enhance the lateral load carrying resistance and to reduce potential damage that could be caused by future earthquakes. A review of previous research on repaired reinforced concrete frames and on retrofit methods utilizing fibre reinforced polymers and steel bracing for reinforcing concrete frames was presented.

This study investigated repairing post-earthquake damaged reinforced concrete frames and used a new, quick and simple retrofit strategy to strengthen deficient non-ductile reinforced concrete frames. The retrofit method utilized square hollow structural sections to form diagonal X-bracing designed as a compression strut to increase the stiffness and lateral load capacity. Two, single-storey, one-bay, non-ductile reinforced concrete frames were observed experimentally and analytically. The reinforced concrete frames, BR-3 and BL-3, were previously designed, built, and tested by Shalouf (2005). As part of this program, the frames were first repaired and renamed BR-3R and BL-3R. Frame BR-3R was tested to assess the seismic performance of the repair strategy, while Frame BL-3R was retrofitted with steel X-bracing. The full description of the specimens, the material properties, the procedures for the repairs, the expected capacity of the repaired frame, the design of the steel X-bracing, and the expected capacity of the retrofitted frame were presented and discussed in this study.

The repaired frame, BR-3R, experienced a maximum lateral load of 149 kN at 30 mm of displacement in the positive direction and the retrofitted frame, BL-3R, experienced a maximum lateral load of 707 kN at a displacement of 40 mm in the negative direction during testing in the laboratory. The finite element models of the repaired and retrofitted frames predicted maximum lateral loads of 152 kN at 20 mm of displacement in the positive direction for BR-3R and 635 kN corresponding to a displacement of 8 mm in the positive direction for BL-3R.

The failure mode predicted by the finite element model of the repaired frame, BR-3R, was in agreement with test observations and included damage at the base of the columns including deficient reinforcement lap splice lengths. Slip of the longitudinal reinforcement and concrete spalling were also noted. The finite element model predicted failure due to buckling of the X-brace in the retrofitted frame, BL-3R. The actual failure of the frame was a result of significant out-of-plane twisting and damage to the base foundation. An increase in the lateral load capacity of approximately 5 times the strength of the repaired frame was recorded during the experimental testing, while an increase in lateral load capacity of approximately 4 times was predicted by the analytical investigation. This enhancement in lateral load carrying capacity is in line with increases in the elastic seismic forces prescribed by current design standards relative to those in practice and corresponding to the design standard used to design the original frames.

7.2 Conclusions

An experimental and analytical investigation was presented to demonstrate the use of HSS diagonal X-bracing compression struts as an alternative retrofit strategy for non-ductile reinforced concrete frames designed and built prior to the enactment of seismic design provisions. This study included repairing two previously damaged frames to their original condition; one frame was tested in the repaired condition, while the second frame was further retrofitted. The retrofitting method was quick and easy and required minimal connection details. The retrofitted frame responded with enhanced stiffness and strength compared to the companion repaired frame in both the experimental testing and analytical models. Therefore, the objectives of a stiffness and strength retrofit strategy were met. The resisting mechanism of the retrofitted frame was primarily truss action, while the repaired frame demonstrated frame action. This was evident in the failure modes; the retrofitted frame experienced significant damage in the foundation during testing, while the X-bracing buckled in the finite element model. The companion repaired frame experienced damage at the base of the columns. The experimental results were reasonably simulated by the finite element model, particularly for the repaired frame. Discrepancies between the experimental observations and analytical results were mainly due to the model not capturing out-of-plane displacements and other simplifying assumptions in the modelling. The enhancement in strength provided during testing and predicted by the modelling was in line with increases in the elastic seismic forces prescribed by current design standards. The stiffness predicted by the models was higher than experienced during testing of the frames.

7.3 Future Work

Further work is necessary to investigate HSS diagonal X-bracing compression struts as an alternative retrofit strategy. To start, a stronger foundation is required to ensure that failure occurs in the frame or in the diagonal X-bracing. An out-of-plane support system should be used to prevent the frame from displacing in the out-of-plane direction. Different sizes of HSS diagonal X-bracing could also be tested. Other testing could investigate filling the HSS section with concrete to increase the compressive strength and prevent buckling. Additionally, analytical studies should be performed to investigate the response of structures retrofitted with HSS diagonal X-bracing compression struts. This should include parametric studies to determine the best location in a structure to place the X-bracing. A more refined analytical study should include the damage experienced in Frames BR-3 and BL-3 in the original tests. Any residual damage should then be carried forward prior to modelling the repair and/or retrofit strategy.

References

Bentz, E. C. (2001). *Response-2000 Reinforced Concrete Section Analysis, User Manual*, Version 1.05, Department of Civil Engineering, University of Toronto, Toronto, ON, Canada.

Canadian Institute of Steel Construction (CISC) (2004). *Handbook of Steel Construction*, Ontario, Canada.

Cement Association of Canada (2006). *Concrete Design Handbook Third Edition*, Ontario, Canada.

Duong, K. V., Sheikh, S. A., & Vecchio, F. J. (2007). Seismic behavior of shear-critical reinforced concrete frame: Experimental investigation. *ACI Structural Journal, 104*(3), 304-313.

Ghobarah, A., & Biddah, A. (1999). Dynamic analysis of reinforced concrete frames including joint shear deformation. *Engineering Structures, 21*(11), 971-987.

Ghobarah, A., & Elfath, H. A. (2001). Rehabilitation of a reinforced concrete frame using eccentric steel bracing. *Engineering Structures, 23*(7), 745-755.

Ghobarah, A., & Said, A. (2002). Shear strengthening of beam-column joints. *Engineering Structures, 24*(7), 881-888.

Islam, S., Skokan, M., & Huang, S. (2010). Innovative seismic retrofit of two high-rise buildings with unique challenges. *9th US National and 10th Canadian Conference on Earthquake Engineering: Reaching Beyond Borders*

Karbhari, V. M. (2001). Materials considerations in FRP rehabilitation of concrete structures. *Journal of Materials in Civil Engineering, 13*(2), 90-97.

Li, Y., Lin, Y., Chen, C., & Lin, C. (2007). Theoretical and experimental studies on repaired and rehabilitated reinforced concrete frames. *Canadian Journal of Civil Engineering, 34*(8), 923-933.

Li, Y., & Sung, Y. (2003). Seismic repair and rehabilitation of a shear-failure damaged circular bridge column using carbon fiber reinforced plastic jacketing. *Canadian Journal of Civil Engineering, 30*(5), 819-829.

Maheri, M. R., and A. Sahebi (1997). Use of steel bracing in reinforced concrete frames, *Engineering Structures* **19:12**, 1018-1024.

Ozcelik, R., & Binici, B. (2010). Seismic upgrading of deficient reinforced concrete frames with internal steel frame. *9th US National and 10th Canadian Conference on Earthquake Engineering: Reaching Beyond Borders*

Packer, J.A., and Henderson, J.E. (1997). Hollow Structural Section: Connections and Trusses – A Design Guide, Canadian Institute of Steel Construction, Toronto, Canada, ISBN-0-88811-086-3, pp 464.

Sahoo, D. R., & Rai, D. C. (2010). Seismic retrofit of a city hall using buckling restrained braces based on nonlinear analyses including soil-structure interaction. *9th US National and 10th Canadian Conference on Earthquake Engineering: Reaching Beyond Borders*

Said, A. 2008. Rehabilitation of RC frame joints using local steel bracing. *Structure and Infrastructure Engineering* 4, (6): 431.

Said, A. M., & Nehdi, M. L. (2004). Use of FRP for RC frames in seismic zones: Part I. evaluation of FRP beam-column joint rehabilitation techniques. *Applied Composite Materials, 11*(4), 205-226.

Serrato, F. (2002). *Seismic retrofit of URM infill panels in reinforced concrete frames using FRP sheets*

Shalouf, F. (2005). *Seismic retrofit of reinforced concrete frames with diagonal prestressing or FRP strips*

Skokan, M., Huang, S., Islam, S., & Oguzmert, M. (2010). Seismic strengthening of non-ductile reinforced concrete frames using aluminum shear links as energy-dissipation devices. *Engingeering Structures*

Toutanji, H., & Balaguru, P. (1998). Durability characteristics of concrete columns wrapped with FRP tow sheets. *Journal of Materials in Civil Engineering, 10*(1), 52-57.

Wang, C., Shih, C., Hong, S., & Hwang, W. (2004). Rehabilitation of cracked and corroded reinforced concrete beams with fiber-reinforced plastic patches. *Journal of Composites for Construction, 8*(3), 219-228.

Wong, P.S., and F. J. Vecchio, 2002. VecTor2 & Formworks user's manual, University of Toronto, Toronto, Canada.

Appendix A

Hand Calculations

A.1 Column Strength Calculation

The General Method was used to determine the shear capacity of the columns. This was done as follows with the aid of Figure A.1 for the repaired frame:

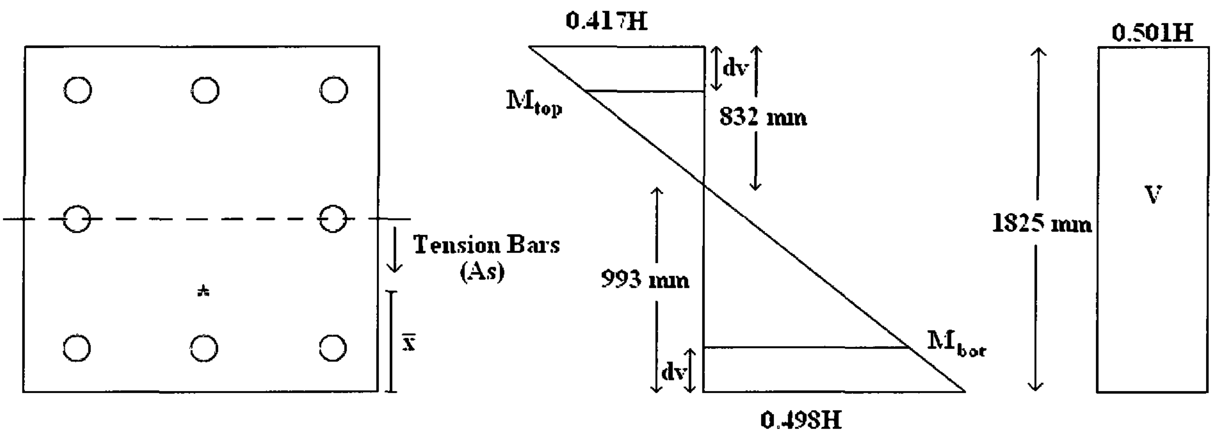

Figure A.1: General Method illustration for the columns of the repaired frame

The calculations are based on the critical loading case which is located at the base of the column.

Base of the column: Assume $\varepsilon_x = 0.001182$

$$S_{ze} = 300$$

$$\bar{x} = \frac{(600)(39.35) + 200(125)}{800} = 60.8\,mm$$

$$d = 250 - 60.8 = 189\,mm$$

$$\beta = \frac{0.4}{1+1500\varepsilon_x} \cdot \frac{1300}{1000+S_{ze}} = \frac{0.4}{1+1500 \cdot 0.001182} \cdot \frac{1300}{1000+300} = 0.144$$

$$\theta = 29° + 7000\varepsilon_x = 29° + 7000 \cdot 0.001182 = 37.24°$$

$$d_v = 0.9d = 0.9 \cdot 189 = 170\ mm$$

$$V_c = \lambda\beta\sqrt{f_c'}b_w d_v = 1.0 \cdot 0.144 \cdot \sqrt{32.1} \cdot 250 \cdot 170 = 35\ kN$$

$$V_s = \frac{A_s f_y d_v \cot\theta}{s} = \frac{\left(\frac{2\pi 6.35^2}{4}\right)500 \cdot 170\cot(37.24)}{125} = 56\ kN$$

$$V_n = V_s + V_c = 56 + 35 = 91\ kN$$

$$V = 0.501H \rightarrow H = \frac{V_n}{0.501}$$

$$\frac{0.498H}{993} = \frac{M_{bot}}{993-d_v}$$

$$M_{bot} = \frac{0.498H}{993}(993-170) = 0.413H = 0.463\frac{V_n}{0.501} = 0.824V_n = 0.824 \cdot 91 = 75.3\ kNm$$

$$N = -400 + 0.437H = -400 + 0.486\frac{V_n}{0.501} = -400 + 0.486 \cdot \frac{91}{0.501} = -311\ kN$$

$$\varepsilon_x = \frac{M_{bot}/d_v + 0.5N + V_n}{2A_s E_s} = \frac{75\,300\,000/(170) - 0.5 \cdot 311\,000 + 91\,000}{2(200\,000 \cdot 800)} = 0.001182 \quad Ok!$$

Therefore, the shear capacity of the columns in the repaired frame is 91 kN.

The General Method was used to determine the shear capacity of the columns of the retrofitted frame with the aid of Figure A.2:

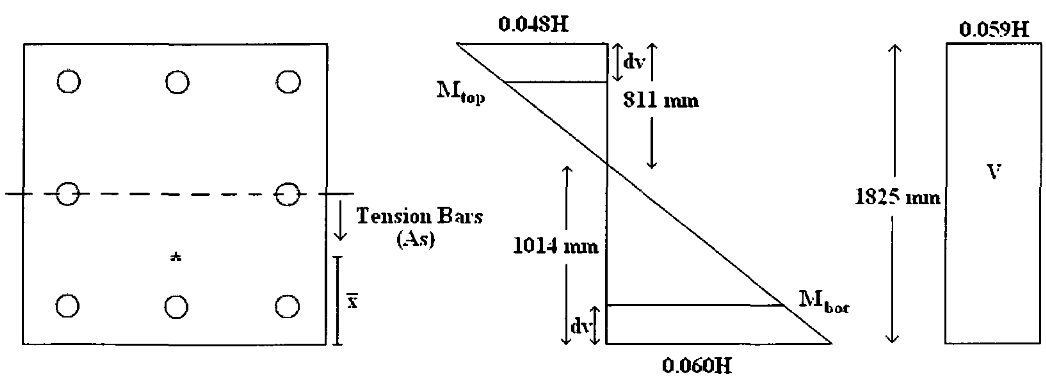

Figure A.2: General Method illustration for the columns of the retrofitted frame

Appendix A

The calculations are based on the critical loading case which is located at the base of the column.

Base of the column: Assume $\varepsilon_x = 0.002204$

$$S_{ze} = 300$$

$$\bar{x} = \frac{(600)(39.35) + 200(125)}{800} = 60.8\,mm$$

$$d = 250 - 60.8 = 189\,mm$$

$$\beta = \frac{0.4}{1+1500\varepsilon_x} \cdot \frac{1300}{1000+S_{ze}} = \frac{0.4}{1+1500 \cdot 0.002404} \cdot \frac{1300}{1000+300} = 0.093$$

$$\theta = 29° + 7000\varepsilon_x = 29° + 7000 \cdot 0.002204 = 44.43°$$

$$d_v = 0.9d = 0.9 \cdot 189 = 170\,mm$$

$$V_c = \lambda\beta\sqrt{f_c'}b_w d_v = 1.0 \cdot 0.093 \cdot \sqrt{32.1} \cdot 250 \cdot 0.9 \cdot 170 = 22\,kN$$

$$V_s = \frac{A_s f_y d_v \cot\theta}{s} = \frac{1.0\left(\frac{2\pi 6.35^2}{4}\right)500 \cdot 170 \cot(44.43)}{125} = 44\,kN$$

$$V_n = V_s + V_c = 44 + 22 = 66\,kN$$

$$V = 0.059H \rightarrow H = \frac{V_n}{0.059}$$

$$\frac{0.060H}{1014} = \frac{M_{bot}}{1014 - d_v}$$

$$M_{bot} = \frac{0.060H}{1014}(1014 - 170) = 0.0499H = 0.0499\frac{V_n}{0.059} = 0.846V_n = 0.846 \cdot 66 = 56.1\,kNm$$

$$N = -400 + 0.911H = -400 + 0.906\frac{V_n}{0.059} = -400 + 0.906 \cdot \frac{66}{0.059} = 618\,kN$$

$$\varepsilon_x = \frac{M_{bot}/d_v + 0.5N + V_n}{2A_s E_s} = \frac{56\,100\,000/(170) + 0.5 \cdot 618\,000 + 66\,000}{2(200\,000 \cdot 800)} = 0.002204 \quad Ok!$$

Therefore, the shear capacity of the columns in the retrofitted frame is 66 kN.

A.2 Beam Strength Calculation

The General Method was used to determine the shear capacity of the beam. This was done as follows with the aid of Figure A.3 for the repaired frame:

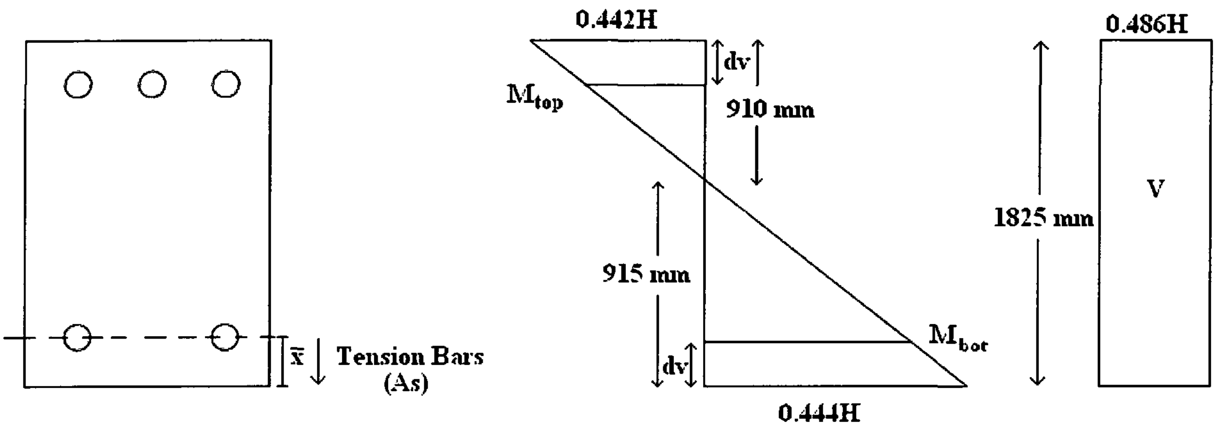

Figure A.3: General Method illustration for the beam of the repaired frame

The calculations are based on the critical loading case which is located at the end of the beam at the support.

Base of the column: Assume $\varepsilon_x = 0.001992$

$S_{ze} = 300$

$d = 350 - 39.5 = 311\ mm$

$$\beta = \frac{0.4}{1+1500\varepsilon_x} \cdot \frac{1300}{1000+S_{ze}} = \frac{0.4}{1+1500 \cdot 0.001992} \cdot \frac{1300}{1000+300} = 0.1003$$

$$\theta = 29° + 7000\varepsilon_x = 29° + 7000 \cdot 0.001992 = 42.94°$$

$$d_v = 0.9d = 0.9 \cdot 311 = 280\ mm$$

$$V_c = \lambda\beta\sqrt{f_c'}b_w d_v = 1.0 \cdot 0.1003 \cdot \sqrt{32.1} \cdot 250 \cdot 0.9 \cdot 280 = 40\ kN$$

$$V_s = \frac{A_s f_y d_v \cot\theta}{s} = \frac{1.0\left(\frac{2\pi 6.35^2}{4}\right)500 \cdot 280 \cot(42.94)}{125} = 76\ kN$$

$$V_n = V_s + V_c = 76 + 40 = 117\ kN$$

$$V = 0.486H \rightarrow H = \frac{V_n}{0.486}$$

$$\frac{0.444H}{915} = \frac{M_{bot}}{915 - d_v}$$

$$M_{bot} = \frac{0.444H}{915}(915 - 280) = 0.308H = 0.308\frac{V_n}{0.486} = 0.634V_n = 0.634 \cdot 116 = 73\ kNm$$

$$N = -0.499H = -0.499\frac{V_n}{0.486} = -0.499 \cdot \frac{116}{0.486} = -119\ kN$$

$$\varepsilon_x = \frac{M_{bot}/d_v + 0.5N + V_n}{2A_sE_s} = \frac{73\,000\,000/(280) - 0.5 \cdot 119\,000 + 119\,000}{2(200\,000 \cdot 400)} = 0.001992 \quad Ok!$$

Therefore, the shear capacity of the beam at the support of the repaired frame is 119 kN.

The shear resistance calculations for the beam at the mid-span are as follows:

Base of the column: Assume $\varepsilon_x = 0.000586$

$$S_{ze} = 300$$

$$d = 350 - 39.5 = 311\ mm$$

$$\beta = \frac{0.4}{1 + 1500\varepsilon_x} \cdot \frac{1300}{1000 + S_{ze}} = \frac{0.4}{1 + 1500 \cdot 0.000586} \cdot \frac{1300}{1000 + 300} = 0.2129$$

$$\theta = 29° + 7000\varepsilon_x = 29° + 7000 \cdot 0.000961 = 33.10°$$

$$d_v = 0.9d = 0.9 \cdot 311 = 280\ mm$$

$$V_c = \lambda\beta\sqrt{f_c'}b_w d_v = 1.0 \cdot 0.2129 \cdot \sqrt{32.1} \cdot 250 \cdot 0.9 \cdot 280 = 84\ kN$$

$$V_s = \frac{A_s f_y d_v \cot\theta}{s} = \frac{1.0\left(\frac{2\pi 6.35^2}{4}\right)500 \cdot 280 \cot(33.10)}{125} = 109\ kN$$

$$V_n = V_s + V_c = 109 + 84 = 193\ kN$$

$$V = 0.486H \rightarrow H = \frac{V_n}{0.486}$$

$$M_{bot} = 0\ kNm$$

$$N = -0.499H = -0.499\frac{V_n}{0.486} = -0.499 \cdot \frac{193}{0.486} = -198\ kN$$

Appendix A

$$\varepsilon_x = \frac{M_{bot}/d_v + 0.5N + V_n}{2A_sE_s} = \frac{0 - 0.5 \cdot 198\,000 + 193\,000}{2(200\,000 \cdot 400)} = 0.000586 \quad Ok!$$

Therefore, the shear capacity of the beam at the mid-span of the repaired frame is 193 kN.

The General Method was used to determine the shear capacity of the beam of the retrofitted frame with the aid of Figure A.4:

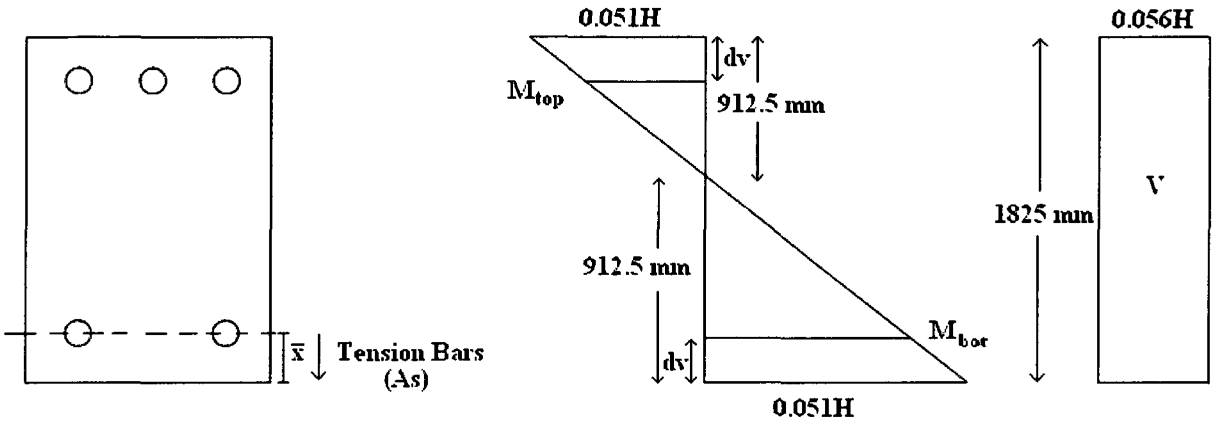

Figure A.4: General Method illustration for the beam of the retrofitted frame

The calculations are based on the critical loading case which is located at the end of the beam.

Base of the column: Assume $\varepsilon_x = 0.001983$

$$S_{ze} = 300$$

$$d = 350 - 39.5 = 311\,mm$$

$$\beta = \frac{0.4}{1+1500\varepsilon_x} \cdot \frac{1300}{1000+S_{ze}} = \frac{0.4}{1+1500 \cdot 0.001983} \cdot \frac{1300}{1000+300} = 0.1006$$

$$\theta = 29° + 7000\varepsilon_x = 29° + 7000 \cdot 0.001983 = 42.88°$$

$$d_v = 0.9d = 0.9 \cdot 311 = 280\,mm$$

$$V_c = \lambda\beta\sqrt{f_c'}b_w d_v = 1.0 \cdot 0.1006 \cdot \sqrt{32.1} \cdot 250 \cdot 0.9 \cdot 280 = 40\,kN$$

$$V_s = \frac{A_s f_y d_v \cot\theta}{s} = \frac{1.0\left(\frac{2\pi 6\,35^2}{4}\right)500 \cdot 280 \cot(42\,88)}{125} = 76\,kN$$

$$V_n = V_s + V_c = 76 + 40 = 116\,kN$$

$V = 0.056H \rightarrow H = \frac{V_n}{0.056}$

$\frac{0.051H}{912.5} = \frac{M_{bot}}{912.5 - d_v}$

$M_{bot} = \frac{0.051H}{912.5}(912.5 - 280) = 0.0354H = 0.0354\frac{V_n}{0.056} = 0.631V_n = 0.631 \cdot 116 = 73\ kNm$

$N = -0.059H = -0.059\frac{V_n}{0.056} = -0.059 \cdot \frac{116}{0.056} = -122\ kN$

$\varepsilon_x = \frac{M_{bot}/d_v + 0.5N + V_n}{2A_sE_s} = \frac{73\,000\,000/(280) - 0.5 \cdot 12\,000 + 116\,000}{2(200\,000 \cdot 400)} = 0.001983 \quad Ok!$

Therefore, the shear capacity of the beam in the retrofitted frame at the support is 116 kN.

The shear resistance calculations for the beam at the mid-span are as follows:

Base of the column: Assume $\varepsilon_x = 0.000573$

$S_{ze} = 300$

$d = 350 - 39.5 = 311\ mm$

$\beta = \frac{0.4}{1+1500\varepsilon_x} \cdot \frac{1300}{1000+S_{ze}} = \frac{0.4}{1+1500 \cdot 0.000573} \cdot \frac{1300}{1000+300} = 0.2151$

$\theta = 29° + 7000\varepsilon_x = 29° + 7000 \cdot 0.000573 = 33.01°$

$d_v = 0.9d = 0.9 \cdot 311 = 280\ mm$

$V_c = \lambda\beta\sqrt{f_c'}b_w d_v = 1.0 \cdot 0.2151 \cdot \sqrt{32.1} \cdot 250 \cdot 0.9 \cdot 280 = 85\ kN$

$V_s = \frac{A_s f_y d_v \cot\theta}{s} = \frac{1.0\left(\frac{2\pi 6.35^2}{4}\right)500 \cdot 280 \cot(33.01)}{125} = 109\ kN$

$V_n = V_s + V_c = 109 + 85 = 194\ kN$

$V = 0.056H \rightarrow H = \frac{V_n}{0.056}$

$M_{bot} = 0\ kNm$

$N = -0.059H = -0.059\frac{V_n}{0.056} = -0.059 \cdot \frac{194}{0.056} = -204\ kN$

$$\varepsilon_x = \frac{M_{bot}/d_v + 0.5N + V_n}{2A_s E_s} = \frac{0 - 0.5 \cdot 204\ 000 + 194\ 000}{2(200\ 000 \cdot 400)} = 0.000573 \quad Ok!$$

Therefore, the shear capacity of the beam at the mid-span of the repaired frame is 194 kN.

A.3 Loading Distribution

The demands imposed by the loading on the repaired and retrofitted frames were determined using the Program SAP 2000. Figures A.5 to A.7 illustrate the loads, shear forces, axial forces and bending moments acting on the frame. The stiffness of the members was calculated using Table 21.1 from CSA A23.3-04 Clause 21.2.5 as follows:

Column:

$$I_e = \propto_c I_g$$

$$\propto_c = 0.5 + 0.6 \frac{P_s}{f_c' A_g} = 0.5 + 0.6 \frac{400\ 000}{32.1 \cdot 250^2} = 0.62$$

$$I_e = 0.62 I_g$$

Beam:

$$I_e = 0.4 I_g$$

Appendix A

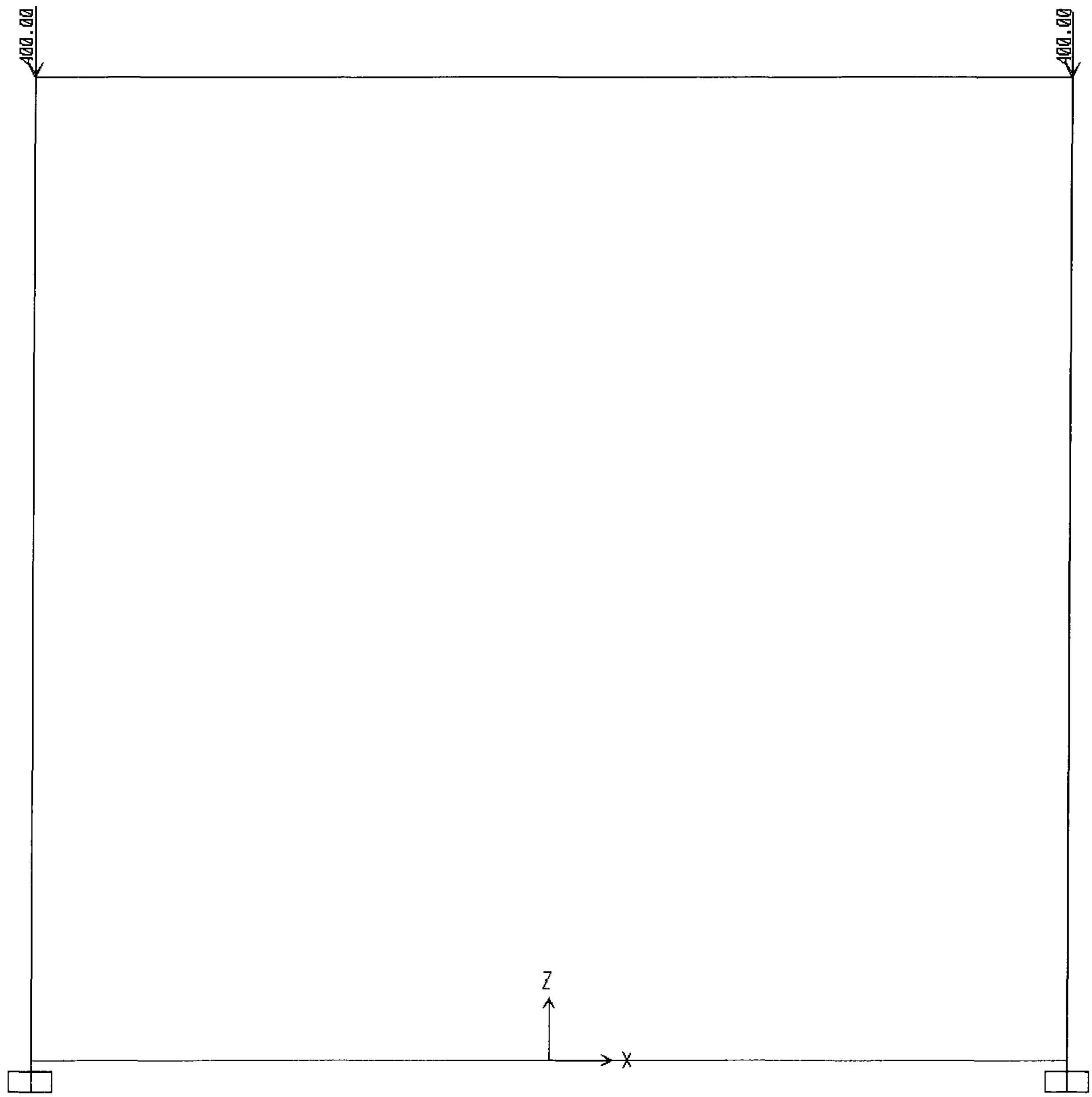

a) Dead load acting on the repaired frame (kN)

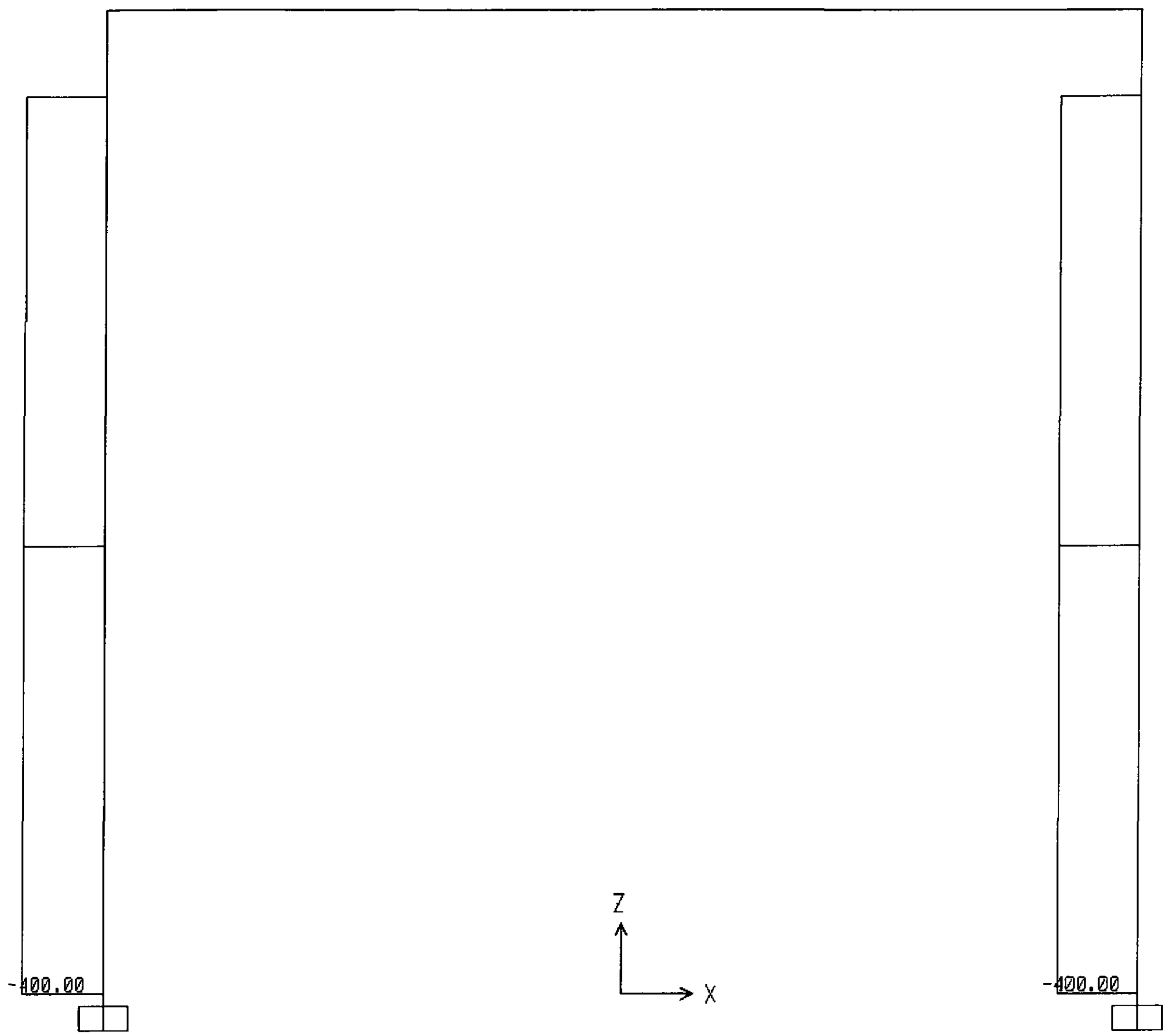

b) Axial forces acting on the repaired frame (kN)

Figure A.5: Member forces on the repaired frame due to dead loads

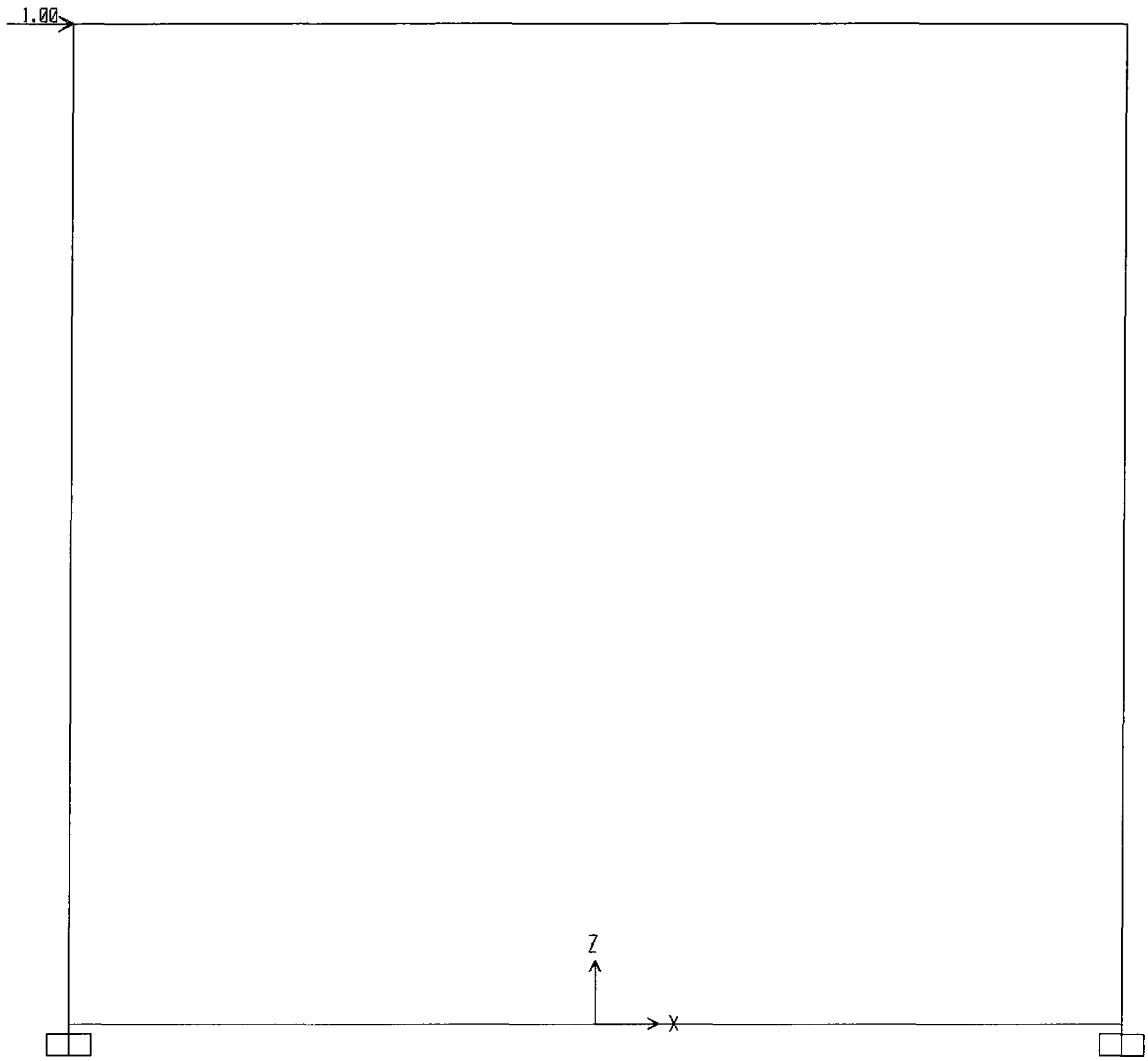

a) Unit lateral load acting on the repaired frame (kN)

Appendix A

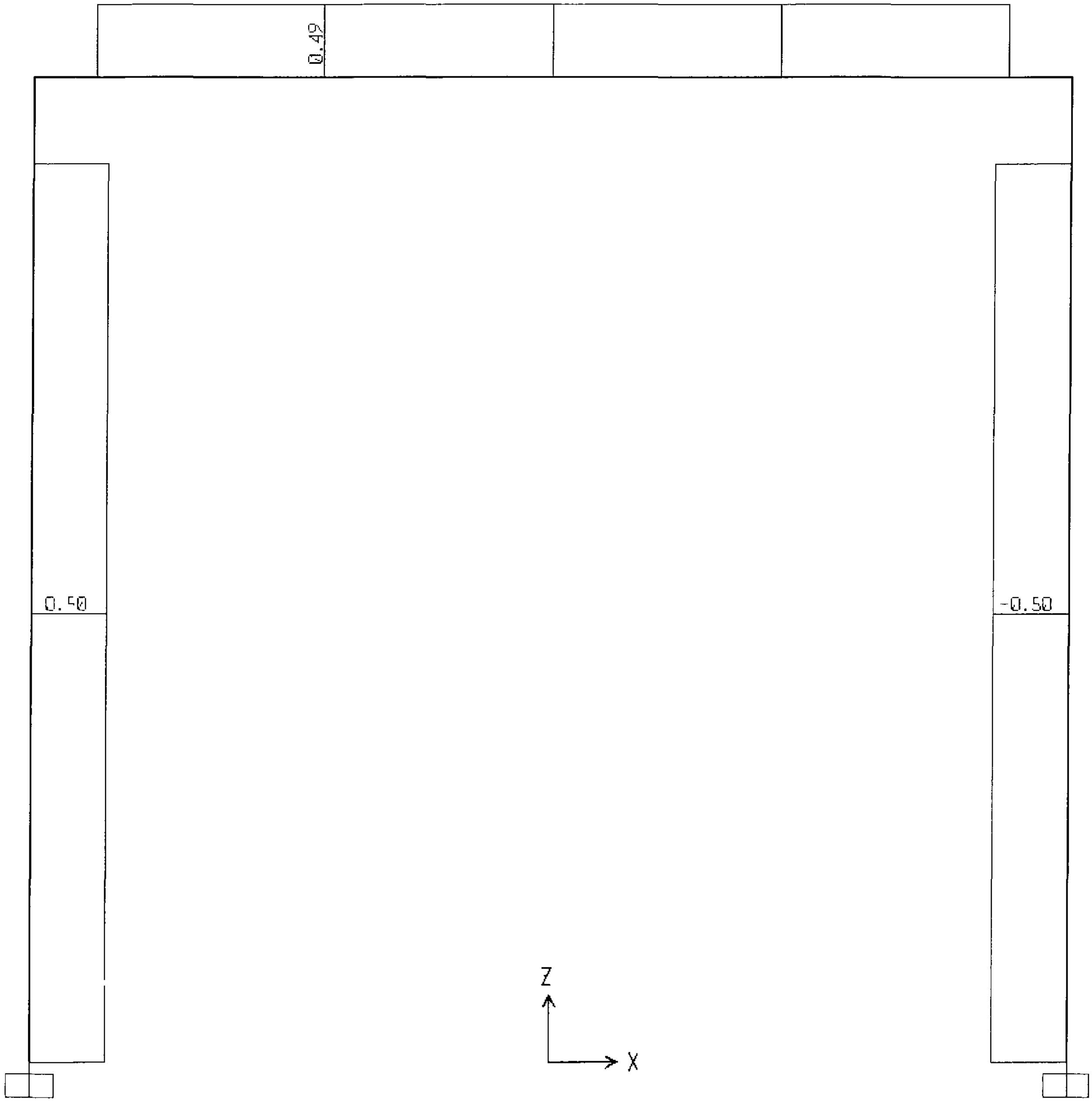

b) Shear forces acting on the repaired frame (kN)

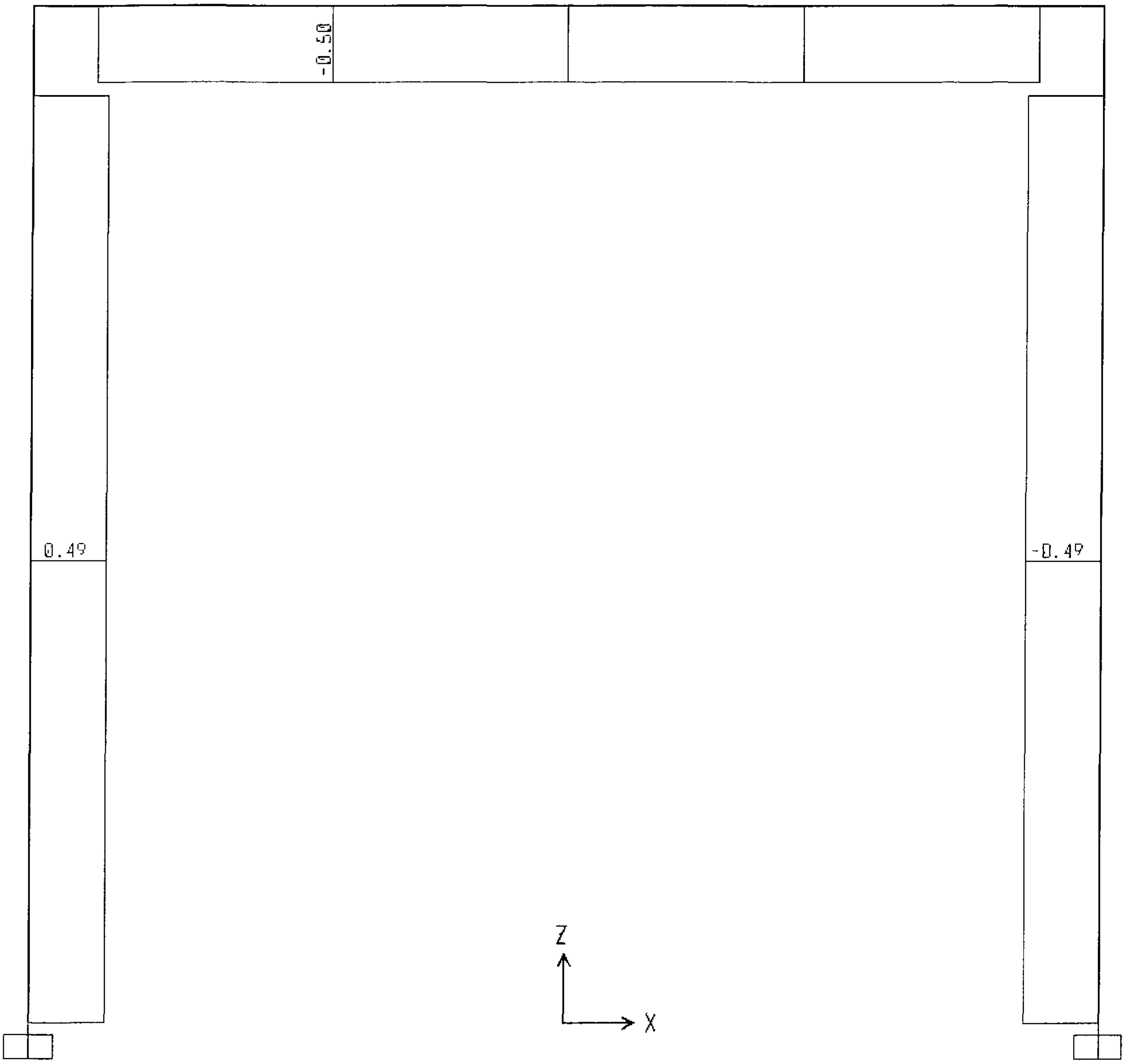

c) Axial forces acting on the repaired frame (kN)

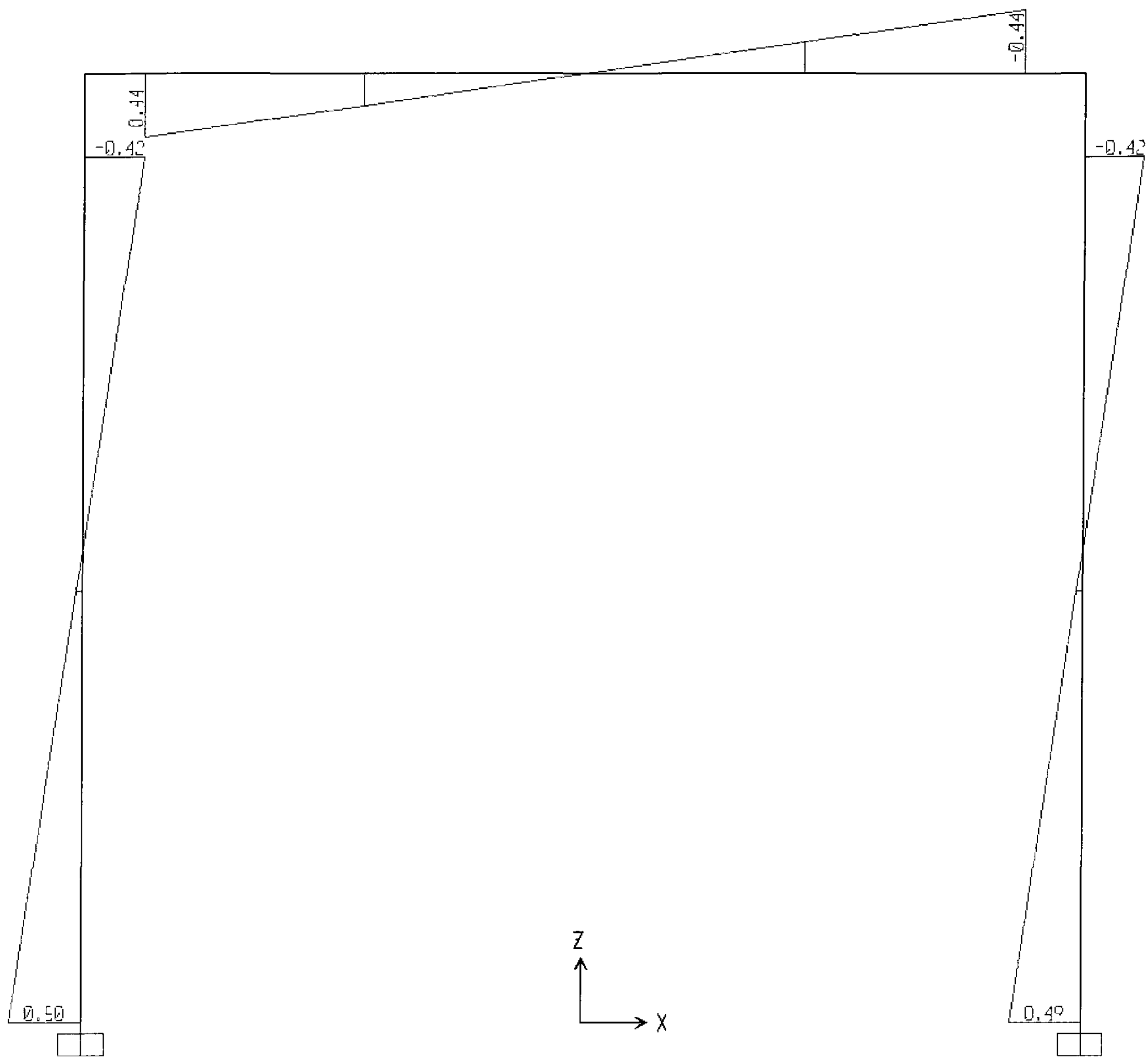

d) Bending moments acting on the repaired frame (kNm)

Figure A.6: Member forces on the repaired frame due to a unit lateral load

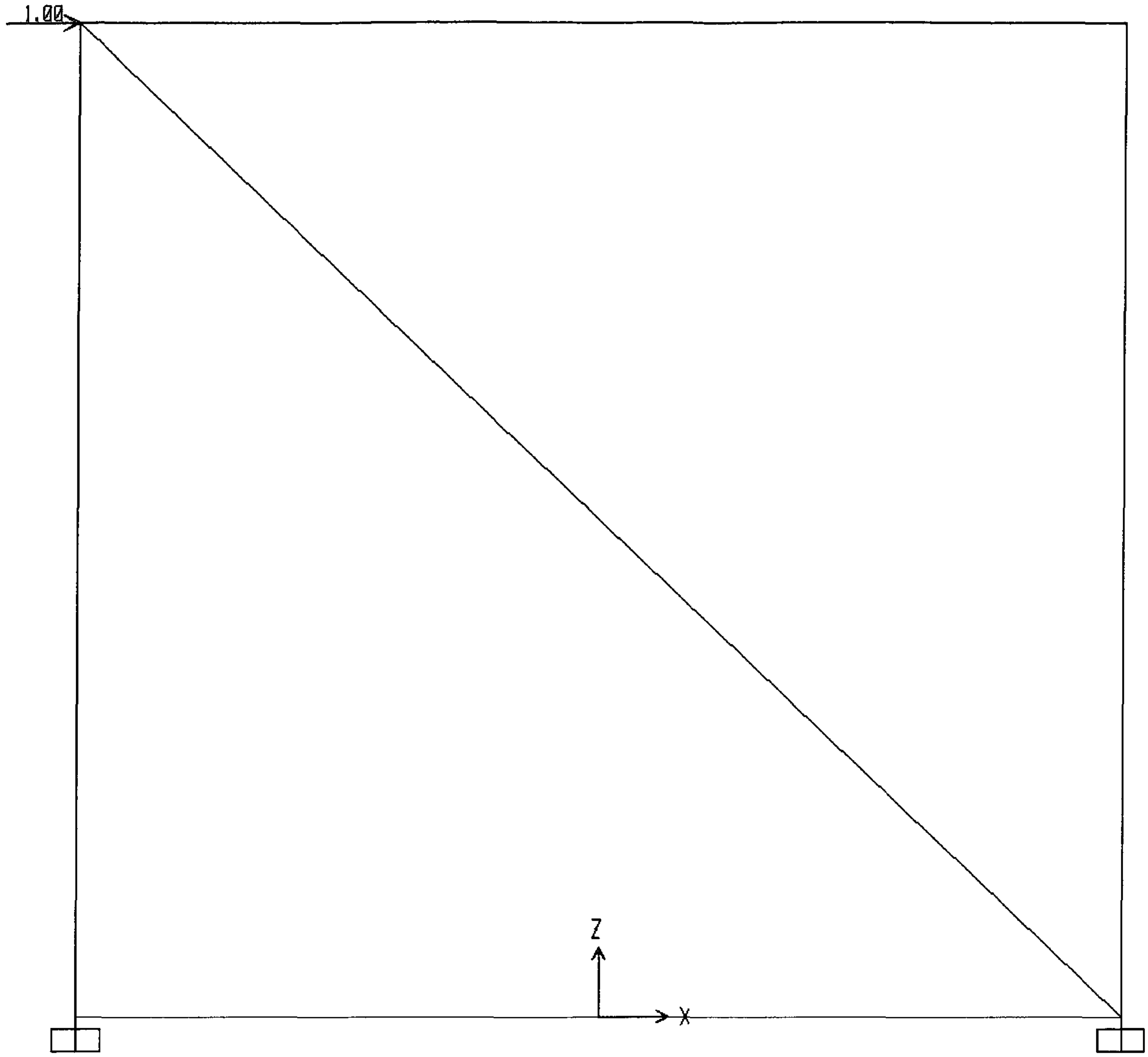

a) Lateral load acting on the retrofitted frame (kN)

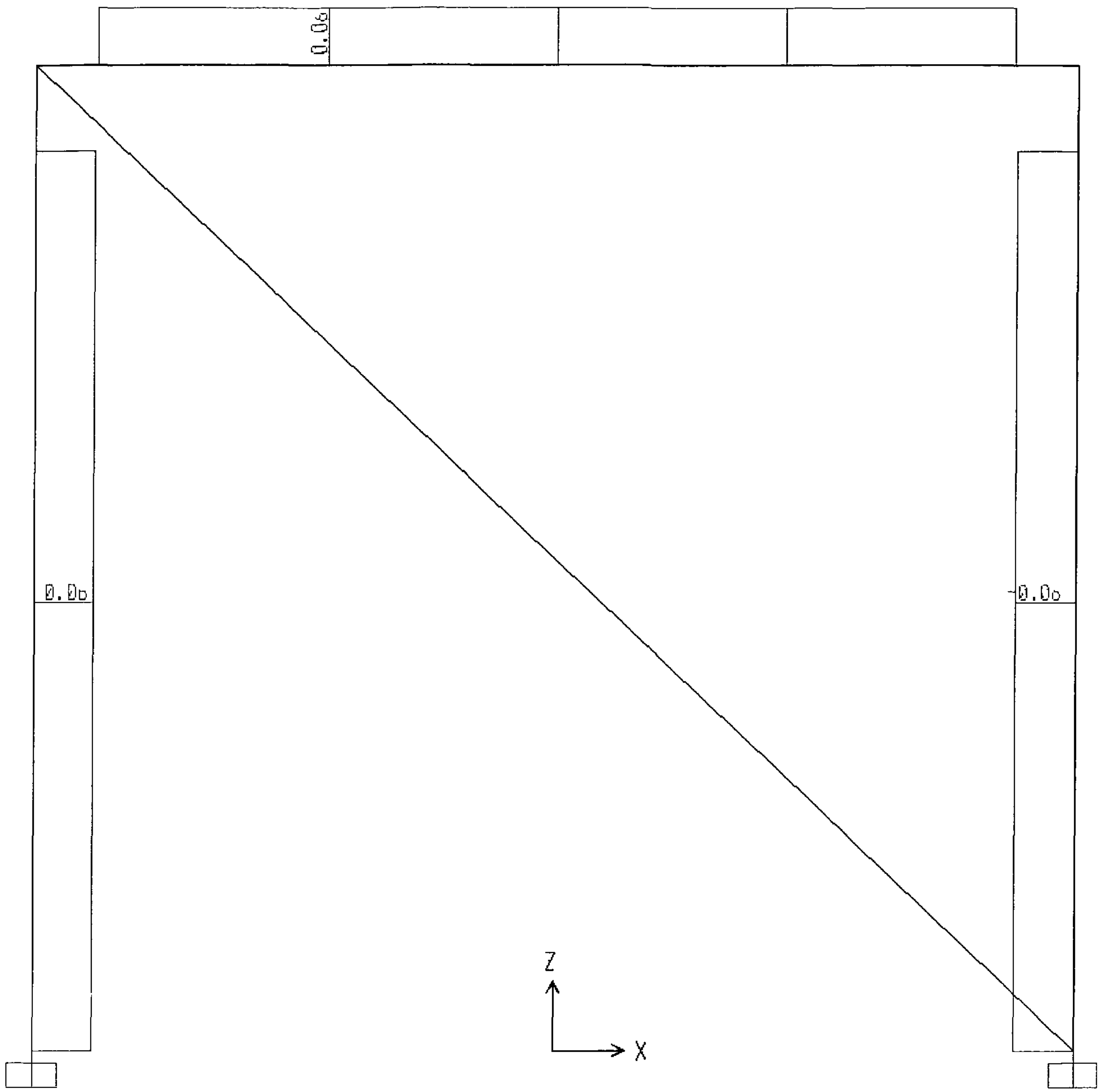

b) Shear forces acting on the retrofitted frame (kN)

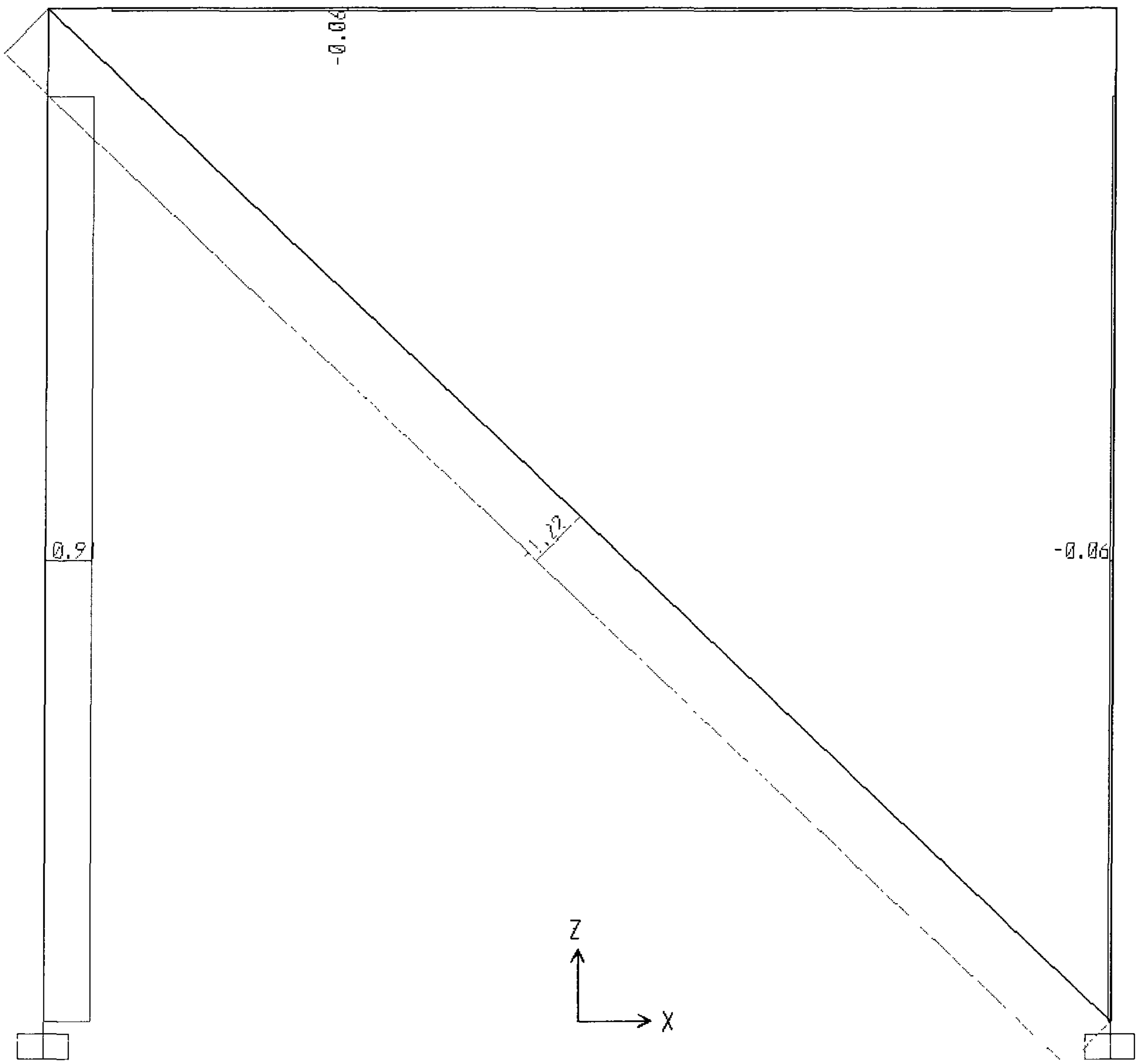

c) Axial forces acting on the retrofitted frame (kN)

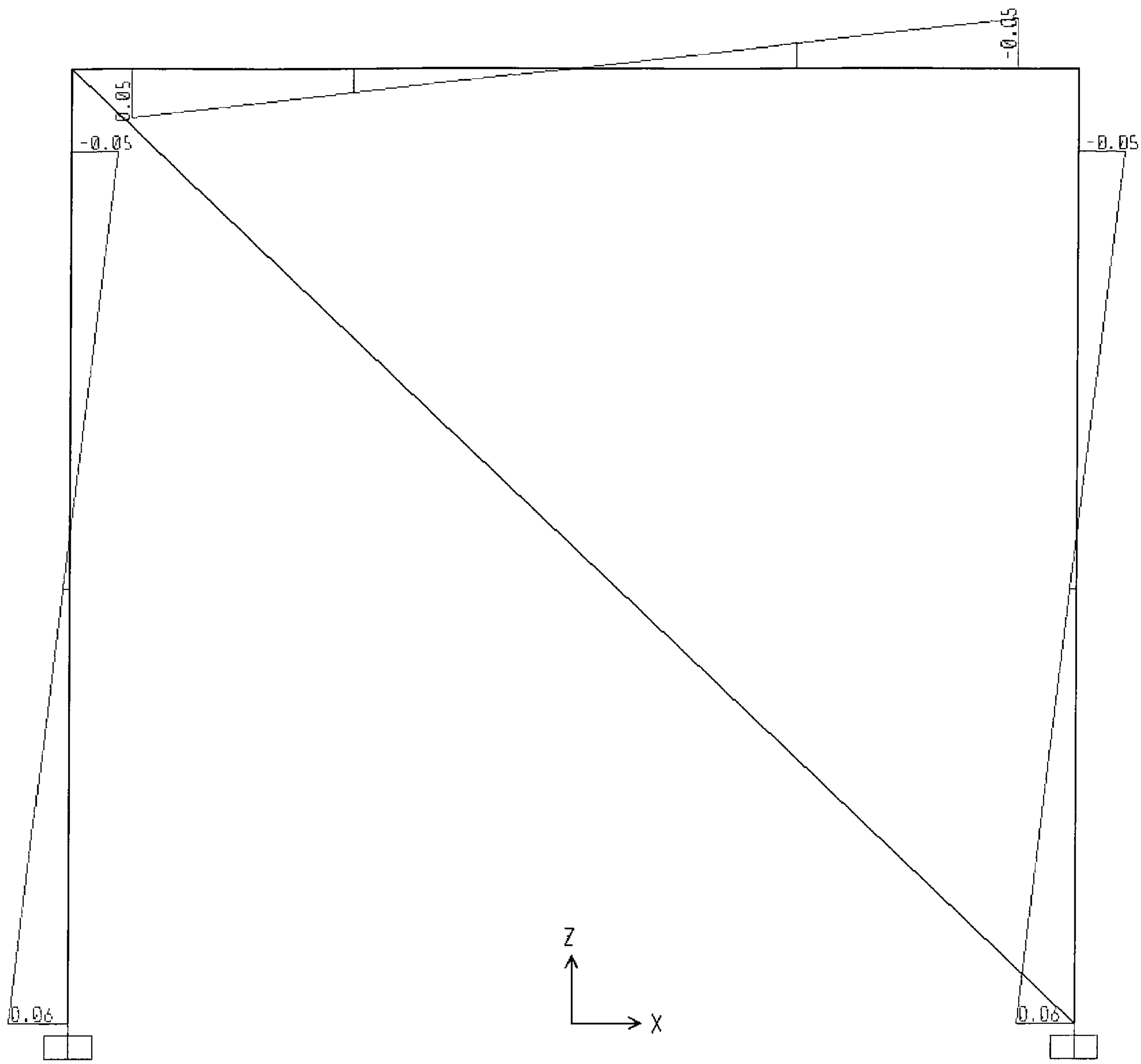

d) Bending moments acting on the retrofitted frame (kNm)

Figure A.7: Member forces on the retrofitted frame due to a unit lateral load

A.4 Steel bracing design

The capacity of the steel brace was calculated according to CSA S16.1-04 as follows:

End condition: Pinned – Pinned, K = 1.0

Class C section, n = 1.34

Maximum length of the steel member, L = 2581 mm

$$\lambda = \frac{KL}{r}\sqrt{\frac{F_y}{\pi^2 E}} = \frac{1.0 \cdot 2581}{36.9}\sqrt{\frac{445}{\pi^2 200000}} = 1.05$$

$$C_r = A_s F_y (1+\lambda^{2n})^{-1/n} = 3280 \cdot 445(1+1.05^{2 \cdot 1.34})^{-1/1.34} = 827\ kN$$

$$P_n = C_r$$

$$P_n = -1.224V \rightarrow V = \frac{P_n}{-1.224} = \frac{C_n}{-1.224} = \frac{-827}{-1.224} = 676\ kN$$

The joint design calculations based on Packer and Hendersen (1997) are as follows:

$$N_1^* \geq P_n = 827\ kN$$

$$\theta_1 = 90°$$

$$F_k = \frac{0.8\,\mathrm{C_r} \sin\theta_1}{A_s} = \frac{0.8 \cdot 827000 \cdot \sin 90°}{3280} = 202\ kN$$

$$N_1^* = \frac{2F_k t_o}{\sin\theta_1}\left[\frac{h_1}{\sin\theta_1} + 5t_0\right] \quad side\ wall\ failure$$

$$N_1^* = \frac{f_y(2h_0 t_0)}{\sqrt{3}\sin\theta_1} \qquad side\ wall\ shear\ failure$$

$$N_1^* = \frac{2 \cdot 202 \cdot 9.5}{\sin 90°}\left[\frac{102}{\sin 90°} + 5 \cdot 9.5\right] = 573\ kN\ Not\ Ok!$$

$N_1^* = \frac{445(2 \cdot 102 \cdot 9.5)}{\sqrt{3}\sin 90°} = 498\ kN\ Not\ Ok!$ Therefore steel plates are required.

Steel plate design:

$$t_p \geq 4t_1 - t_0 = 4 \cdot 9.5 - 9.5 = 28.6\ mm$$

$$t_p = 30\ mm$$

$$N_1^* = 2f_y t_0 \left(t_b + 5(t_0 + t_p)\right) = 2 \cdot 445 \cdot 9.5(102 + 5(9.5 + 30)) = 2532\ kN\ Ok!$$

$$N_1^* = 2F_k t_0 \left(t_b + 5(t_0 + t_p)\right) = 2 \cdot 201 \cdot 9.5(102 + 5(9.5 + 30)) = 1144\ kN\ Ok!$$

Appendix B

Experimental Data

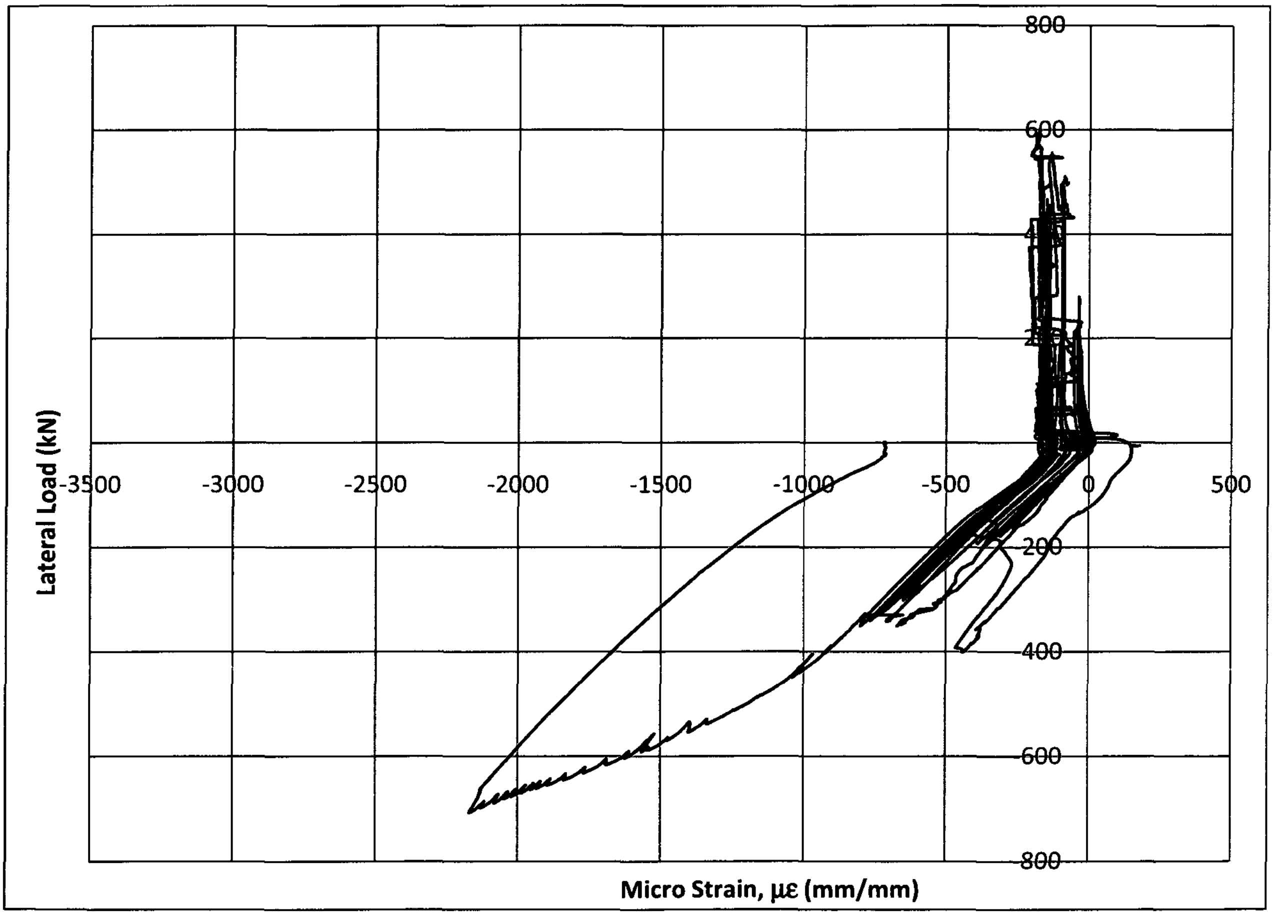

Figure B.1: Lateral load versus strain response of Gauge X1 for BL-3R

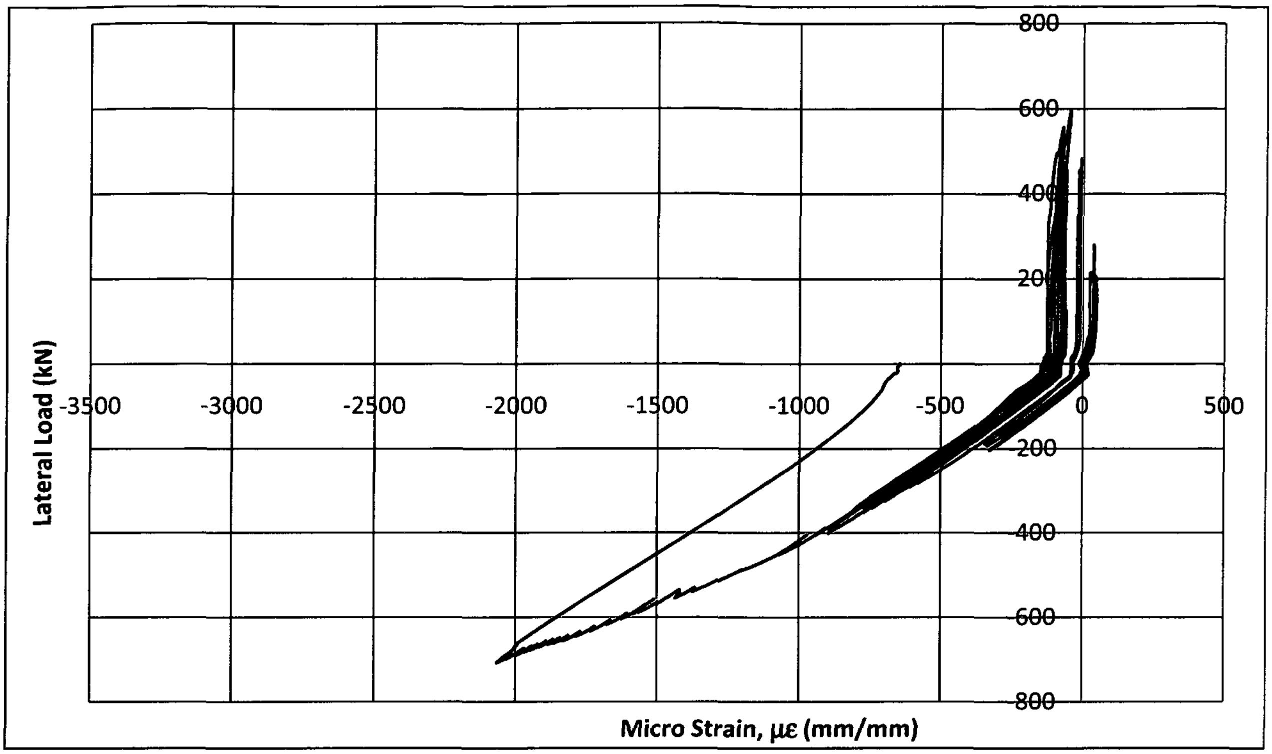

Figure B.2: Lateral load versus strain response of Gauge X2 for BL-3R

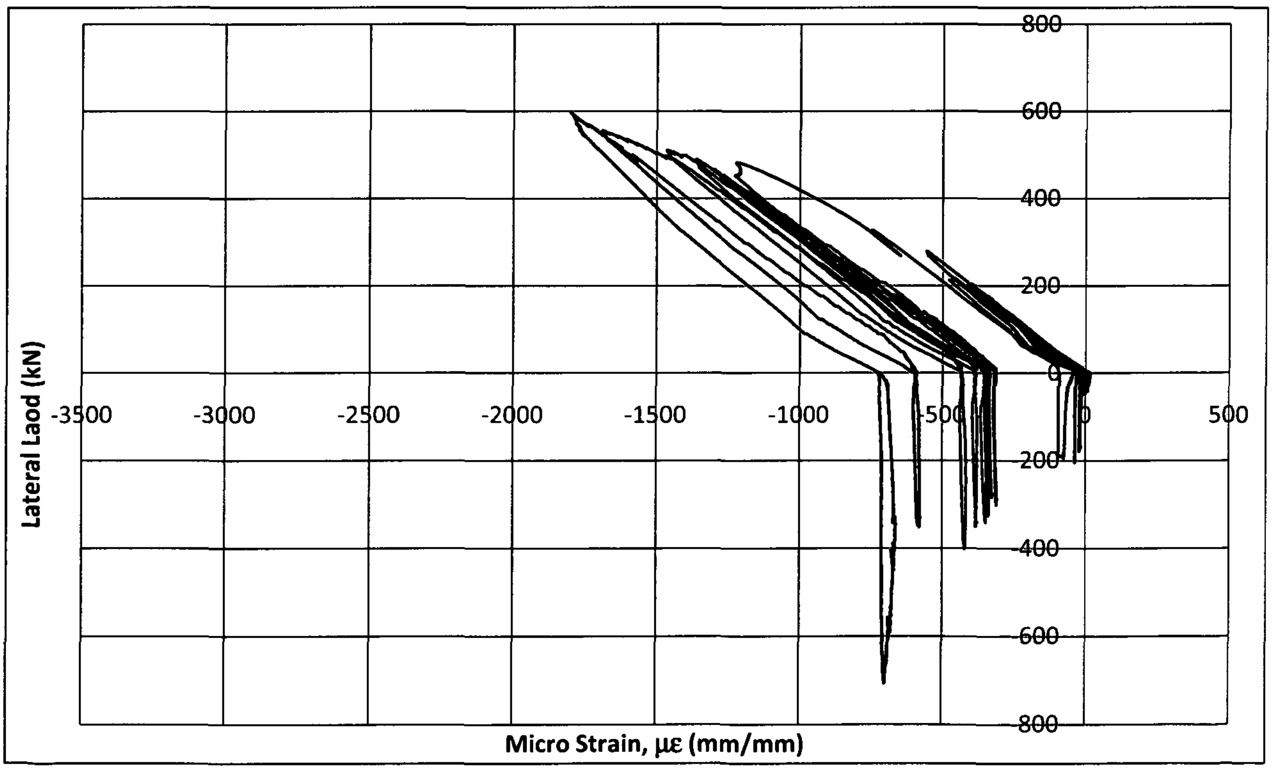

Figure B.3: Lateral load versus strain response of Gauge X4 for BL-3R

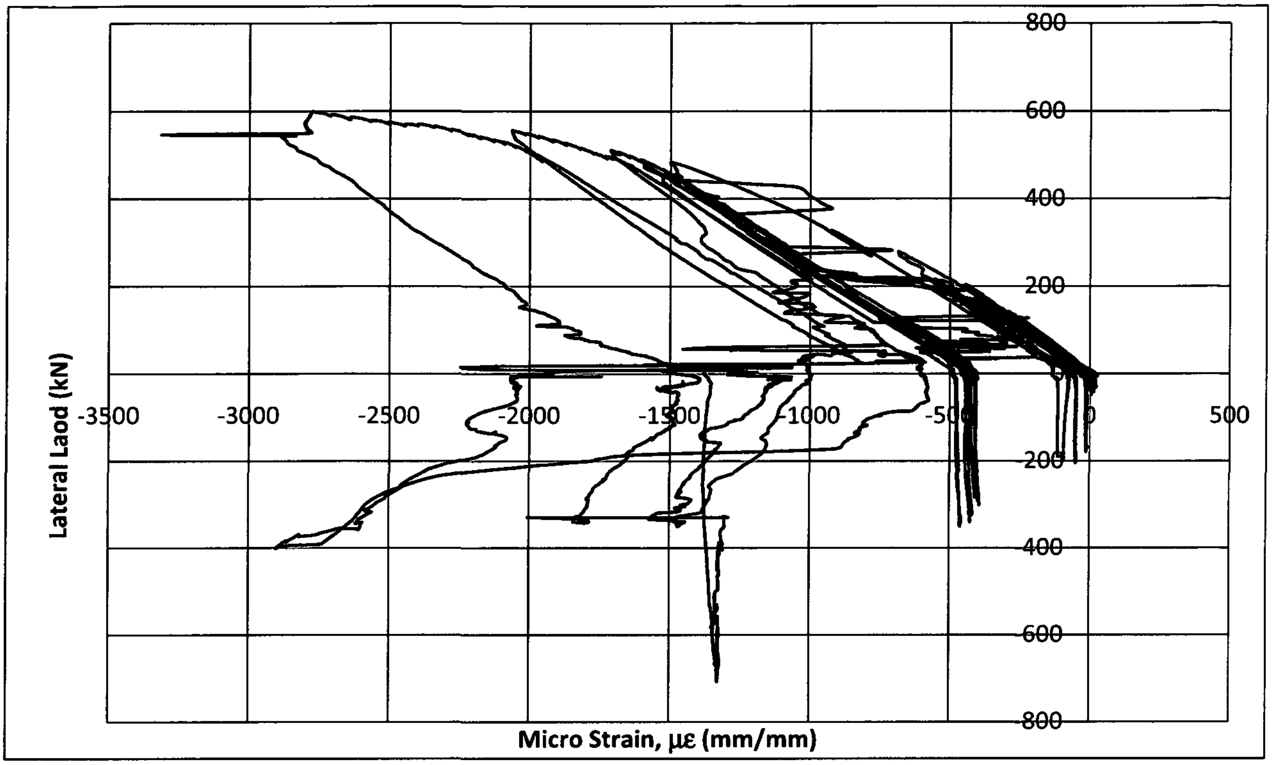

Figure B.4: Lateral load versus strain response of Gauge X7 for BL-3R

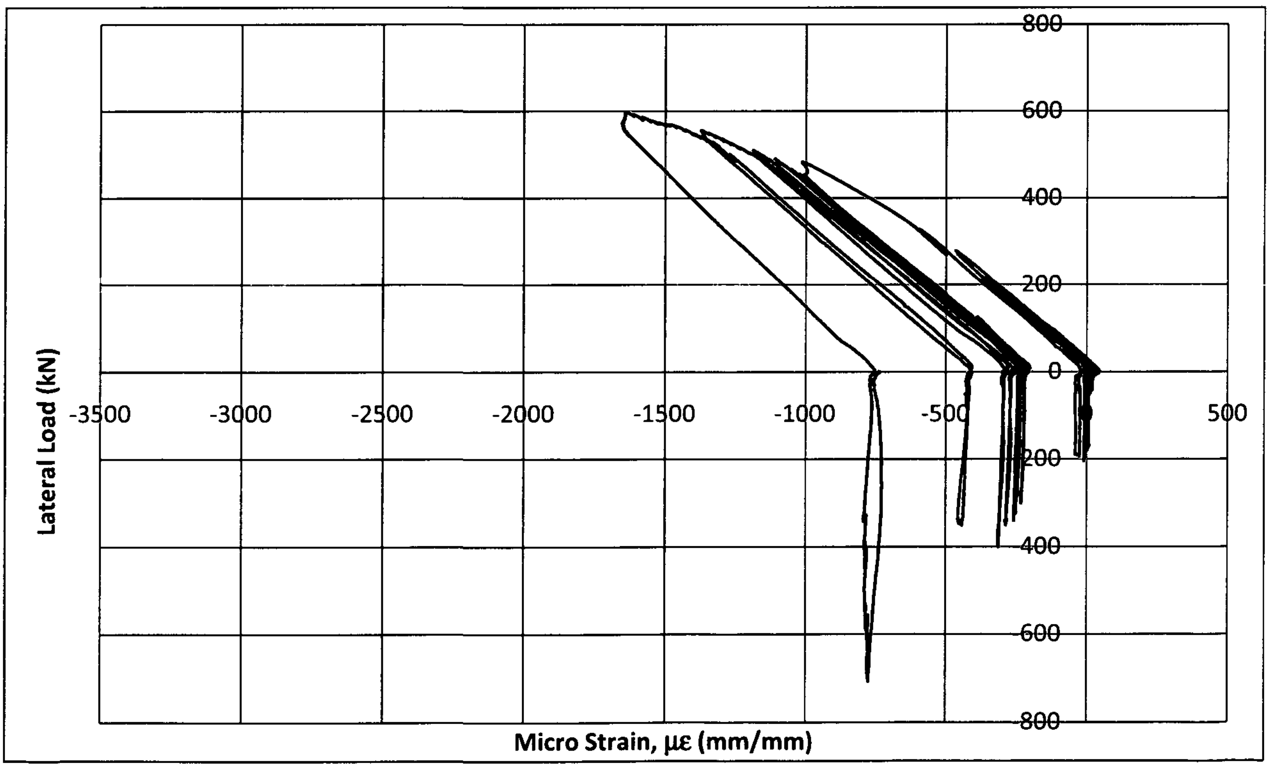

Figure B.5: Lateral load versus strain response of Gauge X8 for BL-3R

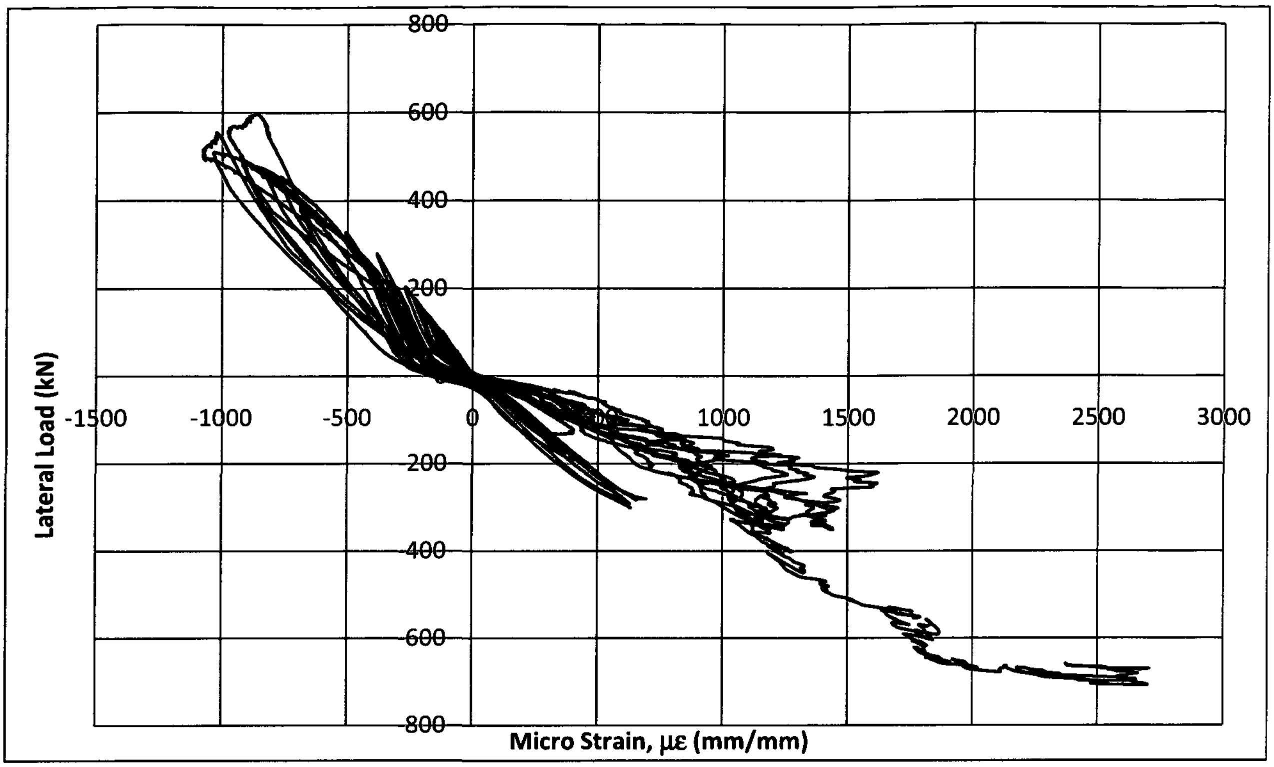

Figure B.6: Lateral load versus strain response of Gauge RC2 for BL-3R

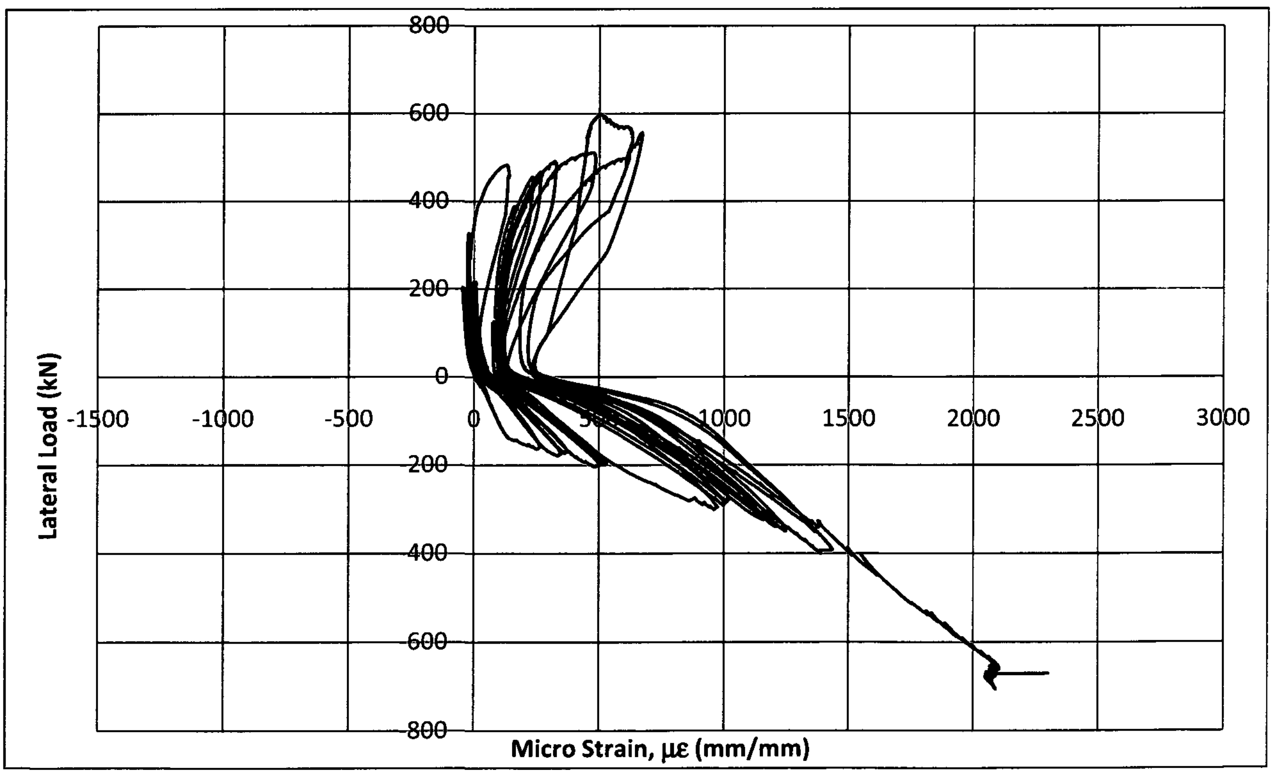

Figure B.7: Lateral load versus strain response of Gauge RC3 for BL-3R

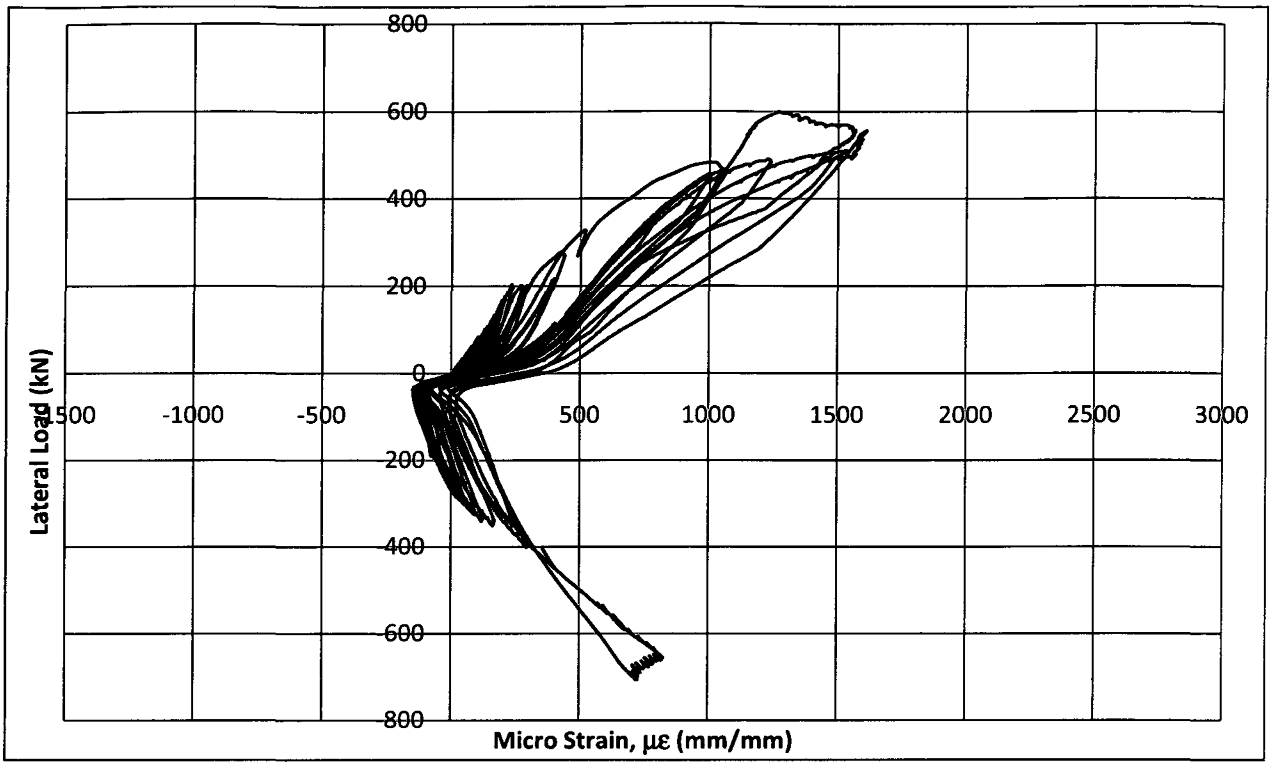

Figure B.8: Lateral load versus strain response of Gauge RC4 for BL-3R

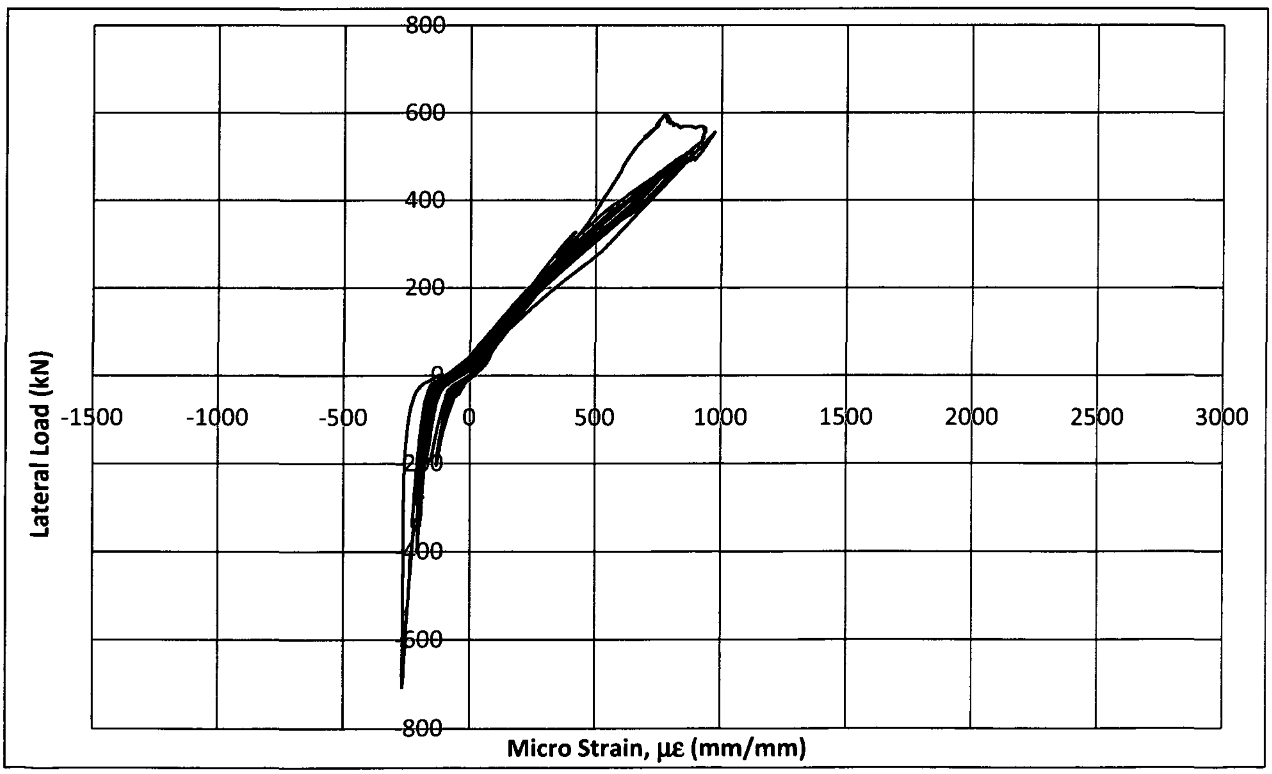

Figure B.9: Lateral load versus strain response of Gauge LC1 for BL-3R

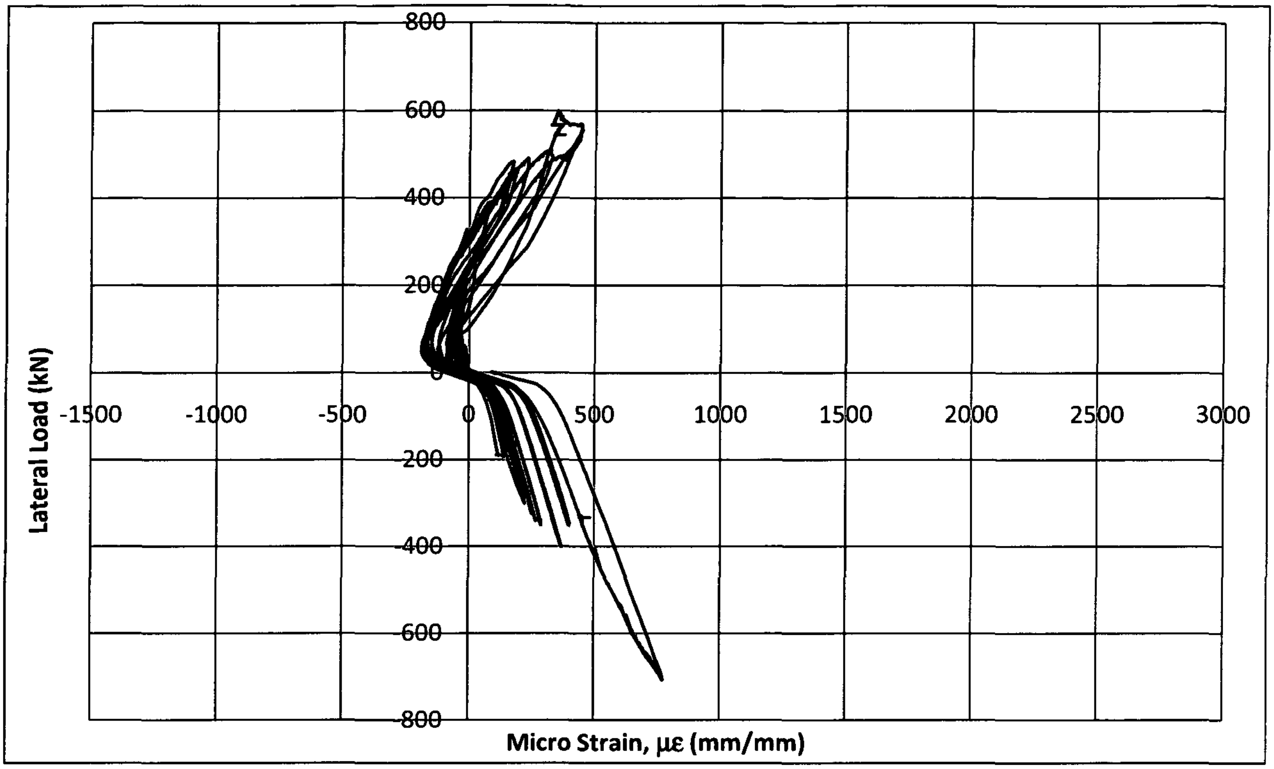

Figure B.10: Lateral load versus strain response of Gauge LC2 for BL-3R

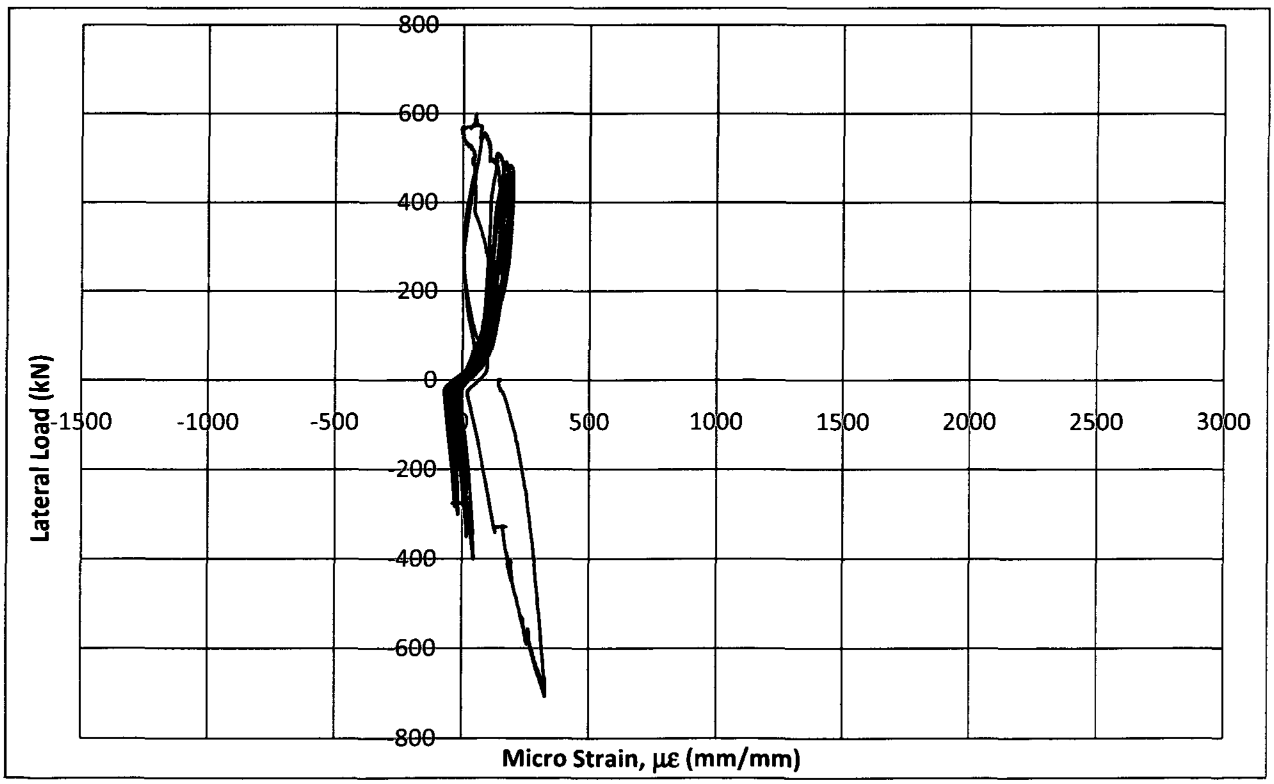

Figure B.11: Lateral load versus strain response of Gauge LC3 for BL-3R

Appendix C

Computer Model Calculations

C.1 Development length sample calculation based on top bars in the beam

According to Table 12.1 of Clause 12.2.3 in CSA A23.3-04, the development length in tension is:

$$l_d = 0.45 k_1 k_2 k_3 k_4 \frac{f_y}{\sqrt{f_c'}} d_b$$

$k_1 = 1.3$ (there is more than 300 mm of concrete below development length)

$k_2 = 1.0$ (uncoated reinforcement)

$k_3 = 1.0$ (normal-density concrete)

$k_4 = 0.8$ (20 M and smaller bars)

$$l_d = 0.45 \cdot 1.3 \cdot 1.0 \cdot 1.0 \cdot 0.8 \frac{495}{\sqrt{32.1}} 16 = 654\ mm$$

C.2 Development length modeling

An example for the calculation of the effective area of the truss bars will be given for the section of 50 mm to 100 mm from the terminated end of the reinforcement.

$$A_{i\rightarrow i+50} = \frac{A_s}{Development\ length}\left(distance_{i+50} - \frac{section\ length}{2}\right)$$

$$A_{50\rightarrow 100} = \frac{200\ mm^2}{650\ mm}\left(100\ mm - \frac{50\ mm}{2}\right) = 23.0\ mm^2 \qquad \text{(1 No. 15 M bar)}$$

$$A_{50\rightarrow 100} = \frac{400\ mm^2}{650\ mm}\left(100\ mm - \frac{50\ mm}{2}\right) = 46.2\ mm^2 \qquad \text{(2 No. 15 M bars)}$$

$$A_{50\rightarrow 100} = \frac{600\ mm^2}{650\ mm}\left(100\ mm - \frac{50\ mm}{2}\right) = 69.2\ mm^2 \qquad \text{(3 No. 15 M bars)}$$

C.3 Calculations of steel bracing properties

The steel bracing properties were calculated as follows:

$$A = 3280\ mm^2$$

$$d_b = 102\ mm$$

$$f_y = 150\ MPa$$

$$f_u = 252\ MPa$$

$$\varepsilon_s = 0.000833\ mm/mm$$

$$\varepsilon_{rup} = 0.001717\ mm/mm$$

$$\varepsilon_{sh} = 0.000834\ mm/mm$$

$$E_s = \frac{f_y}{\varepsilon_s} = \frac{150}{0.000833} = 180\ 000\ MPa$$

$$E_{sh} = \frac{f_u - f_y}{\varepsilon_{rup} - \varepsilon_s} = \frac{252-150}{0.001717-0.000833} = 115\ 385\ MPa$$